



HAL
open science

Precision medicine for the treatment of hepatocellular carcinoma

Emanuele Felli

► **To cite this version:**

Emanuele Felli. Precision medicine for the treatment of hepatocellular carcinoma. Human health and pathology. Université de Strasbourg, 2022. English. NNT : 2022STRAJ030 . tel-04799519

HAL Id: tel-04799519

<https://theses.hal.science/tel-04799519v1>

Submitted on 23 Nov 2024

HAL is a multi-disciplinary open access archive for the deposit and dissemination of scientific research documents, whether they are published or not. The documents may come from teaching and research institutions in France or abroad, or from public or private research centers.

L'archive ouverte pluridisciplinaire **HAL**, est destinée au dépôt et à la diffusion de documents scientifiques de niveau recherche, publiés ou non, émanant des établissements d'enseignement et de recherche français ou étrangers, des laboratoires publics ou privés.

THESE DE DOCTORAT

ÉCOLE DOCTORALE SCIENCES DE LA VIE ET DE LA SANTÉ

Institut de recherche sur les maladies virales et hépatiques, UMR_S1110

thèse présentée par

Emanuele FELLI

Soutenue le 09 Mai 2022

Pour obtenir le grade de **Docteur de l'Université de Strasbourg**

Discipline: Sciences Médicales

Spécialité : Hépatogastroentérologie

**Apport de la médecine de précision dans le traitement
du carcinome hépatocellulaire**

Thèse dirigée par :

**Catherine Schuster
Patrick Pessaux**

**DR Inserm
PU-PH, Université de Strasbourg**

Rapporteurs :

Olivier Soubrane

PU-PH, Université de Paris

Fabrizio Panaro

PU-PH, Université de Montpellier

Examineurs :

**Anne Lejay
Ephrem Salamé
Giuseppe Maria Ettorre**

**PU-PH, Université de Strasbourg
PU-PH, Université de Tours
PU-PH, Université de Rome**

I would like to dedicate this thesis to all the patients around the world, no matter their ethnicity, social status, or beliefs. All this multidisciplinary work exists for them, I admire their every day struggle against diseases.

Aknowledgments:

I particularly thank Catherine Schuster and all my Family for the patience, the advices, and the constant help in the elaboration and realization of the research.

Table of contents

INTRODUCTION

1. The concept of precision medicine.....	1
2. Hepatocellular carcinoma	
a) General overview.....	3
b) Surgical treatment.....	5
3. Imaging.....	6
a) Imaging and surgical strategy.....	6
b) Preoperative 3D reconstruction.....	7
c) Intraoperative imaging.....	8
d) In vivo functional imaging.....	9
4. <i>Ex vivo</i> tumoral models.....	11
5. OBJECTIVES.....	15
6. RESULTS.....	17
6.1a) Preoperative imaging.....	17
6.1b) Publication of the results.....	19
6.1c) Conclusions on the first part.....	46

6.2a) <i>In vivo</i> functional imaging.....	47
i) Ischemic-non ischemic tissue assesement.....	47
ii) Ischemia-reperfusion injury assesement.....	71
iii) Hyperspectral enhanced reality (HYPER) for anatomical liver resection.....	115
iii) Real-time ICG guided anatomical liver resection with the positive and negative staining technique.....	133
6.2b) Publication of the results.....	159
6.2c) Conclusions on the second part.....	194
6.3) <i>Ex vivo</i> tumoral models.....	194
7. CONCLUSIONS.....	201
8. BIBLIOGRAPHY.....	203

INTRODUCTION

1. The concept of precision medicine

Medicine is one of the most wonderful and passionating form of science.

The complexity of the human being, the complexity of diseases and their different possible treatments, the continuous interaction with technology, and finally, the fact that it is the only science that has a « subject » - the person - as the unique and final « object » of investigation, give to medicine a fascinating aura. Life is unique for every one of us, and what is deeply linked to it is naturally associated with respect and confidence. From the pre-hippocratic vision of diseases considered as a punishment of gods, medicine made a long distance, and when diseases started to be considered as an objective entity - independent from personal conduit, ethics, or faith - the never-ending struggle of human being to prolong and to improve quality of life entered the modern era. Two thousand years of observations, reasonments, advances as well as regressions, dogmatisms but also visionary intuitions, prepared us to the XXI century way to find a cure for every disease, to take care of every patient, and finally enhance the quality of life respecting dignity.

It is from this complex picture of hundreds and hundreds of years of evolution, that medicine could synthetize the combination of experience, knowledge, technology, insights

and wealth (but unfortunately only for a part of humankind), that naturally led to the concept and application of precision medicine.

But what is the meaning of this simple and innocent word? Precision medicine can be considered a way of reaching the ultimate form of care and cure, to adapt to a specific patient a tailored medical or surgical treatment, and again, always tailored to that particular form of disease.

To reach this ambitious goal, the effort is tremendous in every field of human application, from basic sciences to engineering, including industrial development or communication - just to cite some of them-, and certainly politics.

After this maybe pindaric flight, let's go back to the present, and certainly the future!

Hepatocellular carcinoma is a very complex disease. The incidence is rising; manifestations are proteus; a diversity of molecular pathways determine different natural evolutions when patients are affected, and today a quite impressive and variegated number of treatment strategies exist. This is our goal, to give to every single patient the best chances of cure, enforce a constant and tight collaboration and interaction between scientists, hepatologists, surgeons, radiologists and oncologists, all working for a transversal and integrated multidisciplinary combination of clinical practice and research, is the only way to translate into reality the forementioned concept of precision medicine.

So, dear reader, this is how the story began.

2. Hepatocellular carcinoma

a) General overview

Hepatocellular carcinoma (HCC) is the most frequent primitive liver cancer, accounting for about 90% of cases and occurring almost exclusively in cirrhotic patients. Its incidence is growing progressively worldwide (1,2), with an estimation of more than 1 million individuals that will be affected by liver cancer annually by 2025 (3). Hepatitis B virus (HBV) infection is the leading risk factor for HCC development, responsible for around 50% of cases (4). Since the introduction of direct antiviral agent treatments, and in patients with sustained virological response, the risk attributed to hepatitis C virus (HCV) infection has substantially decreased (5). Currently, non-alcoholic steatohepatitis (NASH), associated with diabetes or metabolic syndrome, is becoming the fastest growing cause of HCC, especially in western countries (6). Although our understanding of the pathophysiology of the disease has improved, this knowledge is still not fully translated into clinical practice. Understanding the genetic pathways involved in the development of this disease has improved in recent years, with specific mutations found in around 25% of HCC, but the most frequent ones detected in <10% of patients (7,8). Diagnosis of HCC is usually based on non-invasive criteria, with screening programs well established in high-risk patients, especially cirrhotics, associating liver ultrasound and alphafetoprotein testing every 6 months. When pathognomonic radiological features are present at CTscan or MRI -the arterial “wash-in” associated to the venous phases “wash-out”- for diagnosis, no biopsy is needed; procedure reserved in case of doubts or in tumors arising on non-cirrhotic

parenchyma. As in recent years, tumor molecular characterization is gaining importance; biopsies from the lesion and from non-tumoral liver are more and more performed (9,10). Hepatic resection, local ablation and liver transplantation are the three established curative treatments for HCC and progressive improvement in patients' selection (tumoral characteristics, liver function, and patient's performance status), was associated to better longterm outcomes and improved quality of life (11). Transarterial chemoembolization (TACE), transarterial radioembolization (TARE), stereotaxic radiotherapy and systemic therapies (including immunotherapy), are other established -but usually non-curative- options to consider in the armamentarium of treatment strategies in patients affected by HCC (**Fig.1**) (12).

In this thesis we will focus only on surgical resection.

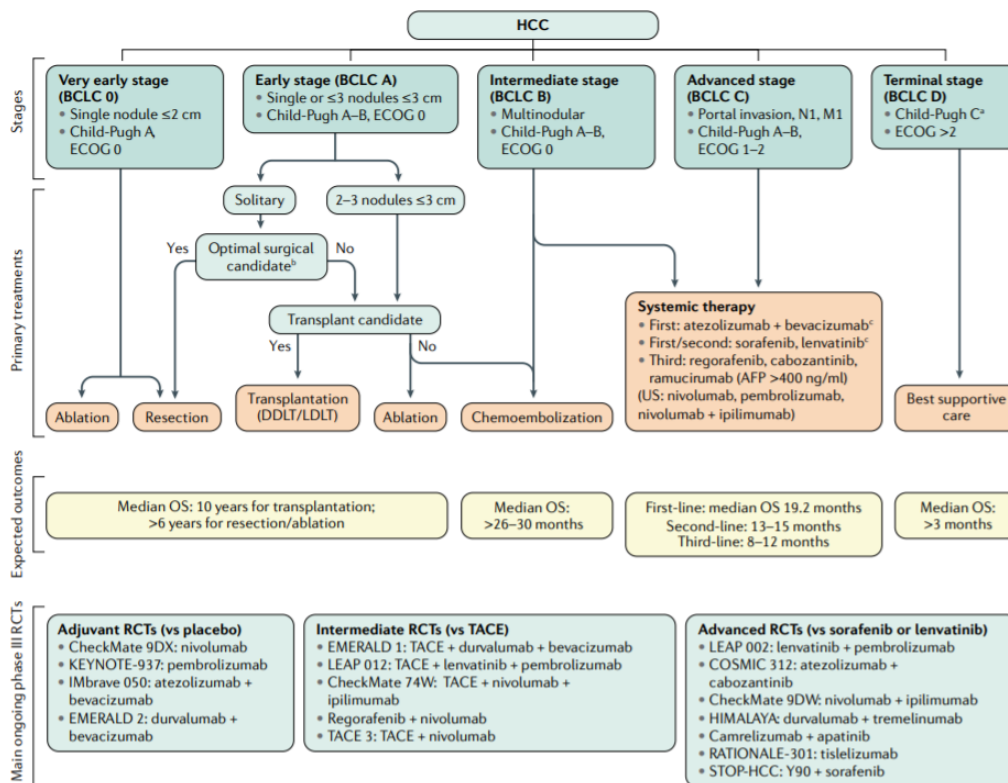


Figure 1. Management of HCC

(from Llovet et al, Nature reviews Nat Rev Dis Primers. 2021 Jan 21;7(1):6)

b) Surgical treatment

Surgical treatments include hepatic resection and liver transplantation, the latest associated with the best 5- year overall survival of 70–80%. Decision between resection and transplantation is usually based on patient’s age, liver function, degree of portal hypertension, and tumoral characteristics such as tumor localization, number and size of nodules, the relationship with vascular and biliary structures, type of resection needed, future liver remnant, and performance status. Resection is considered the treatment of choice, especially in patients with HCC without cirrhosis and for those patients whom post-

operative hepatic decompensation is unlikely, or in case of formal contraindication to liver transplantation (i.e. age, or when resection is considered as a “bridge” to it)(13). Increasing evidence suggests that anatomical liver resection offers a longer postoperative survival and disease-free survival as compared to non-anatomical ones (14-18); this particular point is still today a source of debate, with different attitudes encountered, especially between western and eastern countries. Anatomical resection is a more demanding procedure, especially on cirrhotic livers. In fact, even if after selective arterial and portal vein clamping superficial demarcation between vascularized and ischemic liver segments are easy to discriminate, intraparenchymal landmarks between segments are more difficult to determine. This technical difficulty has become even more determinant in recent years as minimally invasive liver resection has been increasingly performed. Different strategies to overcome this difficulty have been considered; a detailed description is presented in the dedicated chapter of intraoperative navigation.

3. Imaging

a) Imaging and surgical strategy

Modern liver surgery is based on precise imaging evaluation. Surgical strategy is in fact conceived after an accurate analysis of tumoral characteristics and patient’s real anatomy, information that are derived mainly from CT scan and MRI analysis. Anatomical or non-anatomical resections are planned according to the relationship between the tumor (or tumors) and the vascular and biliary structures. It is important to consider that this process

requires high quality images, ideally performed in centers focused on liver surgery. Three phases CT scan is mandatory, including arterial, venous and late phase, obtained with a 64 detector with bolus tracking techniques, to determine the best delay to start arterial acquisition. MRI should be performed with a 1.5 Tesla using a six-channel phased-array body coil for signal detection and an intravenous agent like gadolinium as tracer. As a complement to MRI and CT-scan, fluorodesoxyglucose (FDG) or choline Positron Emission Tomography (PET)-scan, can be performed preoperatively to rule out the presence of extrahepatic disease. Sometimes alternative exams are useful to better clarify the pre-operative diagnosis to confirm surgical strategy (i.e., contrast ultrasound)

b) Preoperative 3D reconstruction

To enhance the strategic planification capacity and to meet the need of calculating the future remnant liver volume, 3D reconstruction has been progressively introduced in clinical practice. Liver anatomy is sometimes complex to determine only on 2D imaging techniques (i.e. CT-scan and MRI). Since the first anatomical 3D simulator used for preoperative liver resection planning, proposed in 1998 by Marescaux et al. (19), 3D technology has developed incredibly. Nevertheless, the real impact of 3D reconstruction on indications and outcomes after liver resection has not been fully demonstrated yet (20,21). Especially for the treatment of HCC, with the aforementioned resection difficulties in presence of cirrhosis, accurate preoperative planning may minimize the risk of

intraoperative variations in the surgical strategy, variations that has been reported to be as high as 20% in general surgery procedure, and often associated with an increase in postoperative morbidity (22). Most research on 3D evaluation is focused on its ability to stereoscopically exhibit anatomy, accurately estimate liver volumes, and precisely determine surgical resection margins (23-26). Few studies describe long-term survival outcomes for the benefits obtained 3D evaluation (27, 28). Until now, no study that analyzed the contribution of 3D reconstruction in the surgical planning for hepatectomy for HCC has been published.

c) Intraoperative imaging

As said, defining the exact planes for resection is often difficult, especially in cirrhotic patients and for postero-superior segments tumors. Defining the correct intraparenchymal anatomical line is technically challenging and anatomical landmarks, such as hepatic veins and portal branches are then used under ultrasound guidance to guide transection (29-32). Makuuchi et al. associated the ultrasound guidance with methylene blue injection in the portal branches to delineate on the liver surface the precise limits of a determined segments or sector. This technique is performed during open surgery; it requires hepatic artery clamping and the wash out of the dye is relatively rapid. Replacing the blue dye with indocyanine green (ICG) and associating the use of near-infrared cameras, fluorescence-based segmentation resections have than been performed (33). This technique allowed in particular a stable parenchymal dying and avoided elective arterial clamping. In 2008, Aoki

et al. (34) first reported an intraoperative technique for subsegments, and segments ICG staining during open hepatectomy; the success rate in identifying the anatomical planes was 93%. The technique was considered safe, reproducible and not time consuming. In parallel, the benefit of laparoscopic liver resection has been established for liver malignancies, especially HCC, confirmed by consensus meetings and international recommendations (35, 36). However, laparoscopic anatomical liver resection (LALR) techniques have not been fully standardized because both inflow portal clamping and portal staining, when used, are difficult to perform in the laparoscopic setting, again especially in cirrhotic livers and for postero-superior segments. To improve the quality and precision of anatomical resection and to guide intraparenchymal transection, combined ICG fluorescence imaging in LALR has been used with direct portal injection of ICG under percutaneous guided laparoscopic ultrasound, the so-called “positive staining” (37, 38). Ishizawa was the first to perform this technique in 2012. The same principle, but with the opposite injection, is the “negative staining”, achieved by the intravenous injection of ICG dye after clamping the segmental portal pedicle following the glissonean concept of anatomical resection (39-42).

d) In vivo functional imaging

Liver ischemia reperfusion injury (IRI) is a dreaded condition after liver resection and liver transplantation (43). Oxygen pressure decreases inside the sinusoids reducing ATP production and increasing reactive oxygen species (ROS), cytokines, and chemokines (44). Currently, there is no intraoperative and non-invasive tool to evaluate liver perfusion to

predict liver viability during post-operative period. This consideration is particularly important in situations such as extensive liver resections on damaged parenchyma (fibrosis or chemotherapy), and especially when future liver remnant volume reaches limit values. Hyperspectral imaging (HSI) is a non-invasive imaging modality that has recently been applied to the medical field as a tool for image-guided surgery, more specifically for an intraoperative quantification of tissue perfusion (45). HSI images are based on the computational analysis of light-tissue interactions through the detection of relative reflectance, giving a quantification of organic compounds such as deoxygenated and oxygenated haemoglobin at different depths (46). Before being applied to the medical field, this technology had largely been explored by NASA since 1985 (47). The application of HSI has recently gained importance for its non-invasiveness and for the accuracy of oxygen quantification. For that reason, HSI is a promising technology that allows to intraoperatively quantify hepatic perfusion and oxygenation and to discriminate among different types of liver ischaemia. HSI camera obtain pictures in which each pixel contains the relative reflectance quantification in a wide range of spectral fields. The data obtained is a spatial (x, y) picture which also has a third dimension (z) in which the information of the spectral field is stored. The result is a 3D cube, which is more informative than the RGB picture. There are different types of HSI cameras, such as whisk broom scanners, single snapshot, and push-broom scanners. The one used in this study is the push-broom scanner, which allows for the extraction of highly informative and sensitive hypercubes (250 bands from 500 to 1000nm) (**Fig. 2a**). The device was engineered to be used during the surgical

procedure (**Fig. 2b**) with a light source composed of 6 lamps (20W Osram Halospot 70 Halogen) (**Fig. 2c**). The HSI camera allows for the extraction of the spectral profile from different tissues and surfaces, proving its ability to distinguish ischaemic from non-ischaemic tissues (**Figs. 2d, e**).

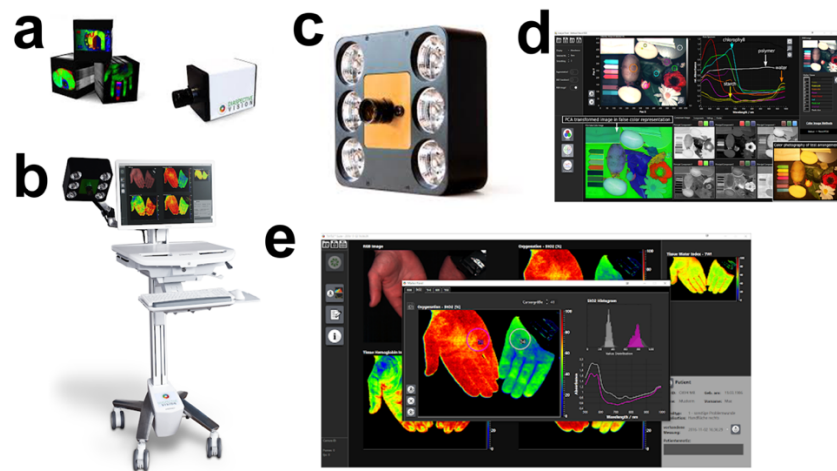


Figure 2. Hyperspectral camera (TIVITA, Diaspective Vision). (a) Push-broom camera. (b) Intraoperative device. (c) Light source. (d, e) TIVITA software analysis.

4. *Ex vivo* liver models

An important limitation in preclinical drug development is the absence of an appropriate cell culture model system. Standard *in vitro* cell culture models are based on conventional hepatocarcinoma cell lines and key features such as cell-cell interactions, tumoral three-dimensional tumor architecture, and cellular heterogeneity are not present. To offer more specific and less toxic treatments to cure or prevent HCC to patients shortly, the liver research community developed elaborated *ex vivo* models able to recapitulate liver fibrosis

or HCC features (48). New *ex vivo* and *in vitro* models have been established and optimized for three dimensional study of hepatic systems, e.g., primary cell-based spheroids and stem cell-derived organoids (Fig.3) as well as chip systems, sandwich cultures, and liver bioprinting (49). Spheroids are three-dimensional (3D) multicellular aggregates obtained from dissociated resections or, more rarely, those that form spontaneously through cell-to-cell adhesion under culture conditions. Liver spheroids demonstrate important relevant features such as superior longevity, enhanced hepatocyte-specific function, and increased cell-to-cell interactions when compared to classical hepatic cell lines. Alternatively, PDX models based on engraftment of liver resections in mice have also been developed and are commonly used to analyze the effect of new potential treatments in preclinical studies. However, PDX models present limits, especially, they are time consuming to establish and are performed in immunocompromised mice making them difficult or even impossible to implement in a precision medicine concept dedicated to individual patients.

Although limited access to patient derived liver tissue is still the major bottleneck for optimal large size experimentations, spheroids have been used for high throughput screening of small molecule libraries to find new treatments. Alternatively, the use of spheroids issued from healthy livers specimens (i.e., non HCC) treated with drugs to modelise liver diseases, such as advanced liver fibrosis, can be combined to state-of-the-art “omics” studies allowing the identification of key cellular player that might be new targets for future treatments. In 2019, our unit, has established the first human liver atlas, using single cell sorting, and single cell RNA sequencing, becoming the world reference

for normal liver cell composition (50). In the future, comparing HCC and adjacent tissue cell gene expression, with the liver atlas data, will allow to decipher cell circuits involved in the early stages of carcinogenesis and identify cellular targets of potential interest for new treatment development to chemoprevent HCC development or recurrence.

From the perspective of precision medicine, the use of liver spheroids and HCC tumorspheres are of utmost importance to improve future patient care. Indeed, patient derived dissociated HCC tumoral tissues, can be reassembled *ex vivo*, to form a set of tumorspheres constituted of hepatocytes and non-parenchymal cells, able to recapitulate the tumoral microenvironment. These spheroids appear as advanced models to test the efficacy of various treatment options and help/guide the clinician to choose the most efficient therapeutic molecule for a specific patient. The generalisation of these kinds of techniques, when patients undergo first line treatment failure, paves the way of personalized patient treatments and improvement of patient's outcome.

In a more global point of view and beside treatment efficacy testing on HCC tumorspheres, analysis of patient tissue-derived liver spheroids treated to modelise advanced liver fibrosis or issued from NASH (Non-Alcoholic Steato Hepatitis) patient's resections, combined to single cell "omics" studies allow to decipher cell circuits and cellular targets engaged in carcinogenesis mechanisms of development. They will at term allow to build chemopreventive strategies to stop fibrosis progression and HCC recurrence. Implementation of personalized medicine research programs relies primarily on very active

and efficient collaborations between surgeons, and translational research teams to obtain optimal quality of specimens.

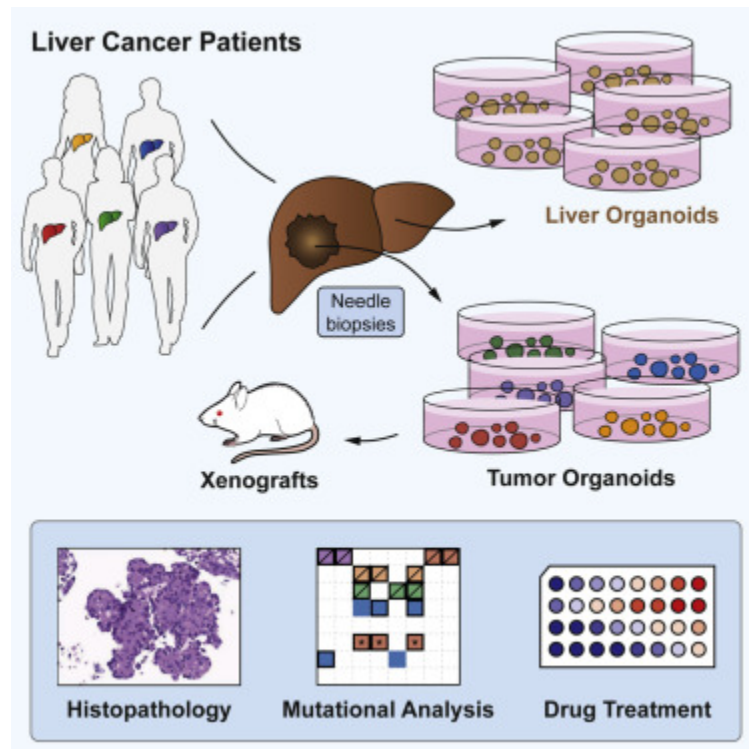


Figure 3. i.e. Organoids from tumoral and non tumoral liver (from Nuciforo et al, Cell Reports, Volume 24, Issue 5, 31 July 2018,1363-1376)

5. OBJECTIVES

This thesis work aimed to integrate the forementioned concept of precision medicine applied to the treatment of HCC on a multidisciplinary basis. The “*leitmotiv*” was to implement a transversal approach that let us integrate innovative technologies and new treatment paradigms in a continuous interaction between clinical needs and expertise coming from different fields of biology and engineering. The whole project, developed in three main fields of application, was so conceived to humbly make a further step in the evolution of precision medicine for the treatment of HCC and to create a homogeneous and coherent path of integration, innovation, and precision for the best cure and care of our patients. The first two parts were realized in tight collaboration with the Institut Hospitalo-Universitaire (IHU), Strasbourg and the Hépato-Digestif Department at the Nouvel Hôpital Civil, University Hospital Strasbourg. The last part was performed more specifically with the Institute for Viral and Hepatic Diseases (Inserm Unit 1110), Strasbourg.

The first part is focused on preoperative imaging and surgical strategy. The goal was to evaluate in a French multicentre prospective non-randomized trial the benefit of the 3D reconstruction over the standard 2D imaging analysis, to see if significant modifications in preoperative strategy and the real operation performed, were present. In the same study, secondary objectives aimed to evaluate if 3D reconstruction could better detect tumor localization, anatomical variations, resection margins, and resected volume. The second part is focused on intraoperative imaging. The recent advances in optical imaging, enhanced reality, and artificial intelligence, encouraged our team to find solutions for

improved patient outcomes by taking advantage of all these novel and promising technologies. The main objectives of the research were as follow: a) to prove that hyperspectral imaging (HSI) could discriminate between ischaemic and non-ischaemic liver; b) to evaluate the correlation between optical and biological properties; c) to demonstrate that HSI could predict liver viability intraoperatively and to automate the process with artificial intelligence; d) to provide enhanced reality to guide liver surgery in a quantitative manner; to establish the principle for HSI molecular imaging in an *in vitro* approach. Finally, we aimed to provide a solid scientific base for these technologies for their translation into the clinical field.

The third part of our interactive and transversal work conceived to optimize the treatment of hepatocellular carcinoma -going from new imaging technologies to operating room- is focused on the tight collaboration with the Institute for Viral and Hepatic Diseases (INSERM Unit 1110). My objective of this part, was to enrich the LIVMOD biobank (UMR_S1110) with high quality operative specimens from cirrhotic and non cirrhotic patients affected by HCC, to contribute 1) to proof-of-concept studies, aiming to find the best treatment strategies for first line non responder patients, or to confirm efficacy of newly identified molecules to prevent liver fibrosis and HCC and 2) to very competitive european and national translational research programs dedicated to better understand advanced liver disease and HCC at the fundamental level.

6. RESULTS

Results related to the two first and main aims of this thesis are an integral part of six manuscripts that are included in the following sections. In addition to project management, with three of the six manuscripts written as first-author, my individual experimental contributions are highlighted in the respective summary sections before the article.

6.1a) Preoperative imaging – results summary and own contribution

The latest imaging technologies applied to the preoperative surgical strategy (operation planning, type of resection, intra-operative navigation, minimally invasive approach, etc) are currently fundamental for an optimal treatment of HCC. Three-D HAPPI (HePatic Procedure PlannIng) is a French prospective multicentric non-randomized trial, developed under the coordination of Pr P. Pessaux (thesis co-director), that had as primary goal to analyze the benefit and use of preoperative 3D reconstruction in the treatment strategy planning before HCC resection. The 3D reconstruction used the same VR RENDER® program, then the images were processed via a plug-in Virtual Surgical Planninc (VSP®, IRCAD).

This study is the first of its kind, as no other prospectively multicentre trials have ever been performed before on the subject. The primary goal was to determine if the preoperative 3D model analysis (named “Plan B”) modified the surgical strategy initially planned, based on conventional 2D imaging (“Plan A”). Measurement was based on the modification rate

analysis between Plan A and Plan B, and from Plan B to the final procedure performed (named “Plan C”).

The primary goal of the study was reached as 3D reconstruction models analysis significantly changed the initial preoperative strategy. No differences were present when considering secondary outcomes, such as tumor localization, anatomical variations, resection margins, and resected volume. Tridimensional reconstruction has proven to be a useful tool to improve preoperative analysis and to establish a correct surgical strategy. Technology has to be implemented and further studies are required to clarify its role in the treatment of hepatocellular carcinoma. My personal contribution to this study was participation to the study design, operative procedures, revision of results and writing and revision of the manuscript.

6.1b) Publication of the results

Article: under review *British Journal of Surgery*

Title:

Paradigm shift: should preoperative 3D reconstruction models become mandatory before hepatectomy for hepatocellular carcinoma (HCC)? Results of a multicenter prospective trial

Benefit of preoperative 3D reconstruction models on surgical strategy before hepatectomy for hepatocellular carcinoma (HCC): a multicenter prospective trial

Emanuele Felli^{1,2,3,4} MD, Emmanuel Boleslawski^{5,6} MD, PhD, Daniele Sommacale^{7,8} MD, PhD, Olivier Scatton⁹ MD, PhD, Raffaele Brustia⁷ MD, PhD, Lilian Schwarz¹⁰ MD, PhD, Daniel Cherqui¹¹ MD, PhD, Thomas Zacharias¹² MD PhD, Alexis Laurent⁷ MD, PhD, Jean-Yves Mabrut^{13,14} MD, PhD, Catherine Schuster PhD⁶, Benoit Gallix³, MD, PhD, Patrick Pessaux^{12,34} MD, PhD

1 Unité Chirurgie HBP, Pôle hépato-digestif Nouvel Hôpital Civil, Strasbourg France

2 Institut of Viral and Liver Disease, Inserm U1110, Strasbourg, France

3 IHU Strasbourg - Institut de Chirurgie Guidée par l'image, Strasbourg, France

4 IRCAD, Research Institute Against Digestive Cancer, Strasbourg, France

5 University Lille, CHU Lille, Service de Chirurgie Digestive et Transplantations, Lille, France.

6 INSERM, U1193, Villejuif, France

7 Department of Digestive and Hepatobiliary and Pancreatic Surgery, AP-HP, Hôpital Henri-Mondor, F-94010, Créteil, France

8 INSERM U955, Team "Pathophysiology and Therapy of Chronic Viral Hepatitis and Related Cancers", Créteil, Assistance Publique-Hôpitaux de Paris, France

9 Department of Hepatobiliary Surgery and Liver Transplantation, Pitié Salpêtrière Hospital, Sorbonne Université, Paris, France.

10 Digestive Surgery Department, Rouen University Hospital, Rouen, France

11 Centre Hepato-Biliaire, AP-HP Paul Brousse Hospital, Paris-Saclay University, Villejuif, France

12 Service chirurgie digestive, Hôpital Emile Muller Mulhouse

13 Service de chirurgie générale, digestive et Transplantation hépatique et intestinale, Hôpital de la Croix-Rousse, Hospices Civils de Lyon, Université Lyon I, Lyon, France.

14 Cancer Research Center of Lyon, Institut national de la santé et de la recherche médicale (INSERM), Unité 1052, Lyon, France.

Corresponding author:

Patrick PESSAUX

Pôle Hépato-digestif, Nouvel Hôpital Civil

1, place de l'hôpital 67000 Strasbourg, France

patrick.pessaux@chru-strasbourg.fr

Non randomized prospective clinical trial

The authors declare that they have no conflict of interest

Abstract

Background: A preoperative surgical strategy before hepatectomy for hepatocellular carcinoma is fundamental to minimize postoperative morbidity and mortality and to reach the best oncologic outcomes. Preoperative 3D reconstruction models may help to better choose the type of procedure to perform and possibly change the initially established plan based on conventional 2D imaging. To determine whether the initial surgical strategy based on the analysis of standard 2D imaging (CT-scan or MR) is modified after 3D reconstruction model analysis.

Methods:

A non-randomized multicenter prospective trial with 136 patients presenting with a resectable hepatocellular carcinoma who underwent open or minimally invasive liver

resection. Measurement was based on the modification rate analysis between conventional 2D imaging based strategy (named “Plan A”) and the 3D model analysis one (“Plan B”), and modification rare from Plan B to the final procedure performed (named “Plan C”).

Results:

The modification rate from Plan B to Plan C (18%) was less frequent than the modification from Plan A to Plan B (35%) (OR= 0.32 [0.15;0.64]). The modification rate from Plan A to Plan C (37%) was more frequent than the one from Plan B to Plan C (18%) (OR= 4.37 [2;10.7]). Concerning secondary objectives, resection margins were underestimated in Plan B as compared to Plan C (- 3.10mm [-5.04;-1.15]).

Conclusion:

The present study suggests that preoperative 3D imaging of the liver is associated with a better prediction of the performed surgical procedure for liver resection in HCC, as compared to classical 2D imaging.

Introduction:

Liver resection (LR) is one of the main curative options for the treatment of hepatocellular carcinoma (HCC), and anatomical LR seems to offer a longer postoperative survival and disease-free survival (1-5) as compared to non-anatomical LR. In patients fit for surgery, oncological principles and future liver remnant are the two main parameters which guide the surgical strategy. The basis of AR relies on tumor position and liver anatomy. Of note, liver anatomy is often complex to be determined solely on 2D imaging techniques (i.e. CT-

scan and MRI). Accurate preoperative planning is essential and may minimize the risk of intraoperative changes in the surgical strategy (reported as high as 20%) often associated with an increase in postoperative morbidity (6).

Since the first anatomical 3D simulator used for preoperative LR planning (7), technology has developed. Nevertheless, the real impact of 3D reconstruction on indications and outcomes after LR have not been fully demonstrated yet (8-9), especially for the treatment of HCC.

The aim of this multi-institutional prospective cohort study was to evaluate the impact of the preoperative 3D model reconstruction analysis on the planned surgical strategy.

Materials and methods:

Number of subjects

The aim of this study was to evaluate the impact of a 3D model analysis on the modification of the surgical strategy and procedure plan, as compared to analysis of conventional preoperative 2D images (i.e. CT-scan or MR) among a target population of patients undergoing LR for HCC. The number of subjects required was obtained on the basis of a risk $\alpha = 5\%$ and a power of 80%, for the comparison of a proportion of 10% of intraoperative modifications of the planned procedure after completion of the 3D reconstruction, and a proportion of 20% intraoperative changes in the 2D group, based on a unilateral proportion comparison test, assuming that 5% of the procedures will be modified from 2D and 3D planning simultaneously.

The number of patients required was estimated at 136 subjects. Simulations have been performed using the R software (R Core Team, 2020). R stands for a language and environment for statistical computing; R Foundation for Statistical Computing, Vienna, Austria. URL: <https://www.R-project.org/> in its most recent version (4.0 and following) with all additional packages necessary.

Study design:

This study was a non-randomized multicenter prospective national French trial. Its total duration was 3 years with a two-year inclusion period, each patient participating during 6 months (from the time of inclusion until the last postoperative follow-up at 3 months). The trial was approved by the French Committee for the protection of persons on October 11, 2016 and registered under Number 16/53. The trial was also registered on clinicaltrials.gov: NCT03382327. The reporting of this study was based on the following: Strengthening the Reporting of Observational Studies in Epidemiology (STROBE) Statement (10).

Participants:

All consecutive patients (>18 years old) with resectable HCC from 12 French specialized HPB centers included from October 2017 to September 2019 were informed for participation in the present study. A written informed consent was obtained from all patients included. All eligible participants had to be covered by the French public health system. Exclusion criteria included concomitant malignancies other than HCC with liver localization, impossibility to obtain MR images, pregnancy, patients unable to give an informed consent for inclusion in the study.

Main outcome: To determine if the preoperative 3D model analysis (named “Plan B”) (Fig. 1) significantly modifies the surgical strategy initially planned, based on conventional 2D imaging (“Plan A”). Measurement was based on the modification rate analysis between Plan A and Plan B, and from Plan B to the final procedure performed in the operating room (named “Plan C”).

Secondary outcomes:

The secondary endpoints were to evaluate preoperatively, before and after 3D reconstruction analysis, HCC localization according to Couinaud’s anatomy, liver vascular supply variations from modal anatomy, estimated resection margins, and resected volume.

Participating centers:

Twelve French centers with an expertise in liver surgery took part in the study. Procedures were performed by senior HPB surgeons according to the center organization using either an open or a minimally invasive approach.

3D model reconstruction:

Tridimensional models were obtained using the program VR RENDER®. They were then processed via a plug-in, i.e. Virtual Surgical Planning (VSP®, IRCAD). For each patient, standard 2D images (i.e. CT-scan and MRI) were sent to a secured online website (Visible Patient) for 3D reconstruction. Vascular and biliary tridimensional views were then available for practitioners for comparison to the initially established plan. Each center was accountable for data collection, and data analysis was then centralized. If CT-scan or MR

images were obtained >6 weeks before inclusion, new updated images were performed to enter the study.

Study timetable:

All centers were accountable for their own inclusion of patients. During outpatient clinics, each patient was informed of the study, data inclusion, primary and secondary outcomes, and a signed informed consent was obtained. Conventional 2D images were discussed in a multidisciplinary team meeting according to the modalities established in each center. The hepatic volumetries were accessible with the software of imaging manufacturers according to the need of the surgeons. The first surgical strategy based on CT-scan and MR images, named “Plan A”, was then reported on a common Internet platform, with mention of tumor localization, anatomical variations, estimated surgical margins and resected liver volume, type of resection and information about open or minimally invasive operations. Images were then sent for a centralized 3D reconstruction and a second analysis was performed. The so-called “Plan B” was then reported with the same features as Plan A. Once the resection was performed, “Plan C” was recorded, representing the final operation performed. Information on resection margins, specimen volumes, and postoperative outcomes were secondarily collected. Morbidity and mortality at 90 days were finally reported and a statistical analysis was performed. Long-term oncological outcomes were not considered in the primary or secondary objectives.

Interventions:

Standard open or minimally invasive hepatectomies

Statistical methods.

Bayesian analyses were an appropriate alternative to Frequentist methods. Generally speaking, they are even thought to be more appropriate in a certain number of cases, such as those in which we want to estimate a probability of being greater or smaller than a cut-off value. We decided to rely on Bayesian methods to estimate posterior distribution for each coefficient. With those distributions, the probability for a coefficient or an odds ratio (OR) to be strictly positive (OR greater than 1) or strictly negative (OR smaller than 1) can be evaluated, contrarily to point estimates which are not informative on the complete distribution (also known as the p-value and the issue of lack of power). Conclusions are formulated in terms of probability for the coefficient to be strictly positive (resp OR greater than 1). If this probability is close to 1, we shall conclude that the probability of the tested hypothesis is very high, or small if close to 0. If this probability is close to 50%, the distribution of the OR is half greater than 1, half smaller, and we shall conclude that the studied OR is not different from 1. Conclusions are then more informative than simple p-values in such cases. A very high (larger than 0.95 or 0.99) or a very low value (smaller than 0.05 or 0.01) of this probability (Pr in the text) can be considered statistically significant. This significance must not be confused with the classical p-value.

Statistical analyses first included a descriptive part of the population and the parameters studied with an evaluation of the effective frequencies and cumulative frequencies for categorical variables, as well as an evaluation of mean and standard deviations, or medians

and interquartiles for quantitative variables. The primary endpoint is defined by the proportion of changes in the surgical plan with or without the use of the 3D reconstruction tool. To model this proportion, a logistic generalized linear model (GLM) was used, and the associated odds ratio was estimated. This OR was compared to 1 by using the posterior Bayesian distribution of the difference coefficient.

Comparison between quantitative variables such as resection volume were also performed and fitted by linear models, in order to get a posterior estimation of all differences. Results are presented in means, or proportions in their 95 credibility intervals, and with the probability for a coefficient to be greater than a threshold value. Priors for coefficient effects were uninformative, namely normal with mean 0 and precision 0.001, and a uniform distribution (0,100) for dispersion parameters. Computations were run JAGS 4.3. For each analysis, a single MCMC chain with 5,000 iterations as burn-in and 100,000 iterations were used to generate the posterior distribution. Convergence was checked and present in every case. Statistical analyses were performed using the R software in its most recent version provided with all packages necessary for data analysis (*R Development Core Team: A language and environment for statistical computing. R Foundation for Statistical Computing, Vienna, Austria*). Statistical analysis was performed in November 2020.

Results:

Population:

Nine of the twelve participating centers enrolled a total of 136 patients (range: 4-39) (Fig. 2). Finally, 124 patients were included (12 were excluded for no available 3D model, 2D

imaging outside inclusion criteria, wrong patient inclusion, lost at follow-up), the analysis was performed as an intention to treat. Patient baseline characteristics are shown in Table 1. Mean age was 67.1 years (range: 28-92 years). Men represented 84.7% (n=105) of the population, and women 15.3% (n=19). The median body mass index (BMI) was 25.7kg/m² (range: 17.4 - 38.9kg/m²). All patients had solitary tumors, no information was available regarding a previous or subsequent project of “bridge” or “salvage” liver transplantation as not concerned with the primary and secondary objectives of the study. ASA score was grade 2 and 3 in 53.2% and 37.9% of patients respectively, and only 1 patient was graded ASA 4. Cirrhosis was diagnosed preoperatively in 50% of patients (n=62), and HBV (Hepatitis B Virus), HCV (Hepatitis C Virus), Alcohol and NASH (nonalcoholic steatohepatitis) were diagnosed as main etiologies in 12.9%, 22.6%, 59%, and 30.6% of patients, respectively. CHILD score had a median of A5 in 91.3% of patients; there was no CHILD C in the study. Indirect signs of portal hypertension were reported in 19.9% of patients (n=21). Concerning comorbidities, diabetes, hypertension, and obesity were present in 41.1%, 62%, and 27.4% of patients, respectively. Previous abdominal surgery was reported in 47.6% of patients.

Planning

Laparoscopic or open resections were indicated in Plan A in 53.2% and 45.2% of patients respectively (robotic resection was indicated in only 1.6% of patients), and no changes in the approach (open or laparoscopic) were reported after 3D analysis. Subjective surgeon confidence in the established plan reported had a median of 7.6 (range: 1-10) for Plan A and 8.6 (range: 1-10.) for Plan B (p=0.21). In Plan A (2D imaging), the initially indicated

resection type was bisegmentectomy (n=13, 10.5%), right hepatectomy (n=20, 16.1%), left hepatectomy (n=8, 6.5%), extended right hepatectomy (n=1, 0.8%), left lobectomy (n=11, 8.9%), tumorectomy (atypical liver resection) (n=24, 19.4%), segmentectomy (n=27, 21.8%), and subsegmentectomy (n=20, 16.1%). In Plan B (3D + 2D imaging), the operations scheduled were bisegmentectomy (11.3%; n=14), right hepatectomy (14.5%; n=18), left hepatectomy (4.8%; n=6), extended right hepatectomy (1.6%; n=2), left lobectomy (11.3%; n=14), tumorectomy (atypical liver resection) (13.7%; n=17), segmentectomy (21%; n=26), subsegmentectomy (21.8%; n=27). Tridimensional modeling reduced potential planning errors by 49% with modifications (in the rate of change from Plan B to Plan C (18%)) significantly less frequent than from Plan A to Plan C (37%) (OR= 4.37 [2 -10.7]). Plan A=B=C was reported in 55.6% of patients (n=69); Plan A≠B and A=C in 6.4% of patients (n=8); Plan A≠B and B=C in 24.1% of patients (n=30) (Fig. 3a, b, c, d); Plan A≠C and Plan B≠C in 12.1% of patients (n=15). In two of the 124 patients, data were incomplete. Concerning the 15 patients where Plan C was different both from Plan A and Plan B, no resection was performed in 3 cases (intraoperative finding of ascites, metastases, and intraoperative vascular injury); a larger resection than initially planned was performed in 5 patients; a more limited one in 3 patients (a left hepatectomy as an alternative to an initially planned central hepatectomy in one patient, a mixed manually assisted laparoscopic hepatectomy in 1 patient; information unavailable in two patients). In 11.3% (n=14) of modified Plan A to Plan B cases, there were a more limited scheduled resections, changing from a major hepatectomy to a minor one, and in 4.5% (n=5) of cases, the

opposite. The modification rate from Plan B to Plan C (18%)(Fig.1)was less frequent than the modification from Plan A to Plan B (35%) (OR= 0.32 [0.15-0.64]). In 81% (99/122) of patients, there was a final correlation of the finally performed procedure when compared to the combined 3D+2D planning versus 63% (77/122) for “standard” 2D alone. The modification rates from Plan A to Plan C (37%) were higher than those from Plan A to Plan B (35%) (OR= 1.41 [0.53-3.9]) (Table 2). Concerning secondary objectives, resection margins were underestimated in Plan B as compared to Plan C (-3.10mm [-5.04-1.15]. Anatomical variations detection was not statistically different between Plan A and Plan B, reported in 24.2 and 33.1% of patients (p=0.16) respectively. There was no difference in the two groups concerning resected volume (intraoperatively a water volume test of the specimen test was performed to compare to the 3D calculated volume) and tumor localization. Intraoperative findings and postoperative outcomes are shown in Table 3. Intraoperative transfusions were necessary in 10.7% of patients (n=13), drainage was left in 45.1% of patients, and the reintervention rate was 4.1% (n=5). The overall morbidity rate was 52.5%, Dindo-Clavien grade 3 complications occurred globally in 13.2% of patients. Ninety-day mortality rate was 5.1%. No differences were found in terms of complications and post-operative mortality in patients with a correctly planned procedure (C=B) and patients with an unplanned performed procedure in the end (C≠B).

Discussion:

Most researches on 3D evaluation focused on its ability to stereoscopically exhibit anatomy, accurately estimate liver volumes, and precisely determine surgical resection

margins (11-14). Few studies described long-term survival outcomes which resulted from the benefits obtained in 3D evaluation (15, 16), and no study analyzed the contribution of 3D reconstruction in the surgical planning for hepatectomy for HCC in practice. In this prospective multi-institutional non-randomized study, analysis of 3D reconstruction models significantly modified the initial surgical strategy based on conventional 2D imaging. 3D modeling reduced potential planning errors by 49% with a change in the modification rate from Plan B to Plan C (18%) significantly less frequent than from Plan A to Plan C (37%) (OR= 4.37 [2 -10.7]). The 3D model was especially useful in approximately 25% of patients where strategy modifications induced by the preoperative reconstructions were actually followed (Plan A≠B and B=C in 24.5% of patients (n=30)). Preoperative 3D evaluation can accurately measure the distance between tumors and major intrahepatic vessels, hence providing better planning to the extent of liver resection and the plane of liver transection. Using 3D, remnant liver volumes can be measured accurately to quantitatively assess the risk of postoperative liver failure after the planned operations. In 11.3% (n=14) of modified Plan A to Plan B cases, there were a more limited scheduled resections, changing from a major hepatectomy to a minor one, and in 4.5% (n=5) of cases, the opposite. The software used has the possibility, beyond 3D reconstruction, to determine the vascularized areas of each portal pedicle, a precious help to visualize the “ideal” anatomical resection. Indeed, the majority of changes included a change in tumorectomies (non-anatomical resections) towards subsegmentectomies (anatomical resections) (17), following the ideal oncological principles of HCC surgical resection (1-5). No center

“effect” was noted in the distribution of preoperative modifications from Plan A to Plan B, and subjective confidence expressed by surgeons in preoperative planning was relatively high, both for initial Plan A, and with further increase after 3D model analysis, with a median progression from 7.6 to 8.6 (scale from 1 to 10). This increase in confidence denotes the ease of understanding the 3D model, despite the fact that the clinical files were evaluated according to the habits of expert teams in HBP surgery in multidisciplinary meetings. This expertise surely explains the fact that 3D modeling did not modify surgical planning in 56.5% of cases. Indeed, it has been reported that 3D models improve the understanding of surgical liver anatomy for surgical residents (18). Secondary outcomes did not reach any statistical significance, and more particularly regarding the exact tumor localization, anatomical variations, resected volume, and surgical margins, with a statistically significant underestimation of 3D of real margins, knowing that the analysis was performed for such specific data only in approximately 40% of patients and as consequences considerations and conclusion on these variables can be done only with caution. Plan A=B=C was reported in 56.5% of patients (n=69), in other words no evident modification was consequent after 3D reconstruction analysis; Plan A≠B and A=C in 6.6% of patients (n=8), the final operation performed similar to the initial strategy based on 2D analysis (actual operation different from the one planned after 3D reconstruction analysis); Plan A≠B and B=C in 24.5% of patients (n=30). In this last group the 3D analysis showed to significantly change surgical strategy and was the primary objective of the study. Finally, concerning 3D reconstruction, it is mandatory the acquisition of good quality 2D images to obtain

appropriated 3D rendering. Finally, despite the highest quality 2D or 3D images, intraoperative findings sometimes modify preoperative planning, situation that occurred approximately in 12% of patients in our study. The 3D models analysis has so to be considered an accurate tool to improve the 2D imaging and not in alternative or opposition to it. In fact, these two modalities have different features that are useful in the preoperative evaluation. It could be also considered a reverse approach, a general 3D view of patient anatomy, tumor localization and distances to main structures successively analyzed on a 2D plan especially for some particular details concerning vascular invasion still today sometimes not so precise with the available 3D computer programs. Another important point for the use of 3D reconstruction is the great importance that today of the patient's understanding of his medical condition, treatment information, and satisfaction. Novel technologies such as 3D models may play a role also in patient education (19,20). It has been reported that 3D models help patients to preoperatively understand their kidney tumor and surgery (21). The results of this study are fully in line with the recommendations made at the expert consensus conference (22), where 3D visualization technology will become a routine for diagnosis and treatment of liver diseases in a reasonably near future. The experts recommended to perform a digitalized classification, resectability evaluation, and surgical planning of blood vessels, as the axis for complicated liver tumors using 3D visualization technology to achieve anatomical, functional, and radical surgical resection of complex HCC (A, Strong recommendation).

In conclusion, this is the first prospective multi-institutional non-randomized trial performed to evaluate the impact of 3D reconstruction on the preoperative surgical strategy for the treatment of hepatocellular carcinoma. Statistical relevance concerning the main outcome has been reached with substantial modifications realized after 3D reconstruction analysis (Plan B). Tridimensional reconstruction has proven to be a useful tool to improve preoperative analysis and to establish a correct surgical strategy. Technology has to be implemented and further studies are required to clarify its role in the treatment of hepatocellular carcinoma.

Acknowledgments:

This work was supported by French state funds managed within the “**Programme d’Investissements d’Avenir**” (Investing for the future program) and by the ANR (National Research Agency) (with the following reference number: ANR-10-IAHU-02).

References:

- 1) Regimbeau JM, Kianmanesh R, Farges O, Dondero F, Sauvanet A, Belghiti J. Extent of liver resection influences the outcome in patients with cirrhosis and small hepatocellular carcinoma. *Surgery*. 2002 Mar;131(3):311-7.
- 2) Kosuge T, Makuuchi M, Takayama T, Yamamoto J, Shimada K, Yamasaki S. Long-term results after resection of hepatocellular carcinoma: Experience of 480 cases. *Hepatology* 1993;40:328–332.
- 3) Hasegawa K, Kokudo N, Imamura H, et al. Prognostic impact of anatomic resection for hepatocellular carcinoma. *Ann Surg* 2005;242:252–259.
- 4) Yamamoto M, Takasaki K, Ohtsubo T, Katsuragawa H, Fukuda C, Katagiri S. Effectiveness of systematized hepatectomy with Glisson’s pedicle transection at the hepatic hilus for small nodular hepatocellular carcinoma: Retrospective analysis. *Surgery* 2001;130:443–448.

-
- 5) Ueno S, Kubo F, Sakoda M, et al. Efficacy of anatomic resection vs nonanatomic resection for small nodular hepatocellular carcinoma based on gross classification. *J Hepatobiliary Pancreat Surg* 2008;15:493–500.
- 6) Gauss T, Merckx P, Brasher C, et al. Deviation from a preoperative surgical and anaesthetic care plan is associated with increased risk of adverse intraoperative events in major abdominal surgery. *Langenbecks Arch Surg*. 2013 Feb;398(2):277-85.
- 7) Marescaux J, Clement JM, Tasseti V, Koehl C, Cotin S, Russier Y, et al. Virtual reality applied to hepatic surgery simulation: the next revolution. *Ann Surg* 1998;228:627–34.
- 8) Miyamoto R, Oshiro Y, Hashimoto S (2014) Three-dimensional imaging identified the accessory bile duct in a patient with cholangiocarcinoma. *World J Gastroenterol* 20:11451–11455
- 9) Hallet J, Gayet B, Tsung A et al (2015) Systematic review of the use of pre-operative simulation and navigation for hepatectomy: current status and future perspectives. *J Hepato Biliary Pancreat Sci* 22:353–362
- 10) von Elm E, Altman DG, Egger M, Pocock SJ, Gøtzsche PC, Vandenbroucke JP; STROBE Initiative. The Strengthening the Reporting of Observational Studies in Epidemiology (STROBE) statement: guidelines for reporting observational studies. *Lancet*. 2007 Oct 20;370(9596):1453-7
- 11) Wigmore SJ, Redhead DN, Yan XJ, et al. Virtual Hepatic Resection Using Three-Dimensional Reconstruction of Helical Computed Tomography Angiograms. *Ann Surg* 2001;233:221-6.
- 12) Saito S, Yamanaka J, Miura K, et al. A novel 3D hepatectomy simulation based on liver circulation: application to liver resection and transplantation. *Hepatology* 2005;41:1297-304.
- 13) Yamanaka J, Saito S, Fujimoto J. Impact of preoperative planning using virtual segmental volumetry on liver resection for hepatocellular carcinoma. *World J Surg* 2007;31:1249-55.
- 14) Radtke A, Sotiropoulos GC, Molmenti EP, et al. Computer-Assisted Surgery Planning for Complex Liver Resections: When Is It Helpful? A Single-Center Experience Over an 8-Year Period. *Ann Surg* 2010;252:876-83.

-
- 15) Mise Y, Hasegawa K, Satou S, et al. How Has Virtual Hepatectomy Changed the Practice of Liver Surgery?: Experience of 1194 Virtual Hepatectomy Before Liver Resection and Living Donor Liver Transplantation. *Ann Surg* 2018;268:127-33.
- 16) Li P, Wang M, Yang Y, Liu H, Pan Z, Jiang B, et al. Preoperative three-dimensional versus two-dimensional evaluation in assessment of patients undergoing major liver resection for hepatocellular carcinoma: a propensity score matching study. *Ann Transl Med.* 2020 Mar;8(5):182.
- 17) Takamoto T, Hashimoto T, Ogata S, et al. Planning of anatomical liver segmentectomy and subsegmentectomy with 3-dimensional simulation software. *Am J Surg* 2013;206:530-8.
- 18) Yang T, Lin S, Xie Q, Ouyang W, Tan T, Li J et al. Impact of 3D printing technology on the comprehension of surgical liver anatomy. *Surg Endosc.* 2019 Feb;33(2):411-417.
- 19) Huettl F, Saalfeld P, Hansen C, Preim B, Poplawski A, Kneist W, Lang H, Huber T. Virtual reality and 3D printing improve preoperative visualization of 3D liver reconstructions-results from a preclinical comparison of presentation modalities and user's preference. *Ann Transl Med.* 2021 Jul;9(13):1074
- 20) Lopez-Lopez V, Robles-Campos R, García-Calderon D, Lang H, Cugat E, Jiménez-Galanes S, Fernández-Cebrian JM, Sánchez-Turrión V, Fernández-Fernández JM, Barrera-Gómez MÁ, de la Cruz J, Lopez-Conesa A, Brusadin R, Gomez-Perez B, Parrilla-Paricio P. Applicability of 3D-printed models in hepatobiliary surgery: results from "LIV3DPRINT" multicenter study. *HPB (Oxford).* 2021 May;23(5):675-684. doi: 10.1016/j.hpb.2020.09.020. Epub 2020 Oct 16. PMID: 33071150.
- 21) Bernhard JC, Isotani S, Matsugasumi T, Duddalwar V, Hung AJ, Suer E et al. Personalized 3D printed model of kidney and tumor anatomy: a useful tool for patient education. *World J Urol.* 2016 Mar;34(3):337-45.
- 22) Fang C, An J, Bruno A, Cai X, Fan J, Fujimoto J et al. Consensus recommendations of three-dimensional visualization for diagnosis and management of liver diseases. *Hepatol Int.* 2020 Jul;14(4):437-453.

Table 1. Baseline patients characteristics (n=124)

Age, y	67.1	(28-92)
BMI (Kg/m²)	27.5	(17.4-38.9)
Gender, No.		
Female	19	15.3%
Male	105	84.7%
Cirrhosis, No.	62	50%
HBV	8	12.9%
HCV	14	22.6%
Alcohol	37	59%
NASH	19	30.6%
CHILD score, mean	5	91.3%
Portal hypertension, No.	21	19.9%
Ascites, No.	0	0%
Esophageal varices, No.	14	11.3%
Comorbidities:		
Diabetes	51	41.1%
Hypertension	77	62%
Obesity	34	27.4%
Chronic kidney disease	10	8.1%
COPD	13	10.5%
Cardiovascular disease	18	14.5%
Previous abdominal surgery	59	47.6%

BMI= body mass index, COPD: chronic obstructive pulmonary disease

HBV= Hepatitis B virus, HCV= Hepatitis C virus, NASH= nonalcoholic steatohepatitis

Table 2: Modification of surgical planning

Type of change	%
Plan A to Plan B	35
Plan B to Plan C	18
Odds ratio	0.32 [0.15-0.64]
Plan A to Plan C	37
Plan B to Plan C	18
Odds ratio	4.37 [2-10.7]
Plan A to Plan C	37
Plan A to Plan B	35
Odds ratio	1.41 [0.53-3.9]

Table 3. Intraoperative features and postoperative outcomes

Transfusions		
Intraoperatively	13	10.7%
Postoperatively	9	7.4%
Antibiotics	14	11.5%
Drainage	55	45.1%
Interventional radiology	8	6.6%
Reoperation	5	4.1%
Overall in hospital morbidity	63	52.5%
Surgical in hospital-related morbidity	41	33.6%
Postoperative hemorrhage	3	2.5%
Biliary fistula	9	7.4%
Ascites	6	31.6%
Portal thrombosis	4	3.3%
Pulmonary effusions	29	23.8
Pulmonary atelectasis	16	13.1%
Kidney failure	9	7.4%
In-hospital mortality	4	3.3%
90-day mortality	6	5.1%

Figure 1. Plan A, B, C



Modifications analysed in 124 patients

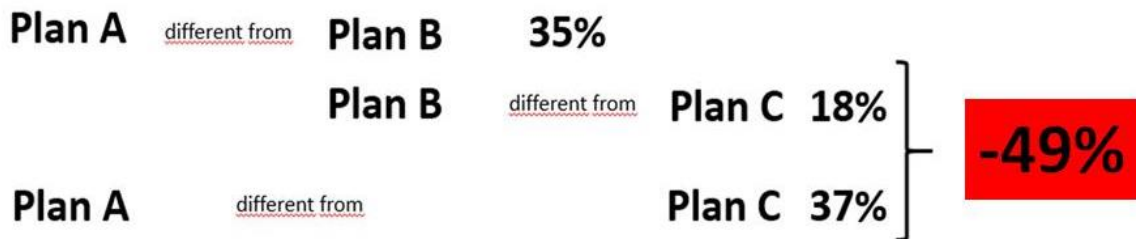


Figure 2. Number of patients enrolled for each of the 12 participating centers

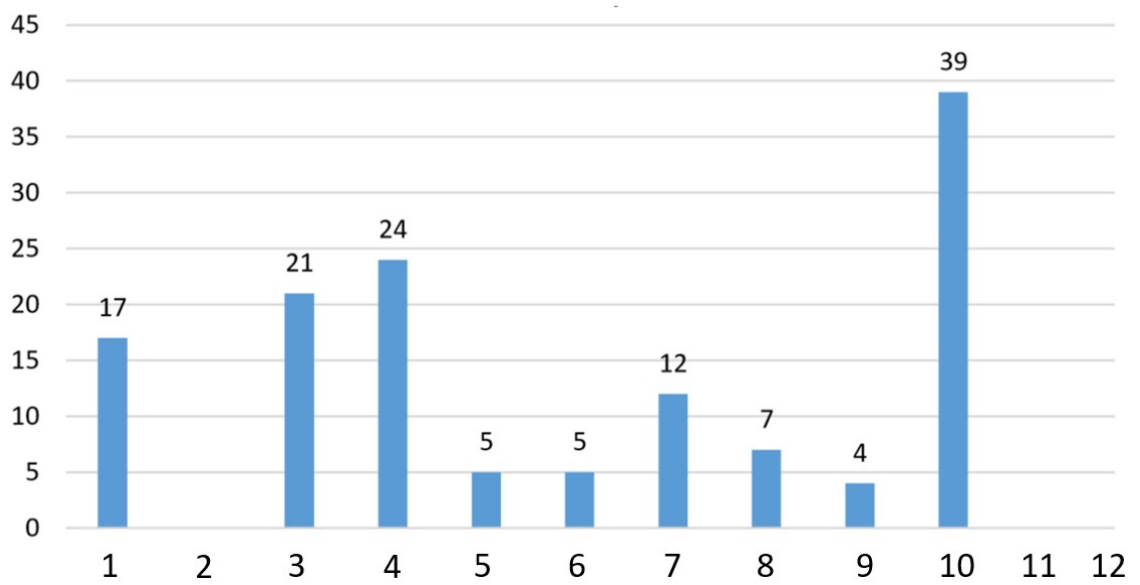


Fig. 3a:

Plan A: extended right hepatectomy with resection of middle hepatic vein. Segment IV resection was considered to prevent venous congestion.

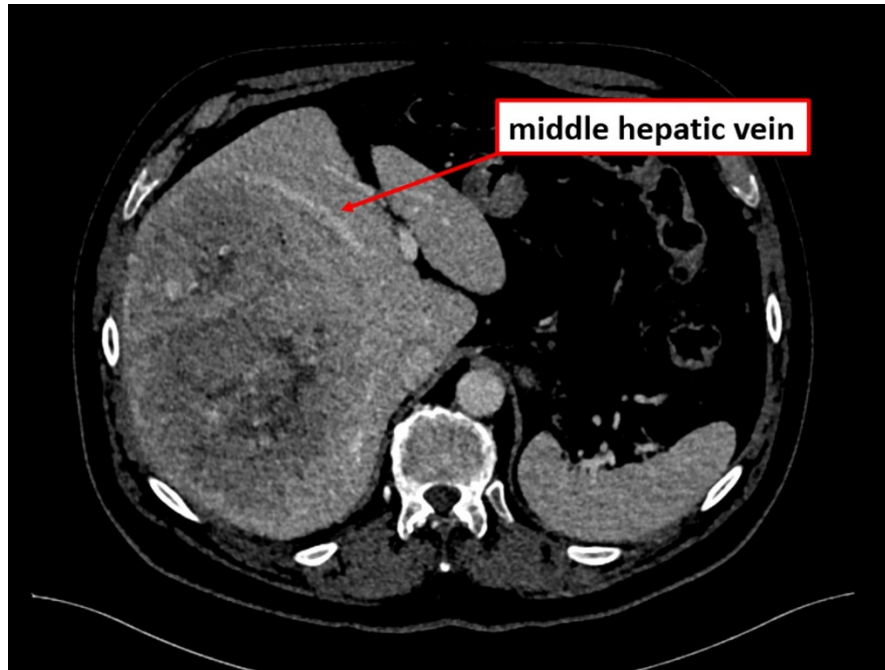


Fig. 3b:

Plan B: 3D reconstruction showed a scissural vein in liver segment IV. Resection was limited to the middle hepatic vein, and no venous congestion was observed intraoperatively.

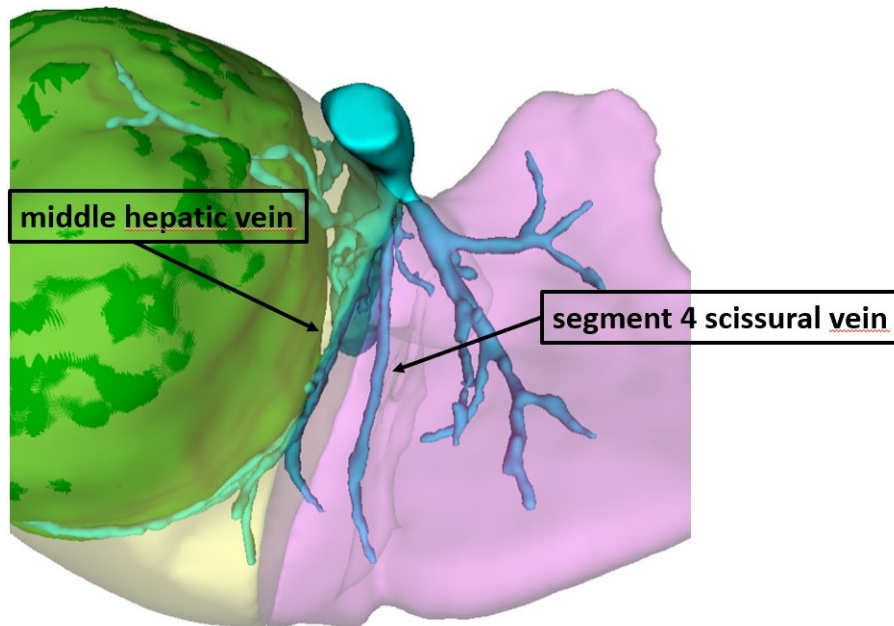


Fig. 3c:

Plan A: left hepatectomy with resection of the middle hepatic vein in a cirrhotic patient.

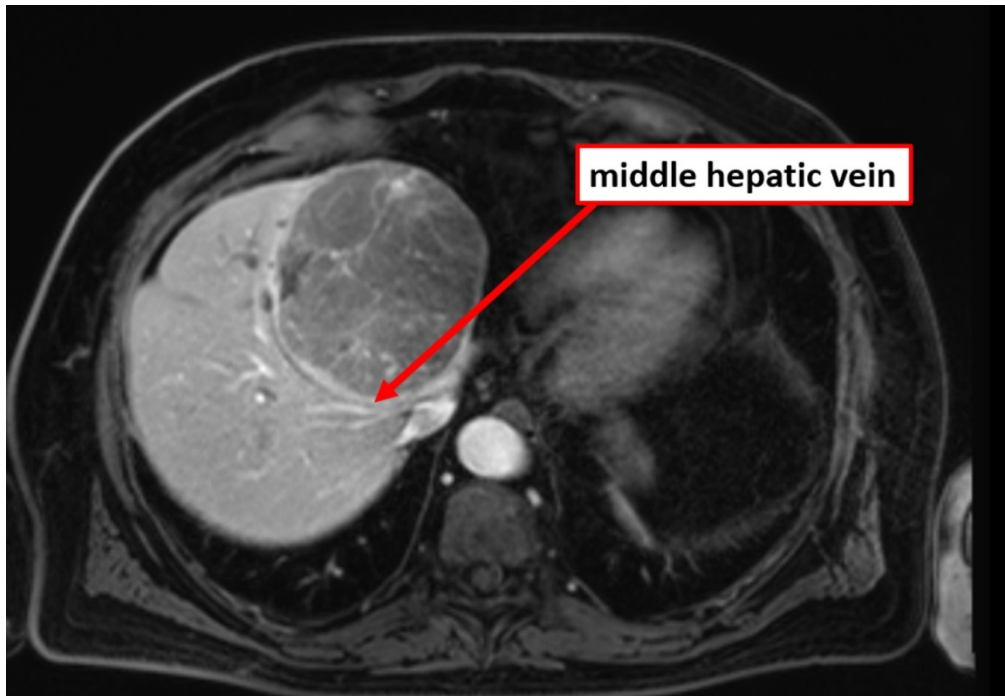
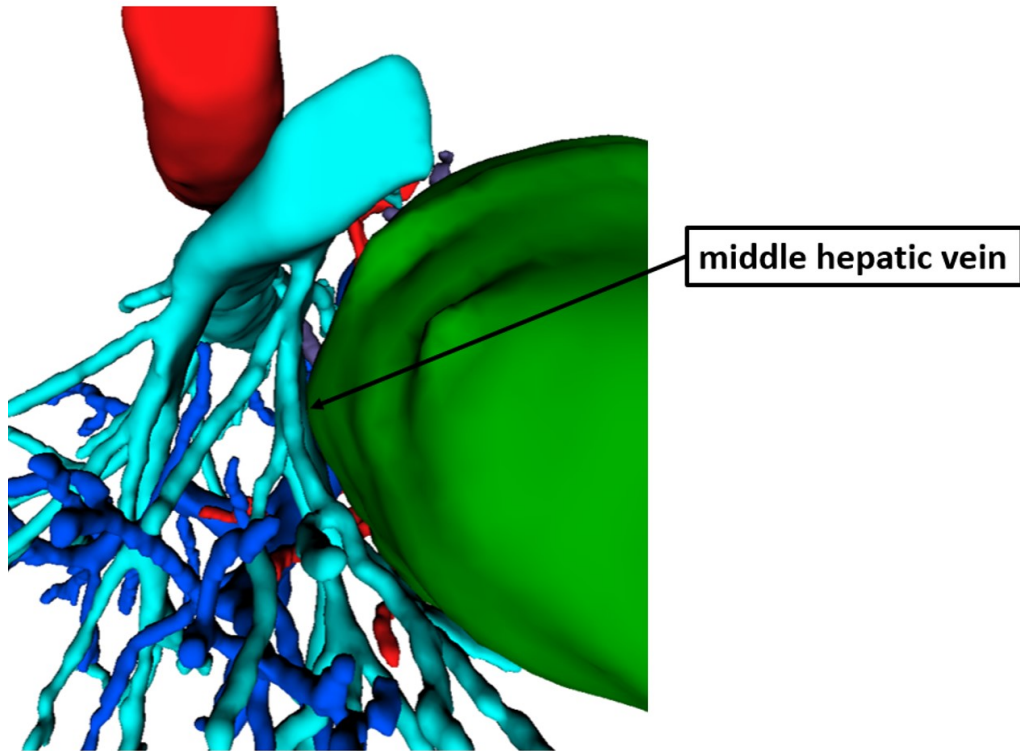


Fig. 3d:

Plan B: 3D reconstruction showed a clear margin on the middle hepatic vein, finally preserved with no venous congestion and no postoperative liver failure.



6.1c) Conclusions on the first part

The reported non-randomized prospective trial showed very interesting results. In fact, analysis of 3D reconstruction models significantly modified the initial surgical strategy based on conventional 2D imaging. Three-D modeling reduced potential planning errors by 49%. The 3D model was especially useful in approximately 25% of patients where strategy modifications induced by the reconstructions were actually realized (Plan A≠B and B=C in 24.5% of patients (n=30)). Preoperative 3D evaluation could accurately measure the distance between tumors and major intrahepatic vessels, providing better planning to the extent of liver resection and the plane of liver transection. Remnant liver volumes could be also measured accurately to quantitatively assess the risk of postoperative liver failure for the planned operations. In about 15% of patients there was a consistent change, either from major to minor resections, either the opposite. This is one of the most important points to consider because changing type of resections may have consequences on post-operative morbidity and mortality. Nevertheless, it has to be considered that the majority of changes included relatively less important modifications such as tumor resections (non-anatomical resections) towards subsegmentectomies (anatomical resections, but with no possibility to really demonstrate if a true anatomical resection has been performed). Secondary outcomes did not reach any statistical significance, and more particularly regarding the exact tumor localization, anatomical variations, resected volume, and surgical margins, with only a statistically significant underestimation by 3D of real margins. These informations were reported only in 40% of patients. Finally, despite the highest quality 2D or 3D images,

intraoperative findings sometimes modify preoperative planning, situation that occurred approximately in 12% of patients in our study.

As a conclusion, tridimensional models analysis has so to be considered as an accurate tool to improve 2D imaging and not in opposition to it.

6.2a) *In vivo* functional imaging – results summary and own contribution

i) Ischemic-non ischemic tissue assesement

We performed a differential intraoperative analysis of the optical properties of the liver to understand if the relative reflectance was a parameter which could discriminate between different levels of blood perfusion. We found that liver HSI could discriminate between total vascular inflow occlusion and hepatic artery occlusion. These results were confirmed via cross-validation of HSI which detected and quantified intestinal congestion in vascular inflow occlusion. A significant correlation between the near-infrared spectra and capillary lactate was found ($r = -0.8645$, $p = 0.0003$ VIO, $r = -0.7113$, $p = 0.0120$ HAO). Finally, a statistically significant negative correlation was found between the histology score and the near-infrared parameter index (NIR) ($r = -0.88$, $p = 0.004$). We infer that HSI, by predicting capillary lactates and the histopathological score, would be a suitable non-invasive tool for intraoperative liver perfusion assessment. My personal contribution to this study was participation to the study design, operative procedures on animal models, revision of results and writing and revision of the manuscript.

Article

Published in: **Scientific Reports (2020)**

Sci Rep. 2020 Sep 22;10(1):15441. doi: 10.1038/s41598-020-72915-6.

Hyperspectral evaluation of hepatic oxygenation in a model of total vs. arterial liver ischaemia

Eric Felli^{1,2*}, Mahdi Al-Taher², Toby Collins⁷, Andrea Baiocchini⁶, **Emanuele Felli**^{3,4}, Manuel Barberio^{2,8}, Giuseppe Maria Ettorre⁵, Didier Mutter^{3,7}, Veronique Lindner⁹, Alexandre Hostettler⁷, Sylvain Gioux¹⁰, Catherine Schuster^{4,11}, Jacques Marescaux^{2,7} & Michele Diana^{1,2,3,7,10}

¹Institute of Physiology, EA3072 Mitochondria Respiration and Oxidative Stress, University of Strasbourg, Strasbourg, France.

²IHU-Strasbourg, Institute of Image-Guided Surgery, Strasbourg, France.

³Department of General, Digestive, and Endocrine Surgery, University Hospital of Strasbourg, Strasbourg, France.

⁴INSERM, Institute of Viral and Liver Disease, U1110 Strasbourg, France.

⁵Department of Transplantation and General Surgery, San Camillo Hospital, Rome, Italy.

⁶Department of Pathology, San Camillo Forlanini Hospital, Rome, Italy.

⁷Surgical Data Science Department, Research Institute Against Digestive Cancer (IRCAD), Strasbourg, France.

⁸Department of Visceral, Transplant, Thoracic and Vascular Surgery, University Hospital of Leipzig, Leipzig, Germany.

⁹Department of Pathology, University Hospital, Strasbourg, France. ¹⁰ICUBE Laboratory, Photonics

Instrumentation for Health, University of Strasbourg, Strasbourg, France. ¹¹University of Strasbourg, Strasbourg,

France. *email: eric.felli@ihu-strasbourg.eu

Liver ischaemia reperfusion injury (IRI) is a dreaded pathophysiological complication which may lead to an impaired liver function. The level of oxygen hypoperfusion affects the level of cellular damage during the reperfusion phase.

Consequently, intraoperative localisation and quantification of oxygen impairment would help in the early detection of liver ischaemia. To date, there is no real-time, non-invasive, and intraoperative tool which can compute an organ oxygenation map, quantify, and discriminate different types of vascular occlusions intraoperatively. Hyperspectral imaging (HSI) is a non-invasive optical methodology which can quantify tissue oxygenation, and which has recently been applied to the medical field. A hyperspectral camera detects the relative reflectance of a tissue in the range of 500 to 1000 nm, allowing the quantification of organic compounds such as oxygenated and deoxygenated haemoglobin at different depths. Here, we show the first comparative study of liver oxygenation by means of HSI quantification in a model of total vascular inflow occlusion (VIO) vs. hepatic artery occlusion (HAO), correlating optical properties with capillary lactate and histopathological evaluation. We found that liver HSI could discriminate between VIO and HAO. These results were confirmed via cross-validation of HSI which detected and quantified intestinal congestion in VIO. A significant correlation between the near-infrared spectra and capillary lactate was found ($r = -0.8645$, $p = 0.0003$ VIO, $r = -0.7113$, $p = 0.0120$ HAO). Finally, a statistically significant negative correlation was found between the histology score and the near-infrared parameter index (NIR) ($r = -0.88$, $p = 0.004$). We infer that HSI, by predicting capillary lactates and the histopathological score, would be a suitable non-invasive tool for intraoperative liver perfusion assessment.

Liver ischaemia and reperfusion injury (IRI) is a dreaded vascular complication characterized by the disruption of parenchymal and microvascular architecture which leads to hepatic functional impairment¹. IRI has practical relevance in liver transplantation and during liver surgery performed with intermittent vascular inflow occlusion. Liver oxygenation impairment and ischaemia can be challenging to detect intraoperatively, which is partly due to multiple hepatic vascular inflows^{1–3}. Parenchymal disruption in the reperfusion phase mainly depends on ischaemic time duration. Consequently, intraoperative localisation and quantification of oxygen impairment may be helpful in quickly detecting future reperfusion injury sites. To date, there is no tool which can spatially visualize and quantify liver oxygenation intraoperatively. Currently, hepatic circulation can be evaluated intraoperatively using ultrasound (US). However, US may be time-consuming, especially during laparoscopic surgical procedures, and has a long learning curve⁴. Additionally, US evaluation might be difficult in obese patients and the interpretation is strongly operator-dependent⁵. Besides, US aims to analyse and quantify blood circulation in a specific area of interest and does not provide an immediate localisation and quantification of oxygenation of the whole liver surface. Hyperspectral imaging (HSI) is a non-invasive technique which has been recently applied to the medical field as a tool for image-guided surgery and specifically for an intraoperative quantification of tissue perfusion^{6,7,8}. HSI detects the relative reflectance of light with a wavelength comprised between 500 and 1000 nm, allowing the quantification of organic compounds, such as oxygenated and deoxygenated haemoglobin⁹. The application of HSI has recently

gained importance for its non-invasiveness and the accuracy of oxygen quantification at different depths¹⁰. For that reason, HSI is a promising technology as it allows for the intraoperative quantification and spatial visualisation of hepatic oxygenation and to discriminate among different types of liver ischaemia.

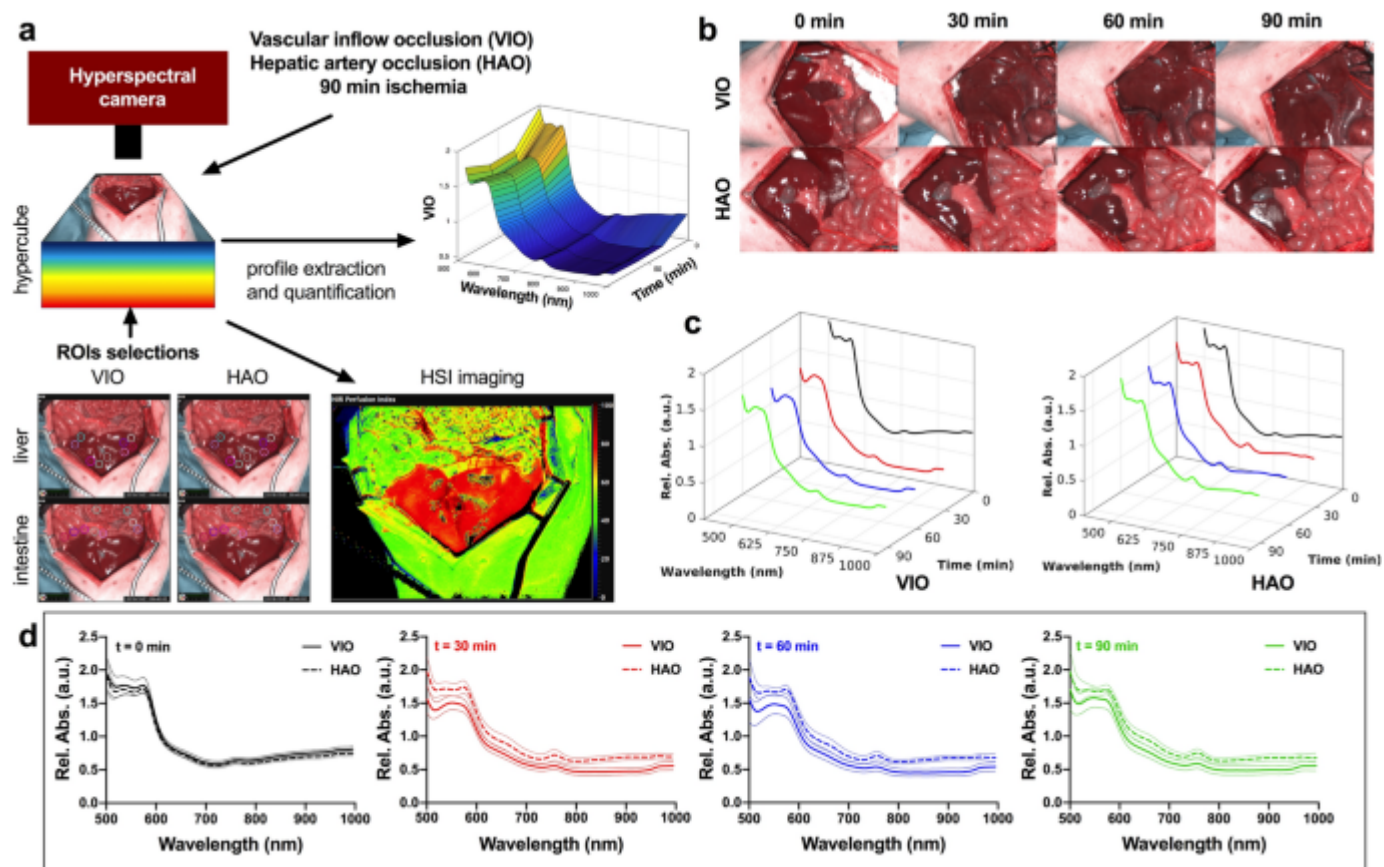
We present a comparative preclinical study of HSI-based liver oxygenation quantification of porcine liver in an experimental model of total vascular inflow occlusion (VIO) versus hepatic artery occlusion (HAO). Optical properties extracted with HSI have been correlated with biological markers to predict the level of ischaemia. The HSI system used in this study provides presets for the quantification of the relative oxygen saturation ($StO_2\%$) at a depth up to ~ 1 mm and of the near-infrared (NIR) spectrum at a depth of up to 3–5mm¹⁰. Water distribution was assessed with the tissue water index (TWI), which quantifies tissue water content¹⁰.

Results

Spectral profile extraction

Hyperspectral images were collected during and before the ischaemic phase, following the selection of ten regions of interest (ROIs) in the intestine and in the liver, which allowed for the extraction of spectral profiles (hypercubes). Images and spectral profiles were extracted from the hypercubes of the ROIs (Fig. 1a). RGB images showed a slight colour difference during the ischaemic phase when compared to the control (Fig. 1b). The overall

spectra of VIO showed a lower relative absorbance during the ischaemic phase when compared to the control and to all HAO timepoints (Fig. 1c,d).



Experimental workflow. **(a)** Hyperspectral imaging was performed 3 times in 30-min intervals for a total period of 90 min in both VIO and HAO models. The images and spectra of 10 ROIs were extracted from the hypercubes and analysed. **(b)** RGB images of liver before ligation and during the ischemic phase, where no major differences were found. **(c)** Spectral profiles of both ischaemia types at different times showed that VIO control was overall higher as compared to the ischaemic phase. This was not the case for the HAO spectra. **(d)** Profiles comparison at each timepoint of VIO and HAO. Spectra extraction was performed with the TIVITA hyperspectral camera (Diaspective Vision GmbH, Germany) from 500 to 1000 nm with a resolution of 5 nm obtaining 250 bands per each image.

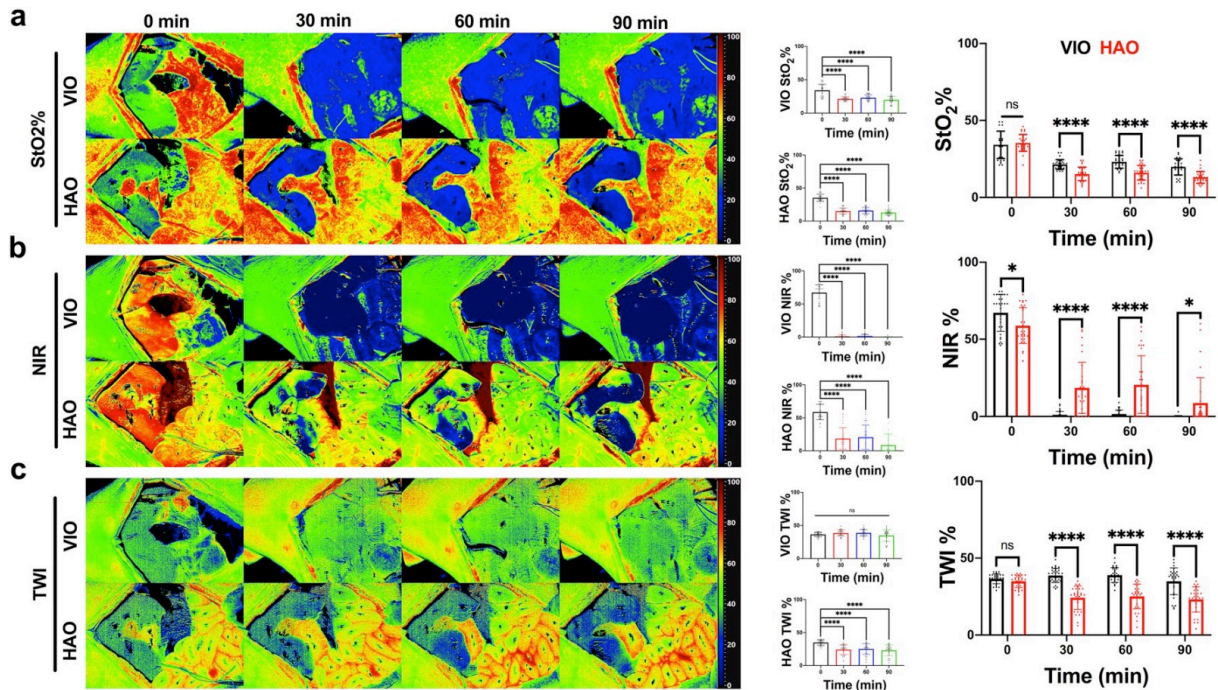


Figure 2. Liver hyperspectral imaging. (a–c) StO₂%, NIR and TWI imaging and quantification. From left to right are displayed hyperspectral images of the two ischaemic models, the quantitative analysis of each model, and the comparison between VIO and HAO. All preset parameter indexes could distinguish different types of ischaemia at each timepoint. The images were quantified and finally compared with one-way and two-way ANOVA. Data are presented as mean ± s.d. and compared to the control, ns $p > 0.05$, * $p \leq 0.05$, ** $p \leq 0.01$, *** $p \leq 0.001$, **** $p \leq 0.0001$. N = 60 (ROIs in 6 pigs).

Liver hyperspectral imaging

The StO₂% index showed a significant decrease during the ischaemic phase in both models ($p < 0.001$ for 30, 60 and 90 min in VIO and HAO) (Fig. 2a). When VIO and HAO were compared, StO₂% in HAO was significantly lower ($p < 0.0001$, for 30, 60, and 90 min). The NIR index showed a visible change in VIO and HAO, similar to StO₂%. However, it could detect a small difference also in the controls ($p = 0.0335$, $p < 0.0001$, $p < 0.0001$, $p = 0.0286$, for 0, 30, 60, and 90 min respectively). Additionally, NIR in HAO showed a localised area of ischaemia which increased in surface area over time (Fig. 2b). TWI did not show any significant difference in VIO ischaemia when compared to the control but

showed a significant difference in HAO ($p < 0.0001$ for 30, 60, and 90 min). The HAO TW index was significantly lower when compared to VIO ($p < 0.0001$ for 30, 60 and 90 min) (Fig. 2c).

Blood gas analysis. Partial oxygen pressure (pO_2) decreased significantly over the ischaemic phase in VIO when compared to HAO after 60 min ($p = 0.232$), reaching a maximum spread after 90 min ($p = 0.0019$) (Fig. 3a). Partial carbon dioxide (pCO_2) showed an overall non-significant increase in both VIO and HAO (Fig. 3b). There was a significant decrease in $cHCO_3^-$ after 60 min in VIO as compared to HAO ($p = 0.0209$) (Fig. 3c). The pH remained constant in HAO presenting a non-significant decrease after 30 min of ischaemia, which decreased significantly in VIO after 90 min ($p = 0.0143$) (Fig. 3d). Creatinine showed a slight increase, which was not statistically significant in VIO and HAO (Fig. 3e). Systemic lactate levels showed a dramatic increase in VIO, which was significant after 60 min, reaching a maximum spread at 90 min as compared to HAO ($p < 0.0001$) (Fig. 3f). The correlation matrix of VIO vital parameters showed that the pH was negatively correlated with pCO_2 ($r = -0.97$, $p = 0.034$) and positively with $cHCO_3^-$ ($r = 0.96$, $p = 0.041$). In addition, it showed that pO_2 was positively correlated with $cHCO_3^-$ ($r = 0.97$, $p = 0.034$) and the pH ($r = 0.98$, $p = 0.019$). Systemic lactate was also found positively correlated with pCO_2 ($r = 0.96$, $p = 0.042$) and negatively correlated with $cHCO_3^-$ ($r = -0.96$, $p = 0.035$), the pH ($r = -1.00$, $p = 0.001$), and pO_2 ($r = -0.99$, $p = 0.011$) (Fig. 3g).

Finally, a positive correlation was found in systemic lactate levels with pCO₂ in HAO ($r = 0.95$, $p = 0.049$) (Fig. 3h).

Liver damage assessment. Capillary lactate sampled on the liver surface showed a significant increase in VIO after 30 min ($p < 0.0001$) followed by a decrease, while HAO showed no significant change (Fig. 4a,b). In addition, the difference between the two techniques was statistically different ($p < 0.0001$) for 30, 60, and 90 min (Fig. 4c). In VIO, the overall damage was represented by steatosis with hepatocyte atrophy and sinusoidal congestion. Similarly to HAO, necrosis was not the main parameter as compared to microvesicular steatosis or to congestion and atrophy. Pale staining was present in both ischaemic types from 30 min with an increasing trend up to 90 min. HAO was characterised by a lobular apoptosis, cholestasis, and neutrophils infiltration. Additionally, after 90 min, a strong congestion was found with a micro-haemorrhage close to the central vein and a microvacuolisation of hepatocytes cytoplasm (Fig. 4d). Sirius red staining did not show any major alteration in the collagen structure which could affect the hyperspectral signal in the control and the ischaemic phase (Fig. 4e). Overall, a significant gradual increase of histology score was found in both ischaemic models. Finally, there was no significant difference between the two histology scores in the two models for all timepoints (Fig. 4f,g).

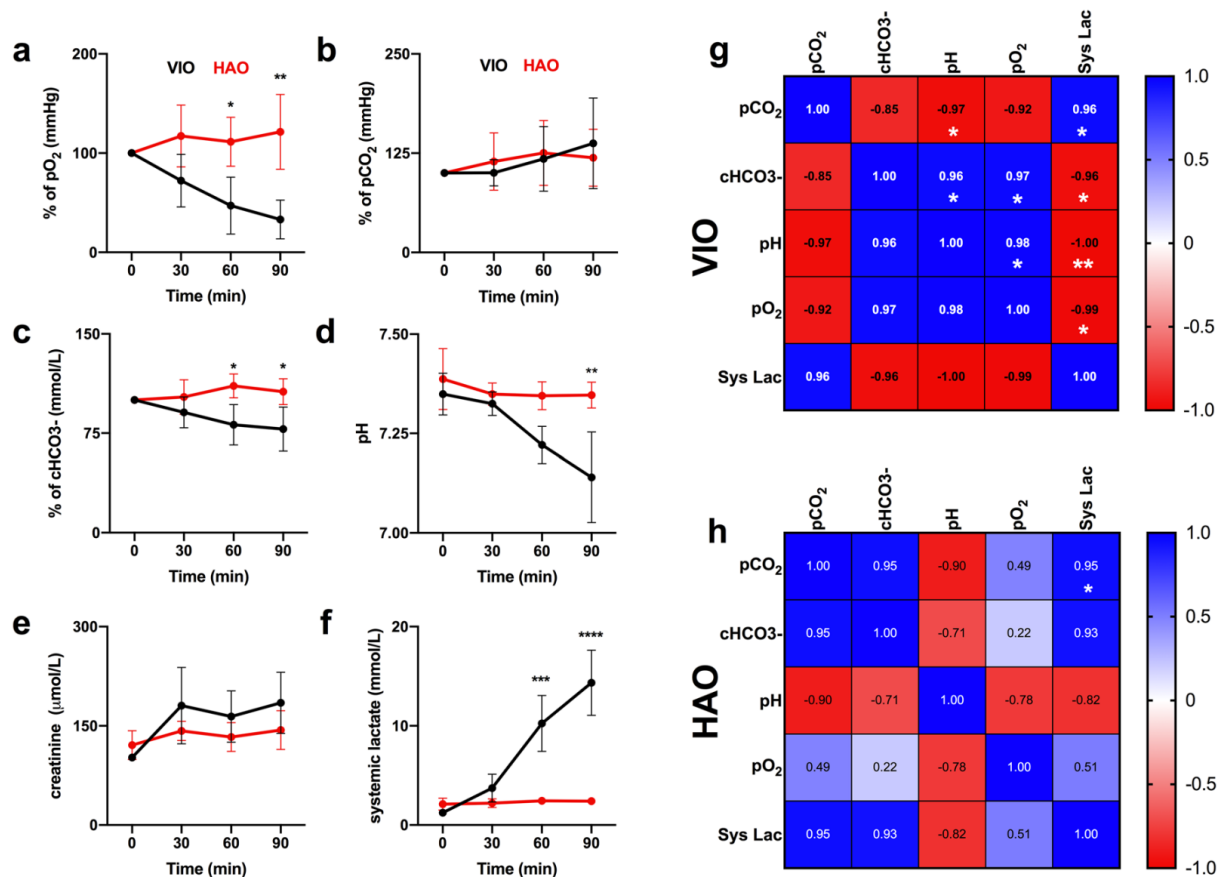


Figure 3. Monitoring of vital parameters with blood gas analysis (BGA). (a–c) pO₂, pCO₂, and cHCO₃⁻ were normalised with the control. (d) The pH was used to monitor the systemic acidosis. (e) Kidney function was monitored with the creatinine level. (f) Systemic lactate. (g) VIO correlation matrix of vital parameters. (h) HAO correlation matrix of vital parameters. Systemic lactates correlated better with pO₂ in both VIO and HAO. Data are presented as mean ± s.d. and compared with one-way ANOVA to the control, ns p > 0.05, *p ≤ 0.05, **p ≤ 0.01, ***p ≤ 0.001, ****p ≤ 0.0001. N = 6 (pigs).

Intestine HSI imaging quantification. Intestinal congestion, if used as a cross-validation test, is potentially an additional element for an automatic diagnosis. We subsequently analysed this parameter to confirm the experimental model. The spectral profile of the intestine showed an increase in relative absorbance in VIO but not in HAO during the ischaemic phase (Fig. 5a,b). The difference between the two spectra at every timepoint was maintained during the whole procedure (Fig. 5c). The VIO StO₂% showed a significant

decrease in oxygenation when compared to the control, which was not observed for HAO (Fig. 5d,e). Intestinal comparison of StO₂% showed a significant difference between VIO and HAO ($p < 0.0001$ for 30, 60, and 90 min) (Fig. 5f). Similar results were observed with NIR and TWI (Fig. 5g, h, i, l, m, n).

Correlation. StO₂% and NIR showed a significant correlation between liver and intestine in VIO, except for TWI (Fig. 6a). No correlation was found in HAO in any of the HSI parameter indexes (Fig. 6b). A stronger correlation between NIR and capillary lactate was found in VIO and HAO when compared to StO₂% and TWI ($p = 0.0003$ and $p = 0.0120$ respectively) (Figs. 6c,d). Finally, the histopathological score showed a significant negative correlation between StO₂% and NIR ($r = -0.79$, $p = 0.018$ and $r = -0.88$, $p = 0.004$ respectively). A positive correlation was also found between StO₂% and NIR ($r = 0.76$, $p = 0.029$) (Fig. 6e).

Discussion

HSI is a non-invasive and easy-to-use imaging technology recently applied to the medical field, providing a contrast-free biochemical analysis of tissues based on optical endogenous properties¹¹. In addition, HSI has been successfully applied as a tool to discriminate healthy from pathological tissue and for the quantification of organ perfusion level in both preclinical and clinical settings^{12–14}. The ability of the HSI system to evaluate the liver oxygenation was already assessed and applied by our group in an intraoperative setting to create hyperspectral enhanced reality (HYPER) in liver anatomical resection^{15–17}. However, doubts remained as to whether or not the system could discriminate different

types of hepatic vascular occlusions. We therefore tested the system to explore this additional feature that we considered important. This is especially true in liver transplantation for dreaded vascular complications such as hepatic artery thrombosis which can lead to up to ~ 60% of retransplantation and a ~ 50% of mortality rates¹⁸.

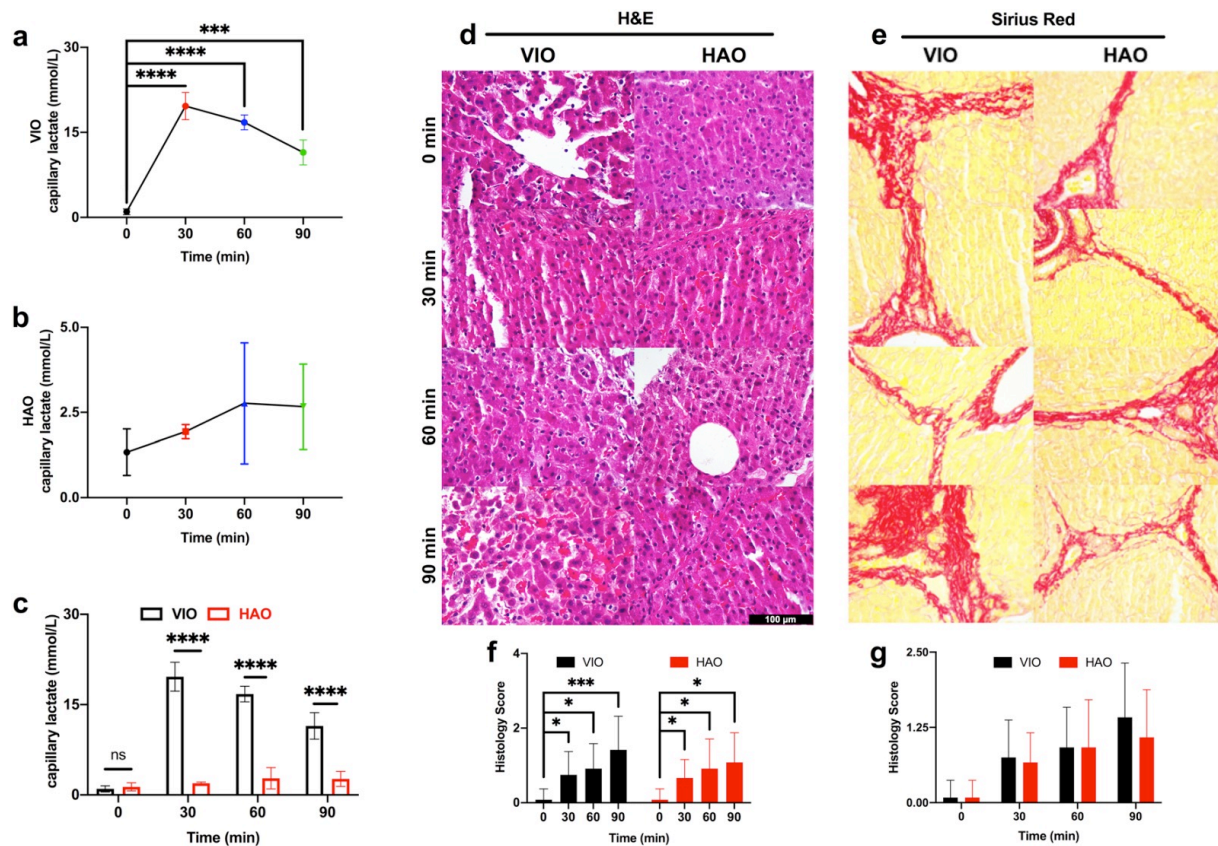


Figure 4. Liver biological analysis. **(a, b)** VIO and HAO capillary lactate. **(c)** Capillary lactate comparison between VIO and HAO. **(d)** H&E showed a gradual congestion increase in both ischaemic phases. **(e)** Sirius red did not show any change in the collagen structure which could affect HSI. **(f)** The histology score showed a significant increase in liver damage although **(g)** no significant difference was found between the two types of ischaemic models. Data are presented as mean \pm s.d. and compared with one-way and two-way ANOVA to the control, ns $p > 0.05$, * $p \leq 0.05$, ** $p \leq 0.01$, *** $p \leq 0.001$, **** $p \leq 0.0001$. N = 6 (pigs).

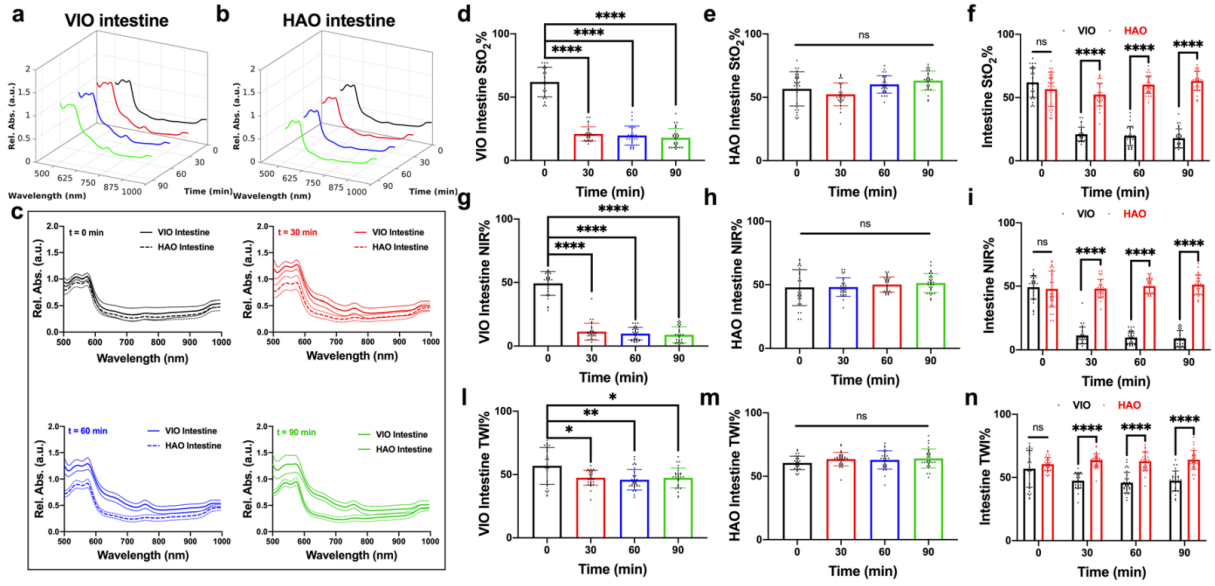


Figure 5. Intestine HSI imaging quantification. (a, b) Intestine spectra profile at different timepoints. (c) Intestine spectra comparison at every timepoint between VIO and HAO. (d-f) VIO and HAO StO₂% quantitative comparison. (g-i) VIO and HAO NIR quantitative comparison (j-l) VIO and HAO TWI quantitative comparison. Data are presented as mean ± s.d. and compared with one-way and two-way ANOVA to the control, ns $p > 0.05$, * $p \leq 0.05$, ** $p \leq 0.01$, *** $p \leq 0.001$, **** $p \leq 0.0001$. N = 60 (ROIs in 6 pigs).

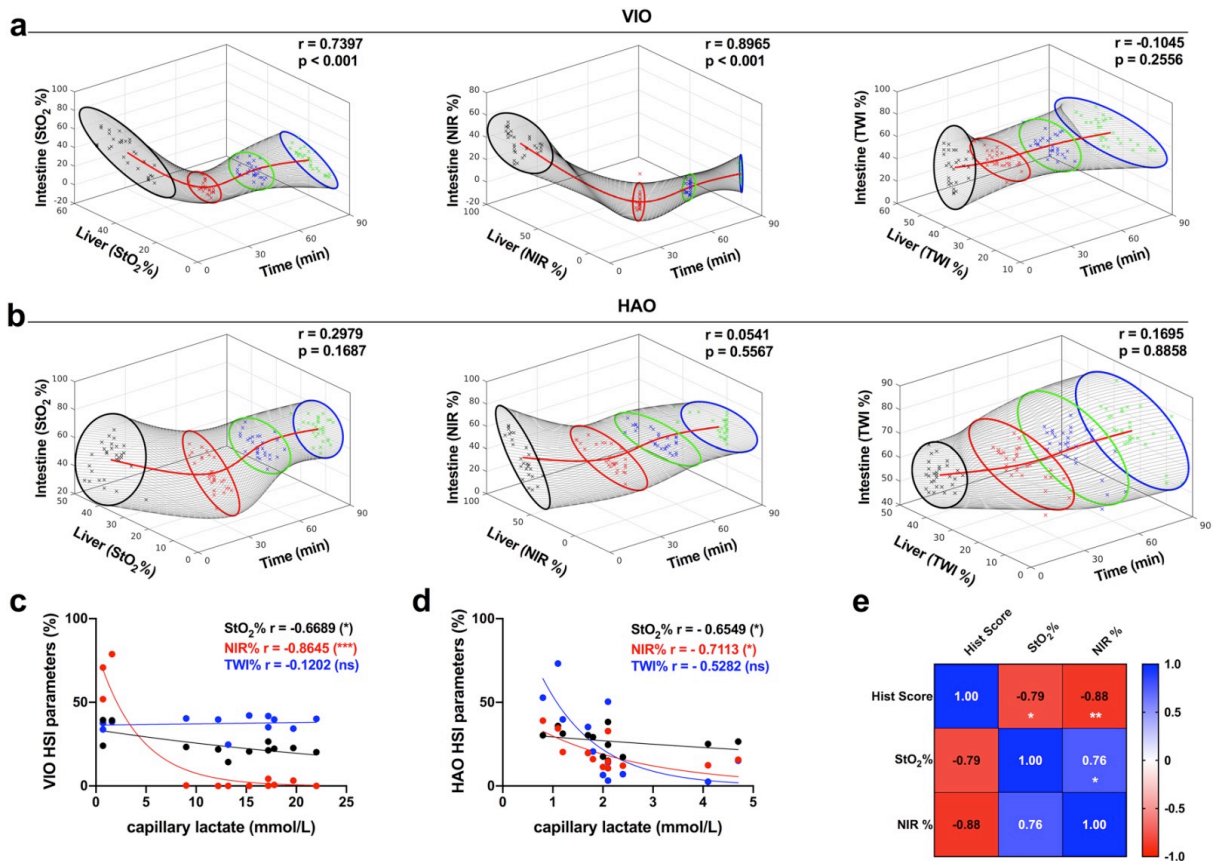


Figure 6. Correlation analysis. (a) VIO HSI parameter correlation of liver and intestine over time (b) HAO HIS parameter correlation of liver and intestine over time. (c, d) Capillary lactate and HSI parameters correlation in VIO. N = 120 (6 pigs, 10 ROIs). (e) Comparison between histology score, StO₂%, and NIR. Data are correlated with Pearson's and Spearman's analysis, ns $p > 0.05$, * $p \leq 0.05$, ** $p \leq 0.01$, *** $p \leq 0.001$, **** $p \leq 0.0001$. Visualisations of the correlation between TWI, StO₂%, and NIR over time. At each timepoint, a scatter plot is visualised, with a best-fitting ellipse at the 95% confidence interval using Principal Component Analysis. N = 24 (6 pigs).

However, US requires specific training and its interpretation may vary among the authors.

Additionally, US does not provide a global map of liver oxygenation intraoperatively, while

HSI provides a spatial resolution which can help the operator to localize the ischemia. To

the best of our knowledge we found some experimental methods to monitor liver ischemia.

All of these promising techniques such as CO₂ sensor, indocyanine green (ICG) and near

infrared spectroscope, presented drawbacks such as invasiveness, the lack of spatial and

informative quantification of ischaemia, the non-intraoperative applicability^{19–23}. These

major drawbacks make it difficult to transfer these methodologies to the clinical practice.

For instance, ICG recently gained importance as intraoperative imaging assessment for

liver perfusion^{21,24}. Although this technique showed positive results, it is still an invasive

methodology due to the need for an injection of an exogenous molecule, which requires

time for the clearance. Additionally, some patients are allergic to the iodine and its

application for imaging purposes has not been approved. The HSI technology overcomes

these problems intraoperatively thanks to its non-invasiveness and its standardised

perfusion assessment which is not operator dependent. Additionally, HSI provide for an

optical quantification of endogenous molecules for which a labelled dye injection is not

needed. In this study, we tested the potential of HSI ability to detect possible complications

in liver surgery associated with oxygen impairment intraoperatively. HSI could precisely predict the level of capillary lactate concentration from changes in optical properties. These results are useful to create an automatic diagnostic system based on optical imaging, which may predict liver graft dysfunction. In our experiments, the camera facilitated the automatic quantification of three parameters which can otherwise be extracted from the hypercube manually¹⁰. Bile has a spectral profile which could interfere with the StO₂% and NIR parameters²⁵. For that reason, the bile duct was left out of the Pringle's manoeuvre to prevent any bile obstruction which could gradually impair the HSI signal. NIR images showed the ability to localise and quantify

the level of ischaemia in the HAO manoeuvre (Fig. 2b). This is probably because NIR wavelengths have deeper tissue penetration as compared to StO₂%¹⁰. This aspect, together with the need to implement the bile signal, may make StO₂% images less informative. However, the lack of a corrective algorithm of the bile spectra profile, limits the applicability of such technology in scenarios on which the bile duct is occluded for long time. Nonetheless, we consider this limit possible to overtake by the creation of an ad hoc plug-in of the proprietary software. TWI did not reveal any changes in VIO, probably due to the full clamp of the vascular inflow which blocked the circulation, as confirmed by the sinusoidal congestion (Fig. 3d). For VIO, TWI did not detect any statistical difference. Given the total inflow occlusion, the blood flow was almost completely stopped and the water contained in tissues and blood stayed inside the organ. The overall significant difference detected by TWI in the HAO ischaemic phase was then likely due to a relative

reduction in blood flow. When the hepatic artery was occluded in HAO, the portal blood flow did not buffer the arterial flow. Indeed, differently from the occlusion of the portal vein, there is no such compensatory mechanism as the HABR effect²⁶. Additionally, the post-sinusoidal pressure was maintained via systemic circulation throughout the inferior vena cava²⁷. Consequently, TWI in the liver may be mainly influenced by blood circulation in the liver. Vital parameters confirmed that the experimental workflow was coherent with the pathophysiology of both ischaemia types. Lactate was the blood marker which correlated with pCO₂% in VIO and HAO. It has been previously used as the main marker to assess correlation between optical and biological properties²⁸. Capillary lactates in VIO increased dramatically after 30 min and started to decrease gradually over time. This was likely due to their distribution into the systemic circulation via the inferior vena cava. The ischemic process could have been non-homogeneous, impairing histology assessment. Bigger biopsies could partially solve this problem but would affect microcirculation, creating a bias in the study. We quantified the following 4 parameters: coagulative necrosis, micro-vacuolisation of the cytoplasm, pale staining, and sinusoidal congestion. A damage increase was characterised by micro-vacuolisation and congestions which appear statistically significant. These alterations appeared more significant after 60 min. Sinusoidal congestion was the most interesting histopathological parameter. This is fundamental in liver vascular thrombosis due to the slowdown in the hematic flow with a dramatic reduction of the sinusoidal pressure which reduces the chance of the blood to wash out into the central vein. Due to its ability to quantify the light scattering, the HSI signal

also depends on the tissue texture. This property has been exploited for diagnostic purposes²⁹. In order to rule out any possible bias given by any potential alteration in liver microarchitecture, Sirius red staining was performed, showing no difference in collagen structure in the control and ischaemic phases. In VIO, the blood flow from the portal vein was interrupted creating a congestion in the intestine, while the blood flowed through the liver in HAO. This was coherently differentiated in HSI as shown in Fig. 5. This was also shown in Fig. 6, where there was no correlation in HAO between the liver and the intestine. However, there was a high correlation in VIO. The overall correlation between the HSI parameters and capillary lactates showed that NIR is a better parameter to detect changes in liver oxygenation and, as a result, in liver hypoxia (Fig. 6c,d). This is due to the similar depth between NIR imaging and blood sampling (~ 3–5 mm) while the StO₂% is more superficial at ~ 1 mm. At that depth, the blood is mainly characterised by arterial circulation. Consequently, the overall evaluation of liver hypoperfusion would be impaired in HAO³⁰. Therefore, StO₂% would be influenced by a higher sensitivity with a dramatic loss of signal as compared to VIO (Fig. 2a,b). Finally, the histopathological score showed a high correlation between StO₂% and NIR, confirming together with the capillary lactate that HSI parameters can predict the overall level of ischaemia. It is still unclear if HSI can distinguish different times of liver ischaemia within the same ischaemic model. To achieve this goal, a possible next step would be to apply an artificial intelligence-based analysis of the whole spectra associated with the automatic recognition of liver tissue to distinguish VIO, HAO, portal vein occlusion (PVO), and bile duct occlusion (BDO) at different

timepoints. The overall correlation with biological data confirmed that HSI is a suitable tool for intraoperative diagnosis and as a result, it merits further investigation for future preclinical and clinical studies using the abovementioned models. Although HSI could discriminate and quantify two different models of hepatic ischaemia, its preset parameters could not discriminate ischaemic time points. In fact, both in liver and intestine, there was no statistical difference among the ischemic time points regarding all parameters. The additional study of time is crucial for an early intervention to prevent the reperfusion damage. Consequently, a future study on the discrimination of the ischemic time points is more than necessary.

Methods

Study design. The primary aim of this study was to evaluate the accuracy of intraoperative HSI in the quantification of liver oxygenation in two models of hepatic ischaemia (VIO and HAO). In order to achieve this goal, HSI was used to extract a relative absorbance between 500 and 1000 nm from hyperspectral images and to quantify the relative absorbance¹⁰. The optical data were compared to capillary lactates to measure the correlation between optical and biological properties. Histopathological characterisation and quantification were performed to confirm the experimental workflow and evaluation. The data were collected before ligation and every 30 min after ligation for a total duration of 90 min.

Animals. This study is part of the ELIOS project (Endoscopic Luminescent Imaging for Oncology Surgery). It was approved by the local Ethical Committee on Animal Experimentation (ICOMETH No. 38.2016.01.085), as well as by the French Ministry of Superior Education and Research (MESR) (APAFIS#8721- 2017013010316298-v2). All animals were managed according to French laws for animal use and care and the directives of the European Community Council (2010/63/EU) and ARRIVE guidelines³¹. Six adult male swine (*Sus scrofa ssp. domesticus*, mean weight: 29.4 ± 4.8 kg) were housed and acclimatised for 48 h in an enriched environment, with constant humidity and temperature conditions. A fasting period was held for 24 h before surgery, with ad libitum access to water. Stress was reduced by means of sedation (zolazepam + tiletamine 10 mg/ kg IM) 30 min before the procedure and respecting circadian cycles of light-darkness. Propofol (3 mg/kg) was injected intravenously (18 gauge IV catheter in ear vein) and maintained with rocuronium 0.8 mg/kg along with inhaled isoflurane 2%. Animals were euthanised with a lethal dose of pentobarbital (40 mg/kg) at the end of the procedure.

Sample size calculation. Correlation between capillary lactate and StO₂% HSI preset parameters was used as a primary outcome to compute sample size. The calculation was based on previous publications on bowel ischaemia, which showed a ρ correlation coefficient of -0.716 ,³². The required paired values were 4, considering $\alpha = 0.05$ with a power $(1 - \beta) = 0.9$. In the present study, 120 paired StO₂% lactate values were obtained in six pigs.

Surgical procedure. After a midline laparotomy and hepatic pedicle dissection, two different vascular inflow occlusions were performed: (1) total occlusion of the vascular inflow (VIO), and (2) hepatic artery isolation and occlusion (HAO). Both manoeuvres were performed for 90 min, which has been shown to be sufficient to induce liver damage in pig models³³. The bile duct was isolated to prevent its ligation.

Hyperspectral imaging. Hyperspectral camera can acquire the spatial 2D image with a third dimension represented by spectroscopic information in a determined wavelength field. In this experimental study, we used a CMOS pushbroom scanning hyperspectral camera (TIVITA, Diaspective Vision GmbH, Germany) to generate hyperspectral images. The distance between the camera and the organ was 40 cm. The distance was monitored by a distance sensor (Bluefruit Feather nRF52832 with Adafruit VL53LOx device) during the whole procedure. The images were acquired using 20 W Osram Halospot 70 Halogen lamp (6 ×) allowing a range of spectra of 500 to 1000 nm. The HSI system took ~ 6 s to perform the imaging. The cube data was transferred to a PC where it was processed creating pseudo-colour images. Data of the cube has dimension of 640 × 480 × 100 (px × px × wavelength). Relative reflectance was extracted within the wavelength range with a gap of 5 nm for a total number of 250 spectral samples. The 3D cube extracted contained the spatial data with the relative reflectance (I/I_0) for each pixel that was converted in relative absorbance via the system through the equation: $A = -\ln(I/I_0)$. Quantitative analysis of StO₂%, NIR, and TWI were performed intraoperatively using the TIVITA software³⁴. HSI was performed before ligation (t = 0 min), and every 30 min for a period of 90 min (t = 30, 60, 90 min) of

ischaemia. Quantitative analysis was performed obtaining the HSI parameters by selecting 10 ROIs in the liver and in the intestine at each timepoint. Average NIR, StO₂%, and TWI preset parameters were computed within each ROI using the TIVITA software.

Biological analysis and quantification. Creatinine, pO₂, pCO₂, cHCO₃⁻, pH, and systemic lactate levels were analysed to monitor global kidney injury, overall acidosis, and lactate production. Blood was sampled through a catheter placed inside the jugular vein (18 gauge IV catheter) under ultrasound guidance and analysed with the epoc Blood Analysis System (Siemens Healthineers). Capillary lactate levels were measured using a strip-based portable lactate analyser (EDGE, ApexBio, Taipei, Taiwan; error margin 0.35 mmol/L), from blood samples obtained from the liver surface by puncturing Glisson's capsule. The order of sampling from liver segments was randomised. HSI preset parameters and capillary lactates were correlated to assess the relationship between optical properties and the actual hypoxic metabolism.

Histology. Liver biopsies were taken randomly from posterior segments. Formalin-fixed paraffin-embedded (FFPE) sections of 5 µm were stained using Harris Hematoxylin formula (Leica Biosystems) and Picro Sirius Red Stain (Sigma Aldrich) according to the manufacturers' instructions. The histopathological score was assigned by a pathologist who was blinded to the experimental conditions, creating a scoring chart similar to Suzuki's³⁵. The score was based on the following variables: (1) cell necrosis, (2) vacuolisation, (3) pale staining, (4) congestion. The score was evaluated using the following scale: (0) none, (1) mild, (2) moderate, and (3) severe.

Statistical analysis. Statistics were performed with GraphPad 8.3 (Prism, GraphPad Software, San Diego, CA, USA). Pearson's and Spearman's rho were calculated to correlate local lactates with HSI parameters. Oneway mixed-effect model ANOVA with Dunnett's multiple comparisons, Kruskal–Wallis with Dunnett's multiple comparison test and Brown Forsythe and Welch ANOVA test with Dunnett's multiple comparison test were performed accordingly with the assumption of the data distribution. Two-way ANOVA with Sidak's multiple comparisons were performed to calculate differences in continuous variables for parametric tests. Pearson's and Spearman's correlations were applied depending on the assumptions of data distribution. A two-tailed analysis with *p value* < 0.05 was considered statistically significant. Three-dimensional scatter plots were performed with MATLAB 2014a. Received: 30 July 2020; Accepted: 8 September 2020

References

1. Itri, J. N., Heller, M. T. & Tublin, M. E. Hepatic transplantation: Postoperative complications. *Abdom. Imaging* **38**, 1300–1333. <https://doi.org/10.1007/s00261-013-0002-z> (2013).
2. Ciobanu, A. O. & Gherasim, L. Ischemic hepatitis - Intercorrelated pathology. *Maedica (Buchar)* **13**, 5–11 (2018).
3. Quiroga, S. *et al.* Complications of orthotopic liver transplantation: Spectrum of findings with helical CT. *Radiographics* **21**, 1085–1102. <https://doi.org/10.1148/radiographics.21.5.g01se061085> (2001).*
4. Rethy, A., Lango, T. & Marvik, R. Laparoscopic ultrasound for hepatocellular carcinoma and colorectal liver metastasis: An overview. *Surg. Laparosc. Endosc. Percutan. Tech.* **23**, 135–144. <https://doi.org/10.1097/SLE.0b013e31828a0b9a> (2013).

-
5. de Moura Almeida, A. *et al.* Fatty liver disease in severe obese patients: diagnostic value of abdominal ultrasound. *World J. Gastroenterol.* **14**, 1415–1418, <https://doi.org/10.3748/wjg.14.1415> (2008).
 6. Lu, G. & Fei, B. Medical hyperspectral imaging: A review. *J. Biomed. Opt.* **19**, 10901. <https://doi.org/10.1117/1.JBO.19.1.010901> (2014).
 7. Jansen-Winkel, B. *et al.* Determination of the transection margin during colorectal resection with hyperspectral imaging (HSI). *Int. J. Colorectal Dis.* **34**, 731–739. <https://doi.org/10.1007/s00384-019-03250-0> (2019).
 8. Li, Q. *et al.* Review of spectral imaging technology in biomedical engineering: Achievements and challenges. *J. Biomed. Opt.* **18**, 100901. <https://doi.org/10.1117/1.JBO.18.10.100901> (2013).
 9. Wang, Q. *et al.* A hyperspectral vessel image registration method for blood oxygenation mapping. *PLoS ONE* **12**, e0178499. <https://doi.org/10.1371/journal.pone.0178499> (2017).
 10. Holmer, A., Marotz, J., Wahl, P., Dau, M. & Kammerer, P. W. Hyperspectral imaging in perfusion and wound diagnostics - Methods and algorithms for the determination of tissue parameters. *Biomed. Tech. (Berl)* **63**, 547–556. <https://doi.org/10.1515/bmt-2017-0155> (2018).
 11. Ortega, S., Halicek, M., Fabelo, H., Callico, G. M. & Fei, B. Hyperspectral and multispectral imaging in digital and computational pathology: A systematic review [Invited]. *Biomed. Opt. Express* **11**, 3195–3233. <https://doi.org/10.1364/BOE.386338> (2020).
 12. Hadoux, X. *et al.* Non-invasive in vivo hyperspectral imaging of the retina for potential biomarker use in Alzheimer's disease. *Nat. Commun.* **10**, 4227. <https://doi.org/10.1038/s41467-019-12242-1> (2019).
 13. Yoon, J. *et al.* A clinically translatable hyperspectral endoscopy (HySE) system for imaging the gastrointestinal tract. *Nat. Commun.* **10**, 1902. <https://doi.org/10.1038/s41467-019-09484-4> (2019).
 14. Wang, J. & Li, Q. Quantitative analysis of liver tumors at different stages using microscopic hyperspectral imaging technology. *J. Biomed. Opt.* **23**, 1–14. <https://doi.org/10.1117/1.JBO.23.10.106002> (2018).
 15. Urade, T. *et al.* Hyperspectral enhanced reality (HYPER) for anatomical; liver resection. *Surg. Endosc.* <https://doi.org/10.1007/s00464-020-07586-5> (2020).

-
16. Barberio, M. *et al.* HYPerspectral Enhanced Reality (HYPER): A physiology-based surgical guidance tool. *Surg. Endosc.* **34**, 1736–1744. <https://doi.org/10.1007/s00464-019-06959-9> (2020).
17. Barberio, M. *et al.* Quantitative fluorescence angiography versus hyperspectral imaging to assess bowel ischemia: A comparative study in enhanced reality. *Surgery* **168**, 178–184. <https://doi.org/10.1016/j.surg.2020.02.008> (2020).
18. Stewart, Z. A. *et al.* Increased risk of graft loss from hepatic artery thrombosis after liver transplantation with older donors. *Liver Transplant* **15**, 1688–1695. <https://doi.org/10.1002/lt.21946> (2009).
19. Pischke, S. E. *et al.* Hepatic and abdominal carbon dioxide measurements detect and distinguish hepatic artery occlusion and portal vein occlusion in pigs. *Liver Transplant* **18**, 1485–1494. <https://doi.org/10.1002/lt.23544> (2012).
20. Levesque, E. *et al.* Plasma disappearance rate of indocyanine green: A tool to evaluate early graft outcome after liver transplantation. *Liver Transplant* **15**, 1358–1364. <https://doi.org/10.1002/lt.21805> (2009).
21. Levesque, E. *et al.* Non-invasive ICG-clearance: A useful tool for the management of hepatic artery thrombosis following liver transplantation. *Clin. Transplant* **25**, 297–301. <https://doi.org/10.1111/j.1399-0012.2010.01252.x> (2011).
22. Kubota, K. *et al.* Intraoperative assessment of reconstructed vessels in living-donor liver transplantation, using a novel fluorescence imaging technique. *J. Hepatobiliary Pancreat. Surg.* **13**, 100–104. <https://doi.org/10.1007/s00534-005-1014-z> (2006).
23. Skowno, J. J., Karpelowsky, J. S., Watts, N. R. & Little, D. G. Can transcutaneous near infrared spectroscopy detect severe hepatic ischemia: A juvenile porcine model. *Paediatr. Anaesth.* **26**, 1188–1196. <https://doi.org/10.1111/pan.13004> (2016).
24. Diana, M. Enabling precision digestive surgery with fluorescence imaging. *Transl. Gastroenterol. Hepatol.* **2**, 97. <https://doi.org/10.21037/tgh.2017.11.06> (2017).
25. Nachabe, R. *et al.* Effect of bile absorption coefficients on the estimation of liver tissue optical properties and related implications in discriminating healthy and tumorous samples. *Biomed. Opt. Express* **2**, 600–614. <https://doi.org/10.1364/BOE.2.000600> (2011).
26. Eipel, C., Abshagen, K. & Vollmar, B. Regulation of hepatic blood flow: The hepatic arterial buffer response revisited. *World J. Gastroenterol.* **16**, 6046–6057. <https://doi.org/10.3748/wjg.v16.i48.6046> (2010).

-
27. Lauth, W. W. in *Hepatic Circulation: Physiology and Pathophysiology Colloquium Series on Integrated Systems Physiology: From Molecule to Function to Disease* (ed New York: Raven Press) 203–226 (1981).
28. Haugaa, H. *et al.* Early bedside detection of ischemia and rejection in liver transplants by microdialysis. *Liver Transplant* **18**, 839–849. <https://doi.org/10.1002/lt.23425> (2012).
29. Halicek, M., Fabelo, H., Ortega, S., Callico, G. M. & Fei, B. In-vivo and ex-vivo tissue analysis through hyperspectral imaging techniques: Revealing the invisible features of cancer. *Cancers (Basel)* **11**, <https://doi.org/10.3390/cancers11060756> (2019).
30. Lauth, W. W., Schafer, J. & Legare, D. J. Hepatic blood flow distribution: Consideration of gravity, liver surface, and norepinephrine on regional heterogeneity. *Can. J. Physiol. Pharmacol.* **71**, 128–135. <https://doi.org/10.1139/y93-018> (1993).
31. Kilkenny, C. *et al.* Animal research: Reporting in vivo experiments: the ARRIVE guidelines. *Br. J. Pharmacol.* **160**, 1577–1579. <https://doi.org/10.1111/j.1476-5381.2010.00872.x> (2010).
32. Barberio, M. *et al.* Quantitative fluorescence angiography versus hyperspectral imaging to assess bowel ischemia: A comparative study in enhanced reality. *Surgery* <https://doi.org/10.1016/j.surg.2020.02.008> (2020).
33. Uchida, M. *et al.* Calcium in pig livers following ischemia and reperfusion. *J. Hepatol.* **20**, 714–719. [https://doi.org/10.1016/s0168-8278\(05\)80140-0](https://doi.org/10.1016/s0168-8278(05)80140-0) (1994).
34. Kulcke, A. *et al.* A compact hyperspectral camera for measurement of perfusion parameters in medicine. *Biomed. Tech. (Berl)* **63**, 519–527. <https://doi.org/10.1515/bmt-2017-0145> (2018).
35. Suzuki, S., Toledo-Pereyra, L. H., Rodriguez, F. J. & Cejalvo, D. Neutrophil infiltration as an important factor in liver ischemia and reperfusion injury. Modulating effects of FK506 and cyclosporine. *Transplantation* **55**, 1265–1272, <https://doi.org/10.1097/00007890-199306000-00011> (1993).

This study was funded by the ARC Foundation for Cancer Research (9 Rue Guy Môquet, 94803 Villejuif, France) through the ELIOS (Endoscopic Luminescent Imaging for precision Oncologic Surgery) grant and partly by the ANR (National Research Agency) through the LiverSURG grant (ANR-18-CE19-0026).

ii) Ischemia-reperfusion injury assesement

We evaluated hte liver viability in a hepatic artery occlusion model with an artificial intelligence-based analysis of HSI. We have combined the potential of HSI to extract quantitative optical tissue properties with a deep learning-based model using convolutional neural networks. The artificial intelligence (AI) score of liver viability showed a significant correlation with capillary lactate from the liver surface ($r = -0.78$, $p = 0.0320$) and Suzuki's score ($r = -0.96$, $p = 0.0012$). CD31 immunostaining confirmed the microvascular damage accordingly with the AI score. Our results ultimately showed the potential of an HSI-AI-based analysis to predict liver viability, thereby prompting for intraoperative tool development to explore its application in a clinical setting. My personal contribution to this study was participation to the study design, operative procedures on animal models, revision of results and writing and revision of the manuscript.

Article

Published in: **Diagnostics (2021)**

Diagnostics (Basel) 2021 Aug 24;11(9):1527.doi: 10.3390/diagnostics11091527.

Automatic Liver Viability Scoring with Deep Learning and Hyperspectral Imaging

Eric Felli 1,2,3,* , Mahdi Al-Taher 4, Toby Collins 4, Richard Nkusi 4 , **Emanuele Felli** 5 , Andrea Baiocchini 6, Veronique Lindner 7 , Cindy Vincent 2, Manuel Barberio 8 , Bernard Geny 3, Giuseppe Maria Ettorre 9, Alexandre Hostettler 4, Didier Mutter 5, Sylvain Gioux 10, Catherine Schuster 11, Jacques Marescaux 4 , Jordi Gracia-Sancho 1,12 and Michele Diana 4,12

1 Hepatology, Department of Biomedical Research, Inselspital, University of Bern, 3008 Bern, Switzerland;jordi.gracia@idibaps.org

2 IHU-Strasbourg, Institute of Image-Guided Surgery, 67000 Strasbourg, France; cindy.vincent@ihu-strasbourg.eu

3 Institute of Physiology, EA3072 Mitochondria Respiration and Oxidative Stress, University of Strasbourg,67000 Strasbourg, France; bernard.geny@chru-strasbourg.fr

4 Research Institute against Digestive Cancer (IRCAD), 67000 Strasbourg, France; mahdi.al-taher@ircad.fr (M.A.-T.); toby.collins@ircad.fr (T.C.); ricardonkusi@gmail.com (R.N.);

alexandre.hostettler@ircad.fr (A.H.); jacques.marescaux@ircad.fr (J.M.); michele.diana@ircad.fr (M.D.)

5 Department of General, Digestive, and Endocrine Surgery, University Hospital of Strasbourg, 67000 Strasbourg, France; emanuele.felli@chru-strasbourg.fr (E.F.); d.mutter@ircad.fr (D.M.)

6 Department of Pathology, San Camillo Forlanini Hospital, 00152 Rome, Italy;baiocchiniandrea@gmail.com

7 Department of Pathology, University Hospital of Strasbourg, 67000 Strasbourg, France; veronique.lindner@chru-strasbourg.fr

8 Department of General Surgery, Cardinale Giovanni Panico Hospital, 73039 Tricase, Italy; manuel.barberio@ircad.fr

9 San Camillo Forlanini Hospital, Department of Transplantation and General Surgery, 00152 Rome, Italy; GmEttorre@scamilloforlanini.rm.it

10 Photonics Instrumentation for Health, iCube Laboratory, University of Strasbourg, 67000 Strasbourg, France; sgioux@unistra.fr

11 INSERM, Institute of Viral and Liver Disease, U1110, 67000 Strasbourg, France;
catherine.schuster@unistra.fr

12 Liver Vascular Biology, IDIBAPS Biomedical Research Institute and CIBEREHD,
08036 Barcelona, Spain

* Correspondence: eric.felli@dbmr.unibe.ch; Tel.: +41-3-1632-3598

Abstract:

Hyperspectral imaging (HSI) is a non-invasive imaging modality already applied to evaluate hepatic oxygenation and to discriminate different models of hepatic ischemia. Nevertheless, the ability of HSI to detect and predict the reperfusion damage intraoperatively was not yet assessed. Hypoxia caused by hepatic artery occlusion (HAO) in the liver brings about dreadful vascular complications known as ischemia-reperfusion injury (IRI). Here, we show the evaluation of liver viability in an HAO model with an artificial intelligence-based analysis of HSI. We have combined the potential of HSI to extract quantitative optical tissue properties with a deep learning-based model using convolutional neural networks. The artificial intelligence (AI) score of liver viability showed a significant correlation with capillary lactate from the liver surface ($r = -0.78$, $p = 0.0320$) and Suzuki's score ($r = -0.96$, $p = 0.0012$). CD31 immunostaining confirmed the microvascular damage accordingly with the AI score. Our results ultimately show the potential of an HSI-AI-based analysis to predict liver viability, thereby prompting for intraoperative tool development to explore its application in a clinical setting.

Keywords: liver viability; artificial intelligence; deep learning; convolutional networks; CNNs; hyperspectral imaging; hepatic artery occlusion

1. Introduction

During the last decade, hyperspectral imaging (HSI) has gained importance in the biomedical field [1–3]. HSI systems aim to build images based on the computational analysis of light-tissue interactions through the detection of relative reflectance. This allows for the quantification of organic compounds such as oxygenated and deoxygenated hemoglobin at different depths in a wide large field of view [4]. Recently applied for the quantitative analysis of liver perfusion assessment [1,5], HSI was also used for the study of arterial perfusion [6–11]. Hypoxia produced by the occlusion of arterial flow causes severe time-dependent complications. For instance, hepatic artery occlusion (HAO) is a dreadful vascular event, which can occur in different clinical scenarios such as hepatic artery thrombosis, hepatic artery ligation during liver surgery, emboli, arterial abnormalities, eclampsia, and sickle cell crisis. Oxygen deprivation is the starting event that induces parenchymal damage, which is further aggravated once blood circulation has been re-established by the ischemia-reperfusion injury mechanism (IRI) [12,13]. IRI is associated with a massive injury to hepatocytes even when diagnosed in the early phase (within 2 h) [14–16]. When the occlusion of the hepatic artery occurs, despite its dual vascular inflows, the liver goes under global hypoxia since the hepatic artery contributes ~50% of the oxygen supply. The portal flow alone is insufficient to prevent the occurrence of anaerobic metabolism, which can be rapidly evaluated with the analysis of capillary and systemic lactate concentration [17,18]. Consequently, warm ischemia like cold ischemia disrupts the microcirculation downregulating the sinusoidal protective phenotype [19–21].

As a result, liver perfusion assessment is an essential target for the diagnosis of hepatic hypoxia in both ischemic types.

Intraoperative Doppler ultrasonography (US) is the standard tool for an immediate evaluation of the HAO, followed by a daily US in combination with transaminase control until postoperative day 5 or 7. If hepatic artery thrombosis (HAT) is suspected, a contrastenhanced

CT scan or less often a magnetic resonance scan is performed to confirm the diagnosis. If US and CT or magnetic resonance do not detect HAT, angiography may be helpful [22]. However, all these techniques have some drawbacks. As a matter of fact, they are time-consuming, they require a long-term learning curve, and their interpretation may vary. Additionally, in the case of arterial revascularization, it is not possible to predict the future graft function and the potential consequences of IRI damage. Early detection or, ideally, intraoperative prediction of graft dysfunction or failure would be crucial for timely treatment.

The ongoing research to predict IRI has considered various solutions. They include indocyanine green (ICG) fluorescence imaging, near-infrared spectroscopy (NIRS), microdialysis, and carbon dioxide sensors [23–28]. However, such methods are limited by the need for the administration of an exogenous dye, and/or by some degree of invasiveness. In addition, these approaches do not provide a direct oxygenation map of the organ, which could allow for an immediate localization of liver ischemic damage. Recently, our group has demonstrated the potential usefulness of HSI as an intraoperative tool during

image-guided liver surgery [29]. In particular, HSI could intraoperatively quantify, discriminate, and visualize different types of liver ischemia, including HAO and total vascular inflow occlusion [30]. We are currently working on exploring the potential of HSI coupled with deep learning-based analysis of HS images to intraoperatively predict the ischemia-reperfusion damage. As a first step and a proof of concept, we focused on the ability of HSI to predict damage given by liver hypoxia ligating only the hepatic artery [31].

This allowed us to exclude only the oxygen variable without the more complex composition of blood supply from the portal vein. Machine learning has recently been used for the automatic analysis of hyperspectral image data [32], mainly driven from the remote sensing community [33,34], but now extending to a range of medical applications [1] such as automatic tumor detection [35,36] and histopathological analysis [37]. However, there have not been prior studies reporting on the use of machine learning models to automatically characterize liver reperfusion damage intraoperatively in a large field of view. Our hypothesis is that machine learning models can be trained to automatically recognize the optical properties associated with the reperfusion damage given by HAO in HSI images using supervised learning. Consequently, a predictive AI analysis can be built to provide an automatic convenient and non-invasive tool for intraoperative ischemic liver disease detection.

2. Materials and Methods

2.1. Study Design

Sample size calculation was performed using the correlation between optical and biological data. The calculation was based on previous publications on bowel ischemia which showed a correlation coefficient of ≈ 0.7 [38,39]. The required sample size in terms of paired values was 4, considering $\alpha = 0.05$ with a power $(1 - \beta) = 0.9$. In the present study, 42 paired values StO₂% and lactates values were obtained in 5 pigs in total. The AI model used a pixel by pixel (640 \times 480) analysis per each of the 42 images providing a large dataset elaboration. The aim of the study was to predict liver viability through the analysis of hyperspectral images using artificial intelligence based on convolutional neural networks (CNNs) to (i) discriminate the liver from the rest of the tissues, (ii) recognize perfused from the non-perfused liver, (iii) predict the level of liver perfusion during the reperfusion phase, and (iv) predict biological data (Figure 1a–c). The control group is represented by the same treated pigs before hepatic artery ligation. The ischemic phase was held for 90 min, collecting optical and biological data every 30 min (Figure 1a,b). The following reperfusion phase was monitored for 5 h, collecting data every hour. The hypercube extracted from hyperspectral images was used to train two CNNs (Figure 1c). Finally, the generated AI score for the reperfusion phase was generated and the quantitative analysis of hyperspectral images was correlated with biological data. Histopathological evaluation and scoring were performed in a blinded fashion. Capillary lactate was sampled randomly through the liver surface.

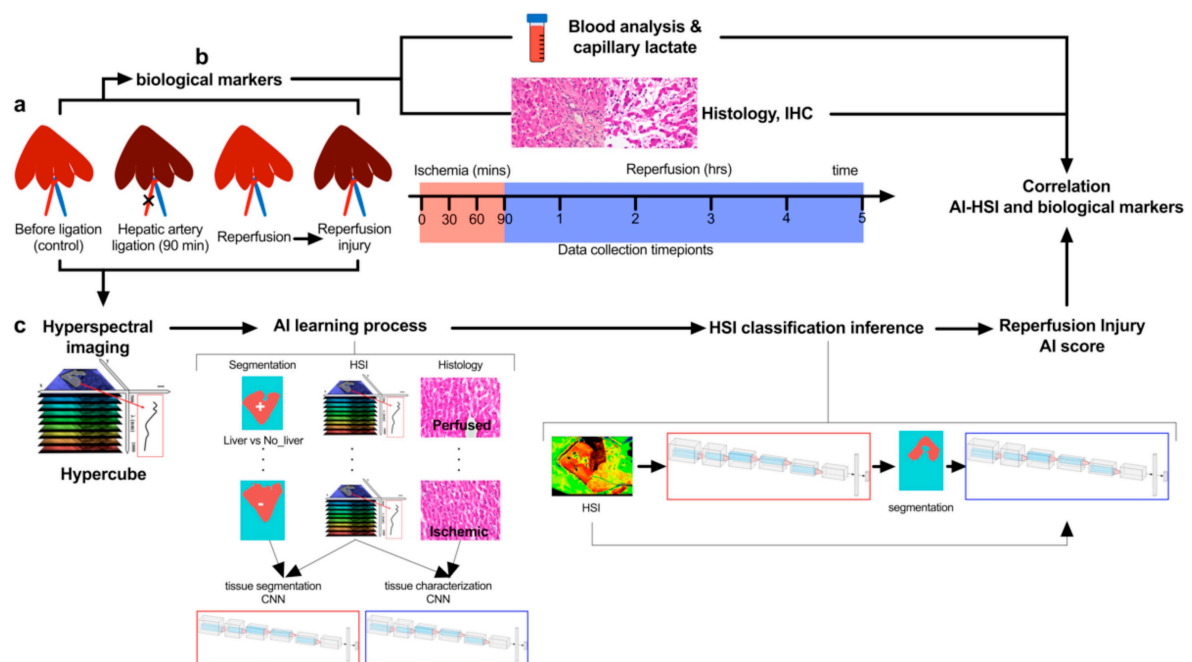


Figure 1. Experimental workflow. (a) Hepatic artery occlusion (HAO) was performed for 90 min followed by a reperfusion phase of 5 h. (b) During ischemia and reperfusion time, biological data and hyperspectral imaging (HSI) were sampled. (c) Hyperspectral imaging was acquired providing the hypercube with a wavelength range from 500 to 1000 nm. Two artificial intelligence-based convolutional neural networks (CNNs) were trained to perform a segmentation that could identify the liver surface and analyze the same surface to predict perfused and not perfused livers during the ischemia phase. Finally, the tissue classification produced by the CNNs was used to create a score of liver viability during the reperfusion phase. While StO₂% and NIR% are calculated with the preset algorithm of the HSI (TIVITA software), the AI score is calculated over the whole spectra using the hypercube.

2.2. Animals

The present study, which is part of the ELIOS project (Endoscopic Luminescent Imaging for Oncology Surgery), was approved by the local Ethical Committee on Animal Experimentation (ICOMETH No. 38.2016.01.085), as well as by the French Ministry of Superior Education and Research (MESR) (APAFIS#8721-2017013010316298-v2). The experimental procedure followed the general indications already published in the protocol

exchange [40]. All animals used in the experiment were managed according to French laws for animal use and care, and according to the directives of the European Community Council (2010/63/EU) and ARRIVE guidelines [41]. Five adult male swine (*Sus scrofa* ssp. *domesticus*, mean weight: 32.4 ± 4.4 kg) were housed and acclimatized for 48 h in an enriched environment, respecting circadian cycles of light-darkness, with constant humidity and temperature conditions. They were fasted 24 h before surgery, with ad libitum access to water, and finally sedated (zolazepam + tiletamine 10 mg/kg IM) 30 min before the procedure to decrease stress. Anesthesia was performed intravenously (18-gauge IV catheter in-ear vein) with Propofol 3 mg/kg and maintained with rocuronium 0.8 mg/kg along with inhaled isoflurane 2% via the automatic standard respiratory system. Vital parameters were monitored through a mechanic ventilator machine. Heartbeat was monitored with a pulse oximeter (Mindray PM-60). At the end of the protocol, animals were euthanized with a lethal dose of pentobarbital (40 mg/kg).

2.3. Surgical Procedure

Midline laparotomy and hepatic pedicle dissection were performed to isolate the hepatic artery. The artery was then ligated with a 3/0 braided suture for 90 min to obtain a model of warm ischemia [42]. The ligature was removed for 5 h in order to observe the reperfusion injury between the early and the beginning of the late stage [43].

2.4. Hyperspectral Imaging

A CMOS push-broom scanning hyperspectral camera (TIVITA, Diaspective Vision GmbH, Am Salzhaff Germany) was used to generate HS images which were performed with a camera-specific software module from the same company. The three-dimensional hypercube is composed of a spatial resolution (x,y) plus a third dimension with the relative reflectance of each pixel (z). The range of the wavelength detected is 500–1000 nm with a 5 nm interval, totaling 100 wavelengths for every pixel. The scanning method is allowed through a slit-shaped aperture motorized with an internal stepper motor [44]. The resolution of the hypercube is 640 × 480 pixels × 100 wavelengths. The acquisition is performed at ~40 cm of distance from the sample and monitored by a distance sensor Bluefruit Feather nRF52832 with Adafruit VL53LOx device (Adafruit, New York, NY, USA) orthogonal to the liver surface. The light source is composed of 6 halogen lamps of 20 W (OSRAM Halospot 70, OSRAM GmbH, Munich, Germany). The HS camera takes ~6 s to perform the acquisition of the hypercube which is transferred to a PC where it is processed creating pseudo-color images. The device used in this experiment provides different algorithms (preset), that quantify the relative oxygen saturation (StO₂%) of the microcirculation at a depth of ~1 mm, and at deeper layers with the near-infrared (NIR) spectrum (3–5 mm) [4]. Quantitative analysis of the StO₂% and NIR index was performed intraoperatively using the TIVITA Suite software module over the whole liver surface. The methods and algorithms of the TIVITA system were explained in more detail by Holmer et al., in 2018 [4]. Briefly, StO₂% is calculated with an algorithm based on the second derivative of the

absorption spectra (570–590 nm and 740–780 nm). The NIR perfusion index is calculated with the absorbance spectra in a spectral range of 655–735 nm and 825–925 nm.

2.5. Artificial Intelligence-Based Analysis

2.5.1. Overview

Two CNNs were created to perform an automatic HS image analysis (Figure S3). The first CNN was trained to automatically recognize liver tissue in any HS image. We refer to this as the organ segmentation CNN. The second CNN was trained to automatically characterize liver tissue which has been recognized by the organ segmentation CNN into two classes, namely perfused and ischemic liver. We refer to this as the tissue characterization CNN (Figure 1c).

2.5.2. Organ Segmentation CNN and Post-Segmentation Filtering

The organ segmentation CNN operated as follows. For each spatial coordinate (x,y) in the HS image, an HS subvolume centered at (x,y) with a spatial window of 5×5 pixels was extracted. The subvolume had the following dimensions: $5 \times 5 \times 100$, with two spatial dimensions and one wavelength dimension of 100 bands. The subvolume was then passed to the organ segmentation CNN, which outputted a binary classification value. Either a value of +1 (positive) or -1 (negative) was outputted, corresponding to a prediction of a liver or non-liver structure occurring at a spatial location (x,y) respectively. Predictions were made for all spatial locations, generating a spatial map (also known as a segmentation mask). Finally, post-segmentation filtering was performed to eliminate spurious regions in

the segmentation masks (typically produced by specular reflections). This was achieved with a connected component analysis to identify the largest region in the segmentation mask, and all positive pixels which did not belong to this largest region were then removed. This filtration stage eliminated small positive ‘islands’ in the segmentation mask which are morphologically unlikely to be liver tissue. Secondly, any small holes that were present in the segmentation mask were automatically filled using the image morphological operations with OpenCV (<https://opencv.org/>, accessed on 1 March 2021). An example of a segmentation mask before and after the filtering stages is shown in Figure S2a.

2.5.3. Tissue Characterization CNN

All positive spatial locations within the segmentation mask were then processed by the tissue characterization CNN. This computed a binary classification where +1 indicated ischemic and -1 indicated healthy liver respectively at each spatial location. Analogous to the organ segmentation CNN, its input is a sub-volume extracted from the HS image of 5 x5 x100 in size, centered at a given spatial location. Classification was performed for all spatial locations, generating a tissue characterization mask. Finally, a single ischemic score for each image was computed by taking the proportion of pixels with positive detections divided by the total number of pixels in the segmentation mask.

2.5.4. CNN Design and Implementation

The two CNNs have identical architecture and they are based on a state-of-the-art 3D CNN [45]. Architecture version 6 from reference 60 was selected because it is a relatively small CNN, so it can be trained with small datasets, yet it can also learn effective multiscale spatio-spectral segmentation features in HSI data. This was demonstrated by its good performance for segmenting remote sensing HSIs with limited data, The CNN is organized such that in early layers, 3D spatio-spectral feature maps are produced, which are then reduced to 1D feature vectors, and then finally processed by a fully connected layer. Network parameters are significantly reduced using ideas from SqueezeNet (<https://arxiv.org/abs/1602.07360>, accessed on 1 March 2021) [46], using a small number of filters combined with 1D convolutions along the spectral dimension in the pooling phase. We illustrate the architecture in Supplementary Figure S3. Layer 1 is a 3D convolution with 20 output channels. Layer 2 is a 1D convolution along the spectral dimension with pooling using a stride of 2. Layers 3 and 4 replicate layers 1 and 2 with 35 output channels. Layers 5 and 6 are 1D convolutions with pooling to further reduce the spectral dimension.

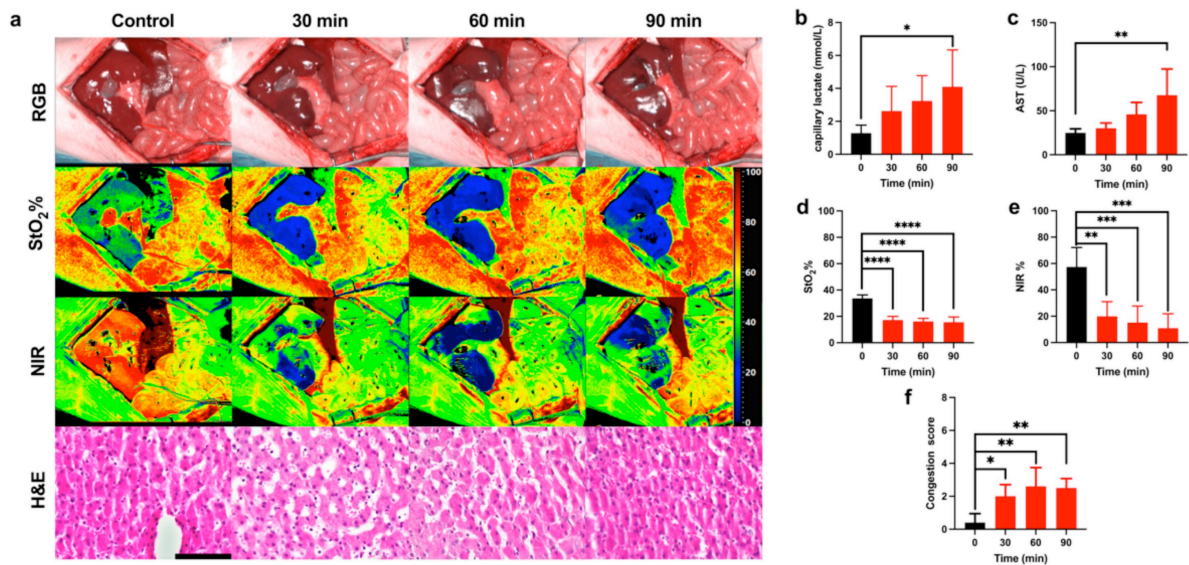


Figure 2. Ischemic phase evaluation. (a) RGB, HSI, and H&E images of the liver during the ischemic phase. Hyperspectral images of StO₂% and NIR% showed an oxygenation decrease during the ischemic phase. H&E images show the gradual congestion increase. (b,c) Capillary lactate (n = 5) and AST (n = 4) levels indicated a gradual liver impairment. (d,e) Both preset software parameter indexes of the oxygenation showed a significant decrease in oxygen levels. (f) The histopathological score of congestion was significant during the ischemic phase. Data are compared to the control, ns p > 0.05, * p < 0.05, ** p < 0.01, *** p < 0.001, **** p < 0.0001 (n = 5). Histology photos were taken with a Leica DM2000 LED microscope, magnification 40_x, scale bar 100 _μm.

The training was performed and implemented in Pytorch using as follows. The HSI images used for training were first concatenated vertically to form a single HSI image, denoted by the HSI image I. The training label images were similarly concatenated to form a single training label image L. The values in L were either +1 (indicating liver), -1 (indicating non-liver), or 0 (indicating a spatial location that was close so close to the border of the liver that its label could not be determined by the annotator thanks to optical blurring around the liver border. Only pixels labeled +1 or -1 were used for training. Class-balanced binary cross-entropy was used as the loss function, implemented by inverse median weighting.

Specifically, the loss of each class $i \in \{-1, +1\}$ was weighted by the value m_i where f_i denotes the proportion of pixels labeled as class i in L and $m = 12 (f_{-1} + f_{+1})$. The CNN weights were initialized with Kaiming initialization [47] and biases were initialized to zero. At each training epoch, a batch of $5 \times 5 \times 100$ subvolumes were randomly selected without replacement from I . Each subvolume was positioned in I such that its center was at a random spatial location in I and whose label in L was either -1 or $+1$. A batch size of 8192 was used. The CNN parameters were updated from each batch with stochastic gradient descent (SGD) using the implementation from Pytorch's "torch.optim" package with a learning rate of 0.01 and a weight decay (L2 regularization) of 0.0005. The training was terminated after 2000 epochs. The time to train was approximately 13 h using a server (DGX 1 equivalent, Nvidia cooperation). The time to train all 5 CNNs for each cross-validation was approximately 65 h.

The tissue characterization CNN was trained in practically the same manner as the organ segmentation CNN. Specifically, all training parameters and processes were identical, and the sole difference was the construction of the training data. LOPOCV was also used where for each animal, one tissue characterization CNN was trained using HSI data from all other animals (4 images per animal corresponding to times 0 min, 30 min, 60 min, and 90 min). Its predictive performance was then evaluated on the 4 images from the held-out animal. The histology score (congestion score) together with the surgical procedure was used as the ground truth. The HSI images used for training were concatenated vertically to form a single HSI image I_0 with a corresponding label image L_0 . A value of $L_0(x,y) = +1$ was

used if the pixel at spatial location (x,y) was annotated as liver and the liver was determined as ischemic from the histology score. A value of $L0(x,y) = 1$ corresponded with an annotated liver pixel that was determined to be healthy from the histology score. A value of $L0(x,y) = 0$ corresponded to all other pixels, and those pixels were not used during training. The training was then performed exactly as described for training the organ segmentation CNN. *

2.6. Blood Analysis

Blood for systemic lactate and liver function was sampled through a central catheter placed in the jugular vein (6 French IV catheter). Capillary lactate was analyzed by puncturing Glisson's capsule with a randomized selection of liver segments. Capillary and systemic lactates were measured using a strip-based portable lactate analyzer, which presents a margin error of 0.35 mmol/L (EDGE, ApexBio, Taipei, Taiwan). The correlation analysis of the data was performed between HSI parameters and capillary lactate concentration. The surgical intervention was monitored to rule out any bias in the hepatic ischemic phase by means of systemic blood gas analysis (BGA) with the epoc Blood Analysis System (Siemens Healthineers, Henkestr, Germany) to measure pO_2 , pCO_2 , pH, glucose, creatinine, urea, and BUN. Liver functionality was assessed by means of aspartate aminotransferase (AST), alanine aminotransferase (ALT), prothrombin time (PT), gamma glutamyl-transferase (GGT), alkaline phosphatase (ALP), total protein (TP), and albumin analysis. Liver injury after the reperfusion phase was assessed also via AST and ALT.

2.7. Histology

Liver biopsies were randomly taken with a 16 G biopsy gun (Temno Biopsy System, Galway, Ireland) from the posterior segments at each timepoint. Sections of 5 μ m were taken from formalin-fixed paraffin-embedded blocks and were dewaxed and rehydrated prior to staining at room temperature. A treatment with hematoxylin Harris' formula (Leica Biosystems, Muttenz, Switzerland) for 10 min and then a wash in acid alcohol for 2 s and in tap water for 2 min were performed. Eosin staining with Eosin 0.5% (Leica Biosystems, Muttenz, Switzerland) for 3 min was performed before washing in tap water for 30 s. Finally, the sections were dehydrated with ethanol 100% and placed in xylene until their mounting with coverslips. A semi-quantitative blinded analysis was performed by a pathologist using Suzuki's criteria [48].

2.8. Immunohistochemistry Staining

Sections were fixed in 10% neutral buffered formalin (NBF) and processed for histological examination, which included paraffin embedding, sectioning, and staining with hematoxylin and eosin. Sections from selected paraffin blocks for each specimen were used for immunohistochemical analysis. Slides of 4 μ m-thick tissue sections were incubated at room temperature in an antigen retrieval process (EDTA citrate buffer, pH 8.3, CC1 buffer), revealed with 'Ultra View' Universal DAB Detection Kit and counterstained with a

hematoxylin solution (Ventana Roche Systems, München, Germany). They were treated on automated VENTANA-Benchmark-XT with CD31 (rabbit monoclonal, EP78 clone, Microm; pre-treatment: CC1 36 min; dilution: 1/200 during 32 min).

2.9. Confocal Endomicroscopy

Confocal endomicroscopy was performed on the anterior surface (the same analysed via HSI) of Glisson's capsule at the end of the procedure. This test evaluated blood microcirculation and arterial supply in randomly selected segments with Cellvizio pCLE system (Mauna Kea Technologies, Paris, France). Confocal images were obtained by intravenously injecting 2 mL of sodium fluorescein (Fluocyne, Serb, Paris, France).

2.10. Statistical Analysis

Statistics were performed using GraphPad 8.3 (GraphPad Software, San Diego, CA, USA). A Spearman's and Person's rho were analyzed to perform the correlation between optical and biological data. All data were expressed as means \pm s.d. One-way ANOVA with Dunnett's multiple comparisons was performed for parametric tests to calculate differences in continuous paired variables. The Friedman test with Dunn's multiple comparison test was applied for paired non-parametric tests. A two-tailed p-value < 0.05 was considered statistically significant. One-tailed significant p-value < 0.05 was applied to the confusion

matrix in the correlation between the AI score and biological data, considering that the correlation among these values was physiologically possible only in one direction.

2. Results

3.1. Ischemic Phase

The surgical intervention was performed under general anesthesia with continuous monitoring of vital parameters (Figure S1). No significant impairments of vital parameters were found during the ischemic phase. However, a significant change in urea and blood urea nitrogen (BUN) was found, although the creatinine level showed no significant changes (Figure S1a–o). HSI images showed an oxygenation decrease in both indexes (StO₂% and NIR%) during the ischemic phase, in congruence with the histological assessment (Figure 2a). Before ligation, the perivenular region presented a regular hepatocellular muralium without any ischemic morphological alteration. After 90 min of ischemia, the parenchyma was characterized by weaker staining in some of the hepatocytes' cytoplasm, which appeared pale with a reduced volume and hyperchromatic nuclei. Capillary lactate and AST showed a significant increase after 90 min of ischemia (4.1 +/- 2.23 mmol/L, p = 0.0102 and 67.50 +/- 29.89 U/L, p = 0.0061 respectively) (Figure 2b,c). The quantitative analysis of StO₂% and NIR% showed a significant decrease with a minimum at 90 min (15.57 +/- 3.98%, p < 0.0001 and 10.90 +/- 11.00%, p < 0.001 respectively) (Figure 2d,e). The ischemic phase was confirmed by the congestion score, which was significantly higher with a plateau phase and a maximum at 60 min (2.5 +/-

0.577 a.u., $p = 0.0015$) (Figure 2f). A convolutional neural network (CNN) was trained to automatically classify each pixel of HS images into two classes: liver tissue and non-liver tissue/other structures (called liver segmentation CNN) (Figures 3a–c and S2a). The performance of liver segmentation CNN was measured with HSI images from the control and ischemic phases using leave-one patient-out cross-validation (LOPOCV). Class predictions (labels) were made for each pixel in each HS image, and predictions from all images and all pixels were combined to produce a normalized confusion matrix (Figure 3d). A sensitivity of 0.993 and a specificity of 0.997 were achieved (top left and bottom right entries in the confusion matrix respectively), showing that the CNN could very accurately discriminate liver tissue from other organs in all images.

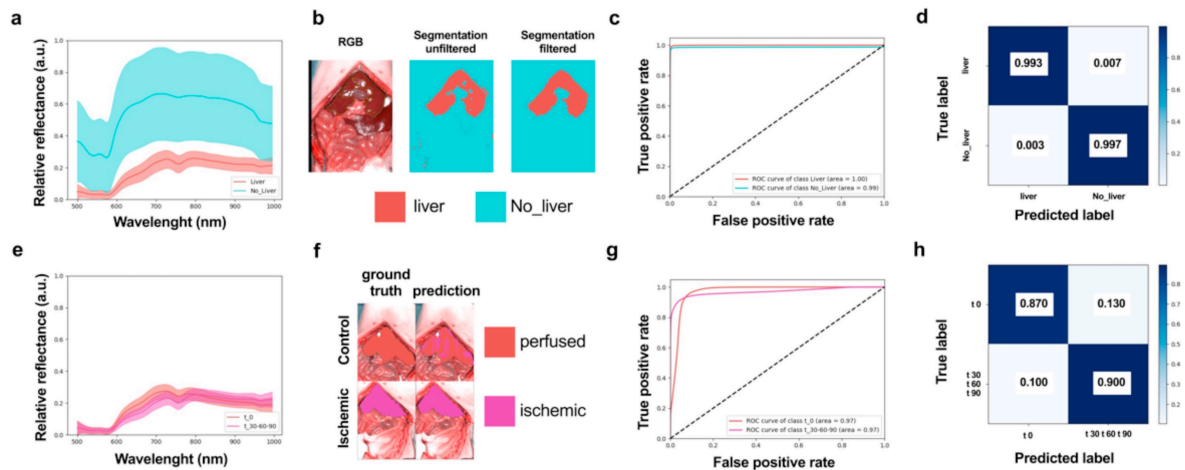


Figure 3. AI-based training and evaluation in the ischemic phase. (a) Liver and non-liver spectral distributions showing mean (central curve) and 1 s.d. (region). (b) Visualization of automatic tissue segmentation of liver and non-liver classes with and without post-segmentation filtration. (c) Receiver operator characteristic (ROC) curves corresponding to liver and non-liver classes, showing the trend

relationship between false positive and true positive rates. **(d)** Confusion matrix showing specificity and sensitivity of tissue segmentation CNN. **(e)** Spectral distributions of perfused and ischemic classes. **(f)** Visualization of tissue automatic tissue characterization results with two classes (perfused and ischemic). **(g)** ROC curves of tissue characterization CNN showing the relationship between false positive and true positive rates. **(h)** Confusion matrix showing specificity and sensitivity of tissue characterization. (n = 5).

by the tissue characterization CNN to automatically predict if the liver was perfused or ischemic (Figure 3e–g). Predictions were accumulated for all pixels and all HS images, and performance was evaluated with a normalized confusion matrix (Figure 3h). This shows a strong potential of the tissue characterization CNN to discriminate between perfused and ischemic liver during the surgical procedure with high sensitivity (0.870) and specificity (0.900). CNN predictions (AI score) were coherent with the experimental workflow. Indeed, the ischemic phase was significantly lower after 30 min of occlusion when compared to the control, and this difference was maintained after 60 and 90 min ($p < 0.0001$ for all timepoints) (Figure S2b,c).

3.2. Reperfusion Phase

CNNs were evaluated on each reperfusion HS image using LOPOCV. The workflow was identical to the processing of the HS images in the control and ischemic phases. First, the liver recognition CNNs detected pixels belonging to the liver, and these were then processed by the tissue characterization CNN to assess perfused or ischemic liver pixels. For each HS image in control and reperfusion phases, a global perfusion AI score was computed as the proportion of detected perfused pixels as compared to the total number of detected liver pixels. A prediction score of 0 indicated total ischemia and 1 indicated total perfusion. The scores for all pigs and timepoints are visualized in Figure 4a,b. The

prediction score showed a common outcome for pigs 1, 2, and 3 (Figure 4a). The score decreased gradually with a minimum value at 5 h of reperfusion (0.246, 0.222, 0.009 a.u. respectively for pig 1,2,3) (Figure 4b). Pig 4 died after 2 h of reperfusion with a score of 0.003; pig 5 had the highest score of 0.959 at the end of the procedure, similar to the control (0.940). Pigs 3 and 5 showed an opposite outcome after 5 h of reperfusion. StO₂% and NIR% parameters were lower in pig 3 and higher in pig 5 (8.14 ± 0.97, 38.32 ± 6.59 StO₂% and 0.04 ± 0.86, 47.20 ± 6.90 NIR%) (Figure 4c,d). Suzuki's score presented a maximum in pig 3 and a minimum in pig 5 (4.0 and 1.3 a.u. respectively) similarly to the AI score (Figure 4e).

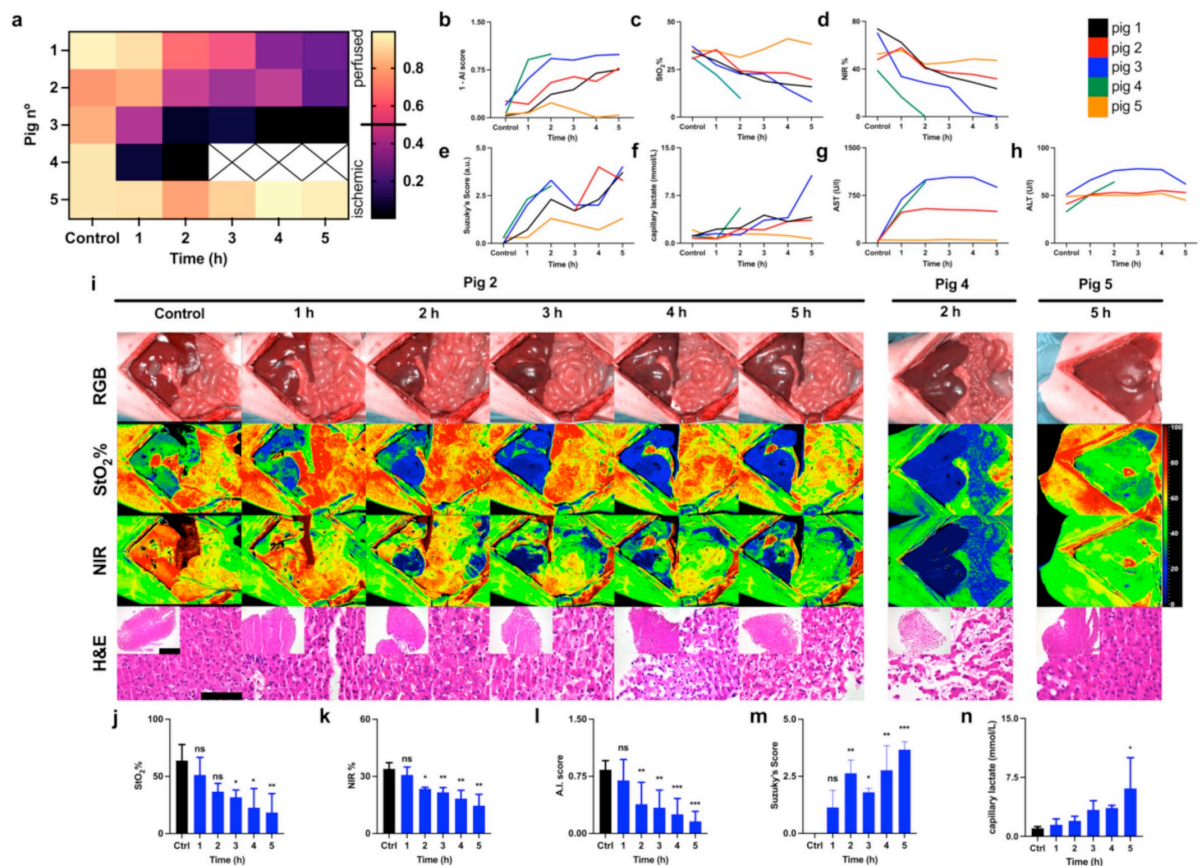


Figure 4. Reperfusion phase. **(a)** Automatic AI score of liver viability for each pig for control and reperfusion times. **(b)** Visualization of AI scores for each pig as a function of time (y-axis was flipped to provide a better visual comparison with Suzuki's score **(c,d)** StO₂% and NIR indexes (n = 5). **(e)** Suzuki's score (n = 5). **(f)** Capillary lactate (n = 5). **(g)** AST (n = 4). **(h)** ALT (n = 4). **(i)** HSI images and H&E images. Pig 2 showed a gradual parenchymal disruption; pig 4 died after 2 h, HSI and H&E showed tissue ischemia and parenchymal disruption respectively. Pig 5 was healthy at the end of the procedure; here, HSI showed a perfused liver and H&E confirmed normal parenchyma. Pigs 1, 2, 3 were grouped (n = 3). **(j,k)** Indexes of StO₂% and NIR showed a significant decrease together with **(l)** the AI score. **(m)** Suzuki's score and **(n)** capillary lactates showed an opposite significant trend. Data are compared to the control, ns p > 0.05, * p ≤ 0.05, ** p ≤ 0.01, *** p ≤ 0.001, (n = 5). Histology photos were taken with a Leica DM2000 LED microscope, magnification 40_ and 10_ scale bars 100_μm and 200_μm respectively.

Save from pig 5, all pigs showed a gradual damage increase. Capillary lactate was higher in pig 3 and lower in pig 5 (10.60 and 0.70 mmol/L respectively) (Figure 4f). Similarly, AST and ALT were high in pig 3 (879.00 U/L, AST, 62.00 U/L, ALT) and low in pig 5 (46.00 U/L, AST, 45.00 U/L, ALT) (Figure 4g,h). In RGB images, which closely correspond to the human eye evaluation, global color changes were slightly visible after 4 h of reperfusion (Figure 4i). The imaging of hyperspectral parameters (StO₂%, NIR%) appeared similar at time 0 (before ligation) and after 1 h of reperfusion. Considering that the apparent red color corresponds to the maximum perfusion and the blue color to the minimum one, after the second hour of reperfusion, all parameters gradually decreased, reaching a minimum after 5 h similarly to the level showed after 90 min of ischemia (Figure 4a). StO₂% presented a higher level of ischemia as compared to NIR% (more diffused and darker blue). Setting NIR% against StO₂% images, NIR% presented sharper limits of the ischemic area, and a higher signal after the first hour of reperfusion was found. The HS data showed more visible and well-defined changes as compared to the RGB

camera. Oxygenation measured with StO₂% and NIR% significantly decreased in both ischemic and reperfusion phases. The last HS image of pig 4 that died after 2 h of reperfusion showed that the liver was not perfused, and H&E confirmed parenchymal and microvascular disruption. Overall, after 5 h of reperfusion, the perivenular region appeared necrotic, probably due to the ischemic damage with a detachment of hepatocytes from the adjacent sinusoidal reticular support. Hepatocytes were reduced in volume with acidophilic cytoplasm and pyknotic nuclei. A mix of inflammatory cells such as lymphocytes and polymorphonuclear elements were visible in the parenchyma (Figure 4i). Grouping pigs 1, 2, and 3, following the AI score, the statistical analysis showed that the HS image quantification of StO₂% and NIR% presented a significant decrease as compared to the control ($p = 0.0014$ StO₂%, $p = 0.0003$ NIR%) (Figure 4j,k). The AI score showed a gradual decrease with a minimum after 5 h (0.160 ± 0.130 a.u., $p < 0.0001$) where Suzuki's score and capillary lactate concentration were significantly high (3.667 ± 0.3512 mmol/L, $p < 0.0001$ and 6.1 ± 3.9 mmol/L, $p = 0.0228$ respectively) (Figure 4l–n). Immunostaining for CD31 revealed stronger staining after 5 h of reperfusion as compared to the control. HSI, H&E, and IHC were displayed together for better visualization of the difference between the control and the damaged liver from different perspectives (Figure 5). Pig 4 showed strong CD31 staining at 2 h and in the control (Figure S2d). Pig 5 showed a similar expression in the control and after the reperfusion phase (Figure S2e). Endomicroscopy confirmed the presence of blood circulation at the end of the reperfusion phase as shown in pigs 3 and 5 (Video S1,2 respectively for pigs 3,5). The liver parenchyma appeared

perfused in both pigs. However, pig 3 presented areas characterized by a slower to absent blood flow on which the microcirculation system appears compromised. Both pigs showed a correct vascular flow in the larger arterial and portal branches of the randomly selected lobes.

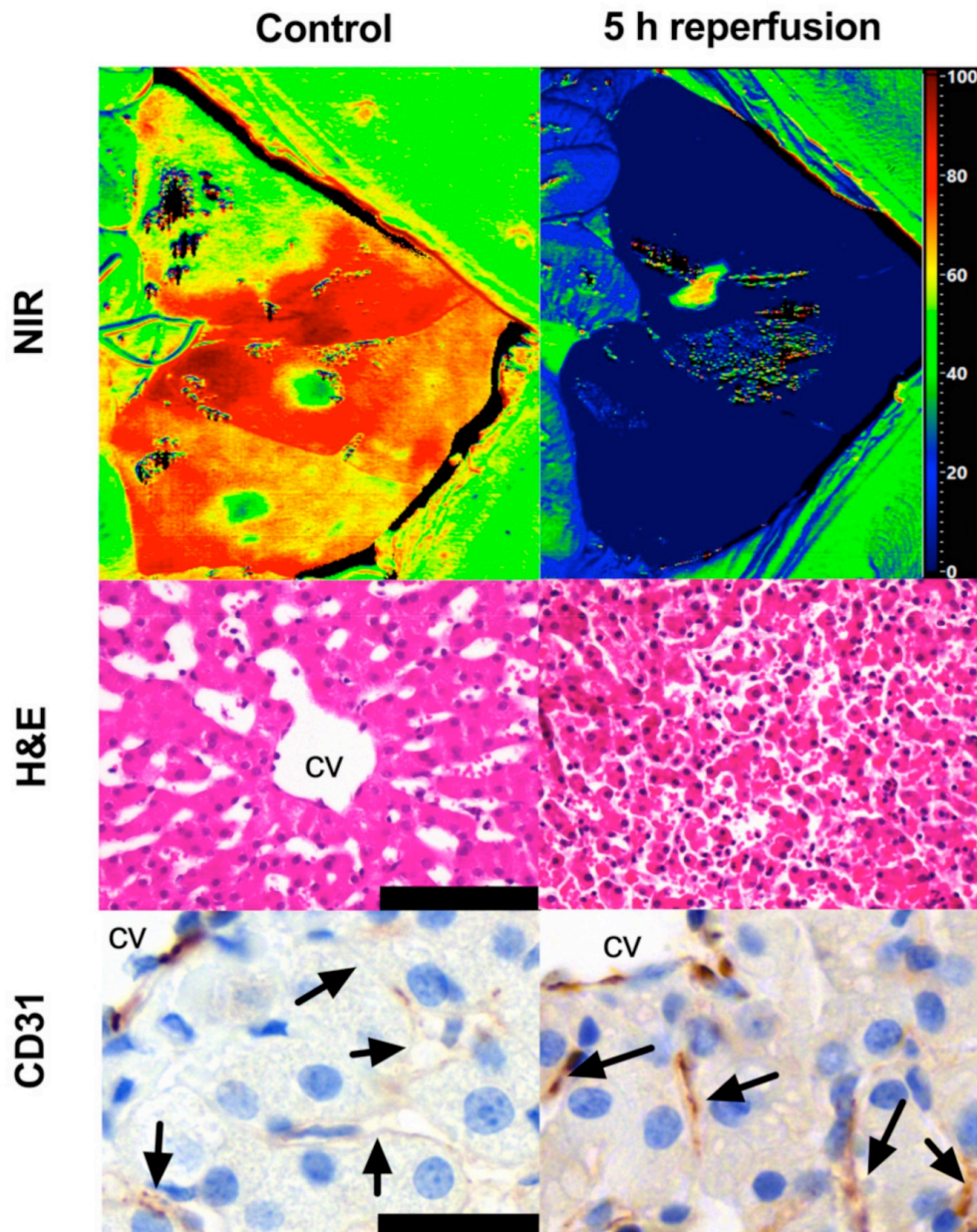


Figure 5. HSI, H&E, and IHC of CD31 expression comparison. The staining for CD31 did not show sinusoidal staining in the control group; this group corresponded to a high level of oxygenation in the HSI

image and a normal microarchitecture of the lobe in H&E. After 5 h of reperfusion, a higher expression of CD31 was observed close to the central vein, which corresponded to a low level of oxygenation in the HS image, a deeply congested microvasculature, and an overall parenchymal disruption in H&E. Histology photos were taken with a Leica DM2000 LED microscope, magnification 40 \times , scale bar 100 μ m (H&E), 160 \times , scale bar 25 μ m (CD31).

3.3. Correlation of HSI with Capillary Lactate

The correlation of HSI indexes with capillary lactate was significant and higher for StO2% as compared to NIR% (Figure 6a). When the images were split into ischemic and reperfusion phases, StO2% and NIR% showed different degrees of correlation. StO2% correlated better with the reperfusion phase and NIR% showed a higher correlation for the ischemic phase (Figure 6b,c). Finally, the AI score of the reperfusion phase was negatively correlated with capillary lactates and Suzuki's score ($r = -0.78$, $p = 0.0320$ and $r = -0.96$, $p = 0.0012$). Additionally, Suzuki's score and capillary lactates were positively correlated ($r = 0.86$, $p = 0.0135$) (Figure 6d).

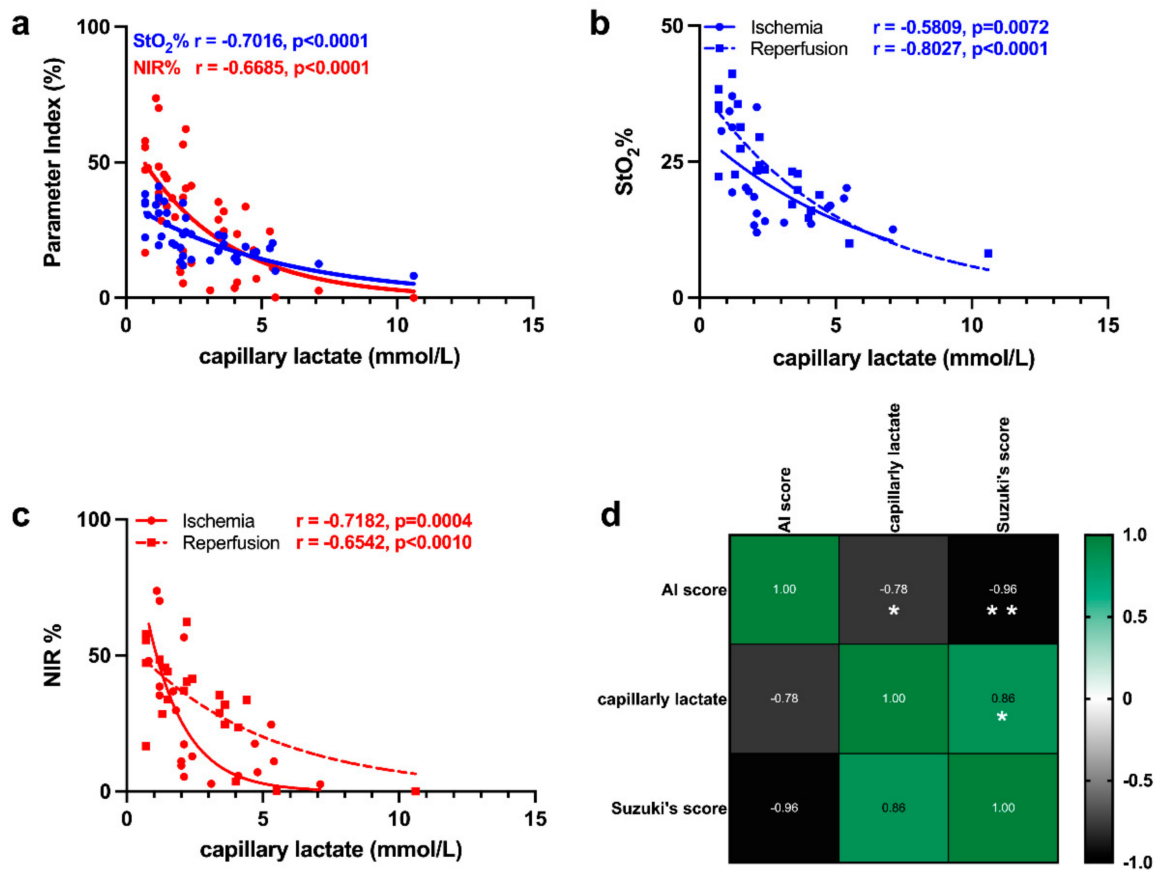


Figure 6. Correlation between optical and biological data. (a) Correlation between StO₂%, NIR, and capillary lactates. (n = 42) (b,c) StO₂% and NIR correlation split into ischemic and reperfusion phases (n = 42). (d) Correlation matrix of AI score, capillary lactates (mmol/L), and Suzuki's score (n = 22 per each variable for 5 pigs). Data are expressed as mean _ s.d. Spearman's and Pearson's correlation significance: * p _ 0.05, ** p _ 0.01.

4. Discussion

4.1. Ischemic Phase

In this study, we explored the potential of the AI-HSI analysis to predict liver viability following a period of 5 h of reperfusion phase after 90 min of hypoxia performed through the occlusion of the hepatic artery [49]. The warm ischemic period was found to be enough to obtain parenchymal damage worsened by the reperfusion phase [42]. Hemodynamic parameters, pH, and systemic oxygenation remained stable during ischemia. A small

increase in pCO₂ was found. However, it was not statistically significant probably due to its continuous delivery into the systemic circulation (Figure S1a–d) [28]. The glucose level was constant during the ischemic phase, in congruence with the literature (Figure S1e) [27]. Liver ischemia-reperfusion injury is known to be the leading cause of acute kidney failure [50]. Although the creatinine increase was not significant, the BUN and urea increase was statistically significant, suggestive of an early kidney dysfunction according to a previous study (Figure S1f–h) [51]. No significant changes were found in liver functionality and systemic lactate levels (Figure S1i–o). HS images could identify the ischemic areas showing the potentiality to exceed the capabilities of human vision which can distinguish only three main ranges corresponding to cone visual pigments (from ~424 to ~563 nm) [52,53]. In our study, HS image AI analysis used 100 bands from 500 to 1000 nm. The following interpretation and translation of relative reflectance quantification at different bands into RGB visible changes via the algorithms enhance the ability of the human eye to evaluate physiological changes (Figure 4i). The image capture took only ~6 s to be ready for its interpretation, which is significantly much faster than any other type of clinically available intraoperative assessment tool. In addition, its simple application reduces the variable of the operator's experience to a marginal value, providing a fast and standardized data extraction. Processing time for each HS image was approximately 1 s, indicating a minimal and acceptable delay to the surgeon for a potential intraoperative tool. The overall analysis of the ischemic phase confirmed the HAO model (Figures 2 and S1). StO₂% and NIR% indexes showed that ischemia was visible during HAO as compared to the control

(Figure 2a). StO₂% showed a larger ischemic area, probably due to the higher arterial blood flow which characterizes the hepatic tissue immediately beneath Glisson's capsule, which corresponds to the depth of StO₂% analysis (~1 mm) [54,55]. NIR% images showed sharper limits of the ischemic area, probably because at a depth of 3 to 5 mm, the lobe is characterized by an increased arterial and portal branch, which almost equally contributes to the oxygen supply [4]. This dual-depth analysis allows HSI to show the differences in oxygenation and may help for a more comprehensive evaluation of the hepatic microvascular circulation. The gross estimation of the mean reduction of StO₂% and NIR% was ~50%, which is close to the theoretical hepatic artery oxygen supply to the liver [56]. The plateau phase highlighted by the congestion score was probably due to the small flow maintained by the portal tract into the inferior vena cava (IVC) (Figure 2f). Although the occlusion of the hepatic artery in the pig 5 was confirmed, as shown by the observation made by the surgeon to check any anatomical variance, by the increase in AST and local lactate (from 26.00 to 43.00 U/l, from 2.10 to 4.10 mmol/L respectively), the AI-score assigned a high value like the control. This anomaly was confirmed by histopathological analysis, CD31, confocal endomicroscopy, and blood tests which showed the absence of microvascular failure. The reason why Pig 5 had a positive response to the ischemic insult is not clear, but it was an interesting case that showed the ability of the AI-score to predict a good outcome that could be considered as a positive control.

4.2. Reperfusion Phase

Five hours of reperfusion phase were considered sufficient for the observation of possible hepatic damage (IRI early phase) and more than the intraoperative time necessary for hepatic surgery [43]. Except for pig 5, systemic lactate levels showed an overall increase, probably due to the flushing out of the presinusoidal capillary lactate into the IVC after the re-establishment of arterial circulation (Figure S2f). Capillary lactate levels supported the findings of hypoxia and the occurrence of the anaerobic metabolism during the ischemia and reperfusion phases. The rapid decrease after the first hour of reperfusion was probably due to the washout of the arterial blood flow. AST and ALT values were higher after the first hour of reperfusion due to the inflammatory response and the hepatic vascular damage observed in HSI images. The acute experimental design may have contributed to the lack of a massive damage spread, which is likely to continue to develop during a longer observation period (late IRI). Oxygenation in both indexes appeared similar before ligation and after the first hour of reperfusion, showing no statistically significant difference. This confirmed the re-establishment of arterial blood perfusion. After 2 h of reperfusion, a visible decrease of oxygenation was detected, indicating the beginning of vascular dysfunction. The gradual reduction in oxygenation reached the same level of the ischemic phase at the end of reperfusion in both oxygen indexes (Figure 4i). This indicates that, after 5 h of reperfusion, the vascular system was heavily compromised. The portion of the small intestine analysed in HSI images did not show any congestion, confirming that the portal branch was not occluded [57]. When the sinusoids are damaged, the capillarization effect

occurs highlighted by the expression of CD31 [58]. Capillarization impedes the normal perfusion of molecules of blood circulation from the lumen of sinusoids. The pericentral zone of the lobe is usually the first one to be positive to CD31 given its distance from the portal triad, which increases the sensitivity to low oxygenation [59,60]. In this study, LSECs appeared to express a higher level of CD31 after 5 h of reperfusion when compared to the control (Figure 5). Pigs 5 and 4 showed low to absent and high levels of CD31 staining in the control and after the reperfusion phase respectively. This highlights the absence of capillarization in pig 5 and a capillarization effect in pig 4. The capillarization of pig 4, confirmed by the necrosis and microvascular disruption found in H&E in the control may contextualize the early liver failure (Figure S2d,e). These results confirm the AI viability score and corroborate the fact that when the AI-HSI score assigned a low score in the reperfusion phase, this was associated with microvasculature damage. Future studies could be based on the histopathological analysis damage of the whole organ, and this would help for the quantification of the amount of necrotic parenchyma over the healthy tissue. In our study, small biopsies were taken to prevent any damage to large vascular branches which could introduce a bias in the HSI analysis. Bile presents a spectra profile, which may interfere with the preset parameters of the

HSI camera which, to the best of our knowledge, are not compensated in order to obtain absolute values of oxygenation close to the real ones [31]. Nevertheless, the correlation of NIR% and StO₂% with capillary lactates, which resulted in a significantly negative correlation confirming the adequacy of the spectra sampling (Figure 6a–c). Consequently,

it may be possible to measure these two indexes as major indicators and predictors of capillary lactates even though their absolute values may be influenced by bile flow fluctuation. We also consider that the “bile effect” is probably of limited relevance in our study, considering that the bile duct was left open. The AI score, which analyses the relative reflectance of the full spectra (500–1000 nm) and is not based on proprietary preset, showed a significant negative correlation with capillary lactates and Suzuki’s score (Figure 6d). This correlation suggests that the analysis of the optical properties of the liver can infer organ viability in this scenario. The possibility to discriminate between the ischemic phase and the reperfusion damage would be the next appropriate step. Dataset size is a very important factor when applying a deep learning approach. This relatively small dataset prohibits end-to-end training of large CNNs with a large number of trainable parameters. However, the test performances give strong empirical evidence that a deep learning approach works well with this dataset despite its small size using the proposed CNNs. We emphasize that using LOPOCV, data from the held-out animal was never used for training. The strong results, particularly liver classification with a sensitivity of 0.993 and a specificity of 0.997, show that the CNNs have learned well because they generalize to data from animals not present in the training set. This has been possible because the CNNs have been trained with mild regularization (weight decay), but more importantly, the CNNs have a relatively small number of trainable parameters (32,444). This greatly reduces the potential to overfit and it is much smaller compared to larger CNNs typically used for image classification with RGB images such as ResNet50 [61] with over 23 million trainable

parameters. Recall that with RGB data, spatial context is extremely important for good classification, which requires filters acting over relatively large spatial distances. In contrast, in HSI, the rich reflectance information reduces the need for spatial context. As a future work, we aim to study the benefit of enlarging the capacity of the CNNs with a larger dataset. This can be both in terms of spatial window (to add more spatial context information) and in terms of network depth (to add more abstract spatio-spectral feature representations into the CNNs). Concerning the CNN model, we believe that a simpler classifier could also be used to perform well on the segmentation task. However, our work shows that the exact same machine learning model (CNN) can be used to effectively solve both tasks without any modification to the model's design or training process, which adds simplicity with a unified approach. As a follow-up study, we aim to compare performance from the CNNs with several other machine learning models such as Support Vector Machines (SVMs) or logistic regression, to investigate how performance is affected by the specific choice of machine learning model. In clinical routine, HAO is evaluated with US and CT in combination with blood analysis. US is still the best clinical tool for postoperative HAO detection. A recent comparison found that US was more accurate with a significantly higher specificity [62,63]. Despite its advantages, for patients with no visible hepatic artery flow, angiography or a contrasted CT scan is performed to obtain a clear diagnosis. Overall, these techniques present their own drawbacks and limitations. CT scan has contraindications such as nephrotoxicity because of iodine contrast medium injection and allergic reactions. When arterial revascularization is performed, there is a "grey zone"

where it is not possible to predict the future graft function and the potential consequences of biliary ischemia. In contrast, US is operator-dependent and requires intensive training to be mastered. The evaluation may be difficult due to a poor penetrance in case of distended bowel loops or obesity, and due to anatomical variations. US cannot provide a precise global map of liver oxygenation intraoperatively. The need for an objective and convenient HAO analysis tool has driven researchers to find alternative solutions. Pischke et al. reported a useful methodology for HAO assessment by using an IscAlert PCO₂ sensor for carbon dioxide [28]. They were able to provide a real-time monitoring system, which could discriminate arterial from portal occlusion. Although this approach was accurate and promising, it required the insertion of a catheter, making this application slightly invasive. Additionally, the analysis of the level of carbon dioxide can provide the level and type of hypoxia only, but not its localization. The development of imaging methods such as fluorescence-based perfusion assessment via the injection of indocyanine green (ICG) and near-infrared spectroscopy (NIRS) showed promising results [23–26]. ICG clearance is achieved by the hepatocytes in the parenchyma and excreted mostly in the bile through the enterohepatic circulation. For that reason, its application in HAO assessment is theoretically more than appropriate. Additionally, ICG was already successfully applied in the study of bowel perfusion [64]. In 2011, Levesque et al., in a study on 14 patients, showed that the ICG disappearance rate (PDRICG) was significantly lower in patients with early and late HAO than in patients without HAO in a HAT context [23]. Although the ICG PDR-based assessment showed

positive results, it has drawbacks such as the need for an injection, the time required for clearance, the contraindications in iodine allergic patients, or those affected by thyrotoxicosis, and its application in the clinical setting is not allowed in many countries. The application of NIRS was the first approach for a non-invasive analysis of hemoglobin without the need for the injection of an exogenous compound for the early diagnosis of HAO. In 2016, Skowno et al. studied transcutaneous hepatic StO₂% monitoring with the NIRS system and they reported that it was not a reliable method for the detection of hepatic ischemia. However, it was potentially useful in small pigs. Liver micro-dialysis was also tested with positive results although this technique is still invasive and can change the surgical workflow, which is not always possible [51]. Our AI HSI-based evaluation may help to predict the extent of ischemia-reperfusion injury, indicating that arterial revascularization is not sufficient to prevent liver failure or massive damage. This study could be the basis for a future prediction model of patient outcomes in a clinical context. Although the HIS system showed the ability to correlate optical and biological properties intraoperatively that ultimately made possible the prediction of liver viability, it presents several limitations. Currently, HSI can be employed exclusively as an intraoperative tool. One possible application would be the detection of perfusion deficits after completion of the vascular anastomoses during liver transplantation. Additionally, spectroscopic probes, acting within the same range of wavelengths and with a similar algorithm, could be inserted percutaneously. US could be applied to guide the probes onto the liver's surface providing reliable perfusion information in selected clinical cases. These cases could be the ones that

are not suitable for US (poorly visible artery) or CT scan (iodine allergy or kidney failure). The oxygenation map and the optical analysis represent only the first 3–5 mm of the tissue; hence it is not possible to detect a specific problem of the vasculature in-depth directly. Additionally, HSI cannot perform video. Our team partially overcame this problem by developing hyperspectral enhanced reality (HYPER) to guide the demarcation line assessment during the hepatectomy [29,38,39]. Finally, its ability to discriminate between ischemia and congestion is not clear as well as the ability to distinguish different ischemic timepoints. Although with its limitations, we consider that HSI-AI is a noninvasive tool that can furnish additional information on liver viability intraoperatively offering an automatic and standardized system.

5. Conclusions

The artificial-intelligence and hyperspectral imaging-based score could predict liver viability during the ischemic and reperfusion phases with a significant correlation with histopathological analysis, capillary lactate concentration, and CD31 staining. Further analysis with different types of vascular occlusion and with an increased number of pigs is necessary to confirm this data. HSI is a valuable non-invasive tool that can predict biological properties of the reperfusion damage produced by HAO intraoperatively.

Supplementary Materials: The following are available online at <https://www.mdpi.com/article/10.3390/diagnostics11091527/s1>, Figure S1: Ischemic phase monitoring. Figure S2: Additional information. Figure S3: CNN architecture. Video S1: endomicroscopy of pig 3. Video S2: endomicroscopy of pig 5.

Author Contributions: Methodology, E.F. (Eric Felli), M.A.-T. and E.F. (Emanuele Felli); Histopathology, A.B. and V.L.; Hyperspectral Imaging, E.F. (Eric Felli) and M.A.-T.; Experimental support, C.V.; Data collection, M.B., Artificial intelligence analysis and its validation, T.C., R.N., A.H., E.F. (Eric Felli) and M.D., Analysis, E.F. (Eric Felli) and T.C.; Supervision E.F. (Eric Felli), G.M.E., B.G., S.G., D.M., C.S., J.M., J.G.-S., M.D.; Project administration, funding acquisition, M.D. All authors, Writing, original draft preparation. E.F. (Eric Felli), M.A.-T., T.C., E.F. (Emanuele Felli), M.D., Writing review and editing. All authors have read and agreed to the published version of the manuscript.

Funding: This study was funded by the ARC Foundation for Cancer Research (9 Rue Guy Môquet, 94803 Villejuif, France) through the ELIOS (Endoscopic Luminescent Imaging for precision Oncologic Surgery) grant and partly by the ANR (National Research Agency) through the Liver SURG grant (ANR-18-CE19-0026). This work was also partially supported by French state funds managed within the “Plan Investissements d’Avenir” and by the ANR (reference ANR-10-IAHU-02).

Institutional Review Board Statement: This experiment was part of the ELIOS project (Endoscopic Luminescent Imaging for Oncology Surgery), approved by the local ethical committee on animal experimentation (ICOMETH No. 38.2016.01.085), and by the French Ministry of Superior Education and Research (MESR) (APAFIS#8721-2017013010316298-v2). All animals were managed according to French laws for animal use and care, and according to the directives of the European Community Council (2010/63/EU) and ARRIVE guidelines.

Informed Consent Statement: Not Applicable.

Data Availability Statement: The data presented in this study are available on request from the corresponding author.

References

1. Lu, G.; Fei, B. Medical hyperspectral imaging: A review. *J. Biomed. Opt.* **2014**, *19*, 10901. [CrossRef]
2. Ortega, S.; Fabelo, H.; Iakovidis, D.K.; Koulaouzidis, A.; Callico, G.M. Use of Hyperspectral/Multispectral Imaging in Gastroenterology. Shedding Some-Different-Light into the Dark. *J. Clin. Med.* **2019**, *8*, 36. [CrossRef] [PubMed]
3. Fei, B. Chapter 3.6—Hyperspectral imaging in medical applications. In *Data Handling in Science and Technology*; Amigo, J.M., Ed.; Elsevier: Amsterdam, The Netherlands, 2020; Volume 32, pp. 523–565.

-
4. Holmer, A.; Marotz, J.; Wahl, P.; Dau, M.; Kammerer, P.W. Hyperspectral imaging in perfusion and wound diagnostics—Methods and algorithms for the determination of tissue parameters. *Biomed. Tech.* **2018**, *63*, 547–556. [CrossRef]
 5. Jansen-Winkel, B.; Holfert, N.; Köhler, H.; Moulla, Y.; Takoh, J.P.; Rabe, S.M.; Mehdorn, M.; Barberio, M.; Chalopin, C.; Neumuth, T.; et al. Determination of the transection margin during colorectal resection with hyperspectral imaging (HSI). *Int. J. Colorectal Dis.* **2019**, *34*, 731–739. [CrossRef] [PubMed]
 6. Chin, J.A.; Wang, E.C.; Kibbe, M.R. Evaluation of hyperspectral technology for assessing the presence and severity of peripheral artery disease. *J. Vasc. Surg.* **2011**, *54*, 1679–1688. [CrossRef]
 7. Poole, K.M.; Tucker-Schwartz, J.M.; Sit, W.W.; Walsh, A.J.; Duvall, C.L.; Skala, M.C. Quantitative optical imaging of vascular response in vivo in a model of peripheral arterial disease. *Am. J. Physiol. Heart Circ. Physiol.* **2013**, *305*, H1168–H1180. [CrossRef] [PubMed]
 8. Best, S.L.; Thapa, A.; Holzer, M.J.; Jackson, N.; Mir, S.A.; Cadeddu, J.A.; Zuzak, K.J. Minimal arterial in-flow protects renal oxygenation and function during porcine partial nephrectomy: Confirmation by hyperspectral imaging. *Urology* **2011**, *78*, 961–966. [CrossRef]
 9. Kazune, S.; Caica, A.; Luksevics, E.; Volceka, K.; Grabovskis, A. Impact of increased mean arterial pressure on skin microcirculatory oxygenation in vasopressor-requiring septic patients: An interventional study. *Ann. Intensive Care* **2019**, *9*, 97. [CrossRef] [PubMed]
 10. Sumpio, B.J.; Citoni, G.; Chin, J.A.; Sumpio, B.E. Use of hyperspectral imaging to assess endothelial dysfunction in peripheral arterial disease. *J. Vasc. Surg.* **2016**, *64*, 1066–1073. [CrossRef]
 11. Grambow, E.; Dau, M.; Sandkühler, N.A.; Leuchter, M.; Holmer, A.; Klar, E.; Weinrich, M. Evaluation of peripheral artery disease with the TIVITA® Tissue hyperspectral imaging camera system. *Clin. Hemorheol. Microcirc.* **2019**, *73*, 3–17. [CrossRef]
 12. Oliveira, T.H.C.; Marques, P.E.; Proost, P.; Teixeira, M.M.M. Neutrophils: A cornerstone of liver ischemia and reperfusion injury. *Lab. Investig.* **2018**, *98*, 51–62. [CrossRef] [PubMed]

-
13. Kelly, D.M.; Shiba, H.; Nakagawa, S.; Irefin, S.; Eghtesad, B.; Quintini, C.; Aucejo, F.; Hashimoto, K.; Fung, J.J.; Miller, C. Hepatic blood flow plays an important role in ischemia-reperfusion injury. *Liver Transpl.* **2011**, *17*, 1448–1456. [CrossRef] [PubMed]
14. Pastacaldi, S.; Teixeira, R.; Montalto, P.; Rolles, K.; Burroughs, A.K. Hepatic artery thrombosis after orthotopic liver transplantation: A review of nonsurgical causes. *Liver Transpl.* **2001**, *7*, 75–81. [CrossRef] [PubMed]
15. Wanner, G.A.; Ertel, W.; Muller, P.; Hofer, Y.; Leiderer, R.; Menger, M.D.; Messmer, K. Liver ischemia and reperfusion induces a systemic inflammatory response through Kupffer cell activation. *Shock* **1996**, *5*, 34–40. [CrossRef]
16. Clavien, P.A.; Camargo, C.A., Jr.; Gorczynski, R.; Washington, M.K.; Levy, G.A.; Langer, B.; Greig, P.D. Acute reactant cytokines and neutrophil adhesion after warm ischemia in cirrhotic and noncirrhotic human livers. *Hepatology* **1996**, *23*, 1456–1463. [CrossRef]
17. Haugaa, H.; Thorgersen, E.B.; Pharo, A.; Boberg, K.M.; Foss, A.; Line, P.D.; Sanengen, T.; Almaas, R.; Grindheim, G.; Pischke, S.E.; et al. Early bedside detection of ischemia and rejection in liver transplants by microdialysis. *Liver Transpl.* **2012**, *18*, 839–849. [CrossRef]
18. Machado, M.; Fernandes, A.; Ferreira, C.; Marum, S.; Marques Vidal, P.; Mourão, L.; Marcelino, P. Value of serial serum lactate evaluation in liver transplant patients at the ICU. *Crit. Care* **2006**, *10*, P313. [CrossRef]
19. Ikeda, T.; Yanaga, K.; Kishikawa, K.; Kakizoe, S.; Shimada, M.; Sugimachi, K. Ischemic injury in liver transplantation: Difference in injury sites between warm and cold ischemia in rats. *Hepatology* **1992**, *16*, 454–461. [CrossRef]
20. Russo, L.; Gracia-Sancho, J.; García-Calderó, H.; Marrone, G.; García-Pagán, J.C.; García-Cardena, G.; Bosch, J. Addition of simvastatin to cold storage solution prevents endothelial dysfunction in explanted rat livers. *Hepatology* **2012**, *55*, 921–930. [CrossRef]
21. Hide, D.; Ortega-Ribera, M.; Garcia-Pagan, J.C.; Peralta, C.; Bosch, J.; Gracia-Sancho, J. Effects of warm ischemia and reperfusion on the liver microcirculatory phenotype of rats: Underlying mechanisms and pharmacological therapy. *Sci. Rep.* **2016**, *6*, 22107. [CrossRef]
22. Mills, A.; Mellnick, V. Imaging features of hepatic arterial and venous flow abnormalities. *Clin. Liver Dis.* **2018**, *11*, 27–32. [CrossRef]

-
23. Levesque, E.; Hoti, E.; Azoulay, D.; Adam, R.; Samuel, D.; Castaing, D.; Saliba, F. Non-invasive ICG-clearance: A useful tool for the management of hepatic artery thrombosis following liver transplantation. *Clin. Transpl.* **2011**, *25*, 297–301. [CrossRef]
24. Levesque, E.; Saliba, F.; Benhamida, S.; Ichai, P.; Azoulay, D.; Adam, R.; Castaing, D.; Samuel, D. Plasma disappearance rate of indocyanine green: A tool to evaluate early graft outcome after liver transplantation. *Liver Transpl.* **2009**, *15*, 1358–1364. [CrossRef]
25. Kubota, K.; Kita, J.; Shimoda, M.; Rokkaku, K.; Kato, M.; Iso, Y.; Sawada, T. Intraoperative assessment of reconstructed vessels in living-donor liver transplantation, using a novel fluorescence imaging technique. *J. Hepatobiliary Pancreat. Surg.* **2006**, *13*, 100–104. [CrossRef]
26. Skowno, J.J.; Karpelowsky, J.S.; Watts, N.R.; Little, D.G. Can transcutaneous near infrared spectroscopy detect severe hepatic ischemia: A juvenile porcine model. *Paediatr. Anaesth.* **2016**, *26*, 1188–1196. [CrossRef]
27. Ungerstedt, J.; Nowak, G.; Ungerstedt, U.; Ericzon, B.G. Microdialysis monitoring of porcine liver metabolism during warm ischemia with arterial and portal clamping. *Liver Transpl.* **2009**, *15*, 280–286. [CrossRef]
28. Pischke, S.E.; Tronstad, C.; Holhjem, L.; Line, P.D.; Haugaa, H.; Tønnessen, T.I. Hepatic and abdominal carbon dioxide measurements detect and distinguish hepatic artery occlusion and portal vein occlusion in pigs. *Liver Transpl.* **2012**, *18*, 1485–1494. [CrossRef] [PubMed]
29. Urade, T.; Felli, E.; Barberio, M.; Al-Taher, M.; Felli, E.; Goffin, L.; Agnus, V.; Ettorre, G.M.; Marescaux, J.; Mutter, D.; et al. Hyperspectral enhanced reality (HYPER) for anatomical; liver resection. *Surg. Endosc.* **2020**, *35*, 1844–1850. [CrossRef] [PubMed]
30. Felli, E.; Al-Taher, M.; Collins, T.; Baiocchini, A.; Felli, E.; Barberio, M.; Ettorre, G.M.; Mutter, D.; Lindner, V.; Hostettler, A.; et al. Hyperspectral evaluation of hepatic oxygenation in a model of total vs. arterial liver ischaemia. *Sci. Rep.* **2020**, *10*, 15441. [CrossRef] [PubMed]
31. Nachabe, R.; Evers, D.J.; Hendriks, B.H.; Lucassen, G.W.; van der Voort, M.; Wesseling, J.; Ruers, T.J. Effect of bile absorption coefficients on the estimation of liver tissue optical properties and related implications in discriminating healthy and tumorous samples. *Biomed. Opt. Express* **2011**, *2*, 600–614. [CrossRef] [PubMed]

-
32. Paoletti, M.E.; Haut, J.M.; Plaza, J.; Plaza, A. Deep learning classifiers for hyperspectral imaging: A review. *Isprs J. Photogramm. Remote Sens.* **2019**, *158*, 279–317. [CrossRef]
33. Camps-Valls, G.; Tuia, D.; Bruzzone, L.; Benediktsson, J.A. Advances in Hyperspectral Image Classification: Earth Monitoring with Statistical Learning Methods. *IEEE Signal Process. Mag.* **2014**, *31*, 45–54. [CrossRef]
34. Goetz, A.F.H. Three decades of hyperspectral remote sensing of the Earth: A personal view. *Remote Sens. Environ.* **2009**, *113*, S5–S16. [CrossRef]
35. Halicek, M.; Lu, G.; Little, J.V.; Wang, X.; Patel, M.; Griffith, C.C.; El-Deiry, M.W.; Chen, A.Y.; Fei, B. Deep convolutional neural networks for classifying head and neck cancer using hyperspectral imaging. *J. Biomed. Opt.* **2017**, *22*, 60503. [CrossRef] [PubMed]
36. Fei, B.; Lu, G.; Wang, X.; Zhang, H.; Little, J.V.; Patel, M.R.; Griffith, C.C.; El-Diery, M.W.; Chen, A.Y. Label-free reflectance hyperspectral imaging for tumor margin assessment: A pilot study on surgical specimens of cancer patients. *J. Biomed. Opt.* **2017**, *22*, 1–7. [CrossRef]
37. Li, X.; Li, W.; Xu, X.; Hu, W.H. Cell classification using convolutional neural networks in medical hyperspectral imagery. In *Proceedings of the 2017 2nd International Conference on Image, Vision and Computing (ICIVC)*, Chengdu, China, 2–4 June 2017; pp. 501–504.
38. Barberio, M.; Longo, F.; Fiorillo, C.; Seeliger, B.; Mascagni, P.; Agnus, V.; Lindner, V.; Geny, B.; Charles, A.L.; Gockel, I.; et al. HYPerspectral Enhanced Reality (HYPER): A physiology-based surgical guidance tool. *Surg. Endosc.* **2020**, *34*, 1736–1744. [CrossRef]
39. Barberio, M.; Felli, E.; Seyller, E.; Longo, F.; Chand, M.; Gockel, I.; Geny, B.; Swanstrom, L.; Marescaux, J.; Agnus, V.; et al. Quantitative fluorescence angiography versus hyperspectral imaging to assess bowel ischemia: A comparative study in enhanced reality. *Surgery* **2020**, *168*, 178–184. [CrossRef]
40. Felli, E.; Al-Taher, M.; Felli, E.; Cinelli, L.; Marescaux, J.; Diana, M. Protocol for the pig liver ischemia/reperfusion injury. *Protoc. Exchagne* **2020**. [CrossRef]
41. Kilkenny, C.; Browne, W.; Cuthill, I.C.; Emerson, M.; Altman, D.G.; NC3Rs Reporting Guidelines Working Group. Animal research: Reporting in vivo experiments: The ARRIVE guidelines. *Br. J. Pharm.* **2010**, *160*, 1577–1579. [CrossRef]

-
42. Uchida, M.; Takemoto, Y.; Nagasue, N.; Kimoto, T.; Dhar, D.K.; Nakamura, T. Calcium in pig livers following ischemia and reperfusion. *J. Hepatol.* **1994**, *20*, 714–719. [CrossRef]
43. Rampes, S.; Ma, D. Hepatic ischemia-reperfusion injury in liver transplant setting: Mechanisms and protective strategies. *J. Biomed. Res.* **2019**, *33*, 221–234. [CrossRef] [PubMed]
44. Kulcke, A.; Holmer, A.; Wahl, P.; Siemers, F.; Wild, T.; Daeschlein, G. A compact hyperspectral camera for measurement of perfusion parameters in medicine. *Biomed. Tech.* **2018**, *63*, 519–527. [CrossRef] [PubMed]
45. Hamida, A.B.; Benoit, A.; Lambert, P.; Amar, C.B. 3-D Deep Learning Approach for Remote Sensing Image Classification. *Ieee Trans. Geosci. Remote Sens.* **2018**, *56*, 4420–4434. [CrossRef]
46. Iandola, F.N.; Han, S.; Moskewicz, M.W.; Ashraf, K.; Dally, W.J.; Keutzer, K. SqueezeNet: AlexNet-level accuracy with 50x fewer parameters and <0.5MB model size. *arXiv* **2016**, arXiv:1602.07360.
47. He, K.; Zhang, X.; Ren, S.; Sun, J. Delving Deep into Rectifiers: Surpassing Human-Level Performance on ImageNet Classification. In *Proceedings of the 2015 IEEE International Conference on Computer Vision (ICCV), Santiago, Chile, 7–13 December 2015*; pp.1026–1034.
48. Suzuki, S.; Toledo-Pereyra, L.H.; Rodriguez, F.J.; Cejalvo, D. Neutrophil infiltration as an important factor in liver ischemia and reperfusion injury. Modulating effects of FK506 and cyclosporine. *Transplantation* **1993**, *55*, 1265–1272. [CrossRef]
49. Brockmann, J.G.; August, C.; Wolters, H.H.; Homme, R.; Palmes, D.; Baba, H.; Spiegel, H.U.; Dietl, K.H. Sequence of reperfusion influences ischemia/reperfusion injury and primary graft function following porcine liver transplantation. *Liver Transpl.* **2005**, *11*, 1214–1222. [CrossRef] [PubMed]
50. Lee, H.T.; Park, S.W.; Kim, M.; D’Agati, V.D. Acute kidney injury after hepatic ischemia and reperfusion injury in mice. *Lab. Invest.* **2009**, *89*, 196–208. [CrossRef]
51. Farnebo, S.; Winbladh, A.; Zettersten, E.K.; Sandstrom, P.; Gullstrand, P.; Samuelsson, A.; Theodorson, E.; Sjoberg, F. Urea clearance: A new technique based on microdialysis to assess liver blood flow studied in a pig model of ischemia/reperfusion. *Eur. Surg. Res.* **2010**, *45*, 105–112. [CrossRef]

-
52. Forrester, J.V.; Dick, A.D.; McMenemy, P.G.; Roberts, F.; Pearlman, E. Chapter 5—Physiology of vision and the visual system. In *The Eye*, 4th ed.; Forrester, J.V., Dick, A.D., McMenemy, P.G., Roberts, F., Pearlman, E., Eds.; W.B. Saunders: Philadelphia, PA, USA, 2016; pp. 269–337.e262.
53. Imamoto, Y.; Shichida, Y. Cone visual pigments. *Biochim. Biophys. Acta* **2014**, 1837, 664–673. [CrossRef]
54. Lauth, W.W. *Hepatic Circulation: Physiology and Pathophysiology*. In *Hepatic Circulation: Physiology and Pathophysiology; Sciences, M.C.L., Ed.; Morgan and Claypool: San Rafael, CA, USA, 2009*.
55. Lauth, W.W.; Schafer, J.; Legare, D.J. Hepatic blood flow distribution: Consideration of gravity, liver surface, and norepinephrine on regional heterogeneity. *Can. J. Physiol. Pharm.* **1993**, 71, 128–135. [CrossRef]
56. Vollmar, B.; Menger, M.D. The hepatic microcirculation: Mechanistic contributions and therapeutic targets in liver injury and repair. *Physiol. Rev.* **2009**, 89, 1269–1339. [CrossRef] [PubMed]
57. Shen, L.; Uz, Z.; Ince, C.; van Gulik, T. Alterations in intestinal serosal microcirculation precipitated by the Pringle manoeuvre. *BMJ Case Rep.* **2019**, 12, e228111. [CrossRef]
58. Baiocchini, A.; Del Nonno, F.; Taibi, C.; Visco-Comandini, U.; D’Offizi, G.; Piacentini, M.; Falasca, L. Publisher Correction: Liver sinusoidal endothelial cells (LSECs) modifications in patients with chronic hepatitis C. *Sci. Rep.* **2020**, 10, 1420. [CrossRef] [PubMed]
59. Scoazec, J.Y.; Feldmann, G. In situ immunophenotyping study of endothelial cells of the human hepatic sinusoid: Results and functional implications. *Hepatology* **1991**, 14, 789–797. [CrossRef] [PubMed]
60. Lalor, P.F.; Lai, W.K.; Curbishley, S.M.; Shetty, S.; Adams, D.H. Human hepatic sinusoidal endothelial cells can be distinguished by expression of phenotypic markers related to their specialised functions in vivo. *World J. Gastroenterol.* **2006**, 12, 5429–5439. [CrossRef]
61. He, K.; Zhang, X.; Ren, S.; Sun, J. Deep Residual Learning for Image Recognition. In *Proceedings of the 2016 IEEE Conference on Computer Vision and Pattern Recognition (CVPR)*, Las Vegas, NV, USA, 27–30 June 2016; pp. 770–778.

-
62. Kim, J.S.; Kim, K.W.; Lee, J.; Kwon, H.J.; Kwon, J.H.; Song, G.W.; Lee, S.G. Diagnostic Performance for Hepatic Artery Occlusion After Liver Transplantation: Computed Tomography Angiography Versus Contrast-Enhanced Ultrasound. *Liver Transpl.* **2019**, *25*, 1651–1660. [CrossRef]
63. Pinna, A.D.; Smith, C.V.; Furukawa, H.; Starzl, T.E.; Fung, J.J. Urgent revascularization of liver allografts after early hepatic artery thrombosis. *Transplantation* **1996**, *62*, 1584–1587. [CrossRef] [PubMed]
64. Diana, M. Enabling precision digestive surgery with fluorescence imaging. *Transl. Gastroenterol. Hepatol.* **2017**, *2*, 97. [CrossRef]

iii) Hyperspectral enhanced reality (HYPER) for anatomical liver resection

We aimed to explore the potential of hyperspectral imaging in an intraoperative setting, to predict liver viability and to enhance the ability of the surgeon to perform anatomical resection. Our group developed a software to overlay HSI images onto the operative field, obtaining HSI-based enhanced reality (HYPER) to identify the demarcation line in an experimental animal model and after a left vascular inflow occlusion during an anatomical resection. After ligation, HSI demonstrated a significantly lower oxygenation (NIR index) in the left medial lobe (LML) ($0.27\% \pm 0.21$) when compared to the right medial lobe (RML) ($58.60\% \pm 12.08$; $p = 0.0015$). Capillary lactates were significantly higher ($3.07 \text{ mmol/L} \pm 0.84$ vs. $1.33 \pm 0.71 \text{ mmol/L}$; $p = 0.0356$) in the LML versus RML, respectively. Concordantly, confocal videos demonstrated the absence of blood flow in the LML and normal perfusion in the RML. HYPER correctly identified the demarcation line and quantified surface liver oxygenation, and it could be an intraoperative tool to guide perfusion-based demarcation line assessment and segmentation. My personal contribution

to this study was participation to the study design, operative procedures on animal models, revision of results and writing and revision of the manuscript.

Article

Published in: **Surgical Endoscopy (2020)**

Surg Endosc 2021 Apr;35(4):1844-1850. doi: 10.1007/s00464-020-07586-5. Epub 2020 Apr 27.

Hyperspectral enhanced reality (HYPER) for anatomical; liver resection

Takeshi Urade¹ · Eric Felli^{1,2} · Manuel Barberio^{1,2} · Mahdi Al-Taher¹ · **Emanuele Felli**³ · Laurent Goffin⁴ · Vincent Agnus¹ · Giuseppe Maria Ettorre⁵ · Jacques Marescaux^{1,6} · Didier Mutter^{1,3,6} · Michele Diana^{1,2,3,4,6}

1 Institute of Image-Guided Surgery, IHU-Strasbourg, Strasbourg, France

2 Institute of Physiology, EA3072 Mitochondria Respiration and Oxidative Stress, University of Strasbourg, Strasbourg, France

3 Department of General, Digestive, and Endocrine Surgery, University Hospital of Strasbourg, Strasbourg, France

4 ICube/CNRS, University of Strasbourg, Strasbourg, France

5 Department of Transplantation and General Surgery, San Camillo Hospital, Rome, Italy

6 Research Institute against Digestive Cancer, IRCAD, 1, place de l'Hôpital, 67091 Strasbourg, France

Abstract

Background Clinical evaluation of the demarcation line separating ischemic from non-ischemic liver parenchyma may be challenging. Hyperspectral imaging (HSI) is a noninvasive imaging modality, which combines a camera with a spectroscope and allows

quantitative imaging of tissue oxygenation. Our group developed a software to overlay HSI images onto the operative field, obtaining HSI-based enhanced reality (HYPER). The aim of the present study was to evaluate the accuracy of HYPER to identify the demarcation line after a left vascular inflow occlusion during an anatomical left hepatectomy.

Materials and methods In the porcine model ($n = 3$), the left branches of the hepatic pedicle were ligated. Before and after vascular occlusion, HSI images based on tissue oxygenation (StO₂), obtained through the Near-Infrared index (NIR index), were regularly acquired and superimposed onto RGB video. The demarcation line was marked on the liver surface with electrocautery according to HYPER. Local lactates were measured on blood samples from the liver surface in both ischemic and perfused segments using a strip-based device. At the same areas, confocal endomicroscopy was performed.

Results After ligation, HSI demonstrated a significantly lower oxygenation (NIR index) in the left medial lobe (LML) ($0.27\% \pm 0.21$) when compared to the right medial lobe (RML) ($58.60\% \pm 12.08$; $p = 0.0015$). Capillary lactates were significantly higher ($3.07 \text{ mmol/L} \pm 0.84$ vs. $1.33 \pm 0.71 \text{ mmol/L}$; $p = 0.0356$) in the LML versus RML, respectively. Concordantly, confocal videos demonstrated the absence of blood flow in the LML and normal perfusion in the RML.

Conclusions HYPER has made it possible to correctly identify the demarcation line and quantify surface liver oxygenation. HYPER could be an intraoperative tool to guide perfusion-based demarcation line assessment and segmentation.

Introduction

Anatomical liver resections (ALRs) are performed by removing a section of the liver visually identified via surface color changes due to selective blood inflow occlusion or staining of the portal tract [1–3]. The resulting demarcation line discriminates the boundaries between ischemic and non-ischemic tissue. This eye-based evaluation suffers from being operator-dependent and from the inability to quantify local oxygenation, particularly beneath the liver surface. Moreover, the inhomogeneity in surface perfusion appreciation in pathologic

conditions, including cirrhosis, steatosis, fibrosis, has been the driver for the development of intraoperative imaging methods such as fluorescence-based segmentation, by means of administration of a fluorophore, mostly Indocyanine Green (ICG) [4]. There are two staining methods to identify anatomical hepatic regions with ICG. Positive staining method is performed to detect anatomical hepatic regions by injection of ICG into the portal branches under IOUS guidance [4–6], and negative staining method is performed to detect anatomical hepatic regions, as the non-fluorescing ones, by the intravenous injection of ICG after clamping the portal branches [5, 7–10]. However, those methods are limited by the need of injecting an exogenous fluorescent molecule to the patient. Hyperspectral imaging (HSI) is a contrast-free optical imaging modality which combines a photo camera and a spectroscope [11]. HSI performs spectral analysis of tissues and allows tumor identification [12, 13], organ perfusion assessment [14, 15], and identification of key anatomical structures intraoperatively [16]. HSI systems build images based on the

computation of light-tissue interactions phenomena, which depend on the tissue concentration of various compounds, up to a certain depth. In the present experiment, we have used a CMOS push-broom scanning hyperspectral

camera (TIVITA®, Diaspective Vision GmbH, Germany). The TIVITA® has preset algorithms, which allow to quantify the relative oxygen saturation (StO₂%) of the superficial

microcirculation at a depth up to ~ 1 mm, whereas it is possible to quantify the relative oxygen saturation in deeper layers, within the near-infrared (NIR) spectrum, with a penetration depth up to 4-6 mm. The tissue water index (TWI) can be used to quantify and image the distribution of water in the observed region of interest (ROI) [17]. The majority of the commercially available HSI systems do not provide an effective video rate and the HSI information is provided as a static side-by-side image. In an attempt to overcome this limitation and improve the use of HSI as a surgical navigation tool, our group has introduced

the concept of HYPerspectral Enhanced Reality (HYPER) [18]. HYPER is based on the superimposing of static HIS images onto an intraoperative video, using augmented reality technologies. Through the mixed reality, informationrich images are overlaid directly on the screen, providing an effective surgical navigation tool. In analogy to our previous experience in bowel ischemia detection and quantification, we hypothesized that HYPER could precisely identify the future liver demarcation line. The aim of this experimental

study was to evaluate the feasibility of HYPER-guided ALR and to assess the accuracy in discriminating ischemic from non-ischemic liver tissue.

Materials and methods Animals

The present study, which is part of the ELIOS project (Endoscopic Luminescent Imaging for Oncology Surgery), was approved by the local Ethical Committee on Animal Experimentation (ICOMETH No. 38.2016.01.085), and by the French Ministry of Superior Education and Research (MESR) (APAFIS#8721-2017013010316298-v2). All animals used in the experimental laboratory were managed according to French laws for animal use and care, and according to the directives of the European Community Council (2010/63/EU) and ARRIVE guidelines [19]. Three adult male swine (*Sus scrofa* ssp. *domesticus*, mean weight: 24.7 ± 0.5 kg) were housed and acclimatized for 48 h in an enriched environment, respecting circadian cycles of lightdarkness, and with constant humidity and temperature conditions. They were fasted 24 h before surgery, with ad libitum access to water, and finally sedated (zolazepam + tiletamine 10 mg/kg IM) 30 min before the procedure to decrease stress. Anesthesia induction was achieved by means of intravenous (18 G IV catheter in ear vein) propofol 3 mg/kg and maintained with rocuronium 0.8 mg/kg along with inhaled isoflurane 2%. At the end of the protocol, animals were euthanized with a lethal dose of pentobarbital (40 mg/kg).

Surgical procedure

The abdominal cavity was accessed via a midline laparotomy. The round ligament, the thin transparent membranes around the liver, and the hepato-gastric ligament were cut to prevent any unexpected traction injuries. During hepatic pedicle dissection, the left hepatic artery and the left portal vein were ligated with 3/0 and 2/0 braided threads, respectively. The demarcation line produced between the right medial (RML) and left medial lobe (LML) was marked on the liver surface with electrocautery following our proprietary software HSI-based enhanced reality (HYPER). The schematic of the set-up in Fig. 1 shows the position of the screen, which allowed the surgeon to follow HYPER and to guide the demarcation line incision. Parenchymal transection was performed to verify if the intraparenchymal perfusion boundaries were matching with the demarcation line suggested by HSI. A clamp crushing method was applied with a special clamp for liver parenchymal transection (Takayama's forceps for liver transection, Yufu Itonaga Co., Ltd., Tokyo, Japan) and a bipolar vessel-sealing device (LigaSure™ Maryland, Covidien, Mansfield, MA, USA). During transection, an intermittent Pringle's maneuver was also performed with a cycle of 15-min clamping with 5 min of perfusion. Finally, hepatic veins were divided with staplers (Endo GIA™, Covidien, Mansfield, MA, USA) and the left median and left lateral lobes were removed.

HSI and HYPER

A commercially available hyperspectral camera (TIVITA®, Diaspective Vision GmbH, Germany) was used to provide intraoperative imaging and quantification of StO₂, NIR perfusion index, and TWI. The TIVITA® was customized

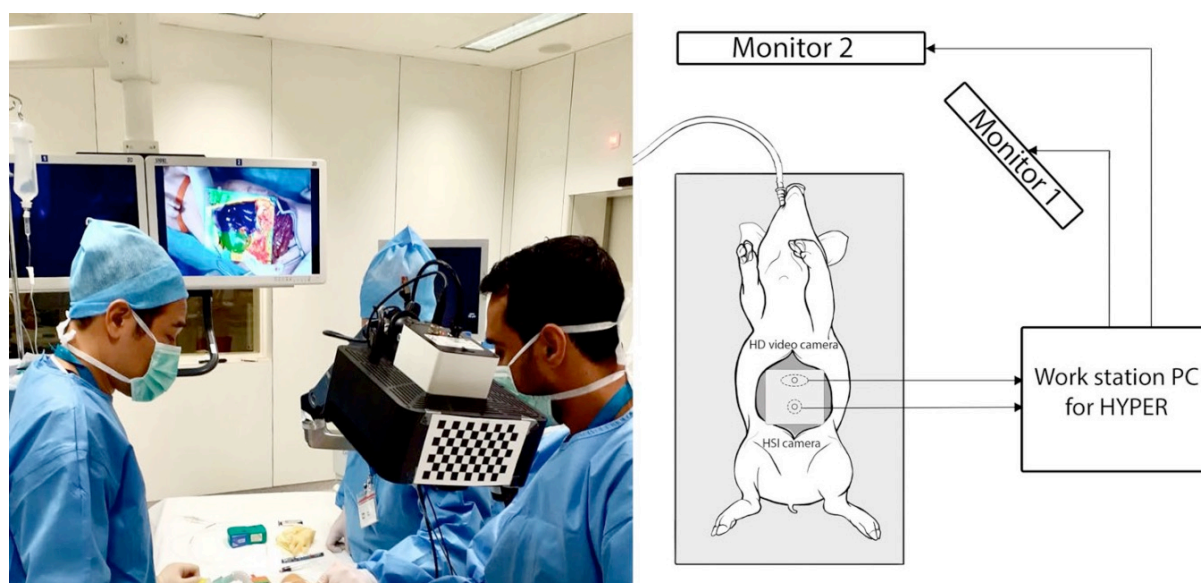


Fig. 1 Schematic of the hyperspectral imaging (HSI)-based enhanced reality (HYPER) system set-up. The workstation PC for HYPER is equipped with TIVITA® software and original software for enhanced reality. The static HSI image is displayed on monitor 1, and the superimposed HSI image on the running video is displayed on monitor 2

integrating an HD video camera (C920 1080p HD Pro Webcam, Logitech, Switzerland). Intrinsic parameters of the hyperspectral camera and of the additional webcam were computed independently, before the procedure. To compute the registration transformation (extrinsic calibration), several poses of a checkerboard are detected simultaneously in both cameras. Checkerboard corners are used to estimate the transformation and to estimate the

error. The HSI system requires 6 s to acquire the tissue spectrum analysis and convert into images depending on the preset algorithms (StO2%, TWI, NIR). Those images are simultaneously displayed side-by-side. For surgical guidance, the HSI-NIR perfusion index was selected to highlight the resulting demarcation line, following vascular ligation, because of the deeper tissue penetration, when compared to the StO2 index. The accuracy of perfusion evaluation between NIR% and StO2 was compared post hoc. A NIR perfusion map (low perfusion (blue)/high perfusion (red) colormap) was superimposed on each live video and was displayed on the screen to guide the resection line in enhanced reality. Four electro-cauterized dots on the liver surface, visible in the RGB and NIR images, were used as landmarks to test the accuracy of the registration and to enable an updated registration in case of a novel HSI image acquisition. Ventilation was stopped during HSI images acquisition. The mean value of the HIS parameters (StO2%, NIR and TWI) was computed on the whole surface of the liver, for each region of interest, before and after ligation.

Probe-based confocal laser endomicroscopy (pCLE)

A Cellvizio® pCLE system (Mauna Kea Technologies, France) was used for endomicroscopic analysis to assess microcirculation, at the same time points of lactate sampling and HSI imaging. Endomicroscopy was performed by applying the tip of the CLE probe directly on the liver surface before vascular ligation (T0), randomly on Glisson's capsule. After vascular ligation, pCLE was repeated during resection on both sides (ischemic and perfused) of the demarcation line (T1). To obtain confocal images, 2 mL of

sodium fluorescein (Fluocyne®, Serb, Paris, France) was injected intravenously. The probe was held manually and the videos were recorded for 1 min.

Local liver lactates

At the same time points, lactates were measured on blood samples obtained by puncturing the liver surface, using a strip-based portable lactate analyzer (EDGE®, ApexBio, Taipei, Taiwan) on the two sides of the demarcation line (which margin error is ~ 0.35 mmol/L [20]). The correlation between HSI parameters and the local capillary lactates was used as primary outcome to establish the sample size. The calculation was based on our previous experiences with bowel ischemia [18, 21], in which the rho correlation coefficient between HSIStO₂ and lactates was -0.7 . Applying an alpha at 0.05 with a power of 0.9, the required sample size in terms of paired values is 4. In the present study, 12 paired values StO₂ lactates were obtained in total in three pigs.

Statistical analysis

Statistics were performed using GraphPad 8.3 (GraphPad Software®, San Diego, CA, USA). A Pearson's rho was calculated to correlate local lactates with HSI parameters. Student's *t* test, one-way and two-way ANOVA with Dunnett's multiple comparisons were performed to calculate differences in continuous variables. A *p* value < 0.05 was considered statistically significant.

Results

The extra time required to register the NIR-derived images was only few seconds. The accuracy of the HYPER registration was subpixel and was around 0.35 pixels. The

demarcation line was marked under HYPER guidance during the procedure (Videoclip). The software elaboration of the HSI hypercube is displayed in Fig. 2A. Under white light observation, the demarcation line was not always sharp, especially in one of the three animals. The HSINIR picture provided a sharper limit of the ischemic area when compared to StO₂%

and TWI% parameters. In the first animal, the demarcation line based on clinical evaluation underestimated the ischemic area, when compared to the HYPER-based one (Fig. 2B). Table 1, the intraoperative data is reported. Briefly, the StO₂% index measured at RML and at the control area of the liver were statistically significantly higher when compared to the LML

($p = 0.0117$ and $p = 0.0130$, respectively). No difference was detected between the control and the RML confirming that the ligation was correctly performed. The NIR% and the TWI index of the LML were both significantly lower when compared to the ones measured at the RML and at the control area. There was no difference between the RML and the control for both indexes. Local lactate was coherently higher in the LML; the difference between the RML and the control when compared to the LML was statistically significant ($p = 0.0356$ and $p = 0.0091$, respectively), where the difference between the RML and the control was not significant. StO₂% and NIR% were statistically significantly different in the control and in the RML. The superficial analysis given by StO₂% was less accurate than the NIR% as shown by the difference between the RML and the LML (Fig. 3).

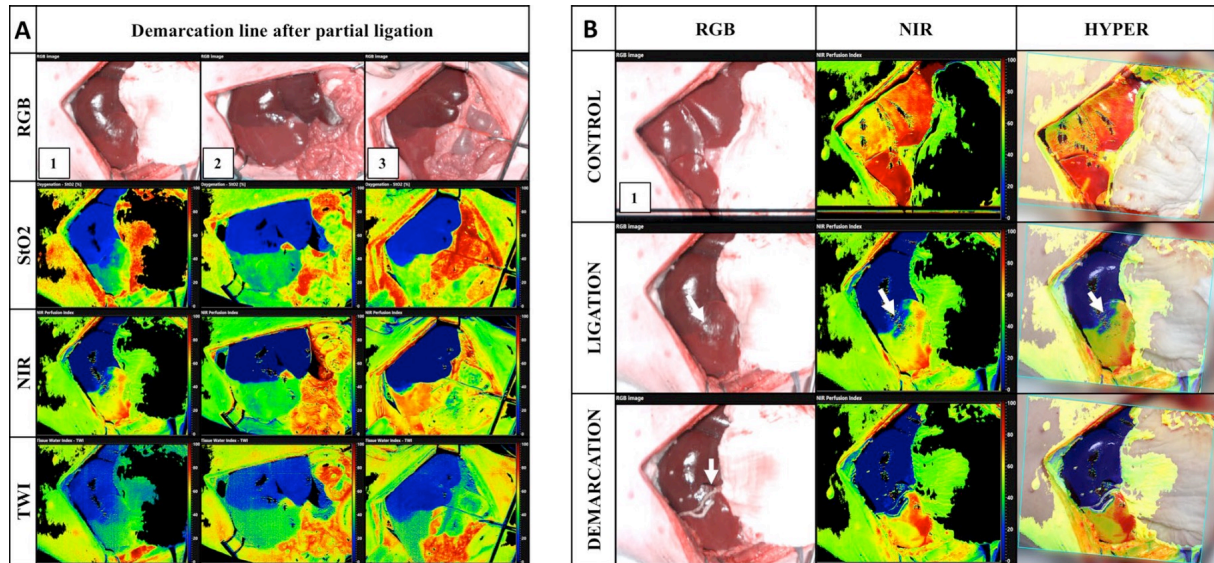


Fig. 2 **A** Hyperspectral liver pictures of the three pig models after the ligation of the left hepatic pedicle branch. **B** Enhanced reality (HYPER) provided by the superimposition of the RGB camera with the Hyperspectral Near-Infrared index obtaining HYPERSPECTRAL of pig 1. Unclear demarcation line solved by HSI is highlighted by the white arrows

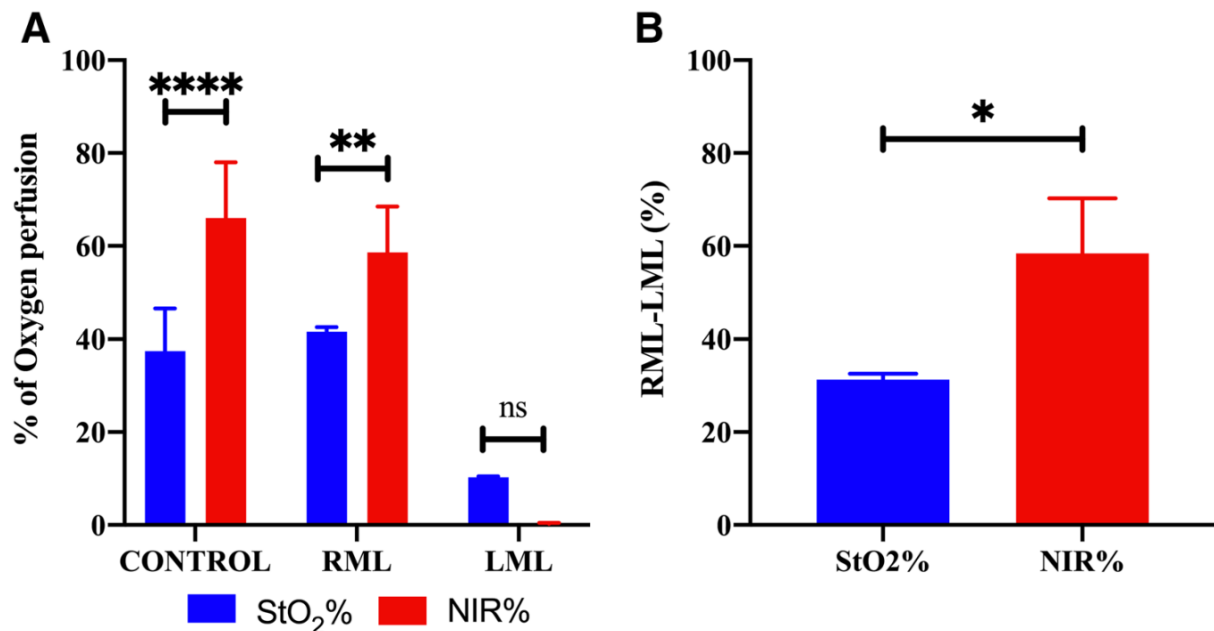


Fig. 3 StO₂% and NIR% comparison. **A** The difference between the two parameters was statistically significantly in the control and in the RML ($p < 0.0001$ and $p = 0.0011$, respectively). **B** The superficial analysis given by StO₂% was less accurate than the NIR% as shown by the difference between the RML and the LML ($p = 0.0326$). Data are expressed as mean \pm sd. p value < 0.05 was considered statistically significant

In addition, the correlation between the local lactate and HSI parameters was statistically significant for (i) local lactate and StO₂% ($r = -0.7805$, 95%CI $-0.95/ -0.24$, $R^2 = 0.6092$, $p = 0.0131$); (ii) local lactate and NIR% ($r = -0.7947$, 95%CI $-0.95/ -0.27$, $R^2 = 0.6316$, $p = 0.0105$); (iii) local lactate and TWI% ($r = -0.7989$, 95%CI $-0.95/ -0.28$, $R^2 = 0.6383$, $p = 0.0098$). Confocal endomicroscopy (Videoclip) performed 1 cm away from the demarcation line in both sides, showed that the perfused region indicated by HSI, i.e., the RML, was characterized by a normal blood circulation, whereas circulation in the LML was absent. Upon injection of fluorescein, the typical emission peak of the fluorophore was noticed as an alteration of the whole HSI spectrum (at around 540 nm). However, this was not interfering with the StO₂% and NIR perfusion indexes that are formed at higher wavelengths (around 800 nm). Finally, a preliminary test for the transection plane was performed. NIR parameter showed low perfusion level in the intraparenchymal plane (Fig. 4).

Discussion

The present acute experiment allowed to demonstrate the feasibility of the HYPER method to intraoperatively identify the demarcation line. The potential clinical relevance of HYPER lies in the accurate discrimination between ischemic and non-ischemic hepatic regions. HSI allowed to clearly identify the demarcation line which could be followed by HSI image superimposition. However, in our setting, the clinically based demarcation line matched with the HYPERbased one in 2 out of 3 cases. The discordant case (Fig. 2B)

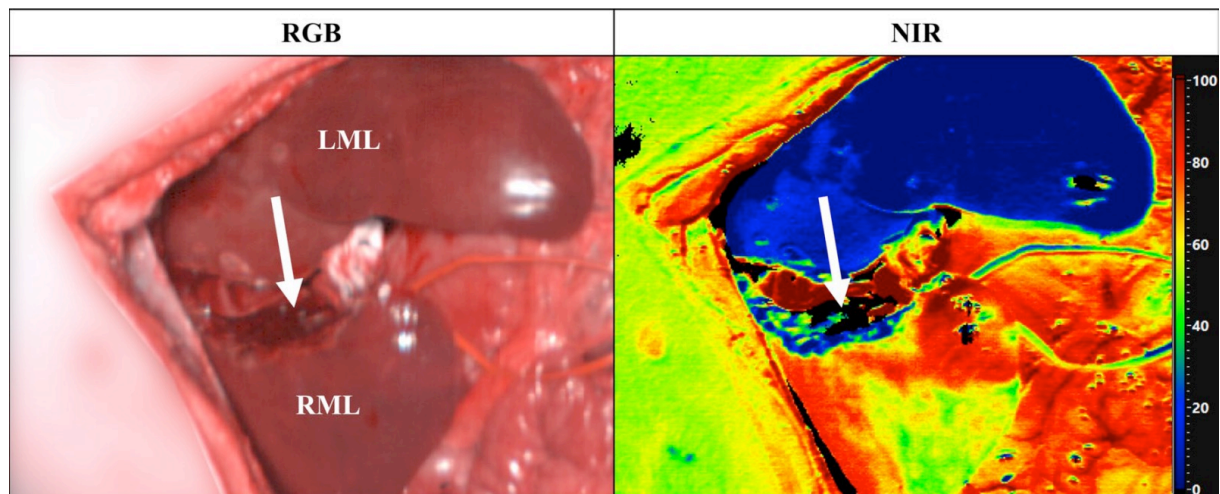


Fig. 4 RGB (left) and NIR perfusion index (right) images of the transection plane. The intraparenchymal HSI analysis of the perfused lobe (RML) shows low level of oxygen perfusion similar to the ischemic lobe (LML) after the resection

provides an example of unclear demarcation, which could be corrected with the HYPER method. The main advantage of HYPER is the possibility to easily acquire new quantitative images during the procedure, representing the actual perfusion status. The oxygen perfusion difference between RML and LML calculated by StO₂% on the surface (depth ~1 mm) was significantly lower when compared to the NIR% which measures in deeper layers (depth 4-6 mm), suggesting that a deeper evaluation of oxygen perfusion could be more accurate. Thus, NIR evaluation through HSI improves the evaluation of the demarcation line compared with the evaluation of the StO₂% and human eye both by being visually sharper and by being quantitatively more discriminating between ischemic and perfused. The high correlation between StO₂%, NIR% and TWI with local lactates confirms the consistency of HSI in discriminating ischemic and non-ischemic areas, with NIR% achieving the highest correlation. In this study, we also performed a preliminary evaluation of the

transection plane. This first attempt showed that HSI detected low level of oxygen perfusion in the transection plane of the perfused lobe (RML) (Fig. 4), most likely due to the action of the electrocautery that altered the hyperspectral signal. This aspect will be separately studied in the next experimental steps, in which different HSI set-up and surgical approaches will be tested to avoid the loss of the signal. To the best of our knowledge, HSI has been applied to anatomical left liver resection in a recently published case report [22].

The future transection line, which was marked according to the Cantlie line and the middle hepatic vein, matched the demarcation line, as identified by the same HSI device used in our experimental study. However, the authors did not superimpose the HSI images, which makes difficult to assess the correspondence between the HSI perfusion images and the actual liver surface demarcation line. Additionally, no ground truth tests were performed to assess the accuracy of HSI parameters. The strong point of our study was the use of superimposition of HSI images onto the RGB video validated by robust metabolic metrics to measure organ perfusion, such as capillary lactates [23–26] and advanced intraoperative microcirculation imaging, such as confocal endomicroscopy [27] which were all concordant with HSI parameters. This supports HYPER as a potential surgical guidance tool despite the multiple limitations of this study, including the low sample size, the acute design, and the focus on the demarcation line rather than on the transection planes. Additionally, the experiments were performed on healthy livers while the real advantages of HSI technology could probably be better defined in clinical conditions (e.g., cirrhosis, steatosis, postchemotherapy liver injury) that alter the liver surface signal. Zuzak et al. [16,

28] developed a near-infrared laparoscopic HSI system to help guide laparoscopic surgeons to visualize biliary anatomy. However, there is currently no commercially available HSI-equipped laparoscope. The availability of an integrated laparoscopic HSI system with video rate would obviate for the need of enhanced reality superimposition methods such as HYPER. Clinically, we are planning to evaluate the method in a prospective observational study to establish the accuracy and evaluate the surgical workflow.

Conclusions

In the experimental setting, HSI was accurate in discriminating ischemic from non-ischemic hepatic areas. HYPER could be a suitable intraoperative tool to guide perfusionbased demarcation line assessment and segmentation.

Acknowledgements

The authors would like to thank Guy Temporal and Christopher Burel for their assistance in medical English proofreading. The authors are also grateful to Catherine Meunier-Cers for her medical illustration.

Funding

This work was funded by the ARC Foundation through the ELIOS (Endoscopic Luminescent Imaging for precision Oncologic Surgery) grant.

Compliance with ethical standards

Disclosures Jacques Marescaux is the President of IRCAD, which is partly funded by KARL STORZ and Medtronic. Michele Diana is member of the scientific board of Diagnostic Green. Michele Diana is the recipient of the ELIOS grant. Takeshi Urade, Eric Felli, Manuel Barberio, Mahdi Al-Taher, Emanuele Felli, Laurent Goffin, Giuseppe Maria Ettore and Didier Mutter have no conflicts of interest or financial ties to disclose.

References

1. Makuuchi M, Hasegawa H, Yamazaki S (1985) Ultrasonically guided subsegmentectomy. *Surg Gynecol Obstet* 161:346–350

-
2. Takasaki K (1998) Glissonean pedicle transection method for hepatic resection: a new concept of liver segmentation. *J Hepatobiliary Pancreat Surg* 5:286–291
 3. Inoue Y, Arita J, Sakamoto T, Ono Y, Takahashi M, Takahashi Y, Kokudo N, Saiura A (2015) Anatomical liver resections guided by 3-dimensional parenchymal staining using fusion indocyanine green fluorescence imaging. *Ann Surg* 262:105–111
 4. Aoki T, Koizumi T, Mansour DA, Fujimori A, Kusano T, Matsuda K, Tashiro Y, Watanabe M, Otsuka K, Murakami M (2020) Ultrasound-guided preoperative positive percutaneous indocyanine green fluorescence staining for laparoscopic anatomical liver resection. *J Am Coll Surg* 230:e7–e12
 5. Ishizawa T, Zuker NB, Kokudo N, Gayet B (2012) Positive and negative staining of hepatic segments by use of fluorescent imaging techniques during laparoscopic hepatectomy. *Arch Surg* 147:393–394
 6. Sakoda M, Ueno S, Iino S, Hiwatashi K, Minami K, Kawasaki Y, Kurahara H, Mataka Y, Maemura K, Uenosono Y, Shinchi H, Natsugoe S (2014) Anatomical laparoscopic hepatectomy for hepatocellular carcinoma using indocyanine green fluorescence imaging. *J Laparoendosc Adv Surg Tech A* 24:878–882
 7. Mizuno T, Sheth R, Yamamoto M, Kang HS, Yamashita S, Aloia TA, Chun YS, Lee JE, Vauthey JN, Conrad C (2017) Laparoscopic glissonean pedicle transection (Takasaki) for negative fluorescent counterstaining of segment 6. *Ann Surg Oncol* 24:1046–1047
 8. Terasawa M, Ishizawa T, Mise Y, Inoue Y, Ito H, Takahashi Y, Saiura A (2017) Applications of fusion-fluorescence imaging using indocyanine green in laparoscopic hepatectomy. *Surg Endosc* 31:5111–5118
 9. Nomi T, Hokuto D, Yoshikawa T, Matsuo Y, Sho M (2018) A novel navigation for laparoscopic anatomic liver resection using indocyanine green fluorescence. *Ann Surg Oncol* 25:3982
 10. Urade T, Sawa H, Iwatani Y, Abe T, Fujinaka R, Murata K, Mii Y, Man-I M, Oka S, Kuroda D (2020) Laparoscopic anatomical liver resection using indocyanine green fluorescence imaging. *Asian J Surg* 43:362–368
 11. Lu G, Fei B (2014) Medical hyperspectral imaging: a review. *J Biomed Opt* 19:10901
 12. Akbari H, Uto K, Kosugi Y, Kojima K, Tanaka N (2011) Cancer detection using infrared hyperspectral imaging. *Cancer Sci* 102:852–857

-
13. Martinez B, Leon R, Fabelo H, Ortega S, Piñeiro JF, Szolna A, Hernandez M, Espino C, O'Shanahan J, Carrera D, Bisshopp S, Sosa C, Marquez M, Camacho R, Plaza ML, Morera J, Callico M (2019) Most relevant spectral bands identification for brain cancer detection using hyperspectral imaging. *Sensors (Basel)* 19:5481
 14. Köhler H, Jansen-Winkel B, Maktabi M, Barberio M, Takoh J, Holfert N, Moulla Y, Niebisch S, Diana M, Neumuth T, Rabe SM, Chalopin C, Melzer A, Gockel I (2019) Evaluation of hyperspectral imaging (HSI) for the measurement of ischemic conditioning effects of the gastric conduit during esophagectomy. *Surg Endosc* 33:3775
 15. Jansen-Winkel B, Maktabi M, Takoh JP, Rabe SM, Barberio M, Köhler H, Neumuth T, Melzer A, Chalopin C, Gockel I (2018) Hyperspectral imaging of gastrointestinal anastomoses. *Chirurg* 89:717–725
 16. Zuzak KJ, Naik SC, Alexandrakis G, Hawkins D, Behbehani K, Livingston E (2008) Intraoperative bile duct visualization using near-infrared hyperspectral video imaging. *Am J Surg* 195:491–497
 17. Holmer A, Marotz J, Wahl P, Dau M, Kämmerer PW (2018) Hyperspectral imaging in perfusion and wound diagnostics - methods and algorithms for the determination of tissue parameters. *Biomed Tech (Berl)* 63:547–556
 18. Barberio M, Longo F, Fiorillo C, Seeliger B, Mascagni P, Agnus V, Lindner V, Geny B, Charles AL, Gockel I, Worreth M, Saadi A, Marescaux J, Diana M (2020) HYPerspectral Enhanced Reality (HYPER): a physiology-based surgical guidance tool. *Surg Endosc* 34:1736–1744
 19. Kilkenny C, Browne W, Cuthill IC, Emerson M, Altman DG (2010) Animal research: reporting in vivo experiments: the ARRIVE guidelines. *Br J Pharmacol* 160:1577
 20. Bonaventura JM, Sharpe K, Knight E, Fuller KL, Tanner RK, Gore CJ (2015) Reliability and accuracy of six hand-held blood lactate analysers. *J Sports Sci Med* 14:203–214
 21. Barberio M, Felli E, Seyller E, Longo F, Chand M, Gockel I, Geny B, Swanstrom L, Marescaux J, Agnus V, Diana M (2020) Quantitative fluorescence angiography versus hyperspectral imaging to assess bowel ischemia: a comparative study in enhanced reality. *Surgery*. <https://doi.org/10.1016/j.surg.2020.02.008>
 22. Sucher R, Athanasios A, Köhler H, Wagner T, Brunotte M, Lederer A, Gockel I, Seehofer D (2019) Hyperspectral Imaging (HSI) in anatomic left liver resection. *Int J Surg Case Rep*

62:108–111

23. Diana M, Noll E, Diemunsch P, Moussallieh FM, Namer IJ, Charles AL, Lindner V, Agnus V, Geny B, Marescaux J (2015) Metabolism-guided bowel resection: potential role and accuracy of instant capillary lactates to identify the optimal resection site. *Surg Innov* 22:453–461

24. Diana M, Agnus V, Halvax P, Liu YY, Dallemagne B, Schlagowski AI, Geny B, Diemunsch P, Lindner V, Marescaux J (2015) Intraoperative fluorescence-based enhanced reality laparoscopic realtime imaging to assess bowel perfusion at the anastomotic site in an experimental model. *Br J Surg* 102:e169–176

25. Diana M, Noll E, Diemunsch P, Dallemagne B, Benahmed MA, Agnus V, Soler L, Barry B, Namer IJ, Demartines N, Charles AL, Geny B, Marescaux J (2014) Enhanced-reality video fluorescence: a real-time assessment of intestinal viability. *Ann Surg* 259:700–707

26. Diana M, Halvax P, Dallemagne B, Nagao Y, Diemunsch P, Charles AL, Agnus V, Soler L, Demartines N, Lindner V, Geny B, Marescaux J (2014) Real-time navigation by fluorescence-based enhanced reality for precise estimation of future anastomotic site in digestive surgery. *Surg Endosc* 28:3108–3118

27. Diana M, Noll E, Charles AL, Diemunsch P, Geny B, Liu YY, Marchegiani F, Schiraldi L, Agnus V, Lindner V, Swanstrom L, Dallemagne B, Marescaux J (2017) Precision real-time evaluation of bowel perfusion: accuracy of confocal endomicroscopy assessment of stoma in a controlled hemorrhagic shock model. *Surg Endosc* 31:680–691

28. Zuzak KJ, Naik SC, Alexandrakis G, Hawkins D, Behbehani K, Livingston EH (2007) Characterization of a near-infrared laparoscopic hyperspectral imaging system for minimally invasive surgery. *Anal Chem* 79:4709–4715 Publisher's Note Springer Nature remains neutral with regard to jurisdictional claims in published maps and institutional affiliations.

iiii) Real-time ICG guided anatomical liver resection with the positive and negative staining technique.

A comprehensive review of the literature on the published series on this technique was performed and published in the peer-reviewed journal HPB (33). Eighty-six articles were

initially found and 11 articles were finally included in the analysis, with 83 patients treated. Sixty-two patients (74.6%) underwent mono-segmentectomies. Thirty-five patients (42.1%) underwent the positive staining technique, and forty-eight patients (57.8%) underwent the negative staining technique. The positive or negative indocyanine green staining technique with real-time fluorescence guidance is an emerging and promising approach. However, the technique has to be standardized and advantages regarding oncologic results still need validation in further studies. My personal contribution to this review was to search and revise the published articles on this subject in English language, and writing and revision of the manuscript.

Article

Published in: **HPB (2021)**

HPB (Oxford) 2021 Nov;23(11):1647-1655. doi: 10.1016/j.hpb.2021.05.006.

Laparoscopic anatomical liver resection for malignancies using positive or negative staining technique with intraoperative indocyanine green-fluorescence imaging

Emanuele Felli^{1,2,3,6}, Takeaki Ishizawa⁴, Zineb Cherkaoui^{1,2}, Michele Diana^{1,3}, Simona Tripon^{5, 6}, Thomas Baumert^{5,6}, Catherine Schuster⁶, Patrick Pessaux^{1,2,3,6}

Running title: a promising technique for minimally invasive anatomical liver resection

-
1. Digestive and Endocrine Surgery, Nouvel Hôpital Civil, University of Strasbourg, Strasbourg, France
 2. IHU Strasbourg, Institute for Image-Guided Surgery, Strasbourg, France
 3. IRCAD, Research Institute against Digestive Cancer, Strasbourg, France
 4. Department of Gastroenterological Surgery, Cancer Institute Hospital, Japanese Foundation for Cancer Research, Ariake, Japan; Hepato-Biliary-Pancreatic Surgery Division, Department of Surgery, Graduate School of Medicine, The University of Tokyo, Tokyo, Japan
 5. Hepatology and Gastroenterology department, Nouvel Hôpital Civil, University of Strasbourg, Strasbourg, France
 6. Institute of Viral and Liver Disease, INSERM U1110, Strasbourg, France

Key words: anatomical liver resection – hepatocellular carcinoma- minimally invasive surgery
Manuscript revision

Abstract

Background: Indications for a minimally invasive resections are increasing worldwide, but respecting anatomical planes during intraparenchymal transection is demanding. Intraoperative ICG fluorescence staining of liver parenchyma has been introduced as a tool for real-time intraoperative guidance. The aim of this study is to make a systematic review of the current relevant literature on indications, techniques, and results of laparoscopic anatomical liver resection (LALR) using intraoperative indocyanine green (ICG) fluorescence for positive and negative staining of liver segments in patients affected by liver malignancies. **Methods:** Electronic bibliographical databases (MEDLINE and PubMed) were searched according to the PRISMA criteria. English language articles meeting the selection criteria and published until June 2020 were retrieved and reviewed. **Results:** a total of 86 articles were initially found and 11 articles were finally included in the analysis with a total of 83 patients treated. Sixty-two patients (74.6%) underwent

monosegmentectomies. Thirty-five patients (42.1%) underwent the positive staining technique, and forty-eight patients (57.8%) the negative staining technique.

Conclusions: The positive or negative indocyanine green staining technique with real-time fluorescence guidance is an emerging and promising approach. However, the technique has to be standardized and advantages in terms of oncologic results still need validation in further studies.

Introduction

Hepatocellular carcinoma (HCC), cholangiocarcinoma, and colorectal liver metastases are the most common liver malignancies for which liver resection is indicated. Anatomical liver resection (ALR) is the current standard for HCC resection as it allows a better postoperative survival and disease-free survival¹⁻⁴. Concerning colorectal liver metastases, there is still no strong evidence to support ALR. However, some authors have recently reported a high rate of positive margins in RAS-mutated lesions and worse cancer-specific survival secondary to remnant liver ischemia^{5, 6}, suggesting that anatomical resection could improve results. For intrahepatic cholangiocarcinoma, a better oncological outcome as compared to nonanatomical resection has been reported in patients with stage IB or II tumors without vascular invasion⁷. The concept of anatomical resection has subsequently become an oncological necessity, which also has to be related to the progressive diffusion of minimally invasive liver resections. The different classifications of liver anatomy currently accepted provide an important, yet idealized, representation of anatomical planes

and structures⁸. Defining the exact planes for resection is often difficult, especially in cirrhotic patients and for posterosuperior segment tumors. In fact, finding the correct intraparenchymal anatomical line is technically challenging and anatomical landmarks, such as hepatic veins and portal branches are then used under ultrasound guidance to guide transection⁹⁻¹². Makuuchi¹⁰ associated the ultrasound guidance to methylene blue injection in portal branches to delineate the precise limits of a determined segment or sector on the liver surface, the technique performed during open surgery. It necessitates as well the hepatic artery clamping, and the dye washout is relatively rapid. Replacing the blue dye with indocyanine green (ICG), and associating the use of near-infrared cameras, fluorescence-based segmentation to guide liver resections have been then introduced¹³. In 2008, Aoki et al. first reported an intraoperative technique for subsegments and segments staining during open hepatectomy, with a success rate of 93% in 4 identifying anatomical planes. The technique was considered safe, reproducible, and not timeconsuming¹⁴. In parallel to this, the role of laparoscopic liver resection (LLR) has been established for liver malignancies, especially HCC, confirmed by consensus meetings and international recommendations^{15, 16}. However, laparoscopic anatomical liver resection (LALR) techniques have not been fully standardized because both selective inflow portal clamping and portal staining, when used, are difficult to perform in the minimally invasive setting, especially in cirrhotic livers and for posterosuperior segments. To improve the quality and precision of anatomical resection, and to guide intraparenchymal transection, combined ICG fluorescence imaging in LALR has been used with direct portal ICG injection under

percutaneous-guided laparoscopic ultrasound, the so-called “positive staining” technique¹⁷⁻¹⁹ (Figures 1a, 2). Ishizawa was the first to perform this technique in 2012. Similarly, but with the opposite principle, is the “negative staining” technique (Figures 1b, 3a, 3b), achieved by the intravenous ICG dye injection after clamping the segmental portal pedicle, following the Glissonian concept of anatomical liver resection¹⁹⁻²³. We aimed to perform a systematic review of the current relevant literature concerning the different techniques and results of minimally invasive liver malignancies resections guided by means of ICG real-time fluorescence, using positive or negative staining.

Materials and methods

Study design

This review included different phases for the methodological algorithm, namely definition of search strategies, selection criteria, assessment of study quality, and analysis of relevant data. The preferred reporting items for systematic reviews and meta-analysis (PRISMA) statements checklist to report a systematic review were used (Fig. 4). Studies were then included in the IDEAL framework to contextualize this emerging technique in the field of surgical innovation.

Study inclusion criteria

At first, selection criteria to identify studies eligible for this review were stated. Prospective and retrospective studies, patient series, and patient reports were included and used for quantitative and qualitative synthesis of data.

Literature search strategy

Electronic bibliographical databases (i.e., MEDLINE, PubMed, EMBASE, and Scopus) were searched. The following terms were used for the search: laparoscopic hepatectomy, and indocyanine green fluorescence. English language articles meeting the selection criteria and published until June 2020 were retrieved and reviewed.

Study selection and quality assessment

The abstracts of the selected studies were blindly and independently screened for relevance by two reviewers (EF and ZC). In order to achieve the highest sensitivity and specificity, records were selected for further analysis only if none of the reviewers rejected it. The selected studies were analyzed and data extraction was performed independently by both reviewers. Any disagreement, if present, between the two reviewers in the selection and analysis was resolved via discussion between two other reviewers (CS and PP).

Data extraction and analysis

Qualitative and quantitative analysis were performed with data from the included studies.

Results

A total of 86 articles were initially found, 75 excluded because of preoperative IGC injection for liver tumors detection or simple IGC injection applications description. Experimental studies were also excluded. Ten articles were finally included in the analysis^{17-20, 22-27}. Three articles were case reports, the others reported single center series with a total of 83 patients treated with this technique (Table 1). Among these ten articles, seven were published in the last two years; sixty-six patients (79.5%) were reported

in 2018-2020 articles. Sixty-two (74.6%) underwent mono-segmentectomies, 5 patients (6%) right anterior sectionectomies, 4 patients (4.8%) right posterior sectionectomies, 4 patients (4.8%) left hepatectomies, 3 patients (3.5%) trisegmentectomy IV-V-VIII, 2 patients (2.4%) right hepatectomies, 2 patient (2.4%) left lateral sectionectomy, 1 patient (1.2%) bisegmentectomy V-VI. Thirty-five patients (42.1%) underwent the positive staining technique, and forty-eight patients (57.8%) the negative staining technique. In the positive staining group, Aoki²⁷ reported 14 patients treated with an intraoperative, yet transcutaneous ultrasound-guided, ICG injection. In two patients, this technique did not succeed because of a small segmental portal branch diameter (<2mm). The other authors reported intraoperative ICG injection under laparoscopic ultrasound guidance through a BK laparoscopic transducer model (BK Medical, 8666) probe characterized by the presence of a needle hole to guide injection. The injection technique was different in terms of needle size and ICG volume and concentration. When reported, needles had a variable size ranging from 18G to 22G. For positive staining, ICG concentration varied from 0.025mg/10mL to 0.025mg/mL. For negative staining, a direct intravenous ICG injection was performed after the use of a Glissonian approach and the clamping of portal pedicles, with a reported ICG dose comprised between 1.5mg to 2.5mg. Fluorescence was reported to appear after a minimum interval of 3 minutes from injection. No vanishing of ICG fluorescence due to ICG diffusion or increased background fluorescence was reported. Fusion 7 real-time imaging was used with a PINPOINT camera in 55 patients (85.9%). The principle of this type of cameras is that near-infrared light source excites the fluorophore and the

fluorescence signal is detected from it. The PINPOINT system is the most frequently used as it allows the possibility of a real time fusion of images; the system is composed by a 0°, 30° or 45° laparoscope, a complementary metal-oxide semiconductor camera head, and a nearinfrared laser diode for ICG excitation at a wavelength of 805 nm. Different types of images are possible to obtain, color images under white-light illumination, a monochromatic fluorescence images under near-infrared light illumination, and finally the fusion images with a green pseudocolor that shows the fluorescent parts of the liver. The vision mode can be changed during the operation, as the different types are simultaneously displayed in subscreens. Concerning the injection time, Aoki reported an average of 15 minutes (9-20 min). ICG injection in the positive staining technique is recommended to be slow to prevent any excessive pressure which could result in a retrograde flow into a portal branch supplying a neighboring segment, with consequent undesired staining. The average operation time in the same series (without initial injection time) was 243 min, and blood loss had an average of 185mL. Considering the resected liver volume, there was no statistically significant difference ($p=0.539$) between the preoperatively estimated average (149mL +/- 42mL), and the average specimen weight (158g +/- 44g). No intraoperative complications were reported, no conversion to laparotomy and no positive margins on the specimen neither. Indication to resection was hepatocellular carcinoma in 33 patients (51.6%), colorectal liver metastases in 12 patients (18.8%), breast cancer liver metastasis in one patient (1.5%), and no information was available in 18 patients (28.1%). Ueno 28 reported an hybrid approach with interventional radiology assistance using a preoperative

intra-arterial infusion of ICG for positive staining in an hybrid operating room. In the preoperative work-up, 3D portal vein branches reconstruction were always performed to identify anatomical variations, first to easily recognize small segmental portal branches, and then to determine the precise injection point and the estimated volume to be resected. In the most recent monocentric retrospective series reported by Xu³⁴, a total of 19 patients underwent positive (n=5) and negative (n=14) staining respectively. The median operative time was 260 with (150-360 min), median intraoperative blood loss was 300cc (50-800ml). No conversion to laparotomy was reported. There were also information on failure rate in both positive (n=4) (wrong portal segment injection, venous branch injection) and negative (n=13) (arterial collaterals staining the excluded segmentsector, wrong glissonean pedicle clamping, multiple single segments branches not entirely clamped) staining. According to IDEAL framework³⁵ this innovative technique is corresponding at present to Stage 1a (stage 0 to 4), where the development of the technique is still limited to single centre/single intervention and case series, or prospective cohort. The purpose at this stage is the development of the procedure to a stable version, the number of treated patients still limited and performed by few innovators and early adopters surgeons. No clear standardization of indications, technique and results exist, with necessity of further research to design appropriated prospective studies.

Discussion ICG was approved by the U.S. Food and Drug Administration in 1954 and was widely used in many different clinical settings. The first clinical applications were to evaluate liver function and cardiac output. In the 1970s, a protein-bound ICG was found to

emit fluorescence with a peak at about 840nm under near-infrared light illumination with (750-810nm)²⁸. Intraoperative ICG use has been also described in visceral surgery (colorectal, upperGI, etc), with an increasing use especially for detection and estimation of stumps vascular perfusion and lymphnodes visualization. Indocyanine green applications in liver surgery have progressively gained attention over recent years and with different applications such as intraoperative guidance for anatomical liver resections, to localize subcapsular and 9 intraparenchymal tumors, or to recognize biliary anatomy²⁹⁻³¹. For anatomical resection, three main techniques are used: positive staining (intraoperative direct intraportal injection in the segment/section to be resected), negative staining (intraoperative intravenous injection of ICG to visualize the remnant perfused liver), and a hybrid combined percutaneous approach (with intra-arterial segmental injection of ICG)

25. Concerning intraoperative image visualization, both classic ICG camera and real-time fusion images vision are reported. Advantages of fluorescence imaging over the blue dye technique include the long-lasting identification of the anatomical part to resect, a clearer visualization of hepatic segments on hepatic surfaces (especially in patients with cirrhosis and/or previous liver resections), and the possibility to identify segmental boundaries not only from the liver surface but also from the raw surfaces during parenchymal dissection³²,

33. In contrast, a major disadvantage is the difficulty in the re-evaluation of segmental boundaries once ICG has been injected. The lack of tactile sensation, the physiological organ deformation according to patient position and liver exposure, the lack of a 3D vision, and the difficulty of precisely conduct an intraoperative laparoscopic ultrasound are some

of the intrinsic difficulties of minimally invasive surgery, enhanced when performing a real anatomical liver resection. In addition, liver anatomy is complex and anatomical planes are difficult to visualize during intraparenchymal transection, especially in cirrhotic patients and for posterosuperior segments. It is well-established that for HCC, anatomical resection is associated with a better overall survival and a lower recurrence rate, and recent evidence suggests its role in the treatment of intrahepatic cholangiocarcinoma and potentially for colorectal liver metastases. It must be stressed that anatomical resection is an oncological necessity and a parameter of the quality of surgical resection. The worldwide progressive diffusion of minimally invasive liver surgery put this technical and oncological challenge as one of the priorities in HPB surgery. In 2008, Aoki reported direct ICG injection during laparotomy¹⁴ modifying the original Makuuchi technique, which consisted in blue dye 10 injection. In 2012, Ishizawa was the first to report positive and negative staining during a laparoscopic resection¹⁷. The positive and negative staining techniques require advanced laparoscopic skills and are technically demanding, though no additional operative time is reported by the different authors, with a mean of 18 minutes necessary for injection in the positive staining group. To overcome some of these difficulties, Aoki proposed a percutaneous preoperative direct ICG injection under trans-abdominal ultrasound guidance, immediately before resection. At present, only small single center series have been published, with a total of 83 patients treated, and no injection protocol standardization, nor strong specific reasons to choose between positive or negative staining. Considering positive staining, difficulties are related to the possibility of correctly inject and visualize

the dye in the segmental portal branch, which can sometimes be multiple according to the patient's anatomy, and most of all difficult to perform for branches less than 2mm in diameter. Reflux to other portal segments and the lesion of biliary or arterial branches are some of the drawbacks of the technique. In fact, only a very small amount of ICG that could totally be taken up by hepatocytes in targeting hepatic segments should be administered, preventing the outflow of ICG from hepatic veins followed by reperfusion into the liver. Considering negative staining, the Glissonian approach can be hemorrhagic and a cause of biliary lesions, as well as technically demanding for posterior segments. Ueno²⁵ proposed a hybrid approach with interventional radiology assistance and intra-arterial ICG injection, hence avoiding previously mentioned difficulties. This strategy is nonetheless not easier, more complex from a logistic point of view, and necessitates additional time and costs, along with the presence of a hybrid operating room and of an experienced and dedicated radiologist. The recent introduction of fusion image cameras allows fluorescence visualization and normal vision simultaneously, preventing the surgeon to continuously switch from one to the other, which is a major advance for this innovating technique. Five out of eleven articles have been published 11 in the last two years, comprising the vast majority of patients (79.5%). It has to be observed that all of these reports come from Asia, where anatomical liver resection for HCC is historically more frequently performed. Very recently the first multicenter robotic series was reported by Chiow³⁶, with a total of 52 patients with negative (n=40) and positive (n=12) technique. Robotic liver surgery is at present still performed in a minority of minimally liver resections, but there is a constant

increase of its use, along with published surgical series. As for laparoscopic surgery, in robotic liver resections clear identification of anatomical margins may help during dissection. It has to be considered that some technical differences exist between laparoscopy and robotics: robotic ultrasound probe is different to the laparoscopic one, in particular there are no probes available with an integrated hole to direct the needle in case of positive staining. A second consideration is that robotic arms usually occupy a large part of the external operative field, with a more difficult approach when inserting the needle percutaneously. Finally, inversely to laparoscopy where the liver surgeon usually performs together ultrasound, percutaneous injection and resection, in a robotic setting the operative surgeon is far from the surgical field. So in case of the positive staining technique, another surgeon with the same technical expertise both in intraoperative ultrasound and percutaneous needle insertion is needed. The advantages in terms of oncological results and technical feasibility of the positive and negative staining technique will necessitate further studies, as well as the standardization of the technique. This promising and interesting technique is a Stage 1a of the IDEAL framework, with only a few of innovators surgeons and early adopters, along with a limited number of patients treated. Consequently, it is still far from standardization, both for indications and technique. The present challenge for the minimally liver surgeon approaching to the positive or negative staining is complex. First, it is necessary the perfect use of the intraoperative ultrasound, with a precise detection of single, often multiples, segmental portal branches, according to the all possible anatomical variations. 12 Secondly, skills for percutaneous ultrasound guided injection with very thin

needles are needed, with possible position variations secondary to respiratory movements and cardiac activity. Finally, the need of a team work, both for ICG dilution and preparation, as well for synchronization of clamping and intravenous injection for the negative staining. Concerning indications and results, another consideration that could possibly be made is in relation to liver transplantation. Bridge or salvage liver transplantation in patients affected by HCC on cirrhotic livers is still a matter of debate in terms of indications and results, but frequently performed in Western countries due the shortage of organs. As precise anatomical laparoscopic liver resection is rarely performed due to previously mentioned difficulties nowadays, the positive or negative IGC staining technique could possibly be a “surgeon”- related variable in this setting as the quality of resection may influence the oncologic results of transplantation 37 .

Conclusions

Minimally invasive precise anatomical liver resection is a major challenge both for technical difficulties and the oncological implications in case of suboptimal resection, especially for HCC. The positive or negative indocyanine green staining technique with real-time fluorescence guidance is an emerging and promising approach, the feasibility of which has been demonstrated by advanced laparoscopic and liver surgeons. However, the technique has to be standardized and advantages in terms of oncologic results still need validation in further studies.

Disclosures: The authors declare that they have no conflict of interest Emanuele Felli have have no conflicts of interest or financial ties to disclose Takeaki Ishizawa have no conflicts of interest or financial ties to disclose Zineb Cherkaoui have no conflicts of interest or financial ties to disclose Michele Diana have no conflicts of interest or financial ties to disclose Simona Tripon have no conflicts of interest or financial ties to disclose Thomas Baumert have no conflicts of interest or financial ties to disclose Catherine Schuster have no conflicts of interest or financial ties to disclose Patrick Pessaux have have no conflicts of interest or financial ties to disclose

Table 1

Author	Year	Patients (n=)	Indication	Type of resection	Staining type	Fusion image	NIR camera system ^o
Ishizawa ¹⁷	2012	2	CRLM/ n/a	Segmentectomy III	1 P,1 N	no	n/a
Sakoda ¹⁸	2014	2	HCC	Segmentectomy V- VI	P P	no	IRI, Olympus
Terasawa ¹⁹	2017	12	HCC, CRLM	1 Segmentectomy II/III 3 segmentectomy III 3 segmentectomy IV 3 segmentectomy V 1 segmentectomy V/VI 1 segmentectomy VI	N P	yes	PINPOINT fusion
Mizuno ²²	2017	1	Breast cancer liver metastasis	Segmentectomy VI	N		N/A

Nomi²³	2018	16	n/a	2 left hepatectomies 3 right anterior sectionectomies 3 right posterior sectionectomies 8 segmentectomies	N	PINPOINT fusion
Urade²⁴	2019	3	2HCC 1CRLM	segmentectomy	N	VISERA ELITE Olympus
Ueno²⁵	2019	10	7HCC 3CRLM	segmentectomy	Phybrid	PINPOINT
Berardi²⁶	2019	1	HCC	segmentectomy	N	n/a
Aoki²⁷	2019	14	9HCC 5CRLM	segmentectomy	P	PINPOINT
Ito²⁰	2020	3	2HCC 1CRLM	1 segmentectomy VI 2 segmentectomy VII	P	PINPOINT
Xu³⁴	2020	19	HCC	8 segmentectomies 6 bisegmentectomies 3 trisegmentectomies 2 right hepatectomies 2 left hepatectomies	14 N 5 P	N/A

NIR: near-infrared

P: positive staining

N: negative staining

HCC: hepatocellular carcinoma

CRLM: colorectal liver metastases

Positive staining

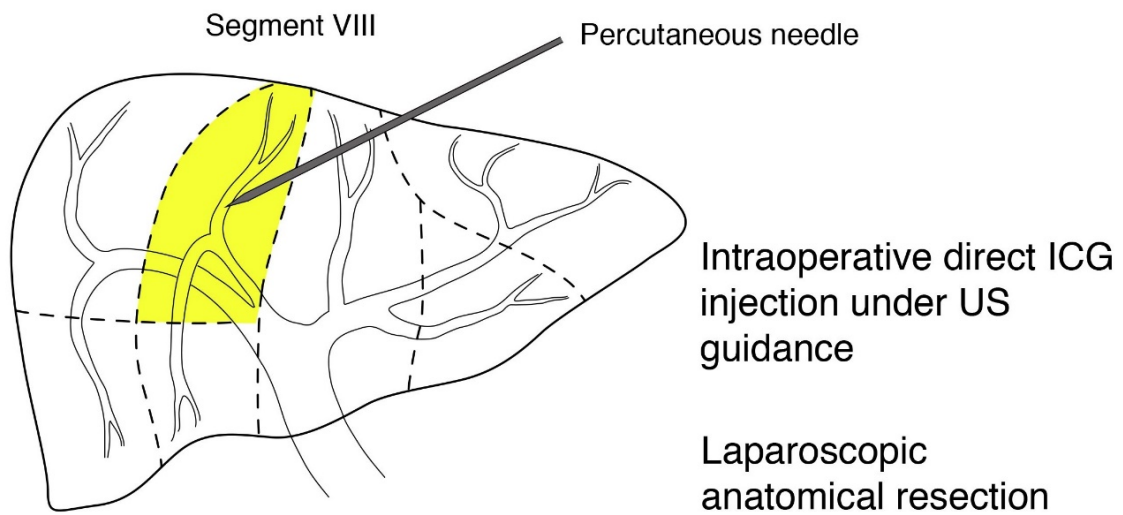


Figure 1a. Schematic representation of ICG positive staining

Negative staining

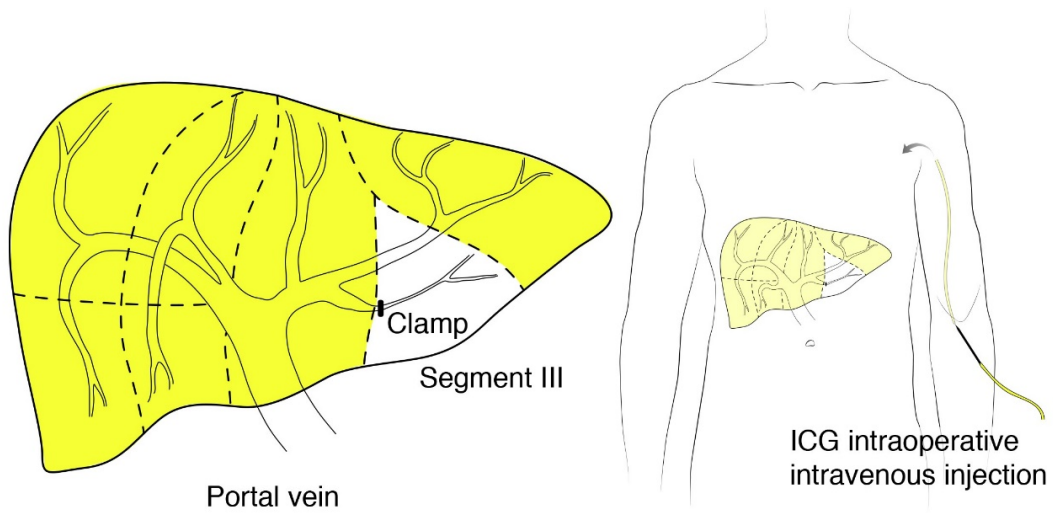


Figure 1b. Schematic representation of ICG negative staining

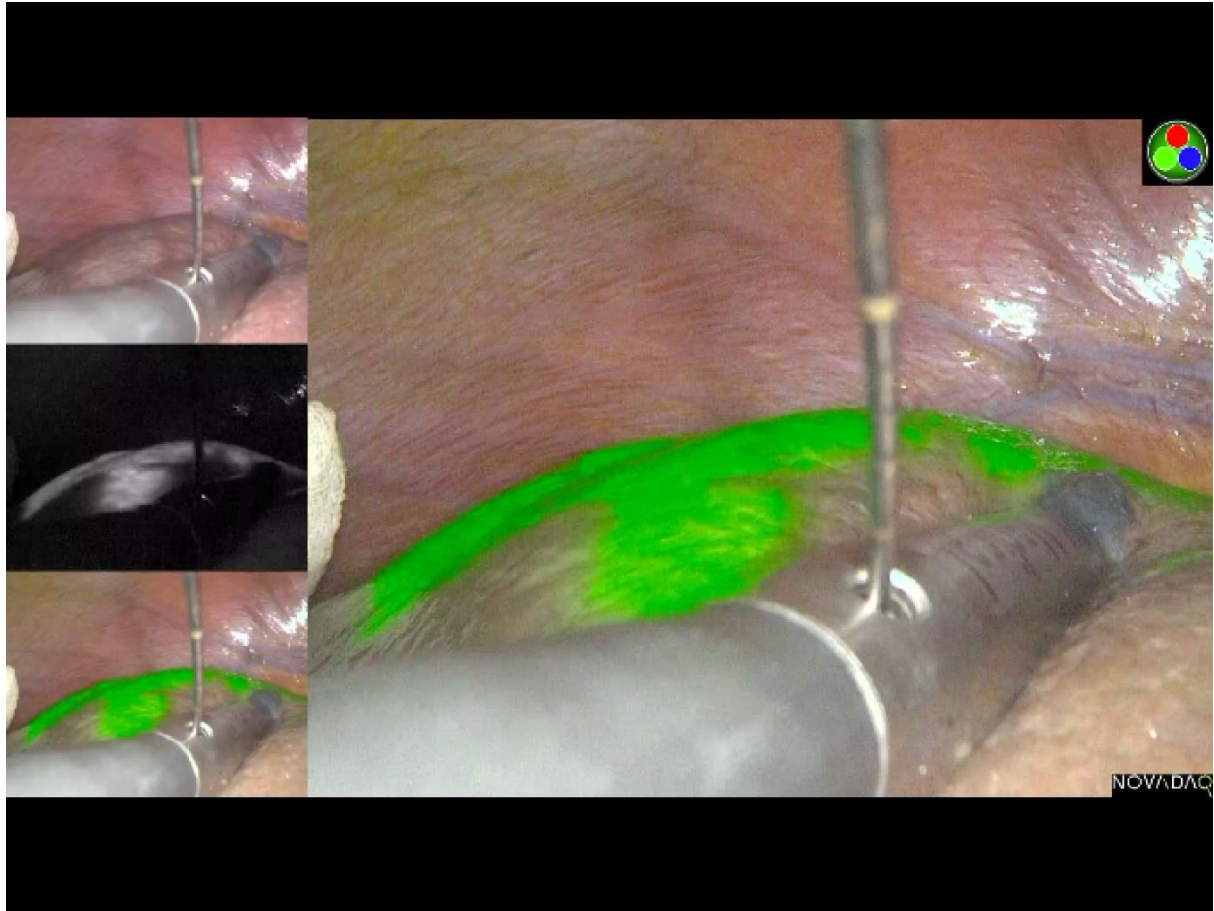


Figure 2. Positive staining: laparoscopic direct intraoperative ICG injection under ultrasound guidance. The stained segment becomes green with a fusion image camera.

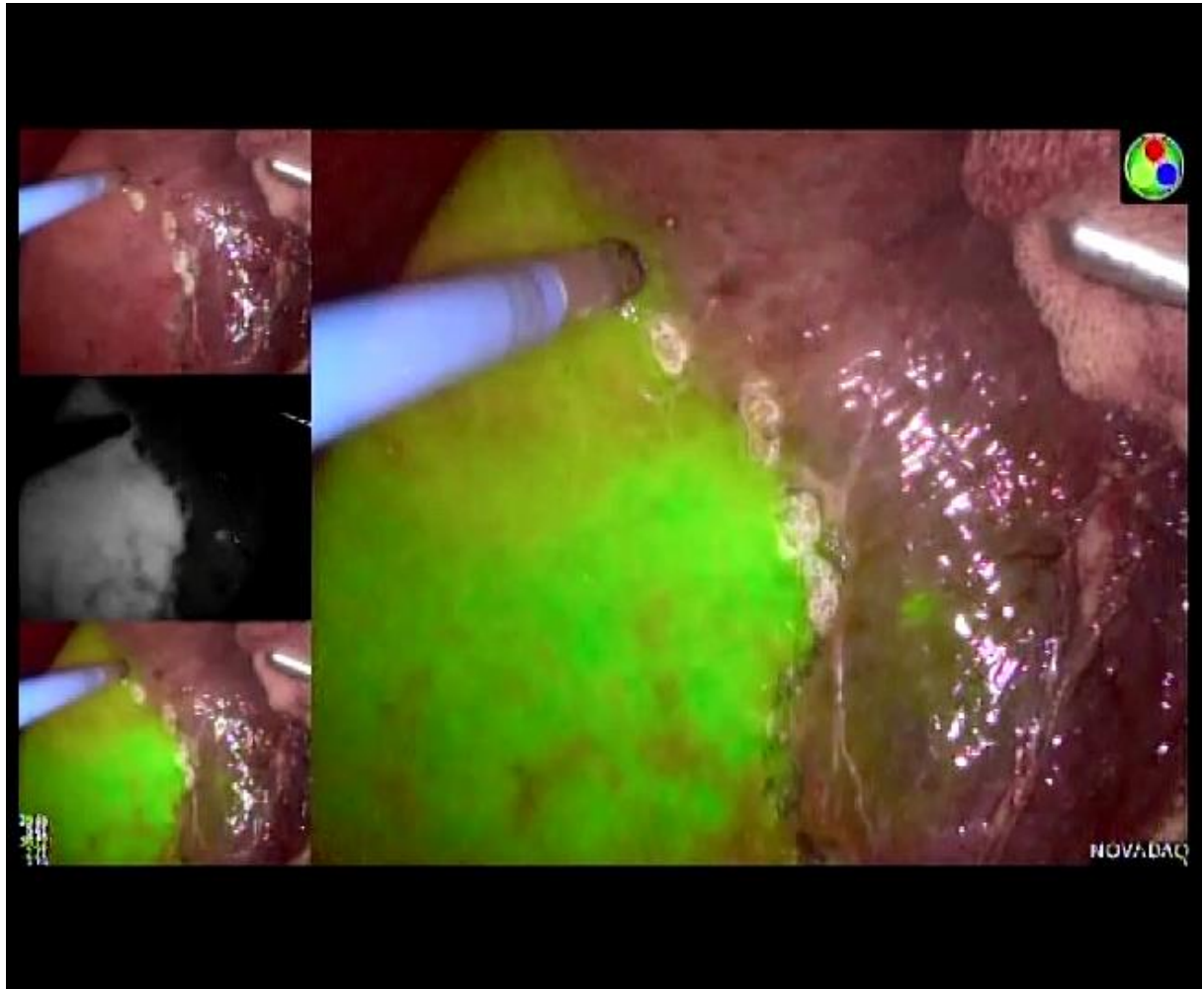


Figure 3a. Negative staining: intravenous ICG injection; fluorescence is present on the remnant liver.

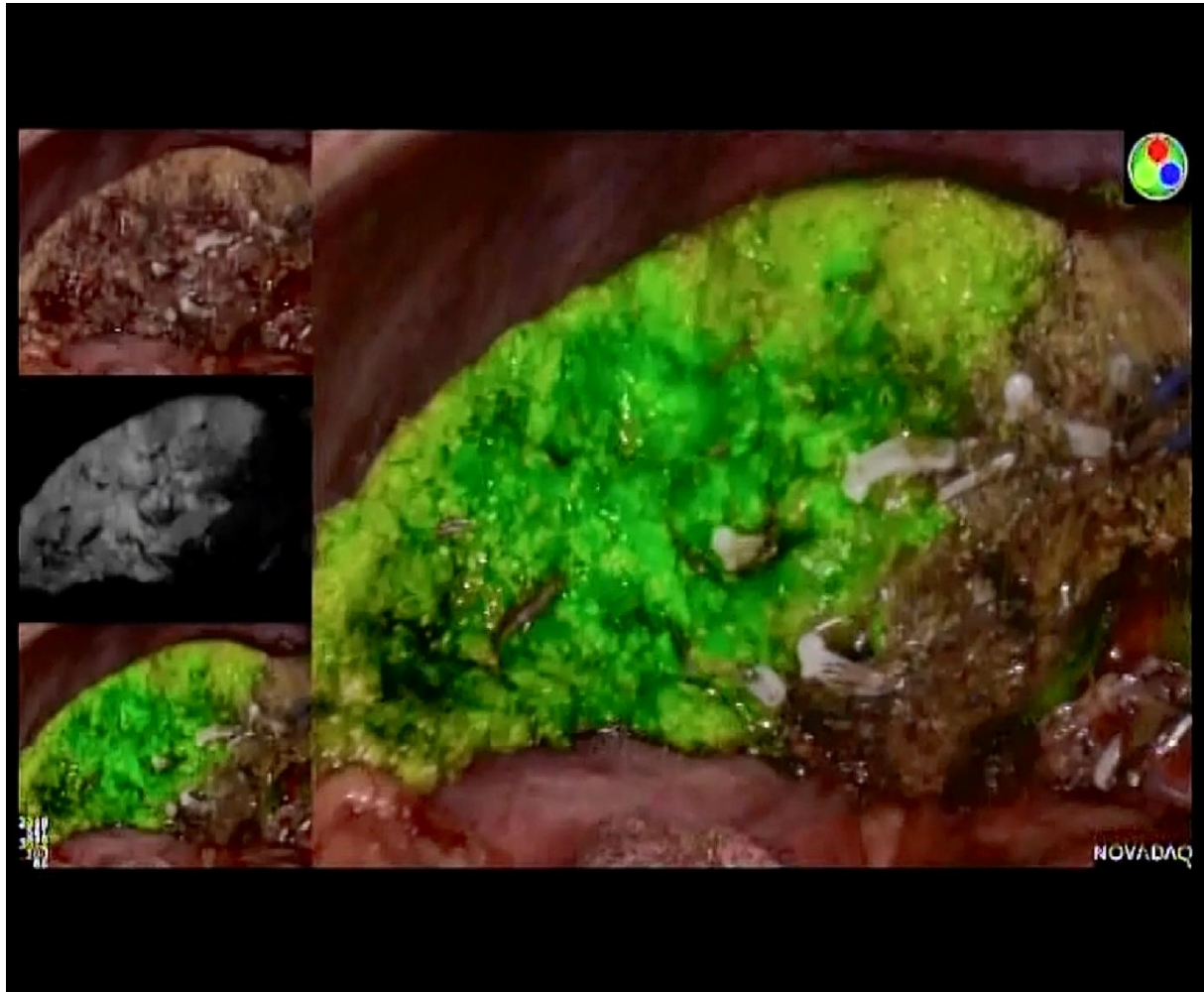


Figure 3b. Negative staining: during resection, the perfused remnant liver is green on the surface as well as intraparenchymally.



PRISMA 2009 Flow Diagram

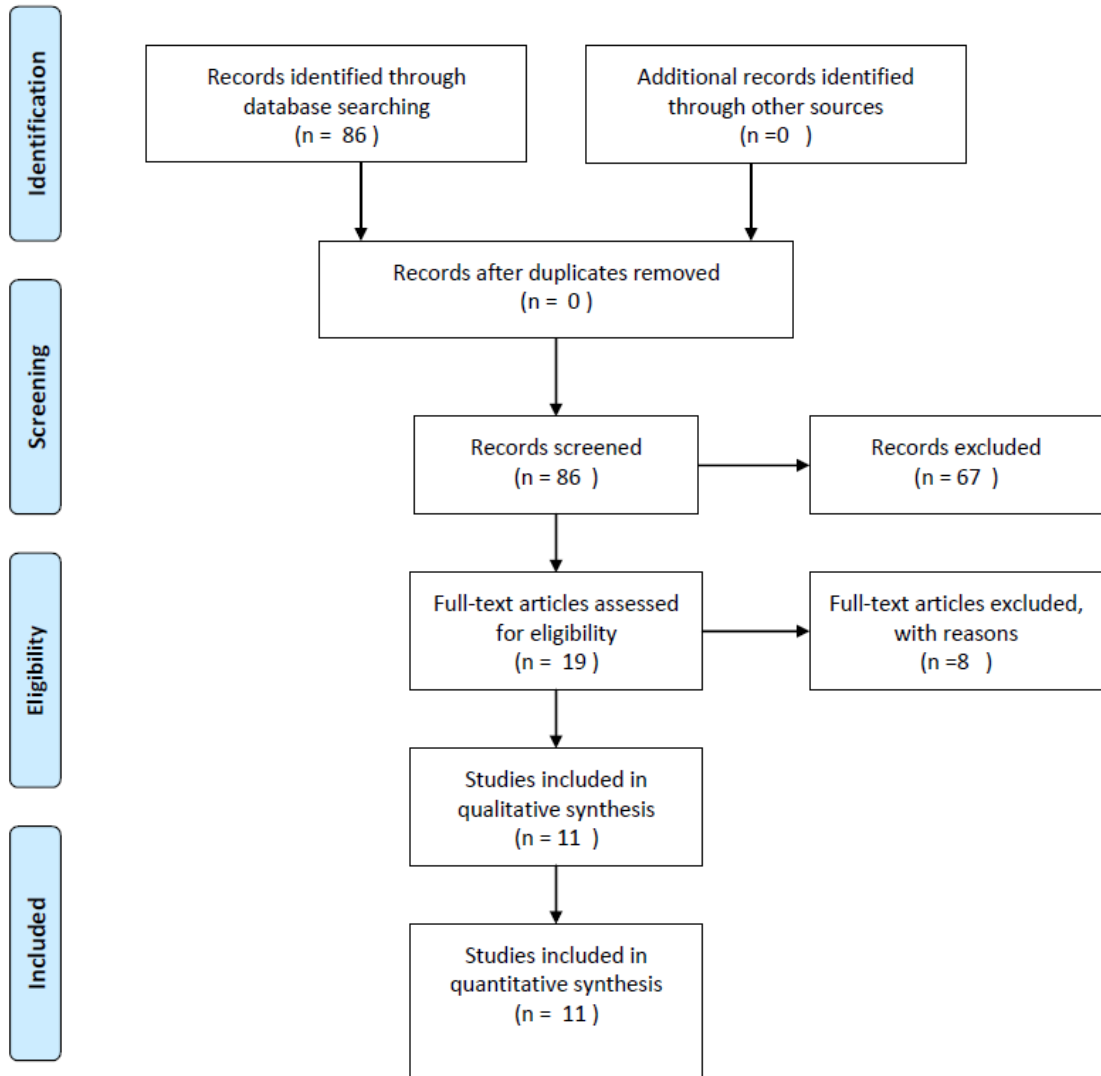


Figure 4. Preferred reporting items for systematic reviews and meta-analysis (PRISMA) flow diagram

References

1. Hasegawa K, Kokudo N, Imamura H, et al. Prognostic impact of anatomic resection for hepatocellular carcinoma. *Ann Surg* 2005; 242(2):252-9.
2. Kosuge T, Makuuchi M, Takayama T, et al. Long-term results after resection of hepatocellular carcinoma: experience of 480 cases. *Hepatogastroenterology* 1993; 40(4):328-32.
3. Ueno S, Kubo F, Sakoda M, et al. Efficacy of anatomic resection vs nonanatomic resection for small nodular hepatocellular carcinoma based on gross classification. *J Hepatobiliary Pancreat Surg* 2008; 15(5):493-500.
4. Yamamoto M, Takasaki K, Ohtsubo T, et al. Effectiveness of systematized hepatectomy with Glisson's pedicle transection at the hepatic hilus for small nodular hepatocellular carcinoma: retrospective analysis. *Surgery* 2001; 130(3):443-8.
5. Brudvik KW, Mise Y, Chung MH, et al. RAS Mutation Predicts Positive Resection Margins and Narrower Resection Margins in Patients Undergoing Resection of Colorectal Liver Metastases. *Ann Surg Oncol* 2016; 23(8):2635-43.
6. Yamashita S, Venkatesan AM, Mizuno T, et al. Remnant Liver Ischemia as a Prognostic Factor for Cancer-Specific Survival After Resection of Colorectal Liver Metastases. *JAMA Surg* 2017; 152(10):e172986.
7. Si A, Li J, Yang Z, et al. Impact of Anatomical Versus Non-anatomical Liver Resection on Short- and Long-Term Outcomes for Patients with Intrahepatic Cholangiocarcinoma. *Ann Surg Oncol* 2019; 26(6):1841-1850.
8. Majno P, Mentha G, Toso C, et al. Anatomy of the liver: an outline with three levels of complexity--a further step towards tailored territorial liver resections. *J Hepatol* 2014; 60(3):654-62.
9. Ferrero A, Lo Tesoriere R, Russolillo N, et al. Ultrasound-guided laparoscopic liver resections. *Surg Endosc* 2015; 29(4):1002-5.
10. Makuuchi M, Hasegawa H, Yamazaki S. Ultrasonically guided subsegmentectomy. *Surg Gynecol Obstet* 1985; 161(4):346-50.
11. Shindoh J, Seyama Y, Matsuda M, et al. Continuous ultrasound navigation for safe and precise anatomic resection of the liver. *Hepatogastroenterology* 2013; 60(123):590-4.

-
12. Torzilli G, Makuuchi M. Ultrasound-guided finger compression in liver subsegmentectomy for hepatocellular carcinoma. *Surg Endosc* 2004; 18(1):136-9.
 13. Tanaka T, Takatsuki M, Hidaka M, et al. Is a fluorescence navigation system with indocyanine green effective enough to detect liver malignancies? *J Hepatobiliary Pancreat Sci* 2014; 21(3):199-204.
 14. Aoki T, Yasuda D, Shimizu Y, et al. Image-guided liver mapping using fluorescence navigation system with indocyanine green for anatomical hepatic resection. *World J Surg* 2008; 32(8):1763-7.
 15. Wakabayashi G, Cherqui D, Geller DA, et al. Recommendations for laparoscopic liver resection: a report from the second international consensus conference held in Morioka. *Ann Surg* 2015; 261(4):619-29.
 16. Abu Hilal M, Aldrighetti L, Dagher I, Edwin B, et al. The Southampton Consensus Guidelines for Laparoscopic Liver Surgery: From Indication to Implementation. *Ann Surg*. 2018 Jul;268(1):11-18
 17. Ishizawa T, Zuker NB, Kokudo N, et al. Positive and negative staining of hepatic segments by use of fluorescent imaging techniques during laparoscopic hepatectomy. *Arch Surg* 2012; 147(4):393-4.
 18. Sakoda M, Ueno S, Iino S, et al. Anatomical laparoscopic hepatectomy for hepatocellular carcinoma using indocyanine green fluorescence imaging. *J Laparoendosc Adv Surg Tech A* 2014; 24(12):878-82.
 19. Terasawa M, Ishizawa T, Mise Y, et al. Applications of fusion-fluorescence imaging using indocyanine green in laparoscopic hepatectomy. *Surg Endosc* 2017; 31(12):5111-5118.
 20. Ito D, Ishizawa T, Hasegawa K. Laparoscopic positive staining of hepatic segments using indocyanine green-fluorescence imaging. *J Hepatobiliary Pancreat Sci* 2020.
 21. Takasaki K. Glissonean pedicle transection method for hepatic resection: a new concept of liver segmentation. *J Hepatobiliary Pancreat Surg* 1998; 5(3):286-91.
 22. Mizuno T, Sheth R, Yamamoto M, et al. Laparoscopic Glissonean Pedicle Transection (Takasaki) for Negative Fluorescent Counterstaining of Segment 6. *Ann Surg Oncol* 2017; 24(4):1046-1047.
 23. Nomi T, Hokuto D, Yoshikawa T, et al. A Novel Navigation for Laparoscopic Anatomic Liver Resection Using Indocyanine Green Fluorescence. *Ann Surg Oncol* 2018; 25(13):3982.
 24. Urade T, Sawa H, Iwatani Y, et al. Laparoscopic anatomical liver resection using indocyanine green fluorescence imaging. *Asian J Surg* 2020; 43(1):362-368.
 25. Ueno M, Hayami S, Sonomura T, et al. Concomitant Use of Indocyanine Green Fluorescence Imaging and Interventional Radiology for Detection of Liver

-
- Segments During Laparoscopic Anatomical Liver Resection: Pilot Feasibility Study. *Surg Laparosc Endosc Percutan Tech* 2019; 29(4):242-246.
26. Berardi G, Wakabayashi G, Igarashi K, et al. Full Laparoscopic Anatomical Segment 8 Resection for Hepatocellular Carcinoma Using the Glissonian Approach with Indocyanine Green Dye Fluorescence. *Ann Surg Oncol* 2019; 26(8):2577-2578.
 27. Aoki T, Koizumi T, Mansour DA, et al. Ultrasound-Guided Preoperative Positive Percutaneous Indocyanine Green Fluorescence Staining for Laparoscopic Anatomical Liver Resection. *J Am Coll Surg* 2020; 230(3):e7-e12.
 28. Landsman ML, Kwant G, Mook GA, et al. Light-absorbing properties, stability, and spectral stabilization of indocyanine green. *J Appl Physiol* 1976; 40(4):575-83.
 29. van Manen L, Handgraaf HJ, Diana M, et al. A practical guide for the use of indocyanine green and methylene blue in fluorescence-guided abdominal surgery. *Journal of surgical oncology* 2018; 118(2):283-300.
 30. Baiocchi GL, Diana M, Boni L. Indocyanine green-based fluorescence imaging in visceral and hepatobiliary and pancreatic surgery: State of the art and future directions. *World journal of gastroenterology* 2018; 24(27):2921.
 31. Diana M. Enabling precision digestive surgery with fluorescence imaging. *Translational gastroenterology and hepatology* 2017; 2.
 32. Miyata A, Ishizawa T, Tani K, et al. Reappraisal of a Dye-Staining Technique for Anatomic Hepatectomy by the Concomitant Use of Indocyanine Green Fluorescence Imaging. *J Am Coll Surg* 2015; 221(2):e27-36.
 33. Inoue Y, Arita J, Sakamoto T, et al. Anatomical Liver Resections Guided by 3-Dimensional Parenchymal Staining Using Fusion Indocyanine Green Fluorescence Imaging. *Ann Surg* 2015; 262(1):105-11.
 34. Xu Y, Chen M, Meng X, LU P, et al Laparoscopic anatomical liver resection guided by real- time indocyanine green fluorescence imaging: experience and lessons learned from the initial series in a single center *Surg End* (2020) 34, 4683-4691
 35. Hirst A, Philippou Y, Blazeby J, Campbell B, et al. No Surgical Innovation Without Evaluation: Evolution and Further Development of the IDEAL Framework and Recommendations. *Ann Surg.* 2019 Feb;269(2):211-220.
 36. Adrian K H Chiow, Seoung Yoon Rho, Ian J.Y. Wee, Lip Seng Lee, Gi Hong Choi. Robotic ICG guided anatomical liver resection in a multicentre cohort: an evolution from “positive staining” into “negative staining” method

-
37. Felli E, Baumert T, Pessaux P. Is minimally invasive true anatomical HCC resection a future way to improve results in bridge or salvage liver transplantation? *Clin Res Hepatol Gastroenterol* 2020.

6.2b) Publication of the results.

We collected prospectively intraoperative hyperspectral images during major hepatectomies in 15 patients. The acquisitions were done after laparotomy, before hepatic pedicle clamping (when needed), during hepatic pedicle clamping, and after declamping. Correlation to post-operative outcome regarding biological tests (liver function and coagulation) and clinical data (morbidity and mortality) was then performed. My personal contribution was the participation to the study design, operative procedures, revision of results and writing and revision of the manuscript. StO₂% values after liver resection were significantly higher in patients who underwent preoperative biliary drainage for jaundice (0.772396 vs 0.491312 ± 0.1123386, p=0.033) and lower in case of unhealthy (steatotic, fibrotic or cirrhotic) liver (0.308659 ± 0.1180001 vs 0.545178 ± 0.1022391, p=0.011). Tissue water Index (TWI) was the only HSI index to correlate with postoperative reintervention. Lower haemoglobin index (OHI) final values showed significant correlation with postoperative sepsis. HSI is a recent and interesting technology still in its experimental phase. This is the first clinical application in a monocentric major hepatectomy series and the reported results suggests that TWI and OHI could be associated to short-term postoperative outcomes. Further experimental and clinical studies are necessary to better explore and evaluate the potential value of this technology in current practice.

Article: under submission to: **British Journal of Surgery**

Hyperspectral imaging and Artificial Intelligence in major hepatectomies: preliminary results from the Ex-Machina trial

Emanuele Felli^{1,2,3,4}, Lorenzo Cinelli^{3,5}, Elisa Bannone¹⁰, Fabio Giannone^{1,2,3,4}, Edoardo Maria Muttillio⁶, Manuel Barberio³, Catherine Schuster⁴, Patrick Pessaux^{1,2,3,4}, Jacques Marescaux³, Sylvain Gioux⁸, Eric Felli^{3,7,9}, Michele Diana^{3,1*}

¹ Digestive and Endocrine Surgery, Nouvel Hôpital Civil, University of Strasbourg, 67000 Strasbourg, France; e.felli@chu-tours.fr (E.F.)

² IHU Strasbourg - Institut de Chirurgie Guidée par l'image, 67000 Strasbourg, France

³ Research Institute against Digestive Cancer (IRCAD), 67000 Strasbourg, France, michele.diana@ircad.fr (M.D.); eric.felli@ircad.fr (Er.F.)

⁴ Université de Strasbourg, Inserm, Institut de Recherche sur les Maladies Virales et Hépatiques UMR_S1110, Strasbourg, France

⁵ Department of Gastrointestinal Surgery, San Raffaele Hospital IRCCS, 20132 Milan, Italy; cinelli.lorenzo@hsr.it (L.C.)

⁶ Dipartimento di Scienze Medico Chirurgiche e Medicina Traslazionale, Sapienza Università di Roma, 00100 Roma, Italy, edoardomariamuttillio@gmail.com (E.M)

⁷ Department of Visceral Surgery and Medicine, Inselspital, Bern University of Bern, 3010 Bern, Switzerland, eric.felli@dbmr.unibe.ch

⁸ ICube Laboratory, University of Strasbourg, 67400 Strasbourg, France; Sylvain.Gioux@intusurg.com (S.G.)

⁹ Department of BioMedical Research, Visceral Surgery and Medicine, University of Bern, 3010 Bern, Switzerland, eric.felli@dbmr.unibe.ch

¹⁰ Department of surgery University of Verona

* Correspondence: michele.diana@ircad.fr

Simple Summary: major hepatectomy may be associated to major morbidity or mortality.

At present no intraoperative tools exist to predict the post-operative course. Hyperspectral imaging is a new and promising technology that may potentially help to evaluate real time liver function during and at the end of the operation. As no clinical data exist concerning a major hepatectomies series our aim was to correlate intraoperative images acquisitions and findings with the postoperative course.

Abstract: Major hepatic resections are associated with higher risk of postoperative complications and post-hepatectomy liver failure. After hepatic pedicle clamping ischemia-reperfusion injury may sometimes lead to post-hepatectomy liver failure. Early detection or, ideally, intraoperative prediction of liver dysfunction or failure would be essential for timely treatment. Fifteen patients who underwent major hepatic resections at Nouvel Hôpital Civil (Strasbourg, France) were retrospectively analyzed. Intraoperative acquisition with the hyperspectral camera system was performed at the beginning of the operation, before any liver manipulation, and at the end of hepatic resection after specimen removal. TWI was the only HSI index to correlate with postoperative reintervention. Lower OHI final values showed significant correlation with postoperative sepsis (0.641417 ± 0.0340463 vs 0.704987 ± 0.0712082 , $p=0.045$), while Δ OHI correlated with PHLF (-0.074822 ± 0.0774023 vs 0.022819 ± 0.0220585 , $p= 0.010$), also showing negative correlation with ALT values observed in POD5 ($\rho = -0.813$, $p=0.001$). This is the first clinical application in a monocentric major hepatectomy series, and the reported results suggest that TWI and OHI could be associated to short-term postoperative outcomes. Further experimental and clinical studies are necessary to better explore and evaluate the potential value of this technology in current practice.

Keywords: Hyperspectral imaging; Liver; Hepatectomy

1. Introduction

Indications for liver resections have increased during the last decades due to a more aggressive and multimodal treatment of primary and secondary liver malignancies[1,2]. Post-operative morbidity and mortality are related to many variables, such as patient performance status, comorbidities, liver function, and future liver remnant volume. Major hepatic resections, defined as the removal of three or more segments, are associated with higher risk of postoperative complications and post-hepatectomy liver failure[3,4]. Morphologic evaluation through magnetic resonance imaging (MRI) and computed tomography (CT) scan, associating the remnant liver volumetry, as well as functional assessment using indocyanine green (ICG) clearance test [5] or sequential hepato-biliary scintigraphy, are useful tools to accurately estimate the volume and function of the future liver remnant (FLR). Nevertheless, all these approaches provide a poor snapshot of preoperative conditions. . The vast majority of major hepatectomies require hepatic pedicle clamping to reduce bleeding during liver transection. The Pringle maneuver results in oxygen deprivation, which is the starting event that induces parenchymal damage, further compounded once blood circulation has been reestablished by the ischemia-reperfusion injury mechanism (IRI). This condition sometimes finally leadsto post-hepatectomy liver failure[6,7]. During the last decade, several solutions were considered to predict IRI and related post-operative liver disfunction, like ICG fluorescence imaging, microdialysis, carbon dioxide sensors, and near-infrared spectroscopy (NIRS)[8-12]. However, such methods are limited by the need for the administration of an exogenous dye, and/or by some degree of invasiveness, and their interpretation may vary. As a result, they are inadequate to estimate the risk of postoperative complications following major hepatectomies. Nevertheless, early detection or, ideally, intraoperative prediction of liver dysfunction or failure would be essential for timely treatment. In this complex scenario, a tool able to

provide a direct oxygenation map of the FLR, could ideally allow for intraoperative localization of liver ischemic damage, giving a prediction of postoperative outcomes. Hyperspectral imaging (HSI) is a non-invasive technique recently applied to the medical field, able to detect the relative reflectance of light at a wavelength comprised between 500 and 1000 nm, allowing the quantification of organic compounds. In a recent study, our group showed the potential usefulness of HSI as an intraoperative tool during image-guided surgery[13,14]. HSI was able to guide and improve the surgical resection line performed via real-time overlay of the hyperspectral image and RGB. Moreover, we demonstrated the quantification and discrimination of different types of liver ischemia, including arterial or total vascular inflow occlusion [15,16] providing a liver viability score in a preclinical model of ischemia-reperfusion injury. In the same way, higher values of water within hepatic tissue could be related to IRI and inflammation[17,18]. Given the above cited evidence and preliminary results in a preclinical setting, we translated the imaging system into a clinical setting. Our aim is to evaluate the HSI potential to predict postoperative outcomes after major hepatectomies

2. Materials and Methods

Study Design

The present study, which was part of the iEXMachyna3 project (Intraoperative EXamination Using MACHine-learning-based HYperspectral for diagNosis & Autonomous Anatomy Assessment), was registered at ClinicalTrials.gov (NCT04589884) and approved by the local ethics committee of the Faculty of Medicine of the University of Strasbourg (ID-RCB: 2020-A01896-33). This is a single-institution, one-arm prospective observational study designed in accordance with the Declaration of Helsinki and the

Strengthening the Reporting of Observational studies in Epidemiology statement (STROBE) guidelines.[19] A dedicated informed consent was obtained from each patient before surgery.

Study Population

Fifteen patients who underwent major hepatic resections with laparotomic approach between September 2020 and June 2021 at Nouvel Hôpital Civil (Strasbourg, France) for malignant lesions of the liver, were retrospectively analyzed from a prospectively maintained database.

Surgical procedure

Laparotomy was performed in all patients with a J-shaped Makuuchi incision, exposition of the surgical field with Tagasako retractor. A full exploration of the abdominal cavity was then performed to look for carcinosis or other anomalies. Liver was mobilized according to the type of hepatectomy. Hepatic pedicle control was made with a tourniquet to prepare intermittent clamping when needed. Hepatic pedicle clamping was 20 minutes and 10 minutes rest in healthy livers, and 10 minutes and 10 minutes rest in cirrhotic livers. Intraoperative ultrasound was performed to confirm the surgical strategy and to look for anatomical landmarks before transection. Portal vein branches and hepatic artery branches were ligated prior to hepatectomy. Hepatic vein control was not systematic. Transection line was then traced with electrocautery once devascularization was complete. Hepatectomy was performed with Cavitronic Ultrasonic Surgical Aspirator (CUSA), hemostasis and biliostasis with 5-0 or 6-0 polypropylene stitches and Hem-o-lock clips. Final ultrasound control was performed to check liver inflow and outflow. Transcystic Escat's external biliary drainage was left according to the type of hepatectomy. Drainage was not systematic.

Hyperspectral Imaging (HSI)

The HSI camera system (TIVITA, Diaspective Vision GmbH, Am Salzhaff, Germany) acquired hypercubes ($640 \times 480 \times 100$ each) and RGB (red, green, blue) images for ten acquisition steps. The hypercube was acquired in around 6 seconds. The TIVITA camera was perpendicularly adjusted at a 40 cm distance to avoid external light irradiations on the measuring area.[20] The system illuminated the area of interest with six halogen spotlights and the light sources in the surgery room were switched off during the HSI acquisition. The HSI camera is equipped with a push-broom imaging spectrometer with a slit-shaped aperture, an internal stepper motor moving the slit of the spectrograph, high quality IR-enhanced CMOS, and data processing equipment. The acquisition of a single hypercube is performed with a camera-specific module of the Perception Studio software (Perception Park GmbH, Graz, Austria). The spectral range of this camera is 500–995 nm. The light source is a 20 W OSRAM Halospot 70 Halogen lamp allowing for intense, broadband, temperature-stable, homogeneous, and fast pulses of radiation. The calibration of the wavelength is performed during camera production. Moreover, dark current effects are corrected after the recording of the data cube by the developed software component. The camera collects and processes the information from the electromagnetic spectrum measuring the reflectance spectra generated by the target of study. To convert image data from radiance to relative reflectance, a white reference object characterized by a high diffuse reflectance is used to create a reference cube before the measurements start. The TIVITA has preset algorithms, which allow to quantify the relative oxygen saturation (StO₂%) of the superficial microcirculation at a depth up to ~1 mm, whereas it is possible to quantify the relative oxygen saturation in deeper layers, within the near-infrared (NIR) spectrum, with a penetration depth up to 4-6 mm. The tissue water index (TWI) and the organ hemoglobin index (OHI) can be used to quantify and image the distribution of water

and hemoglobin, respectively, in the observed region of interest (ROI)[21]. Image acquisition was performed at the beginning of the operation, before any liver manipulation (baseline, T_0), and at the end of hepatic resection, after specimen removal (T_1). $StO_2\%$, NIR, TWI and OHI values were extracted for the same ROIs at T_0 and T_1 and their absolute values at T_1 , and the difference between T_1 and T_0 measurements (Δ) were calculated and analyzed. The intraoperative setting of HSI and acquired images are shown in **Figure 1**.

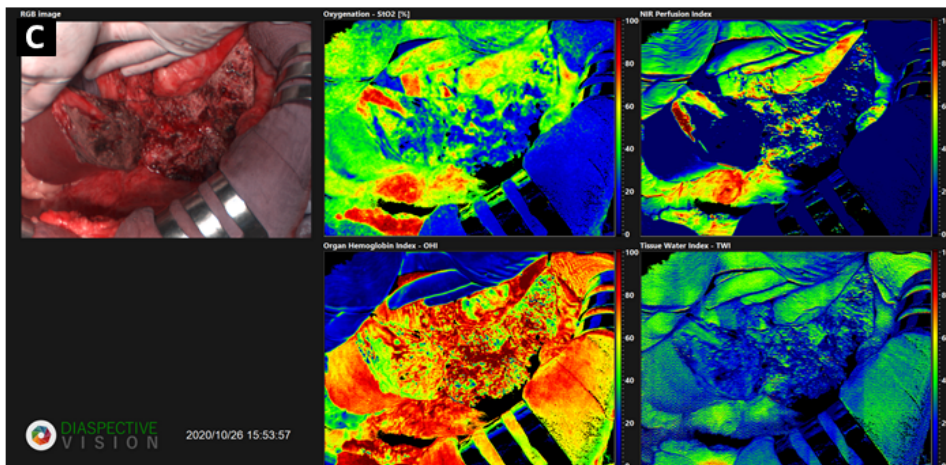
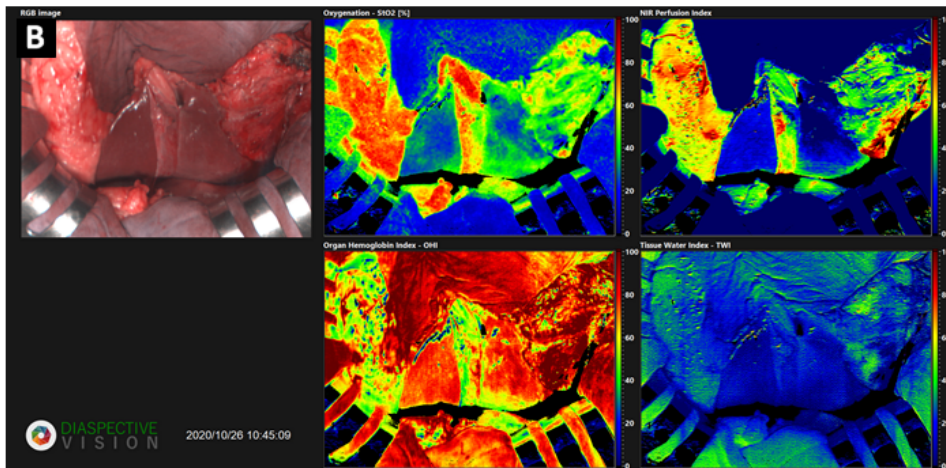
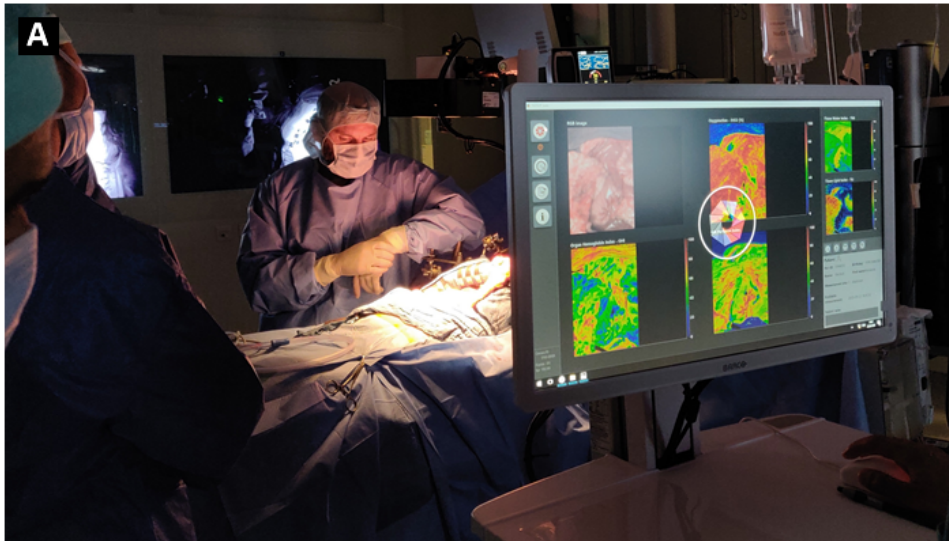


Figure 1. Intraoperative setting of HSI and acquired images. During the acquisition of data, all the lights of the operating room are turned off (A). The acquisition was performed at the beginning of the surgical procedure (B) and after the liver resection, at the end of surgery (C). The RGB (Red-Green-Blue) images and StO2%, NIR, OHI and TWI indexes are reported.

Definition of outcomes

Intraoperative findings and short-term surgical outcomes were analyzed. Intraoperative blood loss was defined as the amount of blood suctioned during the operation. Post-hepatectomy liver failure (PHLF), post-hepatectomy hemorrhage (PHH) and bile leakage were defined and graded according to the latest International Study Group of Liver Surgery (ISGLS) classifications.[22-24]. The same standardized enhanced recovery perioperative pathway[25] was applied to all patients. Reoperation was defined as a new operation that occurred within 60 days of surgery. The prothrombin time (PT) <50% and serum bilirubin >50 µmol/L on postoperative day (POD) 5 were analyzed (“50-50 criteria”) as predictors of liver failure and death after hepatectomy.[26]

Data collection

Preoperative, intraoperative, and postoperative data were retrospectively retrieved from a prospectively maintained electronic database. Preoperative data included: gender, age, body mass index (BMI), comorbidities such as dyslipidemia, diabetes, hypertension, preexisting hepatopathy, preoperative procedures (chemoembolization, portal vein embolization, biliary drainage), type of neoplasia, neoadjuvant chemotherapy, American Society of Anesthesiologists physical status classification (ASA)[27]. Bilirubin, aspartate transaminase (AST), alanine transaminase (ALT), gamma-glutamyltransferase (GGT), alkaline phosphatase (ALP), albumin, hemoglobin, PT, and international normalized ratio (INR) were collected preoperatively. Intraoperative data included duration of surgery, calculated from skin incision to closure of the last surgical wound, intraoperative blood loss, need for blood transfusions, number of resected segments of the liver, type of Pringle maneuver, and total duration of liver ischemia. Bilirubin, AST, ALT, GGT, ALP, albumin, hemoglobin, PT, and INR were routinely measured on POD 1, POD 2 and POD 5.

Histologic data on steatosis, fibrosis, and cirrhosis of non-tumoral liver were always reported in the final pathological report and collected.

All procedures were performed by two experienced HPB surgeons.

Statistical analysis

Categorical data were expressed as numbers and percentages. For continuous variables, median and interquartile range (IQR) were reported. Continuous variables were compared using the Student's t-test or the Mann-Whitney U test, as appropriate. Normality of data distribution was checked by histogram visual inspection. Two-tailed p-values were considered significant when less than 0.05. Statistical analyses were performed using SPSS for Windows, Version 25.0.

The Materials and Methods should be described with sufficient details to allow others to replicate and build on the published results. Please note that the publication of your manuscript implicates that you must make all materials, data, computer code, and protocols associated with the publication available to readers. Please disclose at the submission stage any restrictions on the availability of materials or information. New methods and protocols should be described in detail while well-established methods can be briefly described and appropriately cited.

Research manuscripts reporting large datasets that are deposited in a publicly available database should specify where the data have been deposited and provide the relevant accession numbers. If the accession numbers have not yet been obtained at the time of submission, please state that they will be provided during review. They must be provided prior to publication.

Interventionary studies involving animals or humans, and other studies that require ethical approval, must list the authority that provided approval and the corresponding ethical approval code.

3. Results

Overall, 15 patients submitted to major hepatectomies for liver tumors were included for experimental hyperspectral analysis. The most frequent preoperative diagnosis was hepatocellular carcinoma (HCC, 40%), followed by colorectal liver metastasis (CRLM, 33%). Five patients underwent neoadjuvant chemotherapy, while only one patient presented a biliary drainage for preoperative obstructive jaundice. Descriptive analysis of patients' preoperative characteristics and biochemical assessment is reported in **Table 1**.

Table 1. Descriptive analysis of preoperative variables

Variable	Total Cohort n=15
Gender, male (%)	10 (67)
Age, years*	69 (49; 73)
BMI, Kg/m²*	28.8 (26.6; 30.1)
BMI > 30 (%)	3 (20)
ASA, ≥3 (%)	9 (60)
Dislipidemia (%)	5 (33)
Diabetes (%)	6 (40)
Hypertension (%)	5 (33)
HBV or HCV + (%)	2 (13.5)
Hepatocellular carcinoma (%)	6 (40)
Colorectal metastasis (%)	5 (33)
Colangiocarcinoma (%)	2 (13.5)
Other (%)	2 (13.5)
Overall comorbidities (%)	11 (73.3)
Neoadjuvant therapy (%)	5 (33)
Preoperative chemoembolization (%)	5 (33)
Preoperative portal vein embolization (%)	6 (40)
Preoperative biliary drainage (%)	1 (6.7)
Preoperative bilirubin, μmol/L*	9.4 (5.7; 10.7)
Preoperative serum AST, U/L*	29 (23; 63)
Preoperative serum ALT, U/L*	46 (21; 60)
Preoperative serum ALP, U/L*	103 (73; 174)
Preoperative serum GGT, U/L*	86 (47; 172)
Preoperative serum Hemoglobin, g/dL*	12.8 (11.3; 13.6)
Preoperative serum PT, sec*	87 (75; 100)
Preoperative serum INR*	1.1 (1; 1.21)
Preoperative serum Albumin, g/dL*	43 (41; 46)

* Expressed as median [interquartile range]

BMI body mass index, *ASA* American Society of Anesthesiologists, *AST* ASpartate transaminase, *ALT* ALanine Trasnaminase, *ALP* Alkaline Phosphatase, *GGT* Gamma-Glutamyl Transferase, *PT* Prothrombin Time, *INR* International Normalized Ratio

All these operations were performed by laparotomy, with a median duration of 382 minutes; Pringle maneuver was performed in 10 patients (67%). Overall, the median duration of the vascular intermittent clamping was 53 minutes. Postoperative 90 days mortality was reported in two patients (13.5%), one after extended left hepatectomy associated to distal splenopancreasectomy that had aspiration pneumonia at postoperative day 21 and developed septic shock and multiorgan failure; the second patient had hemorrhagic shock after hepatic artery rupture after left extended hepatectomy and loco-regional lymphadenectomy for intrahepatic cholangiocarcinoma. Liver failure was described in four patients (26.9%), but only one required invasive treatment (grade C PHLF) and was related to postoperative death. Four other patients presented Dindo-Clavien complications ≥ 3 , two developed post-operative bilioma necessitating percutaneous drainage under general anesthesia, one acute kidney dysfunction requiring temporary dialysis and one abdominal abscess drained percutaneously. Descriptive analysis of intraoperative and postoperative variables is reported in **Table 2**.

Table 2. Descriptive analysis of intraoperative and postoperative variables

Variable	Total Cohort n=15
Number of resected hepatic segments*	4 (3; 6)
Duration of surgery, minutes [†]	382 (324; 452)
Vascular clamping (%)	10 (67)
Total time of vascular clamping, minutes*	53 (38; 80)
Intraoperative blood loss, mL [‡]	490 (200; 650)
Intraoperative transfusion (%)	2 (13.5)
Postoperative complications, (Dindo-Clavien) ≥ 3 (%)	6 (40)
Postoperative 90 days mortality (%)	2 (13.5)
Liver failure (%)	4 (26.9)
Grade A (%)	1 (6.7)
Grade B (%)	2 (13.5)
Grade C (%)	1 (6.7)
PHH (%)	2 (13.5)
Biliary leakage (%)	2 (13.5)
Sepsis (%)	5 (33)
30-days reoperation (%)	2 (13.5)
POD 1 serum Bilirubin, $\mu\text{mol/L}$ *	25.7 (16.4; 52.1)
POD 2 serum Bilirubin, $\mu\text{mol/L}$ *	24.1 (11.1; 67.1)
POD 5 serum Bilirubin, $\mu\text{mol/L}$ *	25.5 (10.4; 61.6)
POD 1 serum AST, U/L [‡]	788 (438; 1440)
POD 2 serum AST, U/L [‡]	608 (261; 1228)
POD 5 serum AST, U/L [‡]	75 (36; 128)
POD 1 serum ALT, U/L [‡]	541 (380; 1047)
POD 2 serum ALT, U/L [‡]	531 (352; 1383)

POD 5 serum ALT, U/L*	171 (79; 323)
POD 1 serum ALP, U/L*	75 (53; 106)
POD 2 serum ALP, U/L*	87 (57; 117)
POD 5 serum ALP, U/L*	94 (62; 185)
POD 1 serum GGT, U/L*	97 (57; 126)
POD 2 serum GGT, U/L*	74 (34; 112)
POD 5 serum GGT, U/L*	75 (54; 300)
POD 1 serum PT, sec*	52 (42; 67)
POD 2 serum PT, sec*	49 (32; 64)
POD 5 serum PT, sec*	50 (35; 75)
POD5 serum Bilirubin > 50 µmol/L (%)	5 (33)
POD5 serum PT < 50 sec (%)	6 (40)
50-50 criteria (%)	2 (13.5)

*Expressed as median [interquartile range]

POD postoperative day, CD Clavien-Dindo, PHH post-hepatectomy hemorrhage. AST ASpartate transaminase, ALT ALanine Trasnaminase, ALP Alkaline Phosphatase, GGT Gamma-Glutamyl Transferase, PT Prothrombin Time

Correlation between HSI and perioperative outcomes

StO₂% values after liver resection were significantly higher in patients who underwent preoperative biliary drainage for jaundice (0.772396 vs 0.491312 ± 0.1123386, p=0.033) and lower in case of unhealthy (steatotic, fibrotic or cirrhotic) liver (0.308659 ± 0.1180001 vs 0.545178 ± 0.1022391, p=0.011), while this relationship was not maintained when considering liver steatosis, fibrosis, and cirrhosis separately. Moreover, cirrhotic liver presented higher negative ΔStO₂% values when compared to healthy liver (-0.223228 vs 0.067624 ± 0.1270989, p=0.05). However, preoperative biliary drainage and cirrhosis happened in only one patient. Moreover, StO₂% showed a significant negative correlation with ALT values of POD5 (ρ = -0.602, p=0.030), while ΔStO₂% presented a positive correlation with ALP measured in POD1 (ρ = 0.594, p=0.032).

NIR measurement at the end of operation presented higher values for unhealthy when compared to healthy liver (0.248632 ± 0.2045839 vs 0.020497 ± 0.0068152, p=0.003), and this relationship was maintained when considering the comparison between fibrotic and healthy liver (0.438459 ± 0.1936464 vs 0.155382 ± 0.1690520, p=0.028). Preoperative history of dyslipidemia correlated with lower values of final NIR (0.072035 ± 0.1018278 vs 0.296045 ± 0.2082360). Final NIR values showed negative correlation with ALT values

of POD1 ($\rho = -0.666$, $p=0.013$) and POD5 ($\rho = -0.696$; $p=0.008$), while intraoperative blood loss negatively correlated with Δ NIR ($\rho = 0.629$, $p=0.021$).

TWI was the only HSI index to correlate with postoperative reintervention. In fact, the two patients who presented with biliary leakage, PHH and subsequent reoperations, showed lower values of final TWI (0.133098 ± 0.0615701 vs 0.270123 ± 0.0779744 , $p=0.038$). Preoperative chemoembolization showed significant correlation with higher final values of TWI and Δ TWI ($p=0.027$ and $p=0.036$, respectively). A negative correlation was found between Δ TWI, and PT measured in POD1 ($\rho = -0.567$, $p=0.043$).

Lower OHI final values showed significant correlation with postoperative sepsis (0.641417 ± 0.0340463 vs 0.704987 ± 0.0712082 , $p=0.045$), while Δ OHI correlated with preoperative hypertension (-0.124543 ± 0.0575170 vs -0.019336 ± 0.0646324 , $p=0.013$) and PHLF (-0.074822 ± 0.0774023 vs 0.022819 ± 0.0220585 , $p= 0.010$), also showing negative correlation with ALT values observed in POD5 ($\rho = -0.813$, $p=0.001$).

All the correlations between HSI and perioperative outcomes are reported in **Table 3 (a,b)** and **Table 4 (a,b)**.

Table 3a Comparison of final hyperspectral indexes between patients with different perioperative features

		TWI final	p	OHI final	p	StO₂ final	p	NIR final	p
BMI	< 30	0.239257 ± 0.0863027	.384	0.680372 ± 0.0707513	.520	0.538018 ± 0.1359924	.154	0.237461 ± 0.2099274	.555
	≥ 30	0.291949 ± 0.1044797		0.710483 ± 0.0650543		0.413753 ± 0.0416339			
Pre-existing hepatopathy	No	0.235266 ± 0.0854626	.118	0.682849 ± 0.0661445	.614	0.508318 ± 0.1397226	.840	0.200581 ± 0.2175399	.440
	Yes	0.342238 ± 0.0538465		0.710671 ± 0.1058574		0.529816 ± 0.0962579			
Preoperative chemoembolization	No	0.218855 ± 0.0980174	.027	0.663419 ± 0.0526673	.085	0.513850 ± 0.1545281	.930	0.276932 ± 0.2291223	.364
	Yes	0.307595 ± 0.0131076		0.728952 ± 0.0785237		0.506961 ± 0.0916789			
Neoadjuvant CT	No	0.263105 ± 0.089017	.501	0.668654 ± 0.0579772	.192	0.498806 ± 0.1574234	.650	0.188805 ± 0.1786111	.699
	Yes	0.227945 ± 0.0941956		0.719530 ± 0.0797624		0.534039 ± 0.0750950			
Preoperative portal embolization	No	0.234524 ± 0.0905328	.459	0.673715 ± 0.0489016	.429	0.454457 ± 0.1205904	.057	0.233968 ± 0.2491355	1.000
	Yes	0.271914 ± 0.0902129		0.704302 ± 0.0902349		0.587299 ± 0.1118087			
Preoperative biliary drainage	No	0.244987 ± 0.0900135	.421	0.693930 ± 0.0654900	.169	0.491312 ± 0.1123386	.033	0.217204 ± 0.2139745	1.000
	Yes*	0.322846		0.594439		0.772396			
Dislipidemia	No	0.240269 ± 0.1038706	.583	0.673571 ± 0.0627296	.350	0.528450 ± 0.1551929	.537	0.296045 ± 0.2082360	.029
	Yes	0.269050 ± 0.0589130		0.710679 ± 0.0786646		0.480681 ± 0.0787255			
Diabetes	No	0.230414 ± 0.1056922	.272	0.696561 ± 0.0801249	.496	0.517390 ± 0.1582457	.829	0.263784 ± 0.2182323	.240
	Yes	0.286790 ± 0.0286157		0.669298 ± 0.0415621		0.500588 ± 0.0767515			
Hypertension	No	0.191474 ± 0.0745690	.060	0.677744 ± 0.0503171	.727	0.474390 ± 0.1650029	.455	0.251728 ± 0.2747102	.797
	Yes	0.283367 ± 0.0817567		0.691868 ± 0.0789702		0.531945 ± 0.1147022			
Overall comorbidities	No	0.195183 ± 0.0855704	.147	0.679677 ± 0.0578865	.816	0.496135 ± 0.1820687	.796	0.311862 ± 0.2766107	.304
	Yes	0.272694 ± 0.0841467		0.689683 ± 0.0747739		0.517491 ± 0.1174043			
Intraoperative transfusion	No	0.260331 ± 0.0819605	.333	0.685257 ± 0.0727266	.843	0.503627 ± 0.1396737	.609	0.213809 ± 0.2036642	1.000
	Yes	0.191850 ± 0.1446589		0.696223 ± 0.0476637		0.557963 ± 0.0717409			
Overall morbidity	No	0.270233 ± 0.0505753	.495	0.693441 ± 0.0800839	.767	0.517888 ± 0.0572657	.880	0.224564 ± 0.2435888	.852
	Yes	0.235785 ± 0.1108412		0.681861 ± 0.0633943		0.506516 ± 0.1723634			
Liver failure	No	0.247172 ± 0.0743674	.768	0.681053 ± 0.0705981	.566	0.517901 ± 0.1407749	.738	0.198020 ± 0.2077715	.368
	Yes	0.262925 ± 0.1532453		0.707985 ± 0.0674837		0.487514 ± 0.1105711			
Liver hemorrhage	No	0.270123 ± 0.0779744	.038	0.690250 ± 0.0736359	.664	0.513613 ± 0.1348084	.884	0.214028 ± 0.2034280	.923
	Yes	0.133098 ± 0.0615701		0.666267 ± 0.0052990		0.498051 ± 0.1564696			
Bile leak	No	0.270123 ± 0.0779744	.038	0.690250 ± 0.0736359	.664	0.513613 ± 0.1348084	.884	0.214028 ± 0.2034280	.923
	Yes	0.133098 ± 0.0615701		0.666267 ± 0.0052990		0.498051 ± 0.1564696			
Postoperative Antibiotics	No	0.270731 ± 0.0820834	.190	0.704987 ± 0.0712082	.045	0.516573 ± 0.0742967	.826	0.235174 ± 0.2137565	.635
	Yes	0.200091 ± 0.0965435		0.641417 ± 0.0340463		0.498429 ± 0.2409589			
Reoperation	No	0.270123 ± 0.0779744	.038	0.690250 ± 0.0736359	.664	0.513613 ± 0.1348084	.884	0.214028 ± 0.2034280	.923
	Yes	0.133098 ± 0.0615701		0.666267 ± 0.0052990		0.498051 ± 0.1564696			
Postoperative Bilirubine > 50 in POD5	No	0.254588 ± 0.0756003	.956	0.696863 ± 0.0750111	.653	0.497793 ± 0.1263709	.747	0.167172 ± 0.1705684	.622
	Yes	0.257651 ± 0.1202765		0.677681 ± 0.0686495		0.524469 ± 0.1649255			
Postoperative PT < 50 in POD5	No	0.243983 ± 0.0835275	.726	0.696613 ± 0.0770611	.577	0.519614 ± 0.0878004	.758	0.188439 ± 0.1724098	.639
	Yes	0.264589 ± 0.1153340		0.671418 ± 0.0709153		0.492031 ± 0.2087494			
50-50 criteria	No	0.239900 ± 0.0781888	.533	0.689374 ± 0.0742251	.837	0.482815 ± 0.1320648	.409	0.166844 ± 0.1709078	.283
	Yes	0.277905 ± 0.1286612		0.679598 ± 0.0791150		0.558734 ± 0.1686418			
Healthy vs not-healthy	Healthy	0.265111 ± 0.0760691	.814	0.657303 ± 0.0263142	.531	0.545178 ± 0.1022391	.011	0.020497 ± 0.0068152	.003
	Not-healthy	0.248121 ± 0.0937001		0.691744 ± 0.0725715		0.308659 ± 0.1180001			
Healthy vs steatotic	Healthy	0.247828 ± 0.1062058	.926	0.675116 ± 0.0561137	.599	0.473400 ± 0.1474839	.370	0.288728 ± 0.2424102	.268
	Steatotic	0.252588 ± 0.0814004		0.695605 ± 0.0788087		0.539881 ± 0.1200556			
Healthy vs fibrosis	Healthy	0.266476 ± 0.0816544	.212	0.696815 ± 0.0742775	.073	0.490738 ± 0.1418744	.277	0.155382 ± 0.1690520	.028
	Fibrosis	0.192145 ± 0.1076113		0.650188 ± 0.0134668		0.587111 ± 0.0285334			
Healthy vs cirrhosis	Healthy	0.240566 ± 0.0840258	.135	0.679232 ± 0.0646579	.139	0.515208 ± 0.1360609	.712	0.203737 ± 0.2085892	.442
	Cirrhosis*	0.380313		0.785524		0.461752			
Vascular clamping	No	0.290016 ± 0.0727332	.230	0.677431 ± 0.0785936	.717	0.566543 ± 0.1203236	.258	0.317827 ± 0.2284837	.177
	Yes	0.228621 ± 0.0932619		0.692042 ± 0.0663934		0.480749 ± 0.1338067			

* only 1 case in the present population

Table 3b Comparison of differential values of hyperspectral indexes between patients with different perioperative features

		Delta TWI	p	Delta OHI	p	Delta StO ₂	p	Delta NIR	p
BMI ≥ 30	< 30	-0.020530 ± 0.0814836	.405	-0.063338 ± 0.0710275	.785	0.053490 ± 0.1288035	.727	-0.006279 ± 0.2127378	.257
	≥ 30	0.033784 ± 0.1415086		-0.048008 ± 0.1236632		0.017788 ± 0.2275176		-0.131020 ± 0.1319792	
Hepatopathy	No	-0.002487 ± 0.1012780	.642	-0.068554 ± 0.0812640	.377	0.064900 ± 0.1329345	.273	-0.023769 ± 0.2055404	.769
	Yes	-0.038298 ± 0.0432518		-0.011652 ± 0.0708070		-0.062819 ± 0.2268525		-0.097194 ± 0.2155679	
Preoperative chemoembolization	No	-0.049869 ± 0.0775269	.036	-0.064570 ± 0.0835950	.798	0.024749 ± 0.1744489	.545	-0.001606 ± 0.2410196	.435
	Yes	0.059001 ± 0.0837714		-0.052168 ± 0.0823733		0.078055 ± 0.0922135		-0.088600 ± 0.1097076	
Neoadjuvant CT	No	0.015610 ± 0.0926317	.271	-0.055718 ± 0.0784012	.827	0.052206 ± 0.1710430	.839	-0.052278 ± 0.2167942	1.000
	Yes	-0.045766 ± 0.0934857		-0.066331 ± 0.0910465		0.034124 ± 0.1117891		-0.007523 ± 0.1890109	
Preoperative portal embolization	No	-0.019435 ± 0.1021835	.657	-0.053365 ± 0.0938970	.769	-0.015977 ± 0.1446752	.104	-0.055718 ± 0.2478075	.628
	Yes	0.005349 ± 0.0916297		-0.067308 ± 0.0678286		0.116684 ± 0.1211113		-0.010970 ± 0.1436254	
Preoperative biliary drainage	No	-0.016463 ± 0.0931426	.280	-0.060094 ± 0.0834038	.966	0.024105 ± 0.1300443	.067	-0.054621 ± 0.1950298	.368
	Yes*	0.093601		-0.056274		0.299004		0.199604	
Dyslipidemia	No	-0.001630 ± 0.1192897	.773	-0.071535 ± 0.0708195	.527	0.037493 ± 0.1681291	.820	-0.039616 ± 0.2502065	.943
	Yes	-0.018183 ± 0.0392429		-0.041025 ± 0.0981830		0.057664 ± 0.1190163		-0.027783 ± 0.0992574	
Diabetes	No	-0.016382 ± 0.0852586	.703	-0.085738 ± 0.0743323	.145	0.051519 ± 0.1847046	.854	-0.064239 ± 0.2413175	.724
	Yes	0.005421 ± 0.1164769		-0.018299 ± 0.0772342		0.035223 ± 0.0635521		0.011614 ± 0.1148034	
Hypertension	No	-0.032444 ± 0.0924927	.484	-0.124543 ± 0.0575170	.013	0.075383 ± 0.1506270	.579	-0.052743 ± 0.2667009	.943
	Yes	0.007284 ± 0.0982253		-0.019336 ± 0.0646324		0.026419 ± 0.1500725		-0.024016 ± 0.1651862	
Other comorbidities	No	-0.034312 ± 0.1066924	.526	-0.108263 ± 0.0514208	.152	0.037019 ± 0.1429668	.899	-0.068718 ± 0.3051848	1.000
	Yes	0.003700 ± 0.0925083		-0.038261 ± 0.0829375		0.048910 ± 0.1557534		-0.020108 ± 0.1549617	
Intraoperative transfusion	No	-0.010133 ± 0.0981190	.791	-0.066789 ± 0.0791499	.294	0.043103 ± 0.1522746 vs	.863	-0.037926 ± 0.2081925	1.00
	Yes*	0.017649		0.024067		0.071030		-0.000738	
Overall morbidity	No	-0.039453 ± 0.0502912	.284	-0.038884 ± 0.0727085	.405	0.015760 ± 0.0636814	.503	0.049863 ± 0.1654348	.295
	Yes	0.018967 ± 0.1175734		-0.077728 ± 0.0868181		0.070529 ± 0.1939997		-0.107860 ± 0.2085058	
Liver failure	No	-0.020934 ± 0.0773137	.263	-0.074822 ± 0.0774023	.010	0.069431 ± 0.1331408	.171	-0.004694 ± 0.2018893	.154
	Yes	0.063162 ± 0.1867376		0.022819 ± 0.0220585		-0.087736 ± 0.1916136		-0.202108 ± 0.0671965	
Liver hemorrhage	No	-0.006582 ± 0.0983043	.861	-0.048978 ± 0.0727775	.090	0.029952 ± 0.1411867	.203	-0.038917 ± 0.2079657	1.000
	Yes*	-0.024972		-0.189662		0.228838		0.011158	
Bile leak	No	-0.006582 ± 0.0983043	.861	-0.048978 ± 0.0727775	.090	0.029952 ± 0.1411867	.203	-0.038917 ± 0.2079657	1.000
	Yes*	-0.024972		-0.189662		0.228838		0.011158	
Postoperative Antibiotics	No	-0.018829 ± 0.1023436	.474	-0.045226 ± 0.0796898	.246	0.019211 ± 0.1152786	.257	-0.022478 ± 0.1679342	1.000
	Yes	0.028111 ± 0.0602527		-0.108382 ± 0.0713185		0.132053 ± 0.2310800		-0.077021 ± 0.3296813	
Reoperation	No	-0.006582 ± 0.0983043	.861	-0.048978 ± 0.0727775	.090	0.029952 ± 0.1411867	.203	-0.038917 ± 0.2079657	1.000
	Yes*	-0.024972		-0.189662		0.228838		0.011158	
Postoperative Bilirubine > 50 in POD5	No	-0.027980 ± 0.0786605	.207	-0.060981 ± 0.0798552	.841	0.028645 ± 0.1081746	.549	-0.068636 ± 0.1882200	1.000
	Yes	0.048738 ± 0.1193496		-0.050075 ± 0.1010551		0.088092 ± 0.2329809		-0.048364 ± 0.1973332	
Postoperative PT < 50 in POD5	No	-0.040310 ± 0.0798611	.120	-0.088909 ± 0.0896022	.216	0.074092 ± 0.1154917	.475	-0.013624 ± 0.1219900	.315
	Yes	0.058907 ± 0.1125126		-0.022462 ± 0.0546223		-0.002038 ± 0.2300999		-0.161609 ± 0.2688198	
50-50 criteria	No	-0.033308 ± 0.0765434	.122	-0.087697 ± 0.0830264	.139	0.048370 ± 0.1293280	.951	-0.067149 ± 0.1888789	.921
	Yes	0.073308 ± 0.1332078		-0.003546 ± 0.0482547		0.041177 ± 0.2611780		-0.068204 ± 0.2367461	
Healthy vs not-healthy	Healthy	0.065476 ± 0.0929143	.063	-0.036919 ± 0.0359334	.879	0.037297 ± 0.2253255	.841	-0.177665 ± 0.1651309	.064
	Not-healthy	-0.013591 ± 0.0783757		-0.030435 ± 0.0912430		0.022424 ± 0.1233306		-0.032173 ± 0.1461388	
Healthy vs steatotic	Healthy	0.011850 ± 0.1096453	.571	-0.036910 ± 0.0564948	.438	-0.040565 ± 0.1330348	.094	-0.100822 ± 0.2809984	.370
	Steatotic	-0.020400 ± 0.0889018		-0.074106 ± 0.0922015		0.098886 ± 0.1337132		0.006033 ± 0.1347425	
Healthy vs fibrosis	Healthy	-0.001925 ± 0.1008512	.608	-0.056948 ± 0.0869314	.777	0.043994 ± 0.1586012	.946	-0.072525 ± 0.1873344	.115
	Fibrosis	-0.041389 ± 0.0476232		-0.075489 ± 0.0194722		0.052166 ± 0.0642399		0.170966 ± 0.1636668	
Healthy vs cirrhosis	Healthy	-0.002922 ± 0.0965766	.525	-0.067985 ± 0.0775073	.214	0.067624 ± 0.1270989	.050	-0.017185 ± 0.1972977	.282
	Cirrhosis*	-0.068882		0.038416		-0.223228		-0.249623	
Vascular clamping	No	-0.025682 ± 0.0795543	.615	-0.042327 ± 0.0720511	.556	0.036377 ± 0.1860855	.871	0.079699 ± 0.2115497	.102
	Yes	0.003057 ± 0.1060703		-0.070721 ± 0.0872480		0.050798 ± 0.1290803		-0.106792 ± 0.1656317	

* only 1 case in the present population

Table 4a Correlation between final hyperspectral indexes and perioperative continuous variables

	TWI final		OHI final		StO ₂ final		NIR final	
	rho	p	rho	p	rho	p	rho	p
BMI	0.045	0.878	-0.138	0.638	-0.085	0.773	-0.041	0.890
Preoperative bilirubine	-0.048	0.869	0.048	0.869	-0.009	0.976	-0.026	0.929
Preoperative AST	-0.106	0.719	-0.247	0.395	0.249	0.391	0.456	0.101
Preoperative ALT	-0.480	0.082	-0.436	0.119	0.145	0.620	0.430	0.125
Preoperative ALP	-0.108	0.714	-0.011	0.970	0.359	0.208	0.130	0.658
Preoperative GGT	-0.029	0.923	-0.288	0.318	0.372	0.190	0.513	0.061
Preoperative Hb	0.220	0.450	-0.321	0.263	-0.053	0.858	0.097	0.742
Preoperative PT	-0.147	0.616	0.368	0.196	-0.334	0.243	-0.341	0.233
Preoperative INR	0.088	0.760	-0.333	0.244	0.229	0.432	0.284	0.325
Preoperative Albumin	-0.406	0.150	-0.326	0.255	-0.151	0.607	-0.035	0.904
n. resected Sg	-0.135	0.646	0.042	0.887	0.246	0.396	-0.014	0.962
Total duration of vascular clamping	-0.295	0.306	0.104	0.724	-0.228	0.434	-0.237	0.416
Blood loss	0.357	0.211	0.365	0.199	-0.100	0.735	-0.024	0.934
Operative time	0.322	0.262	0.366	0.199	-0.070	0.811	0.196	0.502
AST POD1	-0.123	0.675	-0.075	0.799	-0.299	0.299	-0.374	0.188
AST POD2	-0.341	0.254	-0.132	0.667	-0.325	0.279	-0.380	0.201
AST POD5	0.105	0.734	-0.050	0.872	0.083	0.788	0.085	0.781
ALT POD1	-0.156	0.594	-0.130	0.658	-0.367	0.196	-0.165	0.573
ALT POD2	-0.325	0.279	-0.127	0.680	-0.517	0.070	-0.666	0.013
ALT POD5	-0.191	0.531	-0.004	0.989	-0.602	0.030	-0.696	0.008
Bilirubin POD1	-0.055	0.852	0.231	0.427	0.108	0.714	0.002	0.994
Bilirubin POD2	0.140	0.648	0.124	0.687	0.003	0.993	0.058	0.851
Bilirubin POD5	0.121	0.693	0.135	0.660	-0.019	0.950	0.121	0.693
ALP POD1	-0.200	0.492	0.007	0.982	0.443	0.113	0.137	0.642
ALP POD2	-0.237	0.436	-0.099	0.747	0.350	0.241	0.171	0.577
ALP POD5	-0.193	0.528	-0.019	0.950	0.284	0.347	-0.113	0.713
GGT POD1	-0.104	0.724	-0.335	0.241	0.304	0.290	0.359	0.207
GGT POD2	0.033	0.915	-0.331	0.270	0.190	0.534	0.259	0.393
GGT POD5	-0.083	0.789	-0.138	0.654	0.242	0.426	0.110	0.720
PT POD1	-0.150	0.609	0.253	0.382	-0.026	0.929	0.011	0.970
PT POD2	-0.025	0.936	0.220	0.469	-0.110	0.720	-0.174	0.571
PT POD5	-0.039	0.905	0.326	0.301	-0.298	0.347	-0.424	0.170

Table 4b Correlation between differential hyperspectral indexes and perioperative continuous variables

	Delta TWI		Delta OHI		Delta StO ₂		Delta NIR	
	rho	p	rho	p	rho	p	rho	p
BMI	0.245	0.420	0.008	0.979	0.305	0.310	0.077	0.802
Preoperative bilirubine	0.467	0.108	0.159	0.603	0.033	0.915	-0.231	0.448
Preoperative AST	0.028	0.929	-0.113	0.714	-0.250	0.409	-0.030	0.922
Preoperative ALT	-0.069	0.823	-0.569	0.042	0.014	0.964	0.171	0.577
Preoperative ALP	0.313	0.297	-0.258	0.394	0.533	0.061	0.022	0.943
Preoperative GGT	0.280	0.354	0.022	0.943	-0.022	0.943	0.088	0.775
Preoperative Hb	0.187	0.541	-0.104	0.734	-0.132	0.668	0.044	0.887
Preoperative PT	-0.304	0.312	-0.008	0.978	-0.014	0.964	0.148	0.630
Preoperative INR	0.271	0.371	-0.162	0.597	0.089	0.771	-0.162	0.597
Preoperative Albumine	-0.442	0.130	-0.287	0.341	-0.180	0.557	0.135	0.659
n. resected Sg	0.356	0.233	-0.347	0.246	0.603	0.029	-0.073	0.811
Total duration of vascular clamping	0.085	0.783	0.178	0.560	-0.229	0.451	-0.490	0.089
Blood loss	0.222	0.467	0.507	0.077	-0.427	0.146	-0.629	0.021
Operative time	0.360	0.226	0.272	0.368	-0.366	0.219	-0.616	0.025
AST POD1	0.445	0.128	0.363	0.223	0.016	0.957	-0.291	0.334
AST POD2	0.294	0.354	0.238	0.457	0.014	0.966	-0.189	0.557
AST POD5	0.263	0.409	0.231	0.470	-0.546	0.066	-0.249	0.436
ALT POD1	0.407	0.168	-0.016	0.957	0.071	0.817	-0.269	0.374
ALT POD2	0.266	0.404	0.140	0.665	0.049	0.880	-0.154	0.633
ALT POD5	-0.105	-0.745	-0.813	0.001	-0.091	0.778	-0.312	0.324
Bilirubine POD1	0.516	0.071	-0.148	0.629	0.500	0.082	-0.121	0.694
Bilirubine POD2	0.545	0.067	-0.056	0.863	0.308	0.331	-0.210	0.513
Bilirubine POD5	0.494	0.103	-0.007	0.983	0.249	0.436	-0.221	0.491
ALP POD1	0.146	0.635	-0.239	0.431	0.594	0.032	0.160	0.603
ALP POD2	0.091	0.778	-0.119	0.712	0.543	0.068	0.294	0.353
ALP POD5	-0.133	0.680	0.263	0.409	0.228	0.477	0.242	0.449
GGT POD1	0.331	0.270	-0.248	0.414	0.328	0.274	0.292	0.333
GGT POD2	0.396	0.203	-0.095	0.770	0.315	0.318	0.074	0.820
GGT POD5	-0.189	0.557	0.462	0.131	-0.210	0.513	0.028	0.931
PT POD1	-0.567	0.043	0.110	0.720	-0.234	0.442	0.267	0.378
PT POD2	-0.508	0.092	0.175	0.586	-0.207	0.519	0.088	0.787
PT POD5	-0.509	0.110	-0.091	0.790	-0.091	0.790	0.018	0.958

4. Discussion

In this study, we explored the potential of the HSI analysis in relation to the postoperative outcomes following major hepatectomies.

As expected, StO₂% showed lower values when considering unhealthy livers, probably due to the higher arterial blood flow which characterizes the healthy hepatic tissue immediately beneath Glisson's capsule, corresponding to the depth of StO₂% analysis (~1 mm)[28,29]. Instead, NIR analysis showed higher values for unhealthy liver, especially regarding fibrosis, probably because NIR measures in deeper layers (depth 4-6 mm), where the lobe is characterized by increased arterial and portal branches, which almost equally contributes to the oxygenation[21]. This oxygen perfusion difference between different depths suggests that a deeper evaluation of oxygen perfusion could be more accurate, as previously reported[16]TWI and OHI seems to be the only parameters to correlate with clinical postoperative outcomes. Especially, lower concentration of water inside hepatic tissue at the end of the operation, could predict postoperative PHH, biliary leakage, and reintervention. Probably, this could reflect the extensive use of vascular inflow clamping and goal-directed fluid therapy with the aim to reduce intraoperative bleeding, especially in patients who underwent major hepatectomies with resection of more than 5 segments. On the same line, hemoglobin concentration recognized by OHI index is affected by Pringle maneuver and a negative Δ OHI% is expected when vascular clamping is performed. Consequently, higher negative Δ OHI% reflects major reductions in hemoglobin and increased liver suffering, explaining its correlation with postoperative liver failure.

Moreover, the negative significant correlation of HSI parameters with higher values of ALT in POD1 and POD5, gives consistency to our results since ALT remains the most specific serum indicator of liver injury[30].

Nowadays, intraoperative evaluation of liver parenchyma that must be preserved or selectively removed, and the qualitative evaluation of the remnant liver, are mainly relied on the naked-eye evaluation, or by ultrasound evaluation and experience of the operating surgeon. This “subjective” evaluation becomes certainly more challenging when underlying liver diseases are present. Ultrasonography (US) is still the gold standard for detecting inadequate blood supply, or outflow obstruction, with high specificity[31]. In contrast, it is operator-dependent, requires intensive training to be mastered and cannot provide a precise global map of liver oxygenation intraoperatively.

The need for an objective and convenient HAO analysis tool has driven researchers to find alternative solutions. Recently, ICG-fluorescence imaging was used to identify segmental boundaries of the liver, enabling more accurate anatomic resections[32,33]. Furthermore, several authors[5,34,35] reported the usefulness of ICG as a predictive factor of PHLF. However, these studies were biased by the high heterogeneity of the included population and retrospective design. In addition, ICG excretion rate is affected not only by the excretion ability of hepatocytes, but also by hepatic blood flow, shunt volume, and bile flow rate[36]. ICG also has drawbacks such as the need for injection, the time required for clearance; the contraindications in kidney failure and hypersensitivity or intolerance to iodine contrast agents, or in patients affected by thyrotoxicosis, and its application in the clinical setting is not allowed in many countries.

HSI has the potential to overcome all these limitations. Our group has previously used HSI to assess StO₂% and intraoperatively localize preselected ROIs during esophagectomy[37], small bowel ischemia[38], and hepatectomy[13]. In particular, HSI was successfully used to guide anatomical liver resections[13] and to discriminate between total and arterial liver ischemia during surgery[15].

The present study is the first monocentric surgical series to apply HSI to major hepatectomies in humans, and our results suggest that HSI is a feasible and promising tool able to potentially help in prediction of short postoperative outcomes. Nevertheless, several limitations must be reported.

First, at present, HSI technology lacks video-rate and time necessary for HSI acquisition is around 10 seconds per image, still not yet fully “real-time”. Our group already developed software to overlay HSI images onto the operative field, obtaining HSI-based enhanced reality (HYPER) on liver[13], but it was not yet applied in clinical setting.

Second, the monocentric and observational design, the small sample size, and the limited number of postoperative major complications, make these results only the starting point to develop new clinical multicenter trials with a larger population. Finally, HIS acquisition is at present feasible only by laparotomy, excluding so all the minimally invasive procedures.

5. Conclusions

HSI is a recent and interesting technology still in its experimental phase. This is the first clinical application in a monocentric major hepatectomy series, and the reported results suggests that TWI and OHI could be associated to short-term postoperative outcomes. Further experimental and clinical studies are necessary to better explore and evaluate the potential value of this technology in current practice.

Author Contributions: “Conceptualization, E.F., Er.F., L.C. and M.D.; methodology, E.F., L.C., Er.F., F.G., E.M.M., E.B. M.B. M.D.; software,; validation, E.F., L.C., E.B., E.M.M, Er.F., M.D.; formal analysis, L.C., E.B.; investigation, E.F., L.C., E.M.M, M.B., E.B., Er.F.; resources, J.M., S.G, M.D.; data curation, L.C.,; writing—original draft

preparation, E.F., L.C., E.M.M, Er.F., M.D.; writing—review and editing, E.F., L.C., E.M.M., Er.F., M.D.; visualization, L.C, E.B.; supervision, E.F., Er.F., C.S., P.P., J.M., S.G., M.D.; project administration, M.D.; funding acquisition, S.G., M.D. All authors have read and agreed to the published version of the manuscript.”

Informed Consent Statement: Informed consent was obtained from all subjects involved in the study.

Data Availability Statement: Not applicable

References

1. Lurje, I.; Czigany, Z.; Bednarsch, J.; Roderburg, C.; Isfort, P.; Neumann, U.P.; Lurje, G. Treatment Strategies for Hepatocellular Carcinoma – a Multidisciplinary Approach. *International journal of molecular sciences* **2019**, *20*, doi:10.3390/ijms20061465.
2. Albertsmeier, M.; Stintzing, S.; Guba, M.; Werner, J.; Angele, M. [Multimodal treatment of colorectal liver metastases]. *MMW Fortschritte der Medizin* **2015**, *157*, 47-49, doi:10.1007/s15006-015-3419-1.
3. Wei, A.C.; Tung-Ping Poon, R.; Fan, S.T.; Wong, J. Risk factors for perioperative morbidity and mortality after extended hepatectomy for hepatocellular carcinoma. *Br J Surg* **2003**, *90*, 33-41, doi:10.1002/bjs.4018.
4. Franken, L.C.; Schreuder, A.M.; Roos, E.; van Dieren, S.; Busch, O.R.; Besselink, M.G.; van Gulik, T.M. Morbidity and mortality after major liver resection in patients with perihilar cholangiocarcinoma: A systematic review and meta-analysis. *Surgery* **2019**, *165*, 918-928, doi:10.1016/j.surg.2019.01.010.
5. Sato, N.; Kenjo, A.; Suzushino, S.; Kimura, T.; Okada, R.; Ishigame, T.; Kofunato, Y.; Marubashi, S. Predicting Post-Hepatectomy Liver Failure Using Intra-Operative Measurement of Indocyanine Green Clearance in Anatomical Hepatectomy. *World journal of surgery* **2021**, *45*, 3660-3667, doi:10.1007/s00268-021-06289-9.
6. Oliveira, T.H.C.; Marques, P.E.; Proost, P.; Teixeira, M.M.M. Neutrophils: a cornerstone of liver ischemia and reperfusion injury. *Laboratory investigation; a journal of technical methods and pathology* **2018**, *98*, 51-62, doi:10.1038/labinvest.2017.90.
7. Kelly, D.M.; Shiba, H.; Nakagawa, S.; Irefin, S.; Eghtesad, B.; Quintini, C.; Aucejo, F.; Hashimoto, K.; Fung, J.J.; Miller, C. Hepatic blood flow plays an important role in ischemia-reperfusion injury. *Liver transplantation : official publication of the American Association for the Study of Liver Diseases and the International Liver Transplantation Society* **2011**, *17*, 1448-1456, doi:10.1002/lt.22424.
8. Levesque, E.; Hoti, E.; Azoulay, D.; Adam, R.; Samuel, D.; Castaing, D.; Saliba, F. Non-invasive ICG-clearance: a useful tool for the management of hepatic artery

-
- thrombosis following liver transplantation. *Clinical transplantation* **2011**, *25*, 297-301, doi:10.1111/j.1399-0012.2010.01252.x.
9. Kubota, K.; Kita, J.; Shimoda, M.; Rokkaku, K.; Kato, M.; Iso, Y.; Sawada, T. Intraoperative assessment of reconstructed vessels in living-donor liver transplantation, using a novel fluorescence imaging technique. *Journal of hepatobiliary-pancreatic surgery* **2006**, *13*, 100-104, doi:10.1007/s00534-005-1014-z.
 10. Skowno, J.J.; Karpelowsky, J.S.; Watts, N.R.; Little, D.G. Can transcutaneous near infrared spectroscopy detect severe hepatic ischemia: a juvenile porcine model. *Paediatric anaesthesia* **2016**, *26*, 1188-1196, doi:10.1111/pan.13004.
 11. Ungerstedt, J.; Nowak, G.; Ungerstedt, U.; Ericzon, B.G. Microdialysis monitoring of porcine liver metabolism during warm ischemia with arterial and portal clamping. *Liver transplantation : official publication of the American Association for the Study of Liver Diseases and the International Liver Transplantation Society* **2009**, *15*, 280-286, doi:10.1002/lt.21690.
 12. Pischke, S.E.; Tronstad, C.; Holhjem, L.; Line, P.D.; Haugaa, H.; Tønnessen, T.I. Hepatic and abdominal carbon dioxide measurements detect and distinguish hepatic artery occlusion and portal vein occlusion in pigs. *Liver transplantation : official publication of the American Association for the Study of Liver Diseases and the International Liver Transplantation Society* **2012**, *18*, 1485-1494, doi:10.1002/lt.23544.
 13. Urade, T.; Felli, E.; Barberio, M.; Al-Taher, M.; Felli, E.; Goffin, L.; Agnus, V.; Ettorre, G.M.; Marescaux, J.; Mutter, D.; et al. Hyperspectral enhanced reality (HYPER) for anatomical liver resection. *Surgical endoscopy* **2021**, *35*, 1844-1850, doi:10.1007/s00464-020-07586-5.
 14. Barberio, M.; Longo, F.; Fiorillo, C.; Seeliger, B.; Mascagni, P.; Agnus, V.; Lindner, V.; Geny, B.; Charles, A.L.; Gockel, I.; et al. HYPerspectral Enhanced Reality (HYPER): a physiology-based surgical guidance tool. *Surgical endoscopy* **2020**, *34*, 1736-1744, doi:10.1007/s00464-019-06959-9.
 15. Felli, E.; Al-Taher, M.; Collins, T.; Baiocchini, A.; Felli, E.; Barberio, M.; Ettorre, G.M.; Mutter, D.; Lindner, V.; Hostettler, A.; et al. Hyperspectral evaluation of hepatic oxygenation in a model of total vs. arterial liver ischaemia. *Scientific reports* **2020**, *10*, 15441, doi:10.1038/s41598-020-72915-6.
 16. Felli, E.; Al-Taher, M.; Collins, T.; Nkusi, R.; Felli, E.; Baiocchini, A.; Lindner, V.; Vincent, C.; Barberio, M.; Geny, B.; et al. Automatic Liver Viability Scoring with Deep Learning and Hyperspectral Imaging. *Diagnostics (Basel, Switzerland)* **2021**, *11*, doi:10.3390/diagnostics11091527.
 17. Mittal, M.; Siddiqui, M.R.; Tran, K.; Reddy, S.P.; Malik, A.B. Reactive oxygen species in inflammation and tissue injury. *Antioxidants & redox signaling* **2014**, *20*, 1126-1167, doi:10.1089/ars.2012.5149.
 18. Cinelli, L.; Felli, E.; Baratelli, L.; Ségaud, S.; Baiocchini, A.; Okamoto, N.; Rodríguez-Luna, M.R.; Elmore, U.; Rosati, R.; Partelli, S.; et al. Single Snapshot Imaging of Optical Properties (SSOP) for Perfusion Assessment during Gastric Conduit Creation for Esophagectomy: An Experimental Study on Pigs. *Cancers* **2021**, *13*, doi:10.3390/cancers13236079.

-
19. von Elm, E.; Altman, D.G.; Egger, M.; Pocock, S.J.; Gøtzsche, P.C.; Vandenbroucke, J.P. The Strengthening the Reporting of Observational Studies in Epidemiology (STROBE) Statement: guidelines for reporting observational studies. *International journal of surgery (London, England)* **2014**, *12*, 1495-1499, doi:10.1016/j.ijssu.2014.07.013.
 20. Kulcke, A.; Holmer, A.; Wahl, P.; Siemers, F.; Wild, T.; Daeschlein, G. A compact hyperspectral camera for measurement of perfusion parameters in medicine. *Biomedizinische Technik. Biomedical engineering* **2018**, *63*, 519-527, doi:10.1515/bmt-2017-0145.
 21. Holmer, A.; Marotz, J.; Wahl, P.; Dau, M.; Kämmerer, P.W. Hyperspectral imaging in perfusion and wound diagnostics - methods and algorithms for the determination of tissue parameters. *Biomedizinische Technik. Biomedical engineering* **2018**, *63*, 547-556, doi:10.1515/bmt-2017-0155.
 22. Rahbari, N.N.; Garden, O.J.; Padbury, R.; Brooke-Smith, M.; Crawford, M.; Adam, R.; Koch, M.; Makuuchi, M.; Dematteo, R.P.; Christophi, C.; et al. Posthepatectomy liver failure: a definition and grading by the International Study Group of Liver Surgery (ISGLS). *Surgery* **2011**, *149*, 713-724, doi:10.1016/j.surg.2010.10.001.
 23. Rahbari, N.N.; Garden, O.J.; Padbury, R.; Maddern, G.; Koch, M.; Hugh, T.J.; Fan, S.T.; Nimura, Y.; Figueras, J.; Vauthey, J.N.; et al. Post-hepatectomy haemorrhage: a definition and grading by the International Study Group of Liver Surgery (ISGLS). *HPB : the official journal of the International Hepato Pancreato Biliary Association* **2011**, *13*, 528-535, doi:10.1111/j.1477-2574.2011.00319.x.
 24. Koch, M.; Garden, O.J.; Padbury, R.; Rahbari, N.N.; Adam, R.; Capussotti, L.; Fan, S.T.; Yokoyama, Y.; Crawford, M.; Makuuchi, M.; et al. Bile leakage after hepatobiliary and pancreatic surgery: a definition and grading of severity by the International Study Group of Liver Surgery. *Surgery* **2011**, *149*, 680-688, doi:10.1016/j.surg.2010.12.002.
 25. Melloul, E.; Hübner, M.; Scott, M.; Snowden, C.; Prentis, J.; Dejong, C.H.C.; Garden, O.J.; Farges, O.; Kokudo, N.; Vauthey, J.-N.; et al. Guidelines for Perioperative Care for Liver Surgery: Enhanced Recovery After Surgery (ERAS) Society Recommendations. *World journal of surgery* **2016**, *40*, 2425-2440, doi:10.1007/s00268-016-3700-1.
 26. Balzan, S.; Belghiti, J.; Farges, O.; Ogata, S.; Sauvanet, A.; Delefosse, D.; Durand, F. The "50-50 criteria" on postoperative day 5: an accurate predictor of liver failure and death after hepatectomy. *Annals of surgery* **2005**, *242*, 824-828, discussion 828-829, doi:10.1097/01.sla.0000189131.90876.9e.
 27. Mayhew, D.; Mendonca, V.; Murthy, B.V.S. A review of ASA physical status - historical perspectives and modern developments. *Anaesthesia* **2019**, *74*, 373-379, doi:10.1111/anae.14569.
 28. Lutt, W.W. Colloquium Series on Integrated Systems Physiology: From Molecule to Function to Disease. In *Hepatic Circulation: Physiology and Pathophysiology*; Morgan & Claypool Life Sciences. Copyright © 2010 by Morgan & Claypool Life Sciences.: San Rafael (CA), 2009.
 29. Lutt, W.W.; Schafer, J.; Legare, D.J. Hepatic blood flow distribution: consideration of gravity, liver surface, and norepinephrine on regional

-
- heterogeneity. *Canadian journal of physiology and pharmacology* **1993**, *71*, 128-135, doi:10.1139/y93-018.
30. Valenti, L.; Pelusi, S.; Bianco, C.; Ceriotti, F.; Berzuini, A.; Iogna Prat, L.; Trotti, R.; Malvestiti, F.; D'Ambrosio, R.; Lampertico, P.; et al. Definition of Healthy Ranges for Alanine Aminotransferase Levels: A 2021 Update. *Hepatology communications* **2021**, *5*, 1824-1832, doi:10.1002/hep4.1794.
 31. Pinna, A.D.; Smith, C.V.; Furukawa, H.; Starzl, T.E.; Fung, J.J. Urgent revascularization of liver allografts after early hepatic artery thrombosis. *Transplantation* **1996**, *62*, 1584-1587, doi:10.1097/00007890-199612150-00010.
 32. Aoki, T.; Yasuda, D.; Shimizu, Y.; Odaira, M.; Niiya, T.; Kusano, T.; Mitamura, K.; Hayashi, K.; Murai, N.; Koizumi, T.; et al. Image-guided liver mapping using fluorescence navigation system with indocyanine green for anatomical hepatic resection. *World journal of surgery* **2008**, *32*, 1763-1767, doi:10.1007/s00268-008-9620-y.
 33. Ishizawa, T.; Zuker, N.B.; Kokudo, N.; Gayet, B. Positive and negative staining of hepatic segments by use of fluorescent imaging techniques during laparoscopic hepatectomy. *Archives of surgery (Chicago, Ill. : 1960)* **2012**, *147*, 393-394, doi:10.1001/archsurg.2012.59.
 34. Sunagawa, Y.; Yamada, S.; Kato, Y.; Sonohara, F.; Takami, H.; Inokawa, Y.; Hayashi, M.; Nakayama, G.; Koike, M.; Kodera, Y. Perioperative assessment of indocyanine green elimination rate accurately predicts postoperative liver failure in patients undergoing hepatectomy. *Journal of hepato-biliary-pancreatic sciences* **2021**, *28*, 86-94, doi:10.1002/jhbp.833.
 35. Kobayashi, Y.; Kiya, Y.; Nishioka, Y.; Hashimoto, M.; Shindoh, J. Indocyanine green clearance of remnant liver (ICG-Krem) predicts postoperative subclinical hepatic insufficiency after resection of colorectal liver metastasis: theoretical validation for safe expansion of Makuuchi's criteria. *HPB : the official journal of the International Hepato Pancreato Biliary Association* **2020**, *22*, 258-264, doi:10.1016/j.hpb.2019.06.013.
 36. Tuñón, M.J.; González, P.; Jorquera, F.; Llorente, A.; Gonzalo-Orden, M.; González-Gallego, J. Liver blood flow changes during laparoscopic surgery in pigs. A study of hepatic indocyanine green removal. *Surgical endoscopy* **1999**, *13*, 668-672, doi:10.1007/s004649901070.
 37. Barberio, M.; Felli, E.; Pop, R.; Pizzicannella, M.; Geny, B.; Lindner, V.; Baiocchi, A.; Jansen-Winkel, B.; Moulla, Y.; Agnus, V.; et al. A Novel Technique to Improve Anastomotic Perfusion Prior to Esophageal Surgery: Hybrid Ischemic Preconditioning of the Stomach. Preclinical Efficacy Proof in a Porcine Survival Model. *Cancers* **2020**, *12*, doi:10.3390/cancers12102977.
 38. Barberio, M.; Felli, E.; Seyller, E.; Longo, F.; Chand, M.; Gockel, I.; Geny, B.; Swanström, L.; Marescaux, J.; Agnus, V.; et al. Quantitative fluorescence angiography versus hyperspectral imaging to assess bowel ischemia: A comparative study in enhanced reality. *Surgery* **2020**, *168*, 178-184, doi:10.1016/j.surg.2020.02.008.

6.2c) Conclusions on the second part

HSI properties were applied in many different experimental settings. We exploited the potential to quantify oxygenation for diagnostic purposes as well as the spatial resolution to create HYPER to improve image-guided surgery. HSI holds great potential given its non-invasiveness and the opportunity to standardize the evaluation without the influence of the operator. The limited penetration of HSI represents the major limitation of this imaging modality. For the first time, HSI was applied to liver surgery and it was possible to intraoperatively assess and predict liver viability; to correlate images to ischemic-reperfusion injury damage, and to enhance the surgeon's eye intraoperatively with Hyperspectral-based enhanced reality.

Anatomical liver resection using ICG-positive or negative staining technique is a promising technique, but it is still performed by a minority of liver surgeons, is technically demanding, and no standardization of the technique exists. Further studies should evaluate the real benefit in terms of post-operative morbidity and mortality and oncologic results.

6.3) *Ex vivo* tumoral models

The programme of this part was focused on the HCC biobank collection of tumoral and adjacent or non-tumoral parenchyma specimens after surgical resection. The goal was to create an efficient pipeline to collect tumor and adjacent very high-quality liver specimens for various purposes, especially, tissue-derived models and “omics” studies. These specimens are collected and conserved in the LIVMOD biobank at Inserm Unit 1110 and used to develop *ex vivo* liver tumor models with spheroids, tumorspheres or PDX models technology. These models are then used to test the anti-tumoral activity of new or currently available drugs for the treatment of HCC. The goal was to perform a proof-of-concept study

to propose to the clinician a personalized “à la carte” chimio sensibility panel, perfectly integrated into the concept of precision medicine.

Results and own contribution

Since May 2018, at my arrival at the Hépatologie Department (Nouvel Hôpital Civil, CHU Strasbourg) I contributed to collect operative liver specimens from cirrhotic and non cirrhotic patients with paired tumor and adjacent samples, associated to patient blood samples in the frame of an active long-lasting collaboration with the researcher of the Institute for viral and hepatic diseases (Inserm U1110). As an official affiliated member since early 2019, I took actively part in the improvement of the liver resection specimens harvesting, by optimizing the specimen conservation, consent documents, and protocols for transfer to the translational research team at Inserm U1110. Besides, I participated in the drafting of the official document allowing the Institute for Viral and Hepatic Research to become by its own a “Centre de Ressources Biologiques” supervised by the Inserm clinical research department. After several rounds of revision, the authorization was obtained in June 2020, and allowed the creation of the LIVMOD (UMR_S1110) biobank.

The collected specimens and blood samples were used to improve liver tumors and liver disease *ex vivo* models like tumor spheres or liver spheroids or patient-derived xenografts (PDX). HCC-derived spheroids have been used to test antitumoral activity of new drugs compared to routinely used therapies to establish “chemograms”, with the objective of a medical treatment “à la carte”. This part needed coordination for specimens transport and logistic considerations to guarantee the perfect timing from resection to *ex vivo* culture, to minimize cellular necrosis. This continuous, efficient and dynamic teamwork lead us to collect in these three years a great amount (near to 100) of operative specimens allowing high quality cultures that were used for many studies, especially to that one that demonstrated the role of the anti-Claudine 1 antibody, developed at the Institute for Viral

and Hepatic Diseases for the prevention of liver fibrosis and HCC development. Beside this main research program, other projects addressed hepatic virus host interactions, especially for HBV and HDV projects, the role of epigenetic modifications in HCC risk after HCV cure, the impact of liver disease on circadian clock and metabolism perturbations, as well as proof-of-concept studies for new molecules identify at the Inserm unit as new therapeutic agents for fibrosis and or HCC development and new cellular targets for chemoprevention of HCC development (for a summary see Fig. 4a,b).

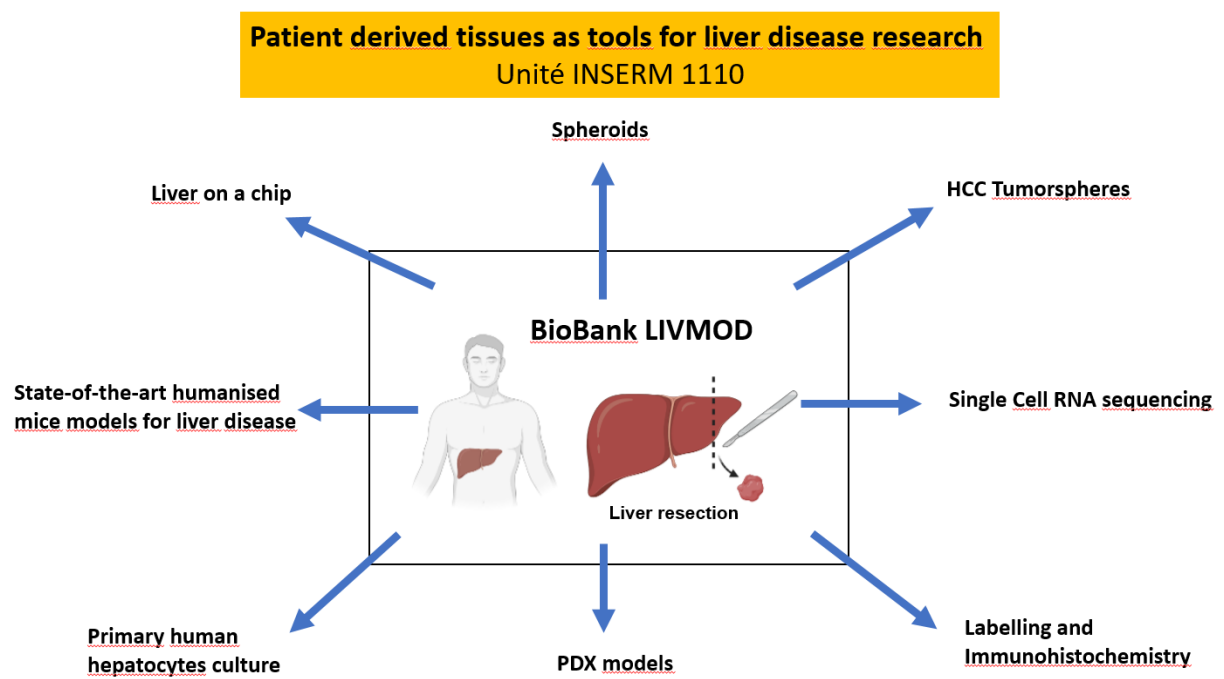


Figure 4a: Patient derived tissues as tools for liver disease research

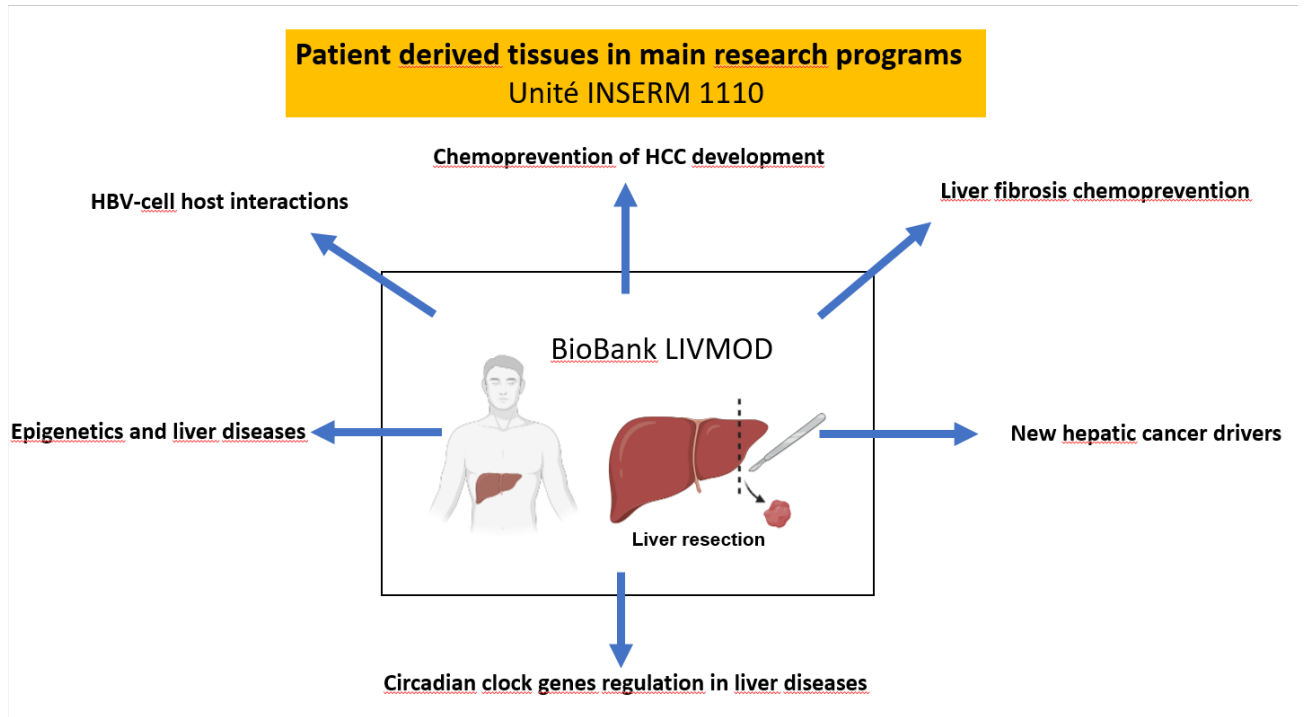
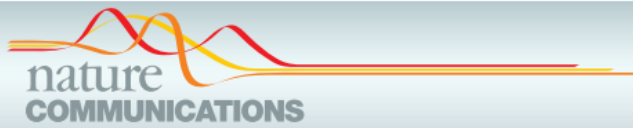


Figure 4b: Patient derived tissues in main research programs

Not every project in this third part has been fully developed, but preliminary results have been published in indexed journals, citing references here reported.

1) A human liver cell-based system modeling a clinical prognostic liver signature for therapeutic discovery.

Nat Commun. 2021 Sep 17;12(1):5525



ARTICLE



<https://doi.org/10.1038/s41467-021-25468-9>

OPEN

A human liver cell-based system modeling a clinical prognostic liver signature for therapeutic discovery

Emilie Crouchet^{1,2}, Simonetta Bandiera^{1,2}, Naoto Fujiwara³, Shen Li⁴, Hussein El Saghire^{1,2}, Mirian Fernández-Vaquero^{5,6}, Tobias Riedl^{5,6}, Xiaochen Sun³, Hadassa Hirschfield³, Frank Jühling^{1,2}, Shijia Zhu³, Natascha Roehlen^{1,2}, Clara Ponsolles^{1,2}, Laura Heydmann^{1,2}, Antonio Saviano^{1,2,7}, Tongqi Qian³, Anu Venkatesh³, Joachim Lupberger^{1,2}, Eloi R. Verrier^{1,2}, Mozhdeh Sojoodi⁴, Marine A. Oudot^{1,2}, François H. T. Duong^{1,2,8}, Ricard Masia⁹, Lan Wei⁴, Christine Thumann^{1,2}, Sarah C. Durand^{1,2}, Victor González-Motos^{1,2}, Danijela Heide⁵, Jenny Hetzer⁵, Shigeki Nakagawa³, Atsushi Ono¹⁰, Won-Min Song¹¹, Takaaki Higashi¹², Roberto Sanchez¹³, Rosa S. Kim¹⁴, C. Billie Bian¹¹, Karun Kiani^{15,16}, Tom Croonenborghs^{15,16,17}, Aravind Subramanian¹⁵, Raymond T. Chung¹⁸, Beate K. Straub¹⁹, Detlef Schuppan^{20,21}, Maliki Ankavay²², Laurence Cocquerel²², Evelyne Schaeffer²³, Nicolas Goossens²⁴, Anna P. Koh³, Milind Mahajan¹¹, Venugopalan D. Nair²⁵, Ganesh Gunasekaran²⁶, Myron E. Schwartz²⁶, Nabeel Bardeesy²⁷, Alex K. Shalek^{16,28,29}, Orit Rozenblatt-Rosen^{16,31}, Aviv Regev^{16,30,31}, Emanuele Felli^{1,2,7}, Patrick Pessaux^{1,2,7}, Kenneth K. Tanabe⁴, Mathias Heikenwälder⁵, Catherine Schuster^{1,2}, Nathalie Pochet^{15,16}, Mirjam B. Zeisel^{1,2,32}, Bryan C. Fuchs^{4,33}, Yujin Hoshida³ & Thomas F. Baumert^{1,2,7}

Abstract

Chronic liver disease and hepatocellular carcinoma (HCC) are life-threatening diseases with limited treatment options. The lack of clinically relevant/tractable experimental models hampers therapeutic discovery. Here, we develop a simple and robust human liver cell-based system modeling a clinical prognostic liver signature (PLS) predicting long-term liver disease progression toward HCC. Using the PLS as a readout, followed by validation in nonalcoholic steatohepatitis/fibrosis/HCC animal models and patient-derived liver spheroids, we identify nizatidine, a histamine receptor H2 (HRH2) blocker, for treatment of advanced liver disease and HCC chemoprevention. Moreover, perturbation studies combined with single cell RNA-Seq analyses of patient liver tissues uncover hepatocytes and HRH2+, CLEC5A^{high}, MARCO^{low} liver macrophages as potential nizatidine targets. The PLS model combined with single cell RNA-Seq of patient tissues enables discovery of urgently needed targets and therapeutics for treatment of advanced liver disease and cancer prevention.

2) Hepatitis B virus compartmentalization and single-cell differentiation in hepatocellular carcinoma.

Life Sci Alliance. 2021 Jul 21;4(9):e202101036





Published Online: 21 July, 2021 | Supp Info: <http://doi.org/10.26508/lsa.202101036>

Downloaded from life-science-alliance.org on 6 March, 2022

Research Article



Hepatitis B virus compartmentalization and single-cell differentiation in hepatocellular carcinoma

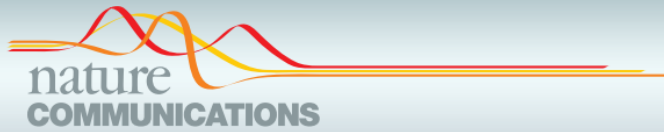
Frank Jühling^{1,*} , Antonio Saviano^{1,2,*}, Clara Ponsolles¹, Laura Heydmann¹, Emilie Crouchet¹, Sarah C Durand¹, Houssein El Saghire¹, Emanuele Felli^{1,2}, Véronique Lindner³ , Patrick Pessaux^{1,2}, Nathalie Pochet^{4,5}, Catherine Schuster^{1,2} , Eloi R Verrier¹, Thomas F Baumert^{1,2,6} 

Abstract

Chronic hepatitis B virus (HBV) infection is a major cause of hepatocellular carcinoma (HCC) world-wide. The molecular mechanisms of viral hepatocarcinogenesis are still partially understood. Here, we applied two complementary single-cell RNA-sequencing protocols to investigate HBV-HCC host cell interactions at the single cell level of patient-derived HCC. Computational analyses revealed a marked HCC heterogeneity with a robust and significant correlation between HBV reads and cancer cell differentiation. Viral reads significantly correlated with the expression of HBV-dependency factors such as *HLF* in different tumor compartments. Analyses of virus-induced host responses identified previously undiscovered pathways mediating viral carcinogenesis, such as E2F- and MYC targets as well as adipogenesis. Mapping of fused HBV-host cell transcripts allowed the characterization of integration sites in individual cancer cells. Collectively, single-cell RNA-Seq unravels heterogeneity and compartmentalization of both, virus and cancer identifying new candidate pathways for viral hepatocarcinogenesis. The perturbation of pro-carcinogenic gene expression even at low HBV levels highlights the need of HBV cure to eliminate HCC risk.

3) **A genome-wide gain-of-function screen identifies CDKN2C as a HBV host factor.**

Nat Commun. 2020 Jun 1;11(1):2707



ARTICLE



<https://doi.org/10.1038/s41467-020-16517-w>

OPEN

A genome-wide gain-of-function screen identifies CDKN2C as a HBV host factor

Carla Eller^{1,11}, Laura Heydmann^{1,11}, Che C. Colpitts^{1,2}, Houssein El Saghire¹, Federica Piccioni³, Frank Jühling¹, Karim Majzoub¹, Caroline Pons⁴, Charlotte Bach¹, Julie Lucifora⁴, Joachim Lupberger¹, Michael Nassal⁵, Glenn S. Cowley³, Naoto Fujiwara⁶, Sen-Yung Hsieh⁷, Yujin Hoshida⁶, Emanuele Felli^{1,8}, Patrick Pessaux^{1,8}, Camille Sureau⁹, Catherine Schuster¹, David E. Root³, Eloi R. Verrier^{1,12} & Thomas F. Baumert^{1,8,10,12}

Abstract

Chronic HBV infection is a major cause of liver disease and cancer worldwide. Approaches for cure are lacking, and the knowledge of virus-host interactions is still limited. Here, we perform a genome-wide gain-of-function screen using a poorly permissive hepatoma cell line to uncover host factors enhancing HBV infection. Validation studies in primary human hepatocytes identified CDKN2C as an important host factor for HBV replication. CDKN2C is overexpressed in highly permissive cells and HBV-infected patients. Mechanistic studies show a role for CDKN2C in inducing cell cycle G1 arrest through inhibition of CDK4/6 associated with the upregulation of HBV transcription enhancers. A correlation between CDKN2C expression and disease progression in HBV-infected patients suggests a role in HBV-induced liver disease. Taken together, we identify a previously undiscovered clinically relevant HBV host factor, allowing the development of improved infectious model systems for drug discovery and the study of the HBV life cycle.

7. CONCLUSIONS

This fascinating research on some specific aspects of HCC treatment is an example of how interactions between different disciplines, “know how” and cutting-edge technologies can be synthesized to provide the highest quality of clinical care.

The word “precision” is the cornerstone of the 21st century paradigm of personalized medicine, the ultimate form of cure and care. The patient as a whole is once again the center of medical science, between modern macroeconomic healthcare necessities (and limits), and continuous need of the best treatment for every specific form of the disease.

We initially focused on preoperative strategy to see if the most recent technologies applied to tridimensional reconstruction significantly improved surgical strategy. The multicentric prospective trial showed that in tertiary referral HPB centers substantial modifications were reported after 3D images analysis. These results suggest that 3D models are a complement and not an opposition to standard imaging. Educational and teaching purposes are also to be considered as 3D reconstruction allows an easier comprehension of the real anatomy of the patient. Details quality is improving and probably soon it will be an integrated and routine part of the surgical process.

We then moved to the intraoperative time exploring the cutting-edge technology of hyperspectral imaging. Experiments showed very interesting, though not fundamental results, but as this new technology is still not explored nor clinically routinely applied, the presented articles are among the first on that kind in this really innovative field. Further research should also be focused on liver transplantation to look for correlations between HIS imaging and liver reperfusion, and postoperative outcome. The review associated with the intraoperative phase focused on an innovative approach, the positive and negative staining with ICG for real time intraoperative guidance during minimally invasive anatomical liver resection. This promising technique is still very rarely used, and future

standardization of the technique may overcome some technical limits. The use of the fusion camera is undoubtedly a great advance to help diffusion in the everyday practice. Finally, the transversal work with the INSERM Unit 1110 was an example of a multidisciplinary approach to clinical and translational research from the bedside to the bench and vice et versa.

Nevertheless, words of caution are necessary. All the mentioned and different forms of innovative approaches need reflexion, planification, and intelligent, constant and humble application to better clarify the real impact in the every day clinical practice.

In conclusion, precision medicine applied to the treatment of HCC is complex and ambitious, and most of all related to different medical specialties, basic science, and engineering. Cutting edge technologies are entering today's clinical practice, and innovation is playing a key role in the decision-making process. Don't miss the boat!

BIBLIOGRAPHY :

- 1) Villanueva, A. Hepatocellular carcinoma. *N. Engl.J. Med.* (2019) **380**, 1450–1462
- 2) Llovet, J. M. *et al.* Hepatocellular carcinoma. *Nat. Rev.Dis. Prim.* (2016) **2**, 16018
- 3) International Agency for Research on Cancer.GLOBOCAN 2018. *IARC*
<https://gco.iarc.fr/today/online-analysis-map?v=2020&mode=population&> (2020).
- 4) Akinyemiju, T. *et al.* The burden of primary liver cancer and underlying etiologies from 1990 to 2015 at the global, regional, and national level. *JAMA Oncol* (2017) **3**, 1683
- 5) Kanwal, F. *et al.* Risk of hepatocellular cancer in HCV patients treated with direct- acting antiviral agents. *Gastroenterology* (2017) **153**, 996–1005.e1
- 6) Estes, C., Razavi, H., Loomba, R., Younossi, Z. & Sanyal, A. J. Modeling the epidemic of nonalcoholic fatty liver disease demonstrates an exponential increase in burden of disease. *Hepatology* (2018) **67**, 123–133
- 7) Schulze, K. *et al.* Exome sequencing of hepatocellular carcinomas identifies new mutational signatures and potential therapeutic targets. *Nat. Genet.* (2015) **47**, 505–511
- 8) Llovet, J. M., Montal, R., Sia, D. & Finn, R. S. Molecular therapies and precision medicine for hepatocellular carcinoma. *Nat. Rev. Clin. Oncol.* (2018) **15**, 599–616
- 9) European Association for the Study of the Liver.EASL clinical practice guidelines: management of hepatocellular carcinoma. *J. Hepatol.* (2018) **69**, 182–236
- 10) Marrero, J. A. *et al.* Diagnosis, staging, and management of hepatocellular carcinoma: 2018 practice guidance by the American Association for the Study of Liver Diseases. *Hepatology* (2018) **68**, 723–750
- 11) Tabrizian, P. *et al.* A US multicenter analysis of 2529 HCC patients undergoing liver transplantation: 10-year outcome assessing the role of down- staging to within Milan criteria [abstract 15]. *Hepatology* (2019) **70**, 10–11
- 12) Llovet, J.M., Kelley, R.K., Villanueva, A. *et al*, Hepatocellular carcinoma. *Nature reviews Nat Rev Dis Primers.* (2021) Jan 21;7(1):6
- 13) Shrager, B., Jibara, G., Schwartz, M. & Roayaie, S. Resection of hepatocellular carcinoma without cirrhosis. *Ann. Surg* (2012) **255**, 1135–1143.
- 14) Regimbeau JM, Kianmanesh R, Farges O, Dondero F, Sauvanet A, Belghiti J. Extent of liver resection influences the outcome in patients with cirrhosis and small hepatocellular carcinoma. *Surgery.*(2002) Mar;131(3):311-7.
- 15) Kosuge T, Makuuchi M, Takayama T, Yamamoto J, Shimada K, Yamasaki S. Long-term results after resection of hepatocellular carcinoma: Experience of 480 cases. *Hepatogastroenterology* (1993);40:328–332.

-
- 16) Hasegawa K, Kokudo N, Imamura H, *et al.* Prognostic impact of anatomic resection for hepatocellular carcinoma. *Ann Surg* (2005);242:252–259.
- 17) Yamamoto M, Takasaki K, Ohtsubo T, Katsuragawa H, Fukuda C, Katagiri S. Effectiveness of systematized hepatectomy with Glisson’s pedicle transection at the hepatic hilus for small nodular hepatocellular carcinoma: Retrospective analysis. *Surgery* (2001);130:443–448.
- 18) Ueno S, Kubo F, Sakoda M, *et al.* Efficacy of anatomic resection vs nonanatomic resection for small nodular hepatocellular carcinoma based on gross classification. *J Hepatobiliary Pancreat Surg* (2008);15:493–500.
- 19) Marescaux J, Clement JM, Tasseti V, Koehl C, Cotin S, Russier Y, *et al.* Virtual reality applied to hepatic surgery simulation: the next revolution. *Ann Surg* (1998);228: 627–34.
- 20) Miyamoto R, Oshiro Y, Hashimoto S Three-dimensional imaging identified the accessory bile duct in a patient with cholangiocarcinoma. *World J Gastroenterol* (2014) 20:11451–11455
- 21) Hallet J, Gayet B, Tsung A *et al.* Systematic review of the use of pre-operative simulation and navigation for hepatectomy: current status and future perspectives. *J Hepato Biliary Pancreat Sci* (2015) 22:353–362
- 22) Gauss T, Merckx P, Brasher C, *et al.* Deviation from a preoperative surgical and anaesthetic care plan is associated with increased risk of adverse intraoperative events in major abdominal surgery. *Langenbecks Arch Surg.* (2013) 398(2):277-85.
- 23) Wigmore SJ, Redhead DN, Yan XJ, *et al.* Virtual Hepatic Resection Using Three-Dimensional Reconstruction of Helical Computed Tomography Angiograms. *Ann Surg* (2001);233:221-6.
- 24) Saito S, Yamanaka J, Miura K, *et al.* A novel 3D hepatectomy simulation based on liver circulation: application to liver resection and transplantation. *Hepatology* (2005) 41:1297-304.
- 25) Yamanaka J, Saito S, Fujimoto J. Impact of preoperative planning using virtual segmental volumetry on liver resection for hepatocellular carcinoma. *World J Surg* (2007) 31:1249-55.
- 26) Radtke A, Sotiropoulos GC, Molmenti EP, *et al.* Computer-Assisted Surgery Planning for Complex Liver Resections: When Is It Helpful? A Single-Center Experience Over an 8-Year Period. *Ann Surg* (2010) 252:876-83.
- 27) Mise Y, Hasegawa K, Satou S, *et al.* How Has Virtual Hepatectomy Changed the Practice of Liver Surgery? : Experience of 1194 Virtual Hepatectomy Before Liver Resection and Living Donor Liver Transplantation. *Ann Surg* (2018) 268:127-33.
- 28) Li P, Wang M, Yang Y, Liu H, Pan Z, Jiang B, *et al.* Preoperative three-dimensional versus two-dimensional evaluation in assessment of patients undergoing major liver

resection for hepatocellular carcinoma: a propensity score matching study. *Ann Transl Med.* (2020) 8(5):182.

29) Makuuchi M, Hasegawa H, Yamazaki S Ultrasonically guided subsegmentectomy. *Surg Gynecol Obstet* (1985) 161:346–350

30) Torzilli G, Makuuchi M. Ultrasound-guided finger compression in liver subsegmentectomy for hepatocellular carcinoma. *Surg Endosc.* (2004) 18:136–139

31) Shindoh J, Seyama Y, Matsuda M, Miyata Y, Shida D, Maeshiro T, Miyamoto S, Inoue S, Umekita N Continuous ultrasound navigation for safe and precise anatomic resection of the liver. *Hepatogastroenterology* (2013) 60:590–594

32) Ferrero A, Lo Tesoriere R, Russolillo N, Vigano L, Forchino F, Capussotti L Ultrasound-guided laparoscopic liver resections. *Surg Endosc* (2015) 29:1002–1005

33) Felli E, Ishizawa T, Cherkaoui Z, Diana M, Tripon S, Baumert TF, Schuster C, Pessaux P. Laparoscopic anatomical liver resection for malignancies using positive or negative staining technique with intraoperative indocyanine green-fluorescence imaging. *HPB* (Oxford). (2021) 23(11):1647-1655

34) Aoki T, Yasuda D, Shimizu Y, Odaira M, Niiya T, Kusano T, Mitamura K, Hayashi K, Murai N, Koizumi T, Kato H, Enami Y, Miwa M, Kusano M. Image-guided liver mapping using fluorescence navigation system with indocyanine green for anatomical hepatic resection. *World J Surg.* (2008) 32(8):1763-7

35) Buell JF, Cherqui D, Geller DA *et al.* The international position on laparoscopic liver surgery: The Louisville Statement, 2008. *Ann Surg* (2009) 250: 825–830

36) Wakabayashi G, Cherqui D, Geller DA *et al.* Recommendations for laparoscopic liver resection: A report from the second international consensus conference held in Morioka. *Ann Surg* (2015) 261: 619–629

37) Ishizawa T, Zuker NB, Kokudo N, Gayet B. Positive and negative staining of hepatic segments by use of fluorescent imaging techniques during laparoscopic hepatectomy. *Arch Surg.* (2012) 147:393e394.

38) Sakoda M, Ueno S, Iino S, *et al.* Anatomical laparoscopic hepatectomy for hepatocellular carcinoma using indocyanine green fluorescence imaging. *J Laparoendosc Adv Surg Tech A.* (2014) 24:878e882.

39) Takasaki K. Glissonean pedicle transection method for hepatic resection: a new concept of liver segmentation. *J Hepatobiliary Pancreat Surg.* (1998) 5:286e291

40) Mizuno T, Sheth R, Yamamoto M, *et al.* Laparoscopic glissonean pedicle transection (Takasaki) for negative fluorescent counterstaining of segment 6. *Ann Surg Oncol.* (2017) 24: 1046e1047

41) Terasawa M, Ishizawa T, Mise Y, *et al.* Applications of fusion fluorescence imaging using indocyanine green in laparoscopic hepatectomy. *Surg Endosc.* (2017) 31:5111e5118

-
- 42) Nomi T, Hokuto D, Yoshikawa T, *et al.* A novel navigation for laparoscopic anatomic liver resection using indocyanine green fluorescence. *Ann Surg Oncol.* (2018) 25(13):3982
- 43) Zhai Y, Petrowsky H, Hong JC, Busuttill RW, Kupiec-Weglinski JW. Ischaemia–reperfusion injury in liver transplantation - from bench to bedside. *Nature Reviews Gastroenterology & Hepatology* (2013)10(2):79-89.
- 44) Selzner M, Selzner N, Jochum W, Graf R, Clavien PA. Increased ischemic injury in old mouse liver: an ATP-dependent mechanism. *Liver Transpl.* (2007) 13(3):382-90.
- 45) Lu G, Fei B. Medical hyperspectral imaging: a review. *J Biomed Opt.* (2014) 19(1):10901.
- 46) Holmer A, Marotz J, Wahl P, Dau M, Kammerer PW. Hyperspectral imaging in perfusion and wound diagnostics - methods and algorithms for the determination of tissue parameters. *Biomed Tech (Berl).* (2018) 63(5):547-56.
- 47) Chiou WC, Sr. NASA image-based geological expert system development project for hyperspectral image analysis. *Appl Opt.* (1985) 24(14):2085.
- 48) Nuciforo S, Fofana I, Matter MS, *et al.* Organoid Models of Human Liver Cancers Derived from Tumor Needle Biopsies. *Cell Reports* (2018) 24(5),1363-1376.
- 49) Serras AS, Rodrigues JS, Cipriano M, *et al.* A Critical Perspective on 3D Liver Models for Drug Metabolism and Toxicology Studies. *Front Cell Dev Biol.* (2021) 22;9: 626805.
- 50) Aizarani, N., Saviano, A., Sagar *et al.* A human liver cell atlas reveals heterogeneity and epithelial progenitors. *Nature* (2019) 572, 199–204.

Dr Emanuele FELLI, MD

Chirurgien, Praticien Hospitalier
Hôpitaux Universitaires de Tours
Institut de recherche sur les maladies virales et hépatiques
Inserm UMR_S1110, Strasbourg

Etat civil:

Né le 08/09/1981 à Rome, Italie
Nationalité : Italienne
Marié, 4 enfants (Emma, Greta, Adriano, Flavio)

Adresse professionnelle : Avenue de la République 37170 Chambray-lès-Tours
e-mail: e.felli@chu-tours.fr e.felli@hotmail.com

Fonction actuelle:

Praticien Hospitalier
Adresse professionnelle : Pôle hépato-digestif, Directeur Pr Salamé
Unité de Chirurgie Hépato-bilio-pancréatique, Service de Chirurgie Digestive
Hôpital Trousseau, Chambray-lès-Tours

Spécialité : **Transplantation Hépatique et Chirurgie Hépatobilio-pancréatique,
chirurgie robotique et coelioscopique**

Membre de l'Unité INSERM UMR_S1110
Institut de recherche sur les maladies Virales et hépatiques, Directeur Pr T Baumert,
Strasbourg- France

Diplômes:

2000 Baccalauréat scientifique, note 97/100
2000-2006 Faculté de Médecine Université Sapienza Rome, Italie
Diplôme Universitaire de Médecine "summa cum laude" (110/110 e lode)
2007 Enregistrement à l'Ordre de Médecins Italien
2007-2012 Internat Chirurgie Viscérale, Hôpital « Umberto I »
Université Sapienza, Rome
30/07/2012 Diplôme de spécialiste en Chirurgie Viscérale « summa cum laude »

Expériences médicales avant obtention du diplôme universitaire en Médecine:

2000-2006 Externe dans le service de Chirurgie Générale
Hôpital Villa Tiberia, Rome, participation à l'activité opératoire

2005 Observership General Surgery ward and theatre,
Whipps Cross University Hospital, London, UK (Juillet-Aout)

Observership Valencia Oncology Institute, Valencia, Espagne (Octobre)

Basic Life Support executor", course et diplôme Rome, Italie
Suturing Techniques", course et diplôme Rome, Italie

2006 Bourse universitaire "Tesi all'Estero" (thèse à l'étranger)
General Surgery Department, ward and theatre
Whipps Cross University Hospital, London, UK (Dec-Feb)

Expériences médicales après obtention du diplôme universitaire:

- 2006: Scholarship en Chirurgie Générale,
Hôpital « Universitario José Eleuterio Gonzales », Nuevo Leon, Mexique
- 2007: Volontaire ONG, Institute for Indian mother & Child
Calcutta, Inde (Avril-Juin)
- 2007 BLSD (Basic Life Support) and PBLSD (Pediatric BLSD), basic
Cours et diplôme, Roma Urgenza, Rome, Italy
- 2008 Colorectal mini-invasive Surgery course”
European Surgical Institute, Hamburg, Allemagne
- 2009 Advanced Life Support (ALS), course et diplome, Rome, Italy
- 2010 Intensive course Laparoscopic General Surgery, IRCAD-Strasbourg
DU de chirurgie laparoscopique- Université de Strasbourg, France
- 2010 Postgraduate Teaching Term (Mai-Juin)
St. Mark’s Hospital, London, laparoscopie (Pr Robin Kennedy), London, UK
- 2011 Advanced Trauma Life Support (ATLS) course et diplôme
Université Cattolica, Hopital A. Gemelli, Rome, Italie
- 2011 Clinical Fellow, Service de Chirurgie Générale
Hôpital “José Maria Gonzales Meseguer” Murcia, Espagne (Mai - Août)
- 2011/2012 FFI (Faisant Fonction d’Interne) , Collège de Médecine des Hôpitaux de
Paris
Nov-Nov Service de Chirurgie Digestive & Hépatobiliaire et Transplantation
Hépatique
Pr Hannoun, Hôpital Pitié-Salpêtrière – Paris, France
- 2012/2013 FFI(Faisant Fonction d’Interne)
Nov-Mai Service de Chirurgie Digestive
Pr Berger HEGP-(Hôpital Européen George Pompidou)
Paris, France
- 2013 FFI (Faisant Fonction d’Interne)
Mai-Nov Service de Chirurgie Digestive & Hépatobiliaire et
Transplantation Hépatique
Pr Azoulay, Hôpital Henri Mondor – Créteil, France
- 2013/2014 Praticien Attaché avec fonction de Chef de Clinique Associé
Nov/Mar Service de Chirurgie Digestive & Hépatobiliaire et Transplantation
hépatique
Pr Azoulay, Hôpital Henri Mondor- Créteil, France
- 2014-15 Praticien Attaché
Mai/Mai Service de Chirurgie Digestive & Hépatobiliaire et Transplantation
Hépatique
Pr Ettorre Hôpital « San Camillo », Rome, Italie

-
- 2015 ESOT multi-organ procurement course, Leyden, Pays Bas
- 2015-2018 Chef de Clinique Assistant
Service de Chirurgie Générale, Endocrinienne et Transplantation
Hépatique
CHU Strasbourg, Strasbourg, France
- 2017 DIU Cancers Hépato-Bilio-Pancréatiques - Stratégies Onco- Chirurgicales
Pr Adam, Hôpital Paul Brousse, Paris, France
- 2018 DIU Pancréatologie médico-chirurgicale
Pr Sauvanet, Hôpital Beaujon, Paris, France
- 2018 - Praticien Hospitalier
Unité Chirurgie Hépato-Biliaire-Pancréatique
Pr Pessaux, Nouvel Hôpital Civil, CHU Strasbourg, France
- 2019 - Membre Unité INSERM S1110
Institut de recherche sur les maladies Virales et hépatiques
Pr Baumert, Strasbourg- France
- hépatique Bourse Hermès ACHBT Observership
Service de Chirurgie Digestive & Hépato-biliaire et Transplantation
Pr Boudjema, Hôpital Pontcaillou- Rennes, France
- Observership chirurgie robotique HPB
Hépto-pancreatic-biliary Unit
Pr Tang Pamela « Youde Nethersole Eastern Hospital » Hong Kong, China
- Observership Chirurgie HBP et Transplantation hépatique
Hospital Clinic, Barcelona – Spain
Pr Fondevila
- 2021 - Praticien Hospitalier
Service de Chirurgie Digestive & Hépato-bilio-pancréatique
et Transplantation hépatique
Pr Salamé, Hôpital Trousseau, CHU Tours, France

Publications : 86 articles indexés, 20 en premier auteur

2022

1. Personalized functional profiling using *ex-vivo* patient-derived spheroids points out the potential of an antiangiogenic treatment in a patient with a metastatic lung atypical carcinoid. Kim H, El-Khoury V, Schulte N, Zhan T, Betge J, Cousin L, **Felli E**, Pessaux P, Ogier A, Opitz O, Ku B, Ebert MP, Kwon YJ. *Cancer Biol Ther.* 2022 Dec 31;23(1):96-102.
2. Combined endoscopic and surgical management of a right intrahepatic bile duct injury during laparoscopic cholecystectomy. Mayer P, Héroin L, Habersetzer F, Vix M, Pessaux P, **Felli E**, Mathis G. *Endoscopy.* 2022 Feb 18.

2021

-
3. Liver resection vs radiofrequency ablation in single hepatocellular carcinoma of posterosuperior segments in elderly patients. Delvecchio A, Inchingolo R, Laforgia R, Ratti F, Gelli M, Anelli MF, Laurent A, Vitali G, Magistri P, Assirati G, **Felli E**, Wakabayashi T, Pessaux P, Piardi T, di Benedetto F, de'Angelis N, Briceño J, Rampoldi A, Adam R, Cherqui D, Aldrighetti LA, Memeo R. *World J Gastrointest Surg*. 2021 Dec 27;13(12):1696-1707
 4. Upper gastrointestinal bleeding due to left side portal hypertension after pancreatic surgery. Mayer P, **Felli E**, Enescu I, Habersetzer F, Tripon S. *Hepatobiliary Pancreat Dis Int*. 2021 Dec 30:S1499-3872(21)00235-6.
 5. Augmented Reality and Image-Guided Robotic Liver Surgery. Giannone F, **Felli E**, Cherkaoui Z, Mascagni P, Pessaux P. *Cancers (Basel)*. 2021 Dec 14;13(24):6268.
 6. Laparoscopic versus open liver resection for hepatocellular carcinoma in elderly patients: a propensity score matching analysis. Delvecchio A, Conticchio M, Riccelli U, Ferraro V, Ratti F, Gelli M, Anelli FM, Laurent A, Vitali GC, Magistri P, Assirati G, **Felli E**, Wakabayashi T, Pessaux P, Piardi T, Di Benedetto F, de'Angelis N, Briceño-Delgado J, Adam R, Cherqui D, Aldrighetti L, Memeo R. *HPB (Oxford)*. 2021 Nov 6:S1365-182X(21)01691-9
 7. The counterclock-clockwise approach for central hepatectomy: A useful strategy for a safe vascular control. Muttillio EM, Felli E, Cinelli L, Giannone F, **Felli E**. *J Surg Oncol*. 2022 Feb;125(2):175-178.
 8. Automatic Liver Viability Scoring with Deep Learning and Hyperspectral Imaging. Felli E, Al-Taher M, Collins T, Nkusi R, **Felli E**, Baiocchini A, Lindner V, Vincent C, Barberio M, Geny B, Ettorre GM, Hostettler A, Mutter D, Gioux S, Schuster C, Marescaux J, Gracia-Sancho J, Diana M. *Diagnostics (Basel)*. 2021 Aug 24;11(9):1527
 9. A human liver cell-based system modeling a clinical prognostic liver signature for therapeutic discovery. Crouchet E, Bandiera S, Fujiwara N, Li S, El Saghire H, Fernández-Vaquero M, Riedl T, Sun X, Hirschfield H, Jühling F, Zhu S, Roehlen N, Ponsolles C, Heydmann L, Saviano A, Qian T, Venkatesh A, Lupberger J, Verrier ER, Sojoodi M, Oudot MA, Duong FHT, Masia R, Wei L, Thumann C, Durand SC, González-Motos V, Heide D, Hetzer J, Nakagawa S, Ono A, Song WM, Higashi T, Sanchez R, Kim RS, Bian CB, Kiani K, Croonenborghs T, Subramanian A, Chung RT, Straub BK, Schuppan D, Ankavay M, Cocquerel L, Schaeffer E, Goossens N, Koh AP, Mahajan M, Nair VD, Gunasekaran G, Schwartz ME, Bardeesy N, Shalek AK, Rozenblatt-Rosen O, Regev A, **Felli E**, Pessaux P, Tanabe KK, Heikenwälder M, Schuster C, Pochet N, Zeisel MB, Fuchs BC, Hoshida Y, Baumert TF. *Nat Commun*. 2021 Sep 17;12(1):5525.
 10. SARS-CoV-2 infection and venous thromboembolism after surgery: an international prospective cohort study. COVIDSurg Collaborative; GlobalSurg Collaborative. *Anaesthesia*. 2022 Jan;77(1):28-39.
 11. Effects of pre-operative isolation on postoperative pulmonary complications after elective surgery: an international prospective cohort study. COVIDSurg Collaborative; GlobalSurg Collaborative. *Anaesthesia*. 2021 Nov;76(11):1454-1464.
 12. Intraoperative Time-Out to Promote the Implementation of the Critical View of Safety in Laparoscopic Cholecystectomy: A Video-Based Assessment of 343 Procedures. Mascagni P, Rodríguez-Luna MR, Urade T, **Felli E**, Pessaux P, Mutter D, Marescaux J, Costamagna G, Dallemagne B, Padoy N. *J Am Coll Surg*. 2021 Oct;233(4):497-505.
 13. Hepatitis B virus compartmentalization and single-cell differentiation in hepatocellular carcinoma. Jühling F, Saviano A, Ponsolles C, Heydmann L, Crouchet E, Durand SC, El Saghire H, **Felli E**, Lindner V, Pessaux P, Pochet N, Schuster C, Verrier ER, Baumert TF. *Life Sci Alliance*. 2021 Jul 21;4(9):e202101036.

-
14. Laparoscopic anatomical liver resection for malignancies using positive or negative staining technique with intraoperative indocyanine green-fluorescence imaging. **Felli E**, Ishizawa T, Cherkaoui Z, Diana M, Tripon S, Baumert TF, Schuster C, Pessaux P. *HPB (Oxford)*. 2021 Nov;23(11):1647-1655.
 15. Laparoscopic surgery versus radiofrequency ablation for the treatment of single hepatocellular carcinoma ≤ 3 cm in the elderly: a propensity score matching analysis. Conticchio M, Delvecchio A, Ratti F, Gelli M, Anelli FM, Laurent A, Vitali GC, Magistri P, Assirati G, **Felli E**, Wakabayashi T, Pessaux P, Piardi T, Di Benedetto F, de'Angelis N, Javier Briceno DF, Rampoldi AG, Adam R, Cherqui D, Aldrighetti L, Memeo R. *HPB (Oxford)*. 2022 Jan;24(1):79-86.
 16. Interpatient heterogeneity in hepatic microvascular blood flow during vascular inflow occlusion (Pringle manoeuvre). Felli E, Muttillio EM, **Felli E**. *Hepatobiliary Surg Nutr*. 2021 Jun;10(3):413-415. doi: 10.21037/hbsn-21-91. PMID: 34159179 Free PMC article. No abstract available.
 17. Prepancreatic common hepatic artery arising from superior mesenteric artery: an exceptional but important finding during pancreaticoduodenectomy. Cinelli L, Felli E, Muttillio EM, Fiorentini G, Diana M, Pessaux P, **Felli E**. *Surg Radiol Anat*. 2021 Sep;43(9):1413-1420.
 18. Radiofrequency ablation vs surgical resection in elderly patients with hepatocellular carcinoma in Milan criteria. Conticchio M, Inchingolo R, Delvecchio A, Laera L, Ratti F, Gelli M, Anelli F, Laurent A, Vitali G, Magistri P, Assirati G, **Felli E**, Wakabayashi T, Pessaux P, Piardi T, di Benedetto F, de'Angelis N, Briceño J, Rampoldi A, Adam R, Cherqui D, Aldrighetti LA, Memeo R. *World J Gastroenterol*. 2021 May 14;27(18):2205-2218.
 19. RE: re: manuscript titled, "Liver transplantation for sickle cell disease: a systematic review". **Felli E**, Felli E, Muttillio EM, Memeo R, Giannelli V, Colasanti M, Pellicelli A, Diana M, Ettore GM. *HPB (Oxford)*. 2021 Jul;23(7):1136.
 20. SARS-CoV-2 vaccination modelling for safe surgery to save lives: data from an international prospective cohort study. COVIDSurg Collaborative, GlobalSurg Collaborative. *Br J Surg*. 2021 Sep 27;108(9):1056-1063.
 21. Timing of surgery following SARS-CoV-2 infection: an international prospective cohort study. COVIDSurg Collaborative; GlobalSurg Collaborative. *Anaesthesia*. 2021 Jun;76(6):748-758.
 22. Primary Hepatic Lymphoma After Lung Transplantation: A Report of 2 Cases. Muttillio EM, Dégot T, Canuet M, Riou M, Renaud-Picard B, Hirschi S, Guffroy B, Kessler R, Olland A, Falcoz PE, Pessaux P, **Felli E**. *Transplant Proc*. 2021 Mar;53(2):692-695.
 23. Can the mutational status of KRAS drive the treatment of colorectal liver metastases? Muttillio EM, **Felli E**. *HPB (Oxford)*. 2021 Apr;23(4):643
 24. Liver transplantation for sickle cell disease: a systematic review. **Felli E**, Felli E, Muttillio EM, Memeo R, Giannelli V, Colasanti M, Pellicelli A, Diana M, Ettore GM. *HPB (Oxford)*. 2021 Jul;23(7):994-999.

2020

25. Clinical efficacy of liver resection combined with adjuvant microwave coagulation for patients with hepatocellular carcinoma: a promising approach to minimize recurrence? **Felli E**, Cherkaoui Z, Pessaux P. *Ann Transl Med*. 2020 Sep;8(18):1123.

-
26. Hepar Lobatum carcinomatosum: A rare cause of portal hypertension. Mathis G, **Felli E**, Mutter D, Pessaux P. Clin Case Rep. 2020 Jun 23;8(10):2082-2083.
 27. Hyperspectral evaluation of hepatic oxygenation in a model of total vs. arterial liver ischaemia. Felli E, Al-TaHER M, Collins T, Baiocchini A, **Felli E**, Barberio M, Ettorre GM, Mutter D, Lindner V, Hostettler A, Gioux S, Schuster C, Marescaux J, Diana M. Sci Rep. 2020 Sep 22;10(1):15441
 28. Demarcation Line Assessment in Anatomical Liver Resection: An Overview. Felli E, Urade T, Al-TaHER M, **Felli E**, Barberio M, Goffin L, Ettorre GM, Marescaux J, Pessaux P, Swanstrom L, Diana M. Surg Innov. 2020 Oct;27(5):424-430
 29. Cattell-Braasch maneuver in pancreatic surgery. No need of venous graft for vascular resection. Muttillio EM, **Felli E**, Pessaux P. J Surg Oncol. 2020 Dec;122(8):1612-1615.
 30. Laparoscopic major hepatectomy for hepatocellular carcinoma in elderly patients: a multicentric propensity score-based analysis. Delvecchio A, Conticchio M, Ratti F, Gelli M, Anelli FM, Laurent A, Vitali GC, Magistri P, Assirati G, **Felli E**, Wakabayashi T, Pessaux P, Piardi T, Di Benedetto F, de'Angelis N, Briceño-Delgado J, Adam R, Cherqui D, Aldrighetti L, Memeo R. Surg Endosc. 2021 Jul;35(7):3642-3652.
 31. Acute abdomen in patients with SARS-CoV-2 infection or co-infection. Seeliger B, Philouze G, Cherkaoui Z, **Felli E**, Mutter D, Pessaux P. Langenbecks Arch Surg. 2020 Sep;405(6):861-866.
 32. Liver necrosis following cholecystectomy in sickle cell disease. Muttillio EM, **Felli E**, Pessaux P. Clin Case Rep. 2020 Mar 31;8(6):1114-1115.
 33. A Standard Set of Value-Based Patient-Centered Outcomes for Pancreatic Carcinoma: An International Delphi Survey. Cherkaoui Z, González C, Wakabayashi T, Delattre B, Léost E, Serra S, Huppertz J, Klein F, Stéphan M, Meyer JM, Schaff A, Martinis E, Bangoura E, Kieffer S, Blanès S, Haddad E, De Guio G, **Felli E**, Pernot S, Marescaux J, Mutter D, Lugiez C, Pessaux P; IHU-VBHC Working Group. Ann Surg Oncol. 2021 Feb;28(2):1069-1078.
 34. A genome-wide gain-of-function screen identifies CDKN2C as a HBV host factor. Eller C, Heydmann L, Colpitts CC, El Saghire H, Piccioni F, Jühling F, Majzoub K, Pons C, Bach C, Lucifora J, Lupberger J, Nassal M, Cowley GS, Fujiwara N, Hsieh SY, Hoshida Y, **Felli E**, Pessaux P, Sureau C, Schuster C, Root DE, Verrier ER, Baumert TF. Nat Commun. 2020 Jun 1;11(1):2707. doi: 10.1038/s41467-020-16517-w. PMID: 32483149 Free PMC article.
 35. Hyperspectral enhanced reality (HYPER) for anatomical liver resection. Urade T, Felli E, Barberio M, Al-TaHER M, **Felli E**, Goffin L, Agnus V, Ettorre GM, Marescaux J, Mutter D, Diana M. Surg Endosc. 2021 Apr;35(4):1844-1850.
 36. Is minimally invasive true anatomical HCC resection a future way to improve results in bridge or salvage liver transplantation? **Felli E**, Baumert T, Pessaux P. Clin Res Hepatol Gastroenterol. 2021 Nov;45(6):101396.
 37. Autologous peritoneal graft for venous vascular reconstruction after tumor resection in abdominal surgery: a systematic review. Lapergola A, **Felli E**, Rebiere T, Mutter D, Pessaux P. Updates Surg. 2020 Sep;72(3):605-615.
 38. Routine pathology examination in the era of value-based healthcare: the case of haemorrhoids specimens. Mascagni P, Eberspacher C, Saraceno F, **Felli E**, Sileri P, Fralleone L, Magliocca F, Mascagni D. Updates Surg. 2020 Mar;72(1):83-88.
 39. Letter to the Editor: Abdominal Surgery in Idiopathic Noncirrhotic Portal Hypertension: Is Preemptive TIPS Reducing Postoperative Complications? **Felli E**, Saviano A, Tripon S, Baumert TF, Pessaux P. Hepatology. 2020 Apr;71(4):1520-1522.

-
40. Formalizing video documentation of the Critical View of Safety in laparoscopic cholecystectomy: a step towards artificial intelligence assistance to improve surgical safety. Mascagni P, Fiorillo C, Urade T, Emre T, Yu T, Wakabayashi T, **Felli E**, Perretta S, Swanstrom L, Mutter D, Marescaux J, Pessaux P, Costamagna G, Padoy N, Dallemagne B. *Surg Endosc*. 2020 Jun;34(6):2709-2714.

2019

41. Radiomics in hepatocellular carcinoma: a quantitative review. Wakabayashi T, Ouhmich F, Gonzalez-Cabrera C, **Felli E**, Saviano A, Agnus V, Savadjiev P, Baumert TF, Pessaux P, Marescaux J, Gallix B. *Hepatol Int*. 2019 Sep;13(5):546-559.
42. Conclusive Identification and Division of the Cystic Artery: A Forgotten Trick to Optimize Exposure of the Critical View of Safety in Laparoscopic Cholecystectomy. Mascagni P, Spota A, **Felli E**, Perretta S, Pessaux P, Dallemagne B, Mutter D. *J Am Coll Surg*. 2019 Nov;229(5):e5-e7.
43. Laparoscopic liver resection in elderly patients: systematic review and meta-analysis. Notarnicola M, **Felli E**, Roselli S, Altomare DF, De Fazio M, de'Angelis N, Piardi T, Acquafredda S, Ammendola M, Verbo A, Pessaux P, Memeo R. *Surg Endosc*. 2019 Sep;33(9):2763-2773.
44. Robotic Central Pancreatectomy for Well-Differentiated Neuroendocrine Tumor: Parenchymal-Sparing Procedure. Wakabayashi T, **Felli E**, Cherkaoui Z, Mutter D, Marescaux J, Pessaux P. *Ann Surg Oncol*. 2019 Jul;26(7):2121.
45. Short-term outcomes of laparoscopic repeat liver resection after open liver resection: a systematic review. Wakabayashi T, **Felli E**, Memeo R, Mascagni P, Abe Y, Kitagawa Y, Pessaux P. *Surg Endosc*. 2019 Mar 18. doi: 10.1007/s00464-019-06754-6. [Epub ahead of print]
46. Aberrant splenic artery rising from the superior mesenteric artery: a rare but important anatomical variation. **Felli E**, Wakabayashi T, Mascagni P, Cherkaoui Z, Faucher V, Pessaux P. *Surg Radiol Anat*. 2019 Jan 3

2018

47. Feasibility and Value of the Critical View of Safety in Difficult Cholecystectomies. **Felli E**, Mascagni P, Wakabayashi T, Mutter D, Marescaux J, Pessaux P. *Ann Surg*. 2018 Nov 9.
48. Autologous peritoneal patch for partial portal vein resection during left hemi hepatectomy (with video). **Felli E**, Lapergola A, Pessaux P. *J Visc Surg*. 2018 Dec;155(6):509-510
49. Robotic Double Purse-String Telescoped Pancreaticogastrostomy: How I Do It. Wakabayashi T, **Felli E**, Pessaux P. *World J Surg*. 2018 Sep 25.
50. Complete resection of the hepatic veins: The role of right inferior vein. **Felli E**, Meniconi RL, Colasanti M, Vennarecci G, Ettore GM. *Hepatobiliary Pancreat Dis Int*. 2018 Feb;17(1):88-90.
51. Salvage Surgery for Esophageal Cancer: How to Improve Outcomes? Cohen C, Tessier W, Gronnier C, Renaud F, Pasquer A, Théreaux J, Gagnière J, Meunier B, Collet D, Piessen G, Mariette C; FREGAT (French Eso-Gastric Tumors working group) – FRENCH (Fédération de Recherche en Chirurgie) – AFC (Association Française de Chirurgie) *Ann Surg Oncol*. 2018 Feb 7. doi: 10.1245/s10434-018-6365-1. [Epub ahead of print]

-
52. Gender Fair Language Matters? **Felli E**. *AnnSurg.* 2018 Jan 4. Doi:10.1097/SLA.0000000000002654.[Epub ahead of print] No abstract available.

2017

53. Incidental Gallbladder Carcinoma Discovered after Laparoscopic Cholecystectomy: Identifying Patients Who will Benefit from Reoperation. Addeo P, Centonze L, Locicero A, Faitot F, Jedidi H, **Felli E**, Fuchshuber P, Bachellier P. *J Gastrointest Surg.* 2017 Dec 22. doi: 10.1007/s11605-017-3655-z. [Epub ahead of print]
54. Antiangiogenic agents after first line and sorafenib plus chemoembolization: a systematic review. Casadei Gardini A, Santini D, Aprile G, Silvestris N, **Felli E**, Foschi G, F, Ercolani G, Marisi G, Valgiusti M, Passardi A, Puzzone M, Silletta M, Brunetti O, Cardellino GG, Frassinetti GL, Scartozzi M. *Oncotarget.* 2017 Jul 22;8(39):66699- 66708. doi: 10.18632/oncotarget.19449. eCollection 2017
55. Discrepancy Between Clinical and Pathologic Nodal Status of Esophageal Cancer and Impact on Prognosis and Therapeutic Strategy. Markar SR, Gronnier C, Pasquer A, Duhamel A, Behal H, Théreaux J, Gagnière J, Lebreton G, Brigand C, Renaud F, Piessen G, Meunier B, Collet D, Mariette C; FREGAT Working Group – FRENCH - AFC.
56. Prognostic value of venous invasion in resected T3 pancreatic adenocarcinoma: Depth of invasion matters. Addeo P, Velten M, Averous G, Faitot F, Nguimpi-Tambou M, Nappo G, **Felli E**, Fuchshuber P, Bachellier P. *Surgery.* 2017 May 30. pii: S0039-6060(17)30164-2. doi: 10.1016/j.surg.2017.03.008. [Epub ahead of print]
57. A Steatotic Pancreas in a Non-obese Patient **Felli E**, Addeo P, Faitot F, Bachellier P. *J Gastrointest Surg.* 2017 May 3. doi: 10.1007/s11605-017-3433-y. [Epub ahead of print] No abstract available
58. Liver transplantation for hereditary hemorrhagic telangiectasia: a systematic review. **Felli E**, Addeo P, Faitot F, Nappo G, Oncioiu C, Bachellier P. *HPB (Oxford).* 2017 Apr 17. pii: S1365-182X(17)30533-6. doi: 10.1016/j.hpb.2017.03.005. [Epub ahead of print] Review.
59. Agenesis of the retro-hepatic inferior vena cava. **Felli E**, Addeo P, Faitot F, Bachellier P. *Dig Liver Dis.* 2017 Mar 25. pii: S1590-8658(17)30263-3. doi: 10.1016/j.dld.2017.03.003. [Epub ahead of print] No abstract available.
60. Surgically treated oesophageal cancer developed in a radiated field: Impact on peri-operative and long-term outcomes. Markar SR, Gronnier C, Pasquer A, Duhamel A, Behal H, Théreaux J, Gagnière J, Lebreton G, Brigand C, Meunier B, Collet D, Mariette C; FREGAT working group – FRENCH - AFC. *Eur J Cancer.* 2017 Apr;75:179-189. doi: 10.1016/j.ejca.2016.12.036.

2016

61. Management of the splenic vein during a pancreaticoduodenectomy with venous resection for malignancy. Addeo P, Nappo G, **Felli E**, Oncioiu C, Faitot F, Bachellier P. *Updates Surg.* 2016 Sep;68(3):241-246. Epub 2016 Sep 20. Review.
62. Right hepatic artery crossing the common hepatic artery: an unusual blood supply to the liver. **Felli E**, Vennarecci G, Santoro R, Guglielmo N, Ettorre GM. *Surg Radiol Anat.* 2016 Apr;38(3):359-60. doi: 10.1007/s00276-015-1522-8. Epub 2015 Jul 22.

-
63. Incidence and Risk Factors Related to Symptomatic Venous Thromboembolic Events After Esophagectomy for Cancer. Mantziari S, Gronnier C, Pasquer A, Gagnière J, Théreaux J, Demartines N, Schäfer M, Mariette C; FREGAT Working Group – FRENCH - AFC. *Ann Thorac Surg.* 2016 Sep;102(3):979-84. doi: 10.1016/j.athoracsur.2016.03.093. Epub 2016 Jun 2.
64. ALPPS for primary and secondary liver tumors. Vennarecci G, Grazi GL, Sperduti I, Busi Rizzi E, **Felli E**, Antonini M, D'Offizi G, Ettore GM. *Int J Surg.* 2016 Jun;30:38-44. doi:10.1016/j.ijsu.2016.04.031. Epub 2016 Apr 22.
65. Significance of Microscopically Incomplete Resection Margin After Esophagectomy for Esophageal Cancer. Markar SR, Gronnier C, Duhamel A, Pasquer A, Théreaux J, Chalret du Rieu M, Lefevre JH, Turner K, Luc G, Mariette C. FREGAT Working Group-FRENCH-AFC. *Ann Surg.* 2016 Apr;263(4):712-8. doi: 10.1097/SLA.0000000000001325.
66. Liver Transplantation and Abuse of Drugs and Alcohol: A Correlation Between Scales of the MMPI-2. Rocco M, Prinzi G, Campagna E, Battaglia T, Barucco T, Polchi S, Kisialiou A, Colasanti M, **Felli E**, Lepiane P, Santoro R, Vennarecci G, Ettore GM. *Transplant Proc.* 2016 Mar;48(2):386-90. doi: 10.1016/j.transproceed.2016.02.006.
67. Multicentre study of neoadjuvant chemotherapy for stage I and II oesophageal cancer. Bekkar S, Gronnier C, Renaud F, Duhamel A, Pasquer A, Théreaux J, Gagnière J, Meunier B, Collet D, Mariette C; French Eso-Gastric Tumors (FREGAT) working group, Fédération de Recherche EN Chirurgie (FRENCH) - Association Française de Chirurgie (AFC). *Br J Surg.* 2016 Jun;103(7): 855-62. doi: 10.1002/bjs.10121. Epub 2016 Apr 4.
68. Role of neoadjuvant treatment in clinical T2N0M0 oesophageal cancer: results from a retrospective multi-center European study. Markar SR, Gronnier C, Pasquer A, Duhamel A, Beal H, Théreaux J, Gagnière J, Lebreton G, Brigand C, Meunier B, Collet D, Mariette C; French Eso-Gastric Tumors (FREGAT) working group – Federation de Recherche EN Chirurgie (FRENCH) - Association Française de Chirurgie (AFC). *Eur J Cancer.* 2016 Mar;56:59-68. doi: 10.1016/j.ejca.2015.11.024. Epub 2016 Jan 23.

2015

69. Laparoscopic liver resection for hepatocellular carcinoma in cirrhotic patients: single center experience of 90 cases. Ettore GM, Levi Sandri GB, Santoro R, Vennarecci G, Lepiane P, Colasanti M, **Felli E**, de Werra E, Colace L, D'Offizi G, Montalbano M, Visco U, Maritti M, Antonini M, Santoro E. *Hepatobiliary Surg Nutr.* 2015 Oct;4(5):320-4. doi: 10.3978/j.issn.2304-3881.2015.06.13.
70. The Impact of Severe Anastomotic Leak on Long-term Survival and Cancer Recurrence After Surgical Resection for Esophageal Malignancy. Markar S, Gronnier C, Duhamel A, Mabrut JY, Bail JP, Carrere N, Lefevre JH, Brigand C, Vaillant JC, Adham M, Msika S, Demartines N, Nakadil E, Meunier B, Collet D, Mariette C; FREGAT (French Eso-Gastric Tumors) working group, FRENCH (Fédération de Recherche EN Chirurgie), and AFC (Association Française de Chirurgie). *Ann Surg.* 2015 Dec;262(6):972-80. doi: 10.1097/SLA.0000000000001011.
71. Is there still a room to improve the safety of ALPPS procedure? A new technical note. Ettore GM, Guglielmo N, **Felli E**, Meniconi RL, Colasanti M, Lepiane P, Santoro R, Vennarecci G. *Eur J Surg Oncol.* 2015 Nov;41(11):1556-7. doi:10.1016/j.ejso.2015.06.013. Epub 2015 Aug 21. No abstract available.
72. The use of Permacol™ surgical implant for subxiphoid incisional hernia repair in cardiac transplant patients. Vennarecci G, Guglielmo N, Pelle F, **Felli E**, Ettore GM. *Int J Surg.* 2015 Sep;21:68-9. doi: 10.1016/j.ijsu.2015.07.641. Epub 2015 Jul 21. No abstract available.

-
73. Salvage liver transplantation after laparoscopic resection for hepatocellular carcinoma: a multicenter experience. **Felli E**, Cillo U, Pinna AD, De Carlis L, Ercolani G, Santoro R, Gringeri E, Di Sandro S, Di Laudo M, Di Giunta M, Lauterio A, Colasanti M, Lepiane P, Vennarecci G, Ettorre GM. *Updates Surg.* 2015 Jun;67(2):215-22. doi: 10.1007/s13304-015-0323-2. Epub 2015 Jul 25.
74. Major hepatectomy for a symptomatic giant liver cavernous hemangioma. de Werra E, Ettorre GM, Levi Sandri GB, Colasanti M, **Felli E**, Vennarecci G. *Hepatobiliary Surg Nutr.* 2015 Jun;4(3):218-9. doi: 10.3978/j.issn.2304-3881.2015.01.08. No abstract available.
75. Total abdominal approach for postero-superior segments (7, 8) in laparoscopic liver surgery: a multicentric experience. Giuliani A, Aldrighetti L, DiBenedetto F, Ettorre GM, Bianco P, Ratti F, Tarantino G, Santoro R, **Felli E**. *Updates Surg.* 2015 Jun;67(2):169-75. doi: 10.1007/s13304-015-0305-4. Epub 2015 Jun 16.
76. Robotic liver surgery: preliminary experience in a tertiary hepato-biliary unit. **Felli E**, Santoro R, Colasanti M, Vennarecci G, Lepiane P, Ettorre GM. *Updates Surg.* 2015 Mar;67(1):27-32. doi: 10.1007/s13304-015-0285-4. Epub 2015 Mar 8.
77. Self-expanding covered metallic stent as a bridge to surgery in esophageal cancer: impact on oncologic outcomes. Mariette C, Gronnier C, Duhamel A, Mabrut JY, Bail JP, Carrere N, Lefevre JH, Meunier B, Collet D, Piessen G; FREGAT WorkingGroup – FRENCH – AFC. *J Am Coll Surg.* 2015 Mar;220(3):287-96. doi: 10.1016/j.jamcollsurg.2014.11.028. Epub 2014 Dec 12.

2014

78. European Initial Hands-On Experience with HEMOPATCH, a Novel Sealing Hemostatic Patch: Application in General, Gastrointestinal, Biliopancreatic, Cardiac, and Urologic Surgery. Fingerhut A, Uranues S, Ettorre GM, **Felli E**, Colasanti M, Scerrino G, Melfa GI, Raspanti C, Gulotta G, Meyer A, Oberhoffer M, Schmoeckel M, Weltert LP, Vignolini G, Salvi M, Masieri L, Vittori G, Siena G, Minervini A, Serni S, Carini M. *Surg Technol Int.* 2014 Nov;25:29-35.
79. Robotic-assisted reversal of Hartmann's procedure for diverticulitis. de'Angelis N, **Felli E**, Azoulay D, Brunetti F. *J Robot Surg.* 2014;8(4):381-3. doi: 10.1007/s11701-014-0458-z. Epub 2014 Mar 16.
80. Impact of neoadjuvant chemoradiotherapy on postoperative outcomes after esophageal cancer resection : results of a European multicenter study. Gronnier C, Tréchet B, Duhamel A, Mabrut JY, Bail JP, Carrere N, Lefevre JH, Brigand C, Vaillant JC, Adham M, Msika S, Demartines N, El Nakadil, Piessen G, Meunier B, Collet D, Mariette C; FREGAT Working Group- FRENCH-AFC, Luc G, Cabau M, Jougon J, Badic B, Lozach P, Cappeliez S, Lebreton G, Alves A, Flamein R, Pezet D, Pipitone F, Iuga BS, Contival N, Pappalardo E, Mantziari S, Hec F, Vanderbeken M, Tessier W, Briez N, Fredon F, Gainant A, Mathonnet M, Bigourdan JM, Mezoughi S, Ducerf C, Baulieux J, Pasquer A, Baraket O, Poncet G, Vaudoyer D, Enfer J, Villeneuve L, Glehen O, Coste T, Fabre JM, Marchal F, Frisoni R, Ayav A, Brunaud L, Bresler L, Cohen C, Aze O, Venissac N, Pop D, Mouroux J, Doncil, Prudhomme M, **Felli E**, Lisunfui S, Seman M, Petit GG, Karoui M, Tresallet C, Ménégauz F, Hannoun L, Malgras B, Lantuas D, Pautrat K, Pocard M, Valleur P. *Ann Surg.* 2014 Nov;260(5):764-70; discussion 770-1. doi: 10.1097/SLA.0000000000000955.
81. Early introduction of everolimus immunosuppressive regimen in liver transplantation with extra- anatomic aortoiliac-hepatic arterial graft anastomosis. **Felli E**, Vennarecci G, Colasanti M, Santoro R, de Werra E, Scotti A, Burocchi M, Levi Sandri GB, Campanelli A, Lepiane P, Ettorre GM. *Case Rep Transplant.* 2014;2014:493095. doi: 10.1155/2014/493095. Epub 2014 Sep 21.
82. Prevention of complications during reoperative thyroid surgery. Pironi D, Pontone S, Vendettuoli M, Podzemny V, Mascagni D, Arcieri S, Panarese A, **Felli E**, Filippini A. *Clin Ter.* 2014;165(4):e285-90. doi: 10.7417/CT.2014.1744.

-
83. Laparoscopic versus open gastric wedge resection for primary gastrointestinal tumors: clinical outcomes and health care costs analysis. de'Angelis N, Brunetti F, **Felli E**, Mehdaoui D, Memeo R, Carra MC, Zuddas V, Azoulay D. Surg Laparosc Endosc Percutan Tech. 2015 Apr;25(2):143-6. doi: 10.1097/SLE.0000000000000080.
84. Open and laparoscopic resection of hepatocellular adenoma: trends over 23 years at a specialist hepatobiliary unit. de'Angelis N, Memeo R, Calderaro J, Felli E, Salloum C, Compagnon P, Luciani A, Laurent A, Cherqui D, Azoulay D. HPB (Oxford). 2014 Sep;16(9):783-8. doi: 10.1111/hpb.12257. Epub 2014 May 23.
85. Robotic right colectomy for hemorrhagic right colon cancer: a case report and review of the literature of minimally invasive urgent colectomy. **Felli E**, Brunetti F, Disabato M, Salloum C, Azoulay D, De'angelis N. World J Emerg Surg. 2014 Apr 26;9:32. doi: 10.1186/1749-7922-9-32. eCollection 2014. Review.

2012

86. Hiding intersphincteric and transphincteric sepsis in a novel pathological approach to chronic anal fissure. Naldini G, Cerullo G, Mascagni D, Orlandi S, Menconi C, Zeri K, **Felli E**, Martellucci J. Surg Innov. 2012 Mar;19(1):33-6. doi:10.1177/1553350611410990. Epub 2011 Jul 7.

-Staging e restaging dei tumori del retto extraperitoneale, Società Italiana di Chirurgia 2008

-Anatomia neurovascolare pelvica, Società Italiana di Chirurgia 2009 ---

-Disfunzioni erettili dopo chirurgia pelvica, Società Italiana di Chirurgia 2010

Participation à des congrès

Participation régulière depuis 2005 aux congrès nationaux et internationaux chirurgie HPB et transplantation hépatique (IHPBA, ILLS, AFC, etc), chirurgie colo-rectale, proctologie, chirurgie mini-invasive), nombreuses présentations orales

Membre de sociétés savantes

IHPBA (International Hepato-Pancreato-Biliary Association)

ACHBT (Association de Chirurgie Hépatobilio-pancréatique et Transplantation)

AFC (Association Française de Chirurgie)

ESOT (European Society of Organ Transplantation)

Expérience de recherche

Circulating neoplastic stem cells in HCV+/- patients affected by hepatocellular carcinoma as a prognostic factors of disease recurrence after surgery

(Cellule staminali neoplastiche circolanti da epatocarcinoma in pazienti HCV+/--come fattore prognostico di recidiva tumorale dopo exeresi chirurgical. En collaboration avec le Pr GM Ettore, Service de Chirurgie Hépatique et Transplantation Hôpital « San Camillo », Roma

Formations :

- conférencier Diplôme Inter Universitaire Chirurgie hépatobilio-pancréatique et Transplantation Hépatique Strasbourg
- conférencier Diplôme Inter Universitaire Chirurgie Digestive Robotique, Strasbourg
- Enseignant Cours Chirurgie Laparoscopique IRCAD, Strasbourg

Langues

Italien (langue maternelle), Anglais (IELTS score 7/10), Français (courant), Espagnol, Russe (bases)

Intérêts extra professionnels : musique (batterie, piano, guitare), histoire de la chirurgie, science politiques, philosophie, histoire, étude de langues étrangères,

Sports : boxe anglaise, running

Tours, 13/03/2022

Dr Emanuele FELLI

INTRODUCTION

1. Le concept de médecine de précision

La médecine est l'une des formes les plus merveilleuses et passionnantes de la science.

Depuis la vision pré-hippocratique des maladies considérées comme un châtiment des dieux, la médecine a fait un long chemin. Lorsque les maladies ont commencé à être considérées comme une entité objective, indépendante de la conduite personnelle, de l'éthique ou de la foi, la lutte sans fin de l'être humain pour prolonger et améliorer la qualité de vie est entrée dans l'ère moderne. Deux mille ans d'observations, de raisonnements, d'avancées ainsi que de régressions, de dogmatismes mais aussi d'intuitions visionnaires, nous ont préparés au XXI^e siècle à trouver un remède à chaque maladie, à prendre soin de chaque patient, et enfin à améliorer la qualité de vie en respectant la dignité.

C'est à partir de ce tableau complexe de centaines et de centaines d'années d'évolution que la médecine a pu combiner l'expérience, les connaissances, la technologie, les idées novatrices et la richesse (malheureusement seulement pour une partie de l'humanité), ce qui a naturellement conduit au concept et à l'application de la médecine de précision.

Le carcinome hépatocellulaire ou CHC est une maladie très complexe. L'incidence est en constante augmentation, les manifestations cliniques variables, une diversité de voies moléculaires détermine des évolutions naturelles différentes, et il existe aujourd'hui un nombre impressionnant et varié de stratégies de traitement. En tant que praticien, l'objectif, est d'offrir à chaque patient les meilleures chances de guérison, en établissant collaboration et interaction constante et étroite entre scientifiques, hépatologues, chirurgiens, radiologues et oncologues, travaillant de concert pour une approche multidisciplinaire, transversale et intégrée de la pratique clinique et de la recherche. L'application de

ce concept interdisciplinaire est indispensable pour traduire dans la réalité le concept de médecine de précision mentionné ci-dessus.

2. Carcinome hépatocellulaire

a) Présentation générale

Le carcinome hépatocellulaire (CHC) est le plus fréquent des cancers primitifs du foie. Il représente environ 90 % des cas et survient presque exclusivement chez les patients cirrhotiques. Son incidence augmente régulièrement dans le monde (1,2), avec une estimation de plus d'un million de personnes qui seront touchées par le CHC chaque année d'ici 2025 (3). L'infection par le virus de l'hépatite B (VHB) est le principal facteur de risque de développement du CHC, responsable d'environ 50 % des cas (4). Depuis l'introduction des traitements antiviraux directs et chez les patients ayant une réponse virologique soutenue, le risque attribué à l'infection par le virus de l'hépatite C (VHC) a considérablement diminué (5). Actuellement, et ceci en particulier dans les pays occidentaux, la stéatohépatite non alcoolique, est responsable de l'augmentation de l'incidence du CHC (6). Bien que notre compréhension de la physiopathologie de la maladie se soit améliorée, ces connaissances ne sont pas encore totalement transposées dans la pratique clinique. La compréhension des voies génétiques impliquées dans le développement du CHC a permis d'identifier des mutations spécifiques trouvées dans environ 25 % des CHC, les plus fréquentes n'étant toutefois détectées que chez <10 % des patients (7,8). De ce fait, les biopsies de la lésion cancéreuse et du foie non tumoral sont de plus en plus réalisées afin de procéder à la caractérisation moléculaire des tumeurs (9,10). La résection hépatique, l'ablation locale et la transplantation hépatique sont les trois traitements curatifs établis pour le CHC. L'amélioration progressive de la sélection des patients (caractéristiques tumorales, fonction hépatique et *performance status*) a été associée à de meilleurs résultats à long terme et à une meilleure qualité de vie (11). La chimioembolisation transartérielle (TACE), la radioembolisation transartérielle (TARE), la radiothérapie stérotaxique et les thérapies systémiques (y compris l'immunothérapie) sont

des options alternatives établies – mais généralement non curatives – à considérer également dans l'arsenal des stratégies de traitement des patients atteints de CHC (**Fig. 1**) (12).

Dans cette thèse, nous nous concentrerons uniquement sur la résection chirurgicale.

a) Traitement chirurgical

Les traitements chirurgicaux comprennent la résection hépatique et la transplantation hépatique, ces derniers associés à une survie globale à 5 ans de 70 à 80 %. La décision entre la résection et la transplantation est généralement basée sur l'âge du patient, la fonction hépatique, le degré d'hypertension portale et les caractéristiques tumorales telles que la localisation tumorale, le nombre et la taille des nodules, la relation avec les structures vasculaires et biliaires, le type de résection nécessaire, le foie résiduel et le *performance status*. La résection est considérée comme le traitement de choix, en particulier chez les patients atteints de CHC survenus sur foies non cirrhotiques et chez les patients pour lesquels la décompensation hépatique post-opératoire est peu probable, ou en cas de contre-indication formelle à la transplantation hépatique (c'est-à-dire l'âge, ou lorsque la résection est considérée comme un traitement d'attente vers celle-ci)(13). De plus en plus d'études suggèrent que la résection anatomique du foie offre une survie postopératoire plus longue et avec un moindre taux de récurrence comparée aux résections non anatomiques (14-18) ; ce point particulier est encore aujourd'hui une source de débat, en particulier entre pays occidentaux et orientaux. La résection anatomique est une procédure plus exigeante, en particulier sur les foies cirrhotiques. Même s'il est facile de distinguer le parenchyme vascularisé de celui ischémique après le clampage sélectif des éléments vasculaires, les points de repère intraparenchymateux entre les segments sont plus difficiles à déterminer. Cette difficulté technique s'est accrue au cours des dernières années, car la résection hépatique par abord mini-invasif a été de plus en plus privilégiée. Différentes stratégies pour surmonter cette difficulté ont été envisagées ; une description détaillée est présentée dans le chapitre dédié à la navigation peropératoire (page 8).

3. Imagerie

a) Imagerie et stratégie chirurgicale

La chirurgie hépatique moderne est basée sur une évaluation précise de l'imagerie. La stratégie chirurgicale est en effet définie après une analyse attentive des caractéristiques de la tumeur et de l'anatomie réelle du patient, informations qui proviennent principalement de l'analyse des images (scanner et IRM). Les résections anatomiques ou non anatomiques sont planifiées en fonction de la relation entre la tumeur (ou les tumeurs) et les structures vasculaires et biliaires. Ce processus nécessite des images de haute qualité, idéalement réalisées dans des centres experts axés sur la chirurgie hépatique

b) Reconstruction 3D préopératoire

Afin d'améliorer la capacité de planification stratégique et de répondre au besoin de calculer le volume du futur foie réstant, la reconstruction 3D s'est progressivement imposée dans la pratique clinique. En effet, l'anatomie réelle est parfois complexe à déterminer à partir des simples images en 2D (scanner et IRM). Depuis le premier simulateur 3D anatomique utilisé pour la planification préopératoire des hépatectomies, proposé en 1998 par Marescaux et al. (19), la technologie 3D s'est développée de manière impressionnante. En effet, pour le traitement du CHC, au vu des difficultés, mentionnées précédemment, c'est-à-dire de réaliser une résection en présence d'un foie cirrhotique, une planification préopératoire précise peut minimiser le risque de variations peropératoires dans la stratégie chirurgicale. Ces variations peuvent atteindre 20% lors des procédures de chirurgie générale, et souvent associées à une augmentation de la morbidité postopératoire (22). Néanmoins, l'impact réel de la reconstruction 3D sur les indications et les résultats en chirurgie hépatique n'a pas encore été démontré (20,21). La plupart des recherches sur l'évaluation 3D se concentrent sur sa capacité à estimer avec précision les volumes des différents segments hépatiques et à déterminer précisément les marges de résection chirurgicale (23-26). Peu d'études comparent les résultats de survie à long terme aux

bénéfices obtenus par l'évaluation 3D (27, 28). Jusqu'à présent, aucune étude prospectif analysant l'apport de la reconstruction 3D dans la planification chirurgicale d'une hépatectomie pour un CHC n'a été publiée.

c) Imagerie peropératoire

Comme déjà mentionné, il est souvent difficile de définir les plans exacts de résection, surtout chez les patients cirrhotiques et pour les tumeurs des segments postéro-supérieurs. La définition de la direction intra parenchymateuse correcte est un défi technique et les repères anatomiques, tels que les veines hépatiques et les branches portales, sont utilisés sous guidage échographique pour guider la résection (29-32). Makuuchi et al. ont associé le guidage par ultrasons à l'injection de bleu de méthylène dans les branches portales pour délimiter sur la surface du foie les limites précises d'un segment ou d'un secteur. Cette technique était réalisée en chirurgie ouverte, elle nécessite un clampage de l'artère hépatique et le lavage du colorant est relativement rapide. En remplaçant le colorant bleu par du vert d'indocyanine (ICG) et en associant l'utilisation de caméras « *near infrared* », des résections anatomiques basées sur la fluorescence ont été réalisées (33). Cette technique permettait notamment une coloration parenchymateuse stable et évitait le clampage artériel électif. En 2008, Aoki et al. (34) ont été les premiers à utiliser cette technique en chirurgie ouverte; le taux de succès pour l'identification des plans anatomiques était de 93 %. La technique a été considérée comme sûre, reproductible et peu/non chronophage. En parallèle, le bénéfice de la résection par voie mini invasive a été établi, en particulier pour le CHC, et a été confirmé lors de réunions de consensus et par des recommandations internationales (35, 36).

d) Imagerie fonctionnelle in vivo

Les lésions d'ischémie-reperfusion (IRI) sont redoutés après hépatectomie ou en transplantation hépatique (43). La pression d'oxygène diminue à l'intérieur des sinusoides, ce qui réduit la production d'ATP et augmente les radicaux libres de l'oxygène, les cytokines et les chemiokines (44). À l'heure

actuelle, il n'existe aucun outil peropératoire et non invasif pour évaluer la qualité de la perfusion hépatique afin de prédire la viabilité du foie dans la période post-opératoire. L'imagerie hyperspectrale (HSI) est une modalité d'imagerie fonctionnelle non invasive qui a récemment été appliquée au domaine médical en tant qu'outil pour la chirurgie guidée par l'image, plus particulièrement pour la quantification peropératoire de l'oxygénation des tissus (45). Les images HSI sont basées sur l'analyse computationnelle des interactions lumière-tissu par la détection de la réflectance relative, permettant une quantification des composés organiques tels que l'hémoglobine désoxygénée et oxygénée à différentes profondeurs dans le parenchyme(46). Son utilité dans l'amélioration de la prise en charge des patients en chirurgie HBP n'a pas encore été documentée.

4. Modèles de foie *ex vivo*

L'absence d'un système de modèle de culture cellulaire approprié constitue une limitation importante dans le développement préclinique de médicament pour les maladies avancées du foie comme la fibrose avancée ou le CHC. Les modèles de culture cellulaire *in vitro* standard sont basés sur des lignées cellulaires d'hépatocarcinome, où des caractéristiques clés telles que les interactions cellule-cellule, l'architecture tumorale tridimensionnelle et l'hétérogénéité cellulaire du microenvironnement tumoral ne sont pas présents. Afin d'offrir des traitements plus spécifiques et moins toxiques pour guérir ou prévenir le CHC rapidement, des modèles *ex vivo* capables de récapituler les caractéristiques de la fibrose hépatique ou du CHC ont été développés (48). De nouveaux modèles *ex vivo* et *in vitro* ont été établis et optimisés pour l'étude tridimensionnelle des systèmes hépatiques, par exemple les sphéroïdes à base de cellules primaires et les organoïdes dérivés de cellules souches (Fig.3) ainsi que les systèmes de puces, les cultures en sandwich et la bio-impression du foie (49). Les sphéroïdes sont des agrégats multicellulaires tridimensionnels (3D) obtenus à partir de résections dissociées puis

réassociées en culture ou, à partir de lignées cellulaires dans des conditions de culture particulières. Les sphéroïdes hépatiques présentent des caractéristiques importantes telles qu'une longévité supérieure aux cultures de cellules primaires classiques, et la préservation des interactions intercellulaires entre les hépatocytes et les cellules non parenchymateuses. Très récemment un modèle de criblage de médicaments pour identifier de nouvelles molécules thérapeutiques capable d'évaluer la réversion d'un profil de mauvais pronostic vers un profil de bon pronostic a été mis au point dans notre laboratoire (Crouchet et al., 2021). Ceci ouvre la porte au criblage de médicaments sur sphéroïdes hépatiques provenant de résections hépatiques. Par ailleurs, des modèles PDX (*patient-derived xenograft*) basés sur la greffe de fragments de résections hépatiques chez la souris ont également été développés et sont couramment utilisés pour analyser l'effet de nouveaux traitements potentiels dans les études précliniques. Au regard, de la médecine de précision, l'utilisation de sphéroïdes hépatiques et de sphères tumorales de CHC est de la plus haute importance pour améliorer les soins futurs aux patients. En effet, les tissus tumoraux CHC dissociés dérivés du patient, peuvent être réassemblés *ex vivo*, pour former un ensemble de tumeurs constituées d'hépatocytes et de cellules non parenchymateuses, capables de récapituler le microenvironnement tumoral. Ces sphéroïdes apparaissent comme des modèles avancés, pour tester rapidement l'efficacité de diverses options de traitement et ainsi aider/guider le clinicien à choisir la molécule thérapeutique la plus efficace pour un patient spécifique.

5. OBJECTIFS

Ce projet de thèse visait à intégrer le concept de médecine de précision susmentionné appliqué au traitement du CHC sur une base multidisciplinaire. L'objectif était de mettre en œuvre une approche transversale permettant d'intégrer les technologies les plus innovantes et de nouveaux paradigmes de traitement en privilégiant une interaction continue entre les besoins cliniques et l'expertise provenant de différents domaines de la biologie et de l'ingénierie. L'ensemble du projet, développé en trois

principaux domaines d'application, a été ainsi conçu pour faire humblement un pas de plus dans l'évolution de la médecine de précision pour le traitement du CHC et pour créer une voie homogène et cohérente d'intégration, d'innovation et de précision pour une meilleure prise en charge et une meilleure chance de guérison de nos patients. Les deux premières parties ont été réalisées en étroite collaboration avec l'Institut Hospitalo-Universitaire (IHU) de Strasbourg et le Service Hépato-Digestif du Nouvel Hôpital Civil, Hôpitaux Universitaires de Strasbourg. La dernière partie a été réalisée plus spécifiquement avec l'Institut des maladies virales et hépatiques (Unité Inserm 1110), Strasbourg.

La première partie est axée sur l'imagerie préopératoire et la stratégie chirurgicale. L'objectif était d'évaluer, dans le cadre d'un essai prospectif non randomisé multicentrique français, les avantages de la reconstruction 3D par rapport à l'analyse d'imagerie 2D standard, afin de déterminer si des modifications significatives de la stratégie préopératoire et de l'opération effectivement réalisée étaient identifiées. Dans la même étude, les objectifs secondaires visaient à évaluer si la reconstruction 3D permettait de mieux détecter la localisation tumorale, les variations anatomiques, les marges de résection et le volume réséqué.

La deuxième partie est axée sur l'imagerie peropératoire. Les progrès récents de l'imagerie optique, de la réalité augmentée et de l'intelligence artificielle nous ont encouragés à trouver des solutions pour obtenir de meilleurs résultats pour les patients, en tirant parti de toutes ces technologies innovantes et prometteuses. Les principaux objectifs de la recherche étaient les suivants : a) prouver que l'imagerie hyperspectrale (HSI) pouvait distinguer entre le foie ischémique et le foie non ischémique ; b) évaluer la corrélation entre les propriétés optiques et biologiques ; c) démontrer que le HSI permettait de prédire la viabilité hépatique en peropératoire et automatiser le processus à l'aide de l'intelligence artificielle ; d) associer l'HSI à la réalité augmentée pour guider les résections hépatiques.

La troisième partie de notre travail interactif et transversal conçu pour optimiser le traitement du CHC – allant des nouvelles technologies d'imagerie à la salle d'opération – s'est concentrée sur la

collaboration étroite avec l'Institut des maladies virales et hépatiques (Unité INSERM 1110). Mon objectif était d'enrichir la biobanque LIVMOD (UMR_S1110) avec des échantillons opératoires de haute qualité provenant de patients cirrhotiques et non cirrhotiques atteints de CHC, et de contribuer 1) à des études *proof of concept*, visant à trouver les meilleures stratégies de traitement pour les patients non répondeurs en première ligne, ou à confirmer l'efficacité de molécules nouvellement identifiées pour prévenir la fibrose hépatique et le CHC, en capitalisant sur des modèles ex vivo obtenus à partir de tissus dérivés de patients, tels les sphéroïdes ; 2) contribuer à des programmes de recherche translationnelle européens et nationaux très compétitifs dédiés à une meilleure compréhension de la maladie hépatique avancée et du CHC au niveau fondamental.

6. RÉSULTATS

Les résultats liés aux deux premiers et principaux objectifs de cette thèse font partie intégrante de six manuscrits qui sont inclus dans les sections suivantes. En plus de la gestion de projet, avec trois des six manuscrits écrits en tant que premier auteur, mes contributions expérimentales individuelles sont mises en évidence dans les sections de résumés respectifs avant chaque article.

6.1) Imagerie préopératoire – résumé des résultats et contribution propre

Les dernières technologies d'imagerie appliquées à la stratégie chirurgicale préopératoire (planification de l'opération, type de résection, navigation intra-opératoire, approche mini-invasive, etc.) sont actuellement fondamentales pour un traitement optimal du CHC. HAPPI 3D (*HepAtic Procedure PlannIng 3D*) est une étude française prospective multicentrique non randomisé, développée sous la coordination du Pr P. Pessaux (co-directeur de thèse), qui avait pour objectif principal d'analyser le bénéfice et l'utilisation de la reconstruction 3D préopératoire dans la planification de la stratégie

chirurgicale avant la résection du CHC. La reconstruction 3D a utilisé le logiciel VR RENDER®, puis les images ont été traitées via un plug-in, Virtual Surgical Planning (VSP®, IRCAD).

Cette étude est la première du genre, car aucun autre essai multicentrique prospectif n'avait été réalisé auparavant sur le sujet. L'objectif principal était de déterminer si l'analyse préopératoire du modèle 3D (appelée « Plan B ») modifiait la stratégie chirurgicale initialement prévue sur la base de l'imagerie 2D conventionnelle (« Plan A »). La mesure était basée sur l'analyse du taux de modification entre le Plan A et le Plan B, et du Plan B à la procédure finale effectuée (appelée « Plan C »). Douze centres ont participé, 124 patients inclus dans l'analyse finale.

La reconstruction tridimensionnelle s'est révélée être un outil important pour améliorer l'analyse préopératoire et établir une stratégie chirurgicale correcte. Ma contribution personnelle à cette étude a été la participation à la conception de l'étude, aux procédures opératoires, à l'analyse des résultats et à la rédaction et la révision du manuscrit (Felli et al, *article soumis, en cours de révision*).

6.2) Imagerie fonctionnelle *in vivo* – résumé des résultats et contribution propre

i) Évaluation des tissus ischémiques et non ischémiques

Nous avons effectué une analyse peropératoire des propriétés optiques du foie pour comprendre si la distinction entre différents niveaux de perfusion était possible. Nous avons constaté que le HSI pouvait distinguer entre l'occlusion totale du flux vasculaire et le clampage exclusif de l'artère hépatique. Ces résultats ont été confirmés par une validation croisée du HSI qui a détecté et quantifié la congestion intestinale en cas d'occlusion vasculaire. On a trouvé une corrélation significative entre les spectres du NIR (*near infrared*) et le lactate capillaire ($r = -0,8645$, $p = 0,0003$ VIO, $r = -0,7113$, $p = 0,0120$ HAO). Une corrélation négative statistiquement significative a été trouvée aussi entre le score histologique et le NIR ($r = -0,88$, $p = 0,004$). Nous en avons déduit que l'HSI, en tenant compte de la corrélation avec les lactates capillaires et le score histopathologique, pouvait être un outil non

invasif approprié pour l'évaluation peropératoire de la perfusion hépatique. Ma contribution personnelle à cette étude a été la participation à la conception de l'étude, aux procédures opératoires sur les modèles animaux de cochon, à l'analyse des résultats et à la rédaction et la révision du manuscrit (Felli et al, Sci Rep 2020).

ii) Évaluation des lésions d'ischémie-reperfusion

Nous avons évalué la viabilité hépatique dans un modèle d'occlusion artérielle avec une analyse de l'HSI associée à l'intelligence artificielle. Le score d'intelligence artificielle (IA) de viabilité hépatique a montré une corrélation significative avec le lactate capillaire de la surface du foie ($r = -0,78$, $p = 0,0320$) et le score de Suzuki ($r = -0,96$, $p = 0,0012$). La détection de CD31 par immunohistochimie a confirmé les lésions microvasculaires en accord avec le score IA déterminé. Nos résultats ont finalement montré le potentiel d'une analyse basée sur le HSI-IA pour prédire la viabilité du foie, encourageant le développement d'outils peropératoires d'exploration non invasifs tel la HSI pour son application dans un contexte clinique. Ma contribution personnelle à cette étude a été la participation à la conception de l'étude, aux procédures opératoires sur les modèles animaux, à l'analyse des résultats et à la rédaction et la révision du manuscrit (Felli et al, Diagn 2021).

iii) Hyperspectral Enhanced Reality (HYPER) pour la résection anatomique du foie

L'équipe a développé un logiciel pour superposer les images HSI sur le champ opératoire, obtenant une réalité augmentée (HYPER) afin d'identifier la ligne de démarcation après clampage vasculaire sélectif gauche pendant une résection anatomique dans un modèle animal expérimental. Après ligature, l'HSI a permis d'observer une oxygénation significativement plus faible (indice NIR) dans le lobe médial gauche (LMG) ($0,27 \% \pm 0,21$) par rapport au lobe médial droit (LMD) ($58,60 \% \pm 12,08$; $p = 0,0015$). Les lactates capillaires étaient significativement plus élevés ($3,07 \text{ mmol/L} \pm 0,84$ vs $1,33 \pm$

0,71 mmol/L ; $p = 0,0356$) dans le LMG que dans le LMD, respectivement. De façon concordante, la microscopie confocale a démontré l'absence de flux sanguin dans le LMG et la perfusion normale dans le LMD. HYPHER a correctement identifié la ligne de démarcation et quantifié l'oxygénation du foie en surface. HYPHER pourrait, de ce fait, être un outil peropératoire pour guider l'évaluation de la ligne de démarcation basée sur la perfusion. Ma contribution personnelle à cette étude a été la participation à la conception de l'étude, aux procédures opératoires sur les modèles animaux, à l'analyse des résultats et à la rédaction et la révision du manuscrit (Felli et al, Surg End 2020).

iv) Résection hépatique anatomique guidée par ICG avec la technique de la coloration positive et négative (*positive* ou *negative staining*).

Une revue exhaustive de la littérature présente concernant cette technique a été effectuée et publiée dans la revue indexée HPB (33). Quarante-six articles ont d'abord été trouvés et 11 articles ont finalement été inclus dans l'analyse, avec 83 patients traités. Soixante-deux patients (74,6 %) ont eu une mono-segmentectomie. Le *positive staining* a été utilisé chez trente-cinq patients (42,1 %), quarante-huit patients (57,8 %) le *negative staining*. La technique doit être standardisée et les avantages concernant les résultats oncologiques doivent encore être validés dans d'autres études. Ma contribution personnelle à cette revue a été de rechercher et de réviser les articles publiés sur ce sujet en langue anglaise, ainsi que la rédaction et la révision du manuscrit (Felli et al, HPB 2021).

6.3) Modèles tumoraux *ex vivo*

Le programme de cette partie était axé sur la collection de la Biobank LIVMOD de spécimens CHC de parenchyme tumoral et adjacent ou de parenchyme non tumoral après résection chirurgicale. L'objectif était de créer un pipeline efficace pour prélever des échantillons de tumeur et de foie adjacent de très haute qualité à des fins diverses, notamment pour des modèles dérivés de tissus de patients et des études « omiques ». Ces échantillons sont recueillis et conservés dans la biobanque LIVMOD de

l'unité Inserm 1110 et utilisés pour développer des modèles de tumeurs hépatiques *ex vivo* avec la technologie des sphéroïdes, des tumorsphères ou des modèles PDX. Ces modèles sont ensuite utilisés pour tester l'activité antitumorale de médicaments nouveaux ou actuellement disponibles pour le traitement du CHC. L'objectif était de réaliser une étude *proof of concept* pour proposer aux cliniciens un panel de sensibilité en établissant des chimiogrammes personnalisés « à la carte », parfaitement intégré au concept de médecine de précision.

Résultats et contribution propre

Depuis mai 2018, à mon arrivée au Pôle Hépato-Digestif (Nouvel Hôpital Civil, CHU Strasbourg) j'ai contribué à la collecte de prélèvements hépatiques opératoires de patients cirrhotiques et non cirrhotiques avec tumeur appariée et prélèvements adjacents, associés à des prélèvements sanguins de patients dans le cadre d'une collaboration active de longue durée avec les chercheurs de l'Institut des maladies virales et hépatiques (Inserm U1110). En tant que membre officiel affilié depuis début 2019, j'ai participé activement à l'amélioration du prélèvement des échantillons des résections hépatiques, en optimisant la conservation des échantillons, les documents de consentement et les protocoles pour le transfert à l'équipe de recherche translationnelle de l'Inserm U1110. Par ailleurs, j'ai participé à la rédaction du document officiel permettant à l'Institut de Recherche Virale et Hépatique de devenir par lui-même un « Centre de Ressources Biologiques » supervisé par le département de recherche clinique de l'Inserm. Après plusieurs séries de révision, l'autorisation a été obtenue en juin 2020, et a permis la création de la biobanque LIVMOD (UMR_S1110).

Les échantillons prélevés et les échantillons de sang ont été utilisés pour améliorer les modèles *ex vivo* de tumeurs et de maladies du foie, comme les tumorsphères, les sphéroïdes hépatiques ou les xénogreffes dérivées de tumeurs de patient (PDX). Les sphéroïdes dérivés du CHC ont été utilisés pour tester l'activité antitumorale de nouveaux médicaments par rapport aux thérapies couramment utilisées afin d'établir des « chimiogrammes », avec pour objectif un traitement médical « à la carte ».

7. CONCLUSIONS

Nous nous sommes initialement concentrés sur la stratégie préopératoire pour voir si les technologies les plus récentes appliquées à la reconstruction tridimensionnelle amélioreraient significativement la stratégie chirurgicale. L'essai prospectif multicentrique a montré que dans les centres de référence tertiaire HBP des modifications substantielles ont été apportées après l'analyse d'images 3D. Les résultats suggèrent que les modèles 3D sont un complément et non en opposition à l'imagerie standard. Les objectifs éducatifs et pédagogiques doivent également être considérés, permettant une compréhension plus facile de l'anatomie réelle du patient.

La deuxième partie, la phase peropératoire, a exploré l'imagerie hyperspectrale (HSI). Nos expériences ont montré des résultats très intéressants, mais pas fondamentaux. Cette nouvelle technologie n'est toujours pas encore appliquée dans la pratique clinique, les articles présentés sont parmi les premiers dans ce domaine. De nouveaux projets de recherche devraient dans le futur être axés sur la transplantation hépatique pour rechercher des corrélations entre l'imagerie, la reperfusion hépatique, et les résultats postopératoires. La revue sur l'utilisation de l'ICG en peropératoire s'est concentrée sur une technique innovante et prometteuse, mais encore trop rarement utilisée. Enfin, le travail transversal avec l'unité INSERM 1110 a été un exemple d'approche multidisciplinaire de la recherche clinique et translationnelle.

Néanmoins, des mises en garde sont nécessaires. Toutes les formes d'approches innovantes nécessitent une réflexion, une planification et une application intelligente, constante et humble pour mieux définir l'impact réel dans la pratique clinique.

En conclusion, la médecine de précision appliquée au traitement du CHC est complexe et ambitieuse, et surtout liée à différentes spécialités médicales et aux sciences fondamentales. Les technologies de

pointe font leur entrée dans la pratique clinique d'aujourd'hui, et l'innovation joue un rôle clé dans le processus décisionnel. Ne ratons pas cette opportunité unique de faire avancer la médecine aux cotés des sciences de l'innovation technique et translationnelle et thérapeutique !

Emanuele FELLI

Apport de la médecine de précision dans le traitement du carcinome hépatocellulaire

Résumé

Résumé en français suivi des mots-clés en français

Le carcinome hépatocellulaire (CHC) est le cancer primitif du foie le plus fréquent et qui survient presque exclusivement sur une cirrhose sous-jacente. Ce travail de thèse avait comme objectif l'intégration du concept de médecine de précision dans le traitement du CHC dans un contexte de multidisciplinarité. L'ensemble du projet a été développé en trois principaux chapitres: le premier basé sur l'imagerie préopératoire et la stratégie chirurgicale. L'objectif d'évaluer dans une étude française prospective multicentrique l'apport des reconstructions 3D dans la détermination de la stratégie préopératoire en regard des l'imagerie 2D traditionnelle. Le deuxième chapitre basé sur l'imagerie intra opératoire. Les récentes avancées dans la réalité augmentée, dans l'intelligence artificielle, et dans les nouvelles technologies d'imagerie, ont encouragé notre équipe à trouver des solutions pour améliorer les suites postopératoires. La troisième partie de ce travail interactif et transversale avait comme objectif d'améliorer les modèles ex-vivo en optimisant les échantillons dérivés de pièces opératoires des hépatectomies pour la bio banque LIVMOD, en collaboration étroite avec l'Institut de Maladies Virales et Hépatiques de Strasbourg.

L'étude prospective multicentrique réalisée dans des centres de référence en chirurgie HBP a montré des changements significatifs dans la stratégie préopératoire après analyse préopératoire des reconstructions 3D. L'imagerie hyper spectrale appliquée à des modèles animaux et en cours des hépatectomies a montré la possibilité de discriminer entre parenchyme hépatique perfusé et non perfusé, et de pouvoir prédire les conséquences de l'ischémie-réperfusion avec un modèle de machine learning. Cette nouvelle technologie n'est pas encore explorée dans la pratique clinique, les articles présentés les premiers publiés dans ce domaine. Pour terminer, le travail transversal a été un exemple de multidisciplinarité entre l'activité clinique et la recherche translationnelle. En conclusion, la médecine de précision appliquée au traitement du CHC est complexe et ambitieuse, et liées à différentes spécialités médicales, science de base, et ingénierie. Des nouvelles technologies de pointe sont en train de rentrer dans la pratique clinique, et l'innovation joue un rôle fondamental dans le processus décisionnel.

Mots clés : carcinome hépatocellulaire – médecine de précision – reconstructions préopératoire 3D – imagerie hyperspectrale – recherche translationnelle – *patient derived tissues - biobank*

Résumé en anglais

Résumé en anglais

Hepatocellular carcinoma (HCC) is the most frequent primitive liver cancer occurring almost exclusively in cirrhotic patients. This thesis work aimed to integrate the concept of precision medicine applied to the treatment of HCC on a multidisciplinary basis. The whole project, developed in three main fields of application: the first part is focused on preoperative imaging and surgical strategy. The goal was to evaluate, in a French multicentric prospective non-randomized trial, the benefit of the 3D reconstruction over the standard 2D imaging analysis. The second part is focused on intraoperative imaging. The recent advances in optical imaging, enhanced reality, and artificial intelligence, encouraged our team to find solutions for improved patient outcomes by taking advantage of all these novel and promising technologies. The third part of our interactive and transversal work aimed to improve ex-vivo models by optimizing the harvesting and conservation of patient-derived hepatic tissue and enrich the collection of patient derived liver specimens of the LIVMOD Biobank based on a tight collaboration with the Institute for Viral and Hepatic Diseases of Strasbourg.

The multicentric prospective trial showed that in tertiary referral HPB centers substantial modifications were reported after 3D images analysis. Hyperspectral imaging applied animal and humans revealed the possibility to discriminate between perfused and not perfused parenchyma, along with the possibility to predict the ischemia reperfusion injury with a machine learning model. This new technology is still not explored nor clinically routinely applied, the presented articles are among the first on that kind in this really innovative field. Finally, the transversal work was an example of a multidisciplinary approach to clinical and translational research from the bedside to the bench.

In conclusion, precision medicine applied to the treatment of HCC is complex and ambitious, and most of all related to different medical specialties, basic science, and engineering. Cutting edge technologies are entering today's clinical practice, and innovation is playing a key role in the decision-making process.

Keywords : hepatocellular carcinoma – precision medicine – preoperative 3D reconstructions – hyperspectral imaging – translational research – patient derived tissues - biobank